SSD

SCIENCE FOR A SUSTAINABLE DEVELOPMENT

BIOGEOCHEMICAL CYCLES IN THE SOUTHERN OCEAN: ROLE WITHIN THE EARTH SYSTEM

BIGSOUTH

F. DEHAIRS, J.-L. TISON, F. FRIPIAT, L. ANDRÉ, H. GOOSSE, B. DELILLE

ENERGY

TRANSPORT AND MOBILITY

AGRO-FOOD

HEALTH AND ENVIRONMENT

CLIMATE

BIODIVERSITY

ATMOSPHERE AND TERRESTRIAL AND MARINE ECOSYSTEMS

TRANSVERSAL ACTIONS

.be

SCIENCE FOR A SUSTAINABLE DEVELOPMENT
(SSD)

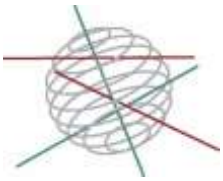

Climate, Antarctica

FINAL REPORT

BIOGEOCHEMICAL CYCLES IN THE SOUTHERN OCEAN: ROLE WITHIN THE EARTH SYSTEM

"BIGSOUTH"

SD/CA/05A

Promotors
F. Dehairs - Vrije Universiteit Brussel (VUB)
J.-L. Tison, F. Fripiat - Université Libre de Bruxelles (ULB)
L. André - (KMMA)
H. Goosse - Université Catholique de Louvain (UCL)
Bruno Delille - Université de Liège (ULg)

Authors
Frank Dehairs, Anne-Julie Cavagna, Arnout Roukaerts, François Fripiat (Vrije Universiteit Brussel)
Jean-Louis Tison, François Fripiat, Gauthier Carnat, Jiayun Zhou, Véronique Schoemann, Jeroen de Jong (Université Libre de Bruxelles)
Luc André (Musée Royal de l'Afrique Centrale)
Hugues Goosse, Sébastien Moreau, Martin Vancoppenolle (Université catholique de Louvain)
Bruno Delille, Bernard Heinesch, Marie Kotovitch, Fanny Van der Linden, Willy Champenois (Université de Liège)
Julien Le Sommer (Laboratoire de Glaciologie et Géophysique de l'Environnement)

Published in 2017 by the Belgian Science Policy
Avenue Louise 231
Louizalaan 231
B-1050 Brussels
Belgium
Tel: +32 (0)2 238 34 11 – Fax: +32 (0)2 230 59 12
http://www.belspo.be

Contact person: Maaike Vancauwenberghe
+32 (0)2 238 36 78

Auteurs. ***Biogeochemical cycles in the Southern Ocean: Role within the Earth system (BIGSOUTH)***. Final Report. Brussels: Belgian Science Policy 2017 – 184 p. (Research Programme Science for a Sustainable Development)

TABLE OF CONTENT

CONTACT INFORMATION

COORDINATOR

- **Dehairs, Frank (Partner 1)**
  Vrije Universiteit Brussel

  Analytical, Environmental and Geo-Chemistry Dept and Earth System Sciences Research Group

  Tel : +3226291265 – Fax : +3226291811 – Email : fdehairs@vub.ac.be

OTHER PARTNERS

- **Tison, Jean-Louis – Fripiat, François (Partner 2)**
  Université Libre de Bruxelles – Laboratoire de Glaciologie

  Tel : +3226502225 – Fax : +326502226 – Email : jtison@ulb.ac.be

- **André, Luc (Partner 3)**
  Musée Royal de l'Afrique Centrale

  Tel : +3227695459 – Fax : +3227695432 – Email : lucandre@africamuseum.be

- **Goosse, Hugues – Moreau, Sébastien – Vancoppenolle, Martin (Partner 4)**
  Université catholique de Louvain

  Tel : +3210473298 – Fax : +3210474722 – Email : hugues.goosse@uclouvain.be

- **Delille, Bruno (Partner 5)**
  Université de Liège – Unité d'Océanographie Chimique

  Tel : +3243663187 – Fax : +3243663367 – Email : Bruno.Delille@ulg.ac.be

- **Schoemann, Véronique (International Partner – Partner 6)**
  Stichting Koninklijk Nederlands Instituut voor Zeeonderzoek (NIOZ)

  Email: via jtison@ulb.ac.be

- **Le Sommer, Julien (International Partner – Partner 7)**
  Laboratoire de Glaciologie et Géophysique de l'Environnement

  Email: julien.lesommer@univ-grenoble-alpes.fr

AUTHORS

- **Dehairs**, Frank – **Cavagna**, Anne-Julie – **Roukaerts**, Arnout – **Fripiat**, François (Vrije Universiteit Brussel)
- **Tison**, Jean-Louis – **Fripiat**, François – **Carnat**, Gauthier – **Zhou**, Jiayun – **Schoemann**, Véronique – **de Jong** Jeroen (Université Libre de Bruxelles)
- **André**, Luc (Musée Royal de l'Afrique Centrale)
- **Goosse**, Hugues – **Moreau**, Sébastien – **Vancoppenolle**, Martin (Université catholique de Louvain)
- **Delille**, Bruno – **Heinesch**, Bernard – **Kotovitch**, Marie – **Van der Linden**, Fanny – **Champenois** Willy (Université de Liège)
- **Le Sommer**, Julien (Laboratoire de Glaciologie et Géophysique de l'Environnement)

PROJECT WEBSITES

- http://www.mio.univ-amu.fr/~queguiner/KEOPS_2.html
- http://yrosiae.blogspot.be/?view=classic
- http://awecs.blogspot.be/2013
- http://seaice.acecrc.org.au/sipex2012/

1. SUMMARY

1.1. CONTEXT

The oceanic system in general and the Southern Ocean in particular, play a crucial role in mediating the carbon dioxide content in the atmosphere and therefore in mitigating global warming. Oceanic biological activity is part of the processes which act on the uptake of CO_2 by the ocean via (1) the process of carbon fixation and export of organic carbon to the deep ocean, (2) controlling the preformed nutrient concentration (i.e., nutrients unused by the phytoplankton and leaving the surface ocean via subduction, downwelling) in the ocean's interior, and (3) controlling the alkalinity of the deep waters. Since these processes are likely to be quite different between the open ocean and sea ice covered systems, differences between both systems need to be properly understood and relative importance of both environments assessed, in order to evaluate the role of the whole Southern Ocean as a climate driver.

Any presence of large stocks of preformed nutrients reflects a missed opportunity for the ocean to sequester CO_2. The Southern Ocean represents the largest reservoir of such unused nutrients and therefore carries most of the potential for increasing the efficiency of the global biological pump. Nutrient-rich and CO_2-charged deep ocean waters ascend mainly in the Southern Ocean, into the surface layer. These waters are returned to the mid-depth ocean before the available pools of nitrates and phosphates are fully used by phytoplankton for carbon fixation despite a close to complete utilization of the silicic acid nutrient by diatoms (Sarmiento et al., 2004). Several factors may a variation in the efficiency of the S.O. biological pump: (1) a change in the exchange of Southern Ocean surface waters with the deep and mesopelagic ocean (Francois et al., 1997; Toggweiler et al., 2006; Sigman et al., 2010); (2) a change in the extent of macro-nutrient consumption by S.O. phytoplankton (Francois et al., 1997; De La Rocha et al., 1998); (3) a change in the Si:N nutrient consumption ratio, subsequently affecting the low latitude productivity (Brzezinski et al., 2002; Beucher et al., 2007; Matsumoto and Sarmiento, 2008); (4) a change in sea ice cover, affecting the ability of CO_2 to escape form supersaturated Southern Ocean surface waters (Stephens and Keeling, 2000). In addition, the mineralization length scale in the mesopelagic ocean is of importance for setting the ocean's carbon sequestration efficiency, as has been clearly recognized recently (e.g., Kwon et al., 2009). For instance, a global deepening of the remineralisation depth by some 25 m could draw down between 10 and 27 ppm of atmospheric CO_2. Until recently, however, research on the biological pump was primarily focused on the surface mixed layer and the deep ocean (Boyd and Trull, 2007). Since intensity, depth and seasonality of mesopelagic mineralization differs significantly between different functional systems (including HNLC open ocean; margin areas; sea ice covered areas) of the Southern Ocean (e.g., Cardinal et al. 2005), it is crucial that the different contributions of these systems to the overall C sequestration capacity in the S.O. be assessed.

While the impact of sea ice on climate through the damping of heat and radiation exchange is relatively well known (Holland et al., 2006), its impact on ocean biogeochemistry could be significant as well. However, at this stage, this has been little studied at large scales. Sea ice affects light distribution in the surface ocean. In addition, sea ice affects atmosphere-ocean gas exchange. Sea ice is not totally impervious, due to open water areas within the pack and to brine inclusions, which connectivity affects permeability of the ice cover. Recent work (e.g. Zemmelink et al., 2006, Delille, 2006, Heinesch et al., 2009, Tison et al., 2010) has shown that more than acting as a passive membrane for gas exchanges, sea ice actually actively contributes to potentially significant fluxes of climate gases such as CO_2 (net sink) and dimethylsulfide (DMS, net source) to the ocean and the atmosphere. Moreover, primary production in, and export production from, sea ice could have a large-scale contribution, though the latter is presently of highly uncertain magnitude. Finally, the melting of sea ice releases organic components, nutrients and trace metals in the surface ocean, which has a potentially important impact on primary production in marginal ice zones of the Southern Ocean (e.g., Lancelot et al., 2009).

1.2. OBJECTIVES

The major aim of BIGSOUTH was to achieve a detailed understanding of the processes controlling functioning and strength of the oceanic biological pump for representative key areas of the S.O., including open ocean and sea ice covered areas, in order to upgrade present day assessments of the carbon sequestration capacity and nutrient cycling in the Southern Ocean and possible impacts on the global ocean. Therefore, we applied a unique combination of stable isotope (natural and spiked isotopic abundances), geochemical tracers, trace element and modeling tools to study the relevant biogeochemical processes and control factors (including Fe) acting on the fluxes of carbon and the two major macronutrients N and Si in the open and seasonally sea ice covered water column.

The main focus of the project wa directed to different contrasting functional entities of the Southern Ocean where diatoms are a key phytoplankton group including the high nutrient low chlorophyll (HNLC) Antarctic circumpolar waters, the sea ice zone and areas subject to natural Fe fertilization such as shelf and margin areas. This observational work was essential for the development and validation of a large-scale bio-physical model of the ocean, the sea ice and of key components of biogeochemical cycles (phytoplankton, nutrients, inorganic and organic carbon). Such a tool is essential to study the role of the Southern Ocean and its sea ice cover in the global ocean carbon cycle.

1.3. GENERAL CONCLUSIONS

Several main field surveys have been carried out since the start of the project. The KEOPS 2 expedition (Kerguelen Ocean and Plateau compared Study) took place from October 6 to November 30, 2011 on board R/V Marion Dufresne, and aimed at understanding the impact of natural iron fertilization from plateau sediments on the efficacy of the biological pump in the vicinity of Kerguelen Island (Indian sector of the Southern Ocean). BIGSOUTH participants focused in particular on the significance of

(1) ammonium vs nitrate uptake under conditions of nitrate repleteness (NO_3^- mostly > 20 µM) and the impact of Fe on this process; (2) euphotic layer nitrification and its impact on new production and export, and the possible role of Fe and (3) the export flux of particles and carbon and the remineralisation of exported matter in the subsurface mesopelagic waters. C, N uptake processes and nitrification were studied via isotope enrichment. Carbon export from the upper mixed layer (biopump) was assessed via the ^{234}Th-deficit method while remineralisation of sinking material in the subsurface, mesopelagic waters was estimated from ^{234}Th excess and the mesopelagic build-up of the biogenic particulate Ba stock. In order to evaluate short term and integrated effects of nitrate uptake, remineralisation – nitrification and spatial variability, possibly induced by varying availability of Fe in the region, on nitrate distribution, we analysed its natural N, O isotopic composition. Nitrate isotopic composition results are unexpected and indicate that a large nitrification rate must persist in the surface mixed layer.

During SIPEX 2 (Sea Ice Physics and Ecosystem eXperiment; Oct.-Nov. 2012; Australian sector; RV Aurora Australis) the focus was on within sea ice biogeochemical processes in an early season situation. We developed an isotope enrichment methodology to assess primary production, ammonium and nitrate uptake, in-situ within sea ice environments.

During YROSIAE leg 1 (October 10 to December 24, 2011), we initiated a one year survey of air-sea ice-ocean fluxes of carbon, nutrients, trace metal and climate gases together with sea ice biogeochemistry in McMurdo Sound in collaboration with Tim Haskell and Antarctica New Zealand. The YROSIAE study lasted till end of 2012. This study involved the set-up of a meteorological observation tower and energy supply devices on Cape Evans shore. The tower was equipped for measurement of air-ice CO_2 fluxes by eddy-correlation and DMS fluxes using the gradient flux method. Two dust collecting towers were also set up to provide a temporal record of a full suite of trace metal and dust measurements at different levels above the ground. Three main labs (cold lab, wet lab and trace metal lab) were set up in dedicated containers at Scott Base. We also carried out a survey of three process stations with the combined objectives of testing the various physical and biogeochemical protocols and providing a reference spring-summer sequence of data acquisition that will be compared to next year's measurements (inter-annual variability). The structure of first-year landfast sea ice at Cape Evans was characterised by typical "calm thermodynamic conditions" controlled by columnar ice down to 85 cm, with a very limited surface frazil layer. Although located in a bay partly protecting the sites from super cooled water inputs originating from the McMurdo Ice Shelf, the ice cover showed a transition to platelet ice, below 85 cm and down to the bottom. Salinities between 4 and 7 were typical of first year sea ice in the Antarctic, but showed a peculiar "break" at about 80 cm, suggesting that there might have been a change in seawater source in the middle of the winter. This hiatus actually corresponded to an accumulation of platelet ice in the ice cover. Besides the expected maximum of DMSP at the bottom of the sea ice layer, where the algal community was clearly visible, another internal maximum was visible between 80 and

100 cm, i.e. at the transition to platelet ice. This usually corresponds to the month of July when light input is quite limited, raising the question of the origin of this internal peak. We also observed that DMSP is not negligible in early winter, and actually increases steadily in the top 60 cm. Finally, the DMSP maximum at 80 cm appears to increase steadily over time suggesting active production. DMS shows a flat profile in the top 50 cm (as expected from the permeability conditions) and increases in the lower half of the ice cover, somewhat mimicking the variability of the DMSP profiles. We observed a general DMS loss at the third station, both at the ice water interface and internally. This internal loss of DMS corresponds to an increase in the concentration of DMS in the atmosphere suggesting that the ice actively releases DMS to the atmosphere during warming. Eddy correlation measurements of CO_2 fluxes reveal a transition of summer air-ice CO_2 fluxes from a source to a sink for atmospheric CO_2. This year-round landfast sea ice survey also provided us with the first opportunity ever to monitor in-situ N_2O concentration in sea ice brine from sackholes. Results demonstrate a clear synergy between a strong increase of N_2O concentrations and CO_2 concentrations during the Winter -Spring transition, supporting active remineralization processes within the sea ice. These concentration peaks can lead to minimal estimates (because bubble release is not assessed here) of ice-air N_2O fluxes of 4 µmol N_2O m^{-2} during spring. Both nitrification and denitrification within sea ice can be responsible for these enhanced N_2O concentrations, and ongoing work is looking at synergies with N-isotopes measurements (NO_3^-, NO_2^-, NH_4^+, DON, PN) to decipher the potential relative contribution of those genetic processes. Finally, samples are now processed in the home laboratories to obtain time series of high resolution gas concentration profiles (O_2, N_2, Ar, CH_4, CO_2) to document primary production, gas production and gas transfer across the sea ice and compare to measured fluxes at the air and ocean interfaces along the season.

The purpose of this work is to develop an explicit representation of gas exchange into a biophysical sea ice model. Between 2012 and 2015, progress was made in terms of one-dimensional modeling of gas dynamics (using argon) and sea ice biogeochemistry (oxygen, O_2, and carbon dioxide, CO_2). In terms of argon dynamics, gas bubble nucleation and rise were major physical processes to represent argon dynamics within sea ice. In addition, modelling results of O_2 dynamics in sea ice seem to validate primary production modelling in sea ice. Modelling results also indicate that ice-atmosphere CO_2 fluxes, primary production and $CaCO_3$ precipitation and dissolution play a major role in CO_2 dynamics within sea ice, but a rather secondary role in terms of a DIC budget. Furthermore, recent observational and modelling evidences point towards a major role of gas bubbles in transporting gases from the under ice water to the atmosphere during ice growth. In perspective, the modelling of nutrients dynamics, including remineralization as observed during the YROSIAE mission, should allow a better determination of primary production and carbon dynamics within sea ice. More modelling studies are needed to better understand and constrain the processes driving the ice-atmosphere CO_2 fluxes, e.g., gas storage by snow, brine wicking, surface ice communities. In addition, preliminary results of sea ice carbon dynamics in a global Earth system model indicate that sea

ice plays a significant role in the carbon cycle of polar oceans, regionally. Further studies are necessary to assess its significance on a global scale.

To better understand how the Antarctic sea ice physical environment affects the seasonal dynamics of biogeochemical cycles, we participated in the 2013 AWECS winter cruise to the Weddell Sea. The applied strategy consisted in studying the variability of sea ice and snow properties on small-regional scales using a multiple platform approach that includes ice coring surveys and instrument deployment on sea ice in an attempt to integrate it into a coherent model for winter sea ice biogeochemical dynamics in the whole of the Weddell Sea. The results document an extremely poorly known time window of the sea ice seasonal cycle in the Antarctic and reveal a much more dynamical winter Antarctic sea ice than was previously thought. The combination of high air temperature fluctuations with heavy snow falls, due to the regular intrusion of cyclonic events well inside the Weddell Sea (down to very close to the coast) sets up favourable conditions for cyclic permeable sea ice sustaining unexpected significant gas exchange with the atmosphere and the ocean and active winter primary production, despite the low amount of light available. Comparison with the rare previous winter expeditions in the Weddell Sea might suggest this is a recent trend associated to our warming climate. This work also entails the investigation of functional relationships between the physical and biogeochemical properties of sea ice and sea ice microbes ranging from viruses to protozoans.

Finally, environmentally controlled sea ice growth and decay experiments at the HSVA facilities in the framework of the INTERICE V EU Infrastructures Project, have allowed us to run process studies focusing on the carbon cycle in sea ice. We have evidenced the tight relationship between ice pCO_2 and fluxes at the ice-air interface during the growth-decay cycle, and proposed values for the exchange coefficient, combining observations and modelling. We have also demonstrated that the observed contrast in ice pCO_2 between the Arctic and the Antarctic sea ice likely resides in their contrasted DOC content available for bacterial respiration. This has allowed validation of the modelling efforts discussed above.

1.4. CONTRIBUTION OF THE PROJECT TO SSD

The BIGSOUTH scientific results contribute to clarifying our insights into fundamental biogeochemical processes ongoing in the open and the sea ice covered Southern Ocean and which define the sink/source strength regarding the exchange of greenhouse gases between ocean and atmosphere and set the carbon sequestration efficiency of the Southern Ocean.

1.5. KEYWORDS

Biological pump - Carbon export flux – Natural Fe fertilization – Sea ice algal productivity – Sea ice organic, inorganic carbon processing – Sea ice biogeochemical modelling – Large scale modeling - Southern Ocean biogeochemistry

2. INTRODUCTION

The BIGSOUTH network focused on the processes controlling the functioning and strength of the oceanic biological carbon pump in representative key areas of the Southern Ocean. To that purpose we applied a unique combination of stable isotope (natural and spiked isotopic abundances), geochemical tracers, trace element and modeling tools to study the relevant biogeochemical processes and control factors (including Fe) acting on the fluxes of carbon.

The main focus of the work was directed to different contrasting functional entities of the Southern Ocean where diatoms are a key phytoplankton group. These functional entities include the high nutrient low chlorophyll (HNLC) Antarctic circumpolar waters, the sea ice zone and areas subject to natural iron fertilization such as shelf and margin areas. In order to obtain a detailed insight in the biogeochemical processes at work in the water column and in the sea ice which control source-sink strengths for climate sensitive gases and essential nutrients, and to evaluate the variability of the biological pump efficiency between different Southern Ocean functional systems, we studied the following three main topics:

1. Impact of surface ocean processes on export and fate of biogenic compounds in the ocean's interior

Here we focused on understanding how the essential Southern Ocean functional systems, including HNLC areas, margin areas naturally fertilized with Fe and sea ice covered areas, differ regarding (1) The primary production system and its potential for carbon export tlo the deep ocean; (2) The export flux of organic carbon from the surface waters and potential drivers; (3) The heterotrophic remineralisation of exported organic carbon in the deeper water column.

2. The physical-biological controls of sea ice on biogeochemical fluxes between atmosphere and ocean

Main questions that were addressed are:

- What are the main processes shaping the seasonal cycle of sea ice biogeochemistry and gas exchanges? How to optimally represent them in climate models?
- Can we better constrain sea ice gross and net primary production, and export using a multi-proxy approach (O_2:Ar, O_2:N_2, δ^{17},$^{18}O_{air}$, TEI and tracers incubations)?
- What is the seasonal evolution of the air – sea ice - ocean CO_2 flux budget associated with ice growth and decay? Do snow processes and $CaCO_3$ precipitation / dissolution play a significant role? How much CO_2 is exchanged with the underlying water? Are carbonate system equilibrium constants in brines (high salinity, low temperature) different from those in sea water?
- What is the balance between key metabolic and physical controls on the DMSP-DMS-DMSO dynamics in the sea ice and the net DMS flux to the atmosphere?

- Is there a link between the observed episodes of sustained production of DMS in sea ice and the sulfur chemistry in the lower atmosphere?
- Does Antarctic sea ice host anoxic micro-environments that promote formation of the other greenhouse biogases CH_4 and N_2O? Can we use $\delta^{15}N$ to trace denitrification processes?
- Can sea ice act as a significant source or sink of trace metals and could this drive subsequent primary production in the ocean? What controls iron bioavailability to the sea ice microbial community?
- How well do short-term isotope dilution experiments (^{13}C, ^{15}N, ^{30}Si) compare with seasonal mass and isotopic balances and how well can we constrain the sea ice – water Si and N fluxes combining both approaches?
- The "silicic acid leakage" and "Antarctic stratification" hypotheses explaining lower atmospheric pCO_2 during ice ages are largely deduced from $\delta^{30}Si$ and $\delta^{15}N$ in Southern Ocean sediments. These assumptions are based on open water studies. Are these assumptions still valid if we take into account the sea ice component?
- Does landfast sea ice biogeochemistry behave differently from that of pack-ice? Does the presence of (very productive) platelet ice sustain larger sinks?

3. Sea ice Biogeochemical model and integration in NEMO-LIM-PISCES

Here we assessed the contribution of the sea ice system to the Southern Ocean biogeochemical cycles at the large-scale, using a coupled physical and biogeochemical sea ice-ocean model.

Main questions that were addressed are:

What are the mechanisms that shape the seasonal cycle of iron, pCO_2, and carbonates in sea ice? How to represent them in a model?

What is the contribution of sea ice to net community and export productions over the whole Southern Ocean? What are the associated uncertainties?

What is the effect of ice-ocean exchanges of organic matter, nutrients and trace metals on primary production and the carbon cycle?

3. METHODOLOGY AND RESULTS

3.1. TOPIC 1: IMPACT OF SURFACE OCEAN PROCESSES ON EXPORT AND FATE OF BIOGENIC COMPOUNDS IN THE OCEAN'S INTERIOR

3.1.1. Carbon processing in the naturally Fe fertilized Southern Ocean: the KEOPS 2 expedition (Oct.-Nov. 2011)

General overview of the KEOPS 2 expedition

The KEOPS 2 expedition (Kerguelen Ocean and Plateau compared Study) took place from October 6 to November 30 on board R/V Marion Dufresne, and aimed at understanding the impact of natural iron fertilization from plateau sediments on the biogeochemical cycles in the vicinity of Kerguelen Island (Indian sector of the Southern Ocean). The Kerguelen Plateau area and adjacent open waters on the lee-ward side of the Island (Figure 1) were studied using a 'C-sequestration' toolbox developed to assess Primary Production, POC export from upper mixed layer and POC remineralization in the mesopelagic water column, thereby providing information on the C-sequestration efficiency of the biopump.

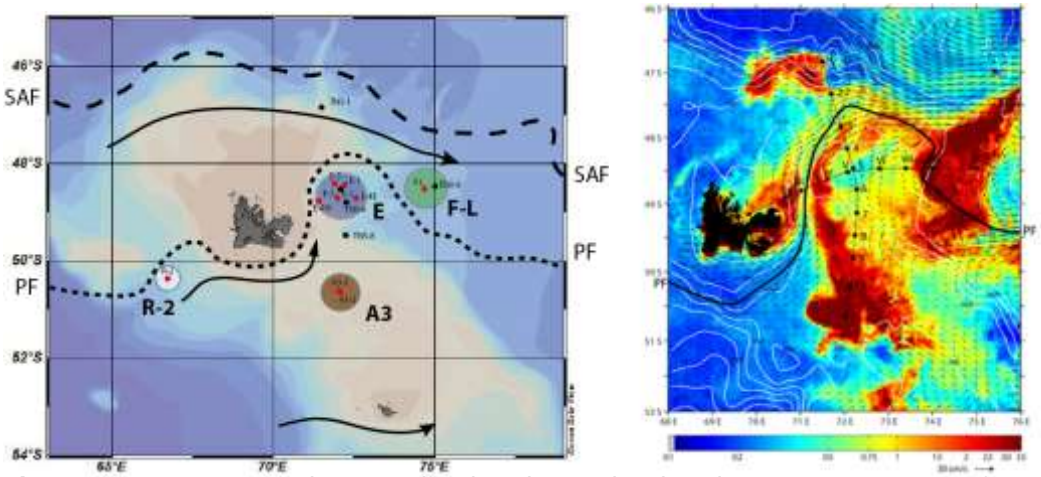

Figure 1: KEOPS 2 study area showing the station locations. R-2 = HNLC reference station; A3 = Plateau station; E = stations in the Polar Front meander; F-L = station north of Polar Front. The dotted line represents the position of the Polar Front. The right graph is a satellite view of surface chl-a with surface velocity fields super imposed (arrows) and corresponding to the last week of the KEOPS 2 cruise (Courtesy F. d'Ovidio and Y.-H. Park).

This task aimed at assessing the impact of environmental conditions (light, temperature, stratification, etc.) and availability of macro and micro-nutrient (Fe) on primary production and N-uptake regime. We focused in particular on the significance of (1) ammonium vs nitrate uptake under conditions of nitrate repleteness (NO3 mostly > 20 µM) and the impact of Fe on this process; (2) euphotic layer nitrification and its impact on new production and export, and the possible role of Fe and (3) the export flux of particles and carbon and the remineralization of exported matter in the subsurface mesopelagic waters. C, N uptake processes and nitrification were studied via isotope enrichment experiments. Carbon export from the upper mixed layer (biopump) was assessed via the ^{234}Th-deficit method while remineralization of

sinking material in the subsurface, mesopelagic waters was estimated from ^{234}Th excess and the mesopelagic build-up of the biogenic particulate Ba inventory. In order to investigate whether processes other than nitrate uptake by phytoplankton are significant and show spatial variability possibly induced by varying availability of Fe in the region, we also analyzed the natural N, O isotopic composition of nitrate.

C-assimilation, nitrate and ammonium uptake rate measurement

Surface waters were sampled at 7 to 8 depths corresponding to 75%, 45%, 25%, 16%, 4%, 1%, 0.3%, 0.01% of the surface photosynthetically active radiation (PAR), using Niskin bottles mounted on a rosette fitted with a PAR sensor. For each light level, two acid-cleaned 1L polycarbonate incubation bottles were filled with seawater. The two bottles were spiked with 200 µmol L^{-1} of ^{13}C-HCO_3^- (^{13}C, 99 atom %), corresponding to a tracer addition equivalent of ≈ 10% of the surface seawater DIC concentration (≈ 2mM), and providing a duplicate of net primary production. One of the bottles was spiked with ^{15}N-NO_3^- and the other with ^{15}N-NH_4^+ (^{15}N, 98 atom %). The amount of spike added was calculated taking into account the original nitrate and ammonium concentrations in order to achieve concentration increments < 10%. Nitrate was measured by continuous flow analysis (Aminot and Kérouel, 2007) and ammonium via fluorimetry (Holmes et al., 1999).

Once spiked, one bottle of each pair was immediately filtered to assess initial conditions (t_0), while the other bottles were transferred to on-deck incubators wrapped in neutral density screens simulating the photometric depths and cooled with circulating surface seawater. Incubation experiments were stopped after 24h (t_f). The relatively long incubation time of 24 hours implies that we probably underestimated uptake rates in case of (1) release of ^{15}N and ^{13}C to the dissolved organic pool during the course of the experiment (Bronk et al., 1994; Laws et al., 2002) and (2) ammonification, which would result in diluting the ^{15}N-spiked ammonium pool with ^{14}N. By applying a steady state model assuming that uptake and regeneration rates are equal for each nitrogen pool the factor by which ammonium uptake rates are underestimated is 1.17 ± 0.23 (1 SD; minimum = 1.00; maximum = 2.36). Also, the uncorrected and corrected *f*-ratios (i.e., NO_3^- uptake/$\sum NO_3^-$ and NH_4^+ uptake; Dugdale and Goering, 1967) are close to 1 (0.96 +/- 0.01; R^2 = 0.99, p value < 0.001) indicating there was no significant effect of any enriched isotope release on *f*-ratio. We therefore only considered uncorrected ammonium uptake rates.

Both, at the initial (i.e., just after spiking) and final incubation times, nitrate and ammonium concentrations were measured and samples taken for ^{15}N-NO_3^- analysis. The remaining seawater was filtered on pre-combusted (450°C) glass fiber filters (Sartorius, MGF, nominal porosity 0.7 µm, 25 mm diameter). Filters were placed in pre-combusted scintillation vials, dried at 50°C and stored in the dark at room temperature until further analysis at the home based laboratory.

Particulate organic nitrogen (PON) and particulate organic carbon (POC) concentrations along with their ^{15}N and ^{13}C abundances (atom ^{13}C and ^{15}N %) were

analysed via an elemental analyser - isotope ratio mass spectrometer (EA-IRMS) using the method described in Savoye et al. (2004).

Atom ^{15}N % for nitrate at initial and final time was measured using the denitrifier method (Sigman et al., 2001; see details further below when discussing natural N, O isotopic composition of nitrate).

C-assimilation and ammonium uptake rates (ρNH_4^+) were calculated from the equations of Dugdale and Goering (1967) where Atom% $^{13}C_{DIC\text{-}toriginal}$ and Atom%$^{15}N_{NH4\text{-}toriginal}$ were calculated and the other parameters were measured. For C-fixation this equation writes (see also Elskens et al., 2005).

$$V = \frac{(atom\%^{13}C_{POCtf})}{time \cdot (atom\%^{13}C_{DIC\,tinit})} \quad (1)$$

$$\mathrm{NPP} = \left[\mathrm{POC_{tf}}\right] \cdot \mathrm{V} \qquad (2)$$

Where V is the specific C assimilation rate (in d^{-1}), NPP net primary production (in µmol C L^{-1} d^{-1}), atom % ^{13}C the measured abundances minus the natural abundances, and t_f and t_{init} refer to the final and initial time of incubation, respectively. Except for nitrate for which initial abundances were measured, the initial abundances for both DIC and NH_4^+ were calculated by taking into account the spike addition and isotopic abundance.

The nitrate uptake rate (ρNO_3^-) was first corrected for any isotope dilution effect during incubation and then calculated as follows:

$$V\,NO_3^- = \frac{atom\%\ ^{15}N_{PONtf}}{time \,.\sqrt{atom\%\ ^{15}NO_{3ti}^- \,.\, atom\%\ ^{15}NO_{3tf}^-}} \qquad (3)$$

$$\rho NO_3^- = \left[PON_{tf}\right].VNO_3^- \qquad (4)$$

The nitrification (RNO_3^-) rate was assessed using the integrated rate equation of the Blackburn model (Blackburn, 1979; Elskens et al. 2005):

$$RNO_3^- = \frac{\ln\left(atom\%\ ^{15}NO_{3tinit}^- / atom\%\ ^{15}NO_{3tf}^-\right)\left[NO_{3tf}^- - NO_{3tinit}^-\right]}{time\ \left(\left[NO_{3tf}^-\right] / \left[NO_{3tinit}^-\right]\right)} \qquad (5)$$

The uncertainty on uptake (NPP, ρNH_4 and ρNO_3) and nitrification (RNO_3) rates were assessed using Monte-Carlo simulations assuming normal distributions for all variables.

The modelled nitrification rates were screened for consistency between observed evolutions of nitrate concentrations over the duration of the incubation experiment and measured nitrate uptake rates. The difference between nitrate uptake and nitrification should be compatible with the change in nitrate concentration over the duration of the incubation experiment, taking into account a 10% precision (relative standard deviation SD) on rates and concentrations measurements. When the rates given by the model were incompatible with temporal evolution of nitrate concentration, nitrification experiments were considered as being flawed and were left out of the dataset.

The significance of surface ocean nitrification in the Kerguelen Plateau area

The N-nutrient (nitrate, nitrite, ammonium) distributions in the upper 500m at the different sites were C, N assimilation measurements were conducted reflect the extent of nitrate uptake and the effects of mineralisation-ammonification and nitrification (Figure 2). Profiles of C uptake, N-uptake and nitrification rates are shown in Figure 3, while integrated N-uptake rates and *f*-ratio values are shown in Table 1. The latter lie in the upper range of values reported for the Southern Ocean and are indicative of a nearly complete NO_3^--based primary production (Sambrotto and Mace, 2000; Savoye et al., 2004, Mulholland and Lomas, 2008).

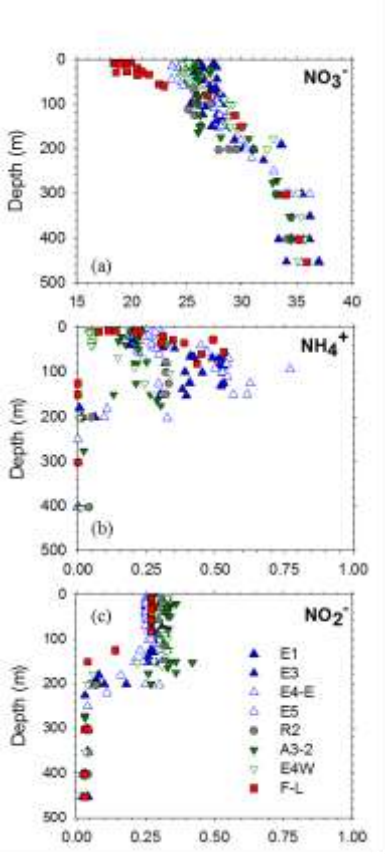

Figure 2: Vertical profiles of NO_3^-, NO_2^-, NH_4^+ concentrations at the different sites investigated for C, N assimilation (Cavagna et al., 2015).

The *f*-ratio increases with increasing N-uptake rate (combined NO_3^- + NH_4^+ uptake) from ~0.3 in the less productive HNLC reference station to ~0.8 in the productive areas over the Kerguelen Plateau and north of the Polar Front (Figure 4a; Table 1).

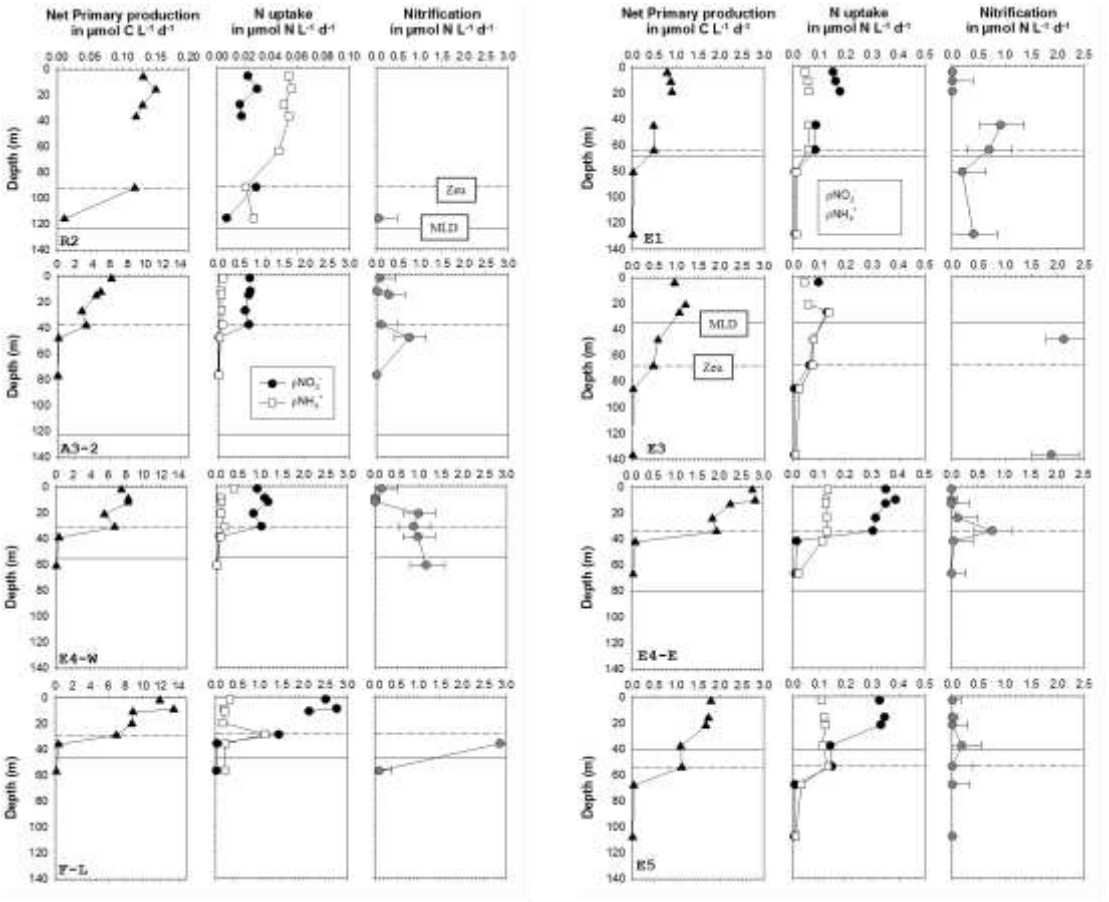

Figure 3: Vertical distribution of Net Primary Production NPP (left column), N-uptake (middle column), and nitrification (right column; error bar corresponds to the 5 and 95% percentiles) rates between stations (rows). Note that there is a change of scale between reference R site, high productivity sites (A3-2, F-L, E4W) and meander sites (E1, E3, E4E, E5). The dashed line represents the euphotic layer depth (Zeu = 1% PAR attenuation) and the full line represents the mixed layer depth.

Below the euphotic layer, ammonium is preferentially assimilated over nitrate, with *f*-ratio ranging between 0.1 and 0.5 (not shown). Assimilation of nitrate is more energetically demanding than ammonium and should be more dependent on light. At the end of summer the *f*-ratio over the Plateau decreases rapidly, from 0.6 to 0.2, indicating that the system evolved from a nitrate-based to an ammonium-based primary production (Mosseri et al., 2008; P. Raimbault, KEOPS 1 database).

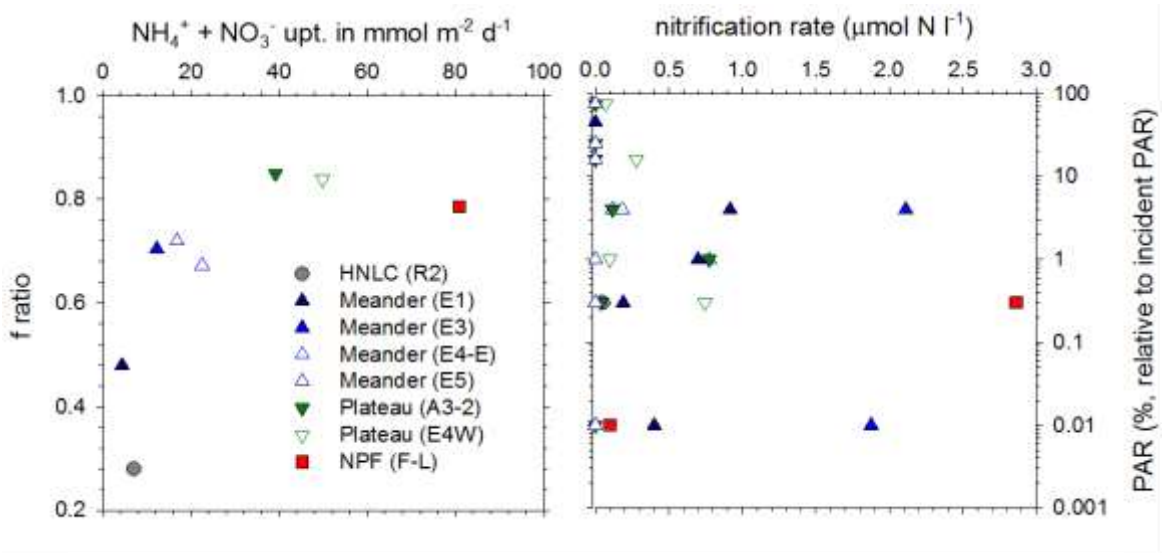

Figure 4: Relationship between mixed layer depth integrated N-uptake (NH_4^+ + NO_3^-) and *f*-ratio (a), and between PAR (%) and nitrification rates (b).

	date	POC	NPP	NH_4^+ upt.	NO_3^- upt.	NO_3^- + NH_4^+ upt.	nitr.*	f ratio	corr. f ratio
		mmol m^{-2}	mmol m^{-2} d^{-1}	mmol m^{-2} d^{-1}	mmol m^{-2} d^{-1}	mmol m^{-2} d^{-1}	mmol m^{-2} d^{-1}	no Unit	no Unit
HNLC reference station									
RK2	26 Oct. 2011	**240,3**	**13,2**	**5,1**	**2,0**	**7,0**		**0,3**	
Meander station									
E1	30 Oct. 2011	436,2	43,5	3,6	8,6	12,2	27,3	0,7	0.0**
E3	4 Nov. 2011	325,8	34,5	2,3	2,1	4,3		0,5	
E4E	14 Nov. 2011	891,0	86,9	7,4	15,2	22,5	8,8	0,7	0,3
E5	19 Nov. 2011	465,4	53,4	4,7	12,1	16,8	2,0	0,7	0,6
average		**529,6**	**54,6**	**4,5**	**9,5**	**14,0**	**12,7**	**0,6**	**0,3**
sd		**248,3**	**22,9**	**2,2**	**5,6**	**7,7**	**13,1**	**0,1**	**0,3**
Kerguelen Plateau and margin									
E4W	12 Nov. 2011	1276,8	252,8	8,0	41,8	49,8	37,7	0,8	0,1
A3-2	17 Nov. 2011	2146,0	179,9	5,9	33,3	39,2	18,1	0,8	0,4
average		**1711,4**	**216,3**	**7,0**	**37,5**	**44,5**	**27,9**	**0,8**	**0,2**
sd		**614,7**	**51,5**	**1,5**	**6,0**	**7,5**	**13,8**	**0,0**	**0,2**
Polar Front									
NPF	7 Nov. 2011	**1565,9**	**314,6**	**17,4**	**63,5**	**80,8**		**0,8**	

*Only 5 stations had a sufficient depth resolution to allow an integration to be made

**As the f ratio is giving the proportion of primary production sustained by new nutrients. If 100% of the nutrient are considerated as regenerated nutrients

Table 1: Mixed layer integrated values for particulate organic C (POC), net primary production (NPP), ammonium uptake (NH_4^+ upt.), nitrate uptake (NO_3^- upt.), ammonium + nitrate uptake (NH_4^+ + NO_3^- upt.), nitrification (Nitr.), f-ratio, and corrected f-ratio by taking into account the contribution of nitrification (Yool et al., 2007).

Nitrification rates are high (up to 3 µmol L^{-1} d^{-1}, with ~90% of the cases <1 µmol L^{-1} d^{-1}) at low light intensities, and insignificant (below our detection limit) at high light intensities (Figures 3 and 4). Such rates are well above the maximum rates reported for the open ocean (up to 0.75 µmol L^{-1} d^{-1}) in the Peru Upwelling (Lipschultz et al., 1991; Ward, 2008), and for the Southern Ocean (< 0.1 µmol L^{-1} d^{-1}; Olson, 1981; Bianchi et al., 1997). The Southern Ocean nitrification data available in the literature pertain to fall and winter, seasons during which primary production and remineralization are expected to be low.

The observed variation of nitrification with depth supports the fact that the process is partly light-inhibited (Figure 3). High nitrification rates are usually reported near the bottom of the euphotic layer where organic matter is still abundant and light is much reduced, allowing the nitrifiers to compete with phytoplankton for the ammonium produced by remineralization (Lipschultz et al., 1991; Ward, 2008). Below the euphotic layer, organic matter degradation and organic matter export lead to ammonium release which is *in fine* nearly-quantitatively converted into nitrate. As the process closing the internal N cycle ($NO_3^- \rightarrow PON \rightarrow NO_3^-$) nitrification likely tracks primary production. The unusual high rates of nitrification across the study area likely result from the particularly high primary production rates which are in the upper range for oceanic systems.

The particularity of our study area is that a significant fraction of the mixed layer (except for stations E3 and E5) extends below the euphotic layer (Figure 3). The nitrate produced by nitrification at low-light intensities can thus easily be transported into the euphotic layer to support regenerated primary production there. Such findings have profound consequences on the concept of new production (Dugdale and Goering, 1967; Eppley and Peterson, 1979).

The *f*-ratio expresses the relative importance of nitrate uptake vs. the combined uptake of nitrate and ammonium, whereby it is assumed that all nitrate is provided to the surface waters by vertical advection of deep waters, while ammonium represents the recycled nutrients (Eppley and Peterson, 1979). Under steady state conditions this uptake of nitrate (supposedly fueling New Production) should be balanced by the export of particulate N (and C) to the deep sea, and measuring the flux of nitrate consumed by the phytoplankton would thus reflect the system's potential for N and C export to the deep sea. Any nitrification in surface waters will of course lead to an overestimation of New Production and of the potential N, C export flux. We estimate that mixed layer nitrification in the Kerguelen area decreases *f*-ratio and thus on New Production by 50 to 75%, bringing estimates of New Production in closer agreement with measured rates of export (see below).

<u>Evidence for significant surface nitrification from nitrate isotopic compositions</u>

Despite silicic acid and nitrate uptake ratios being close to 1 over the Kerguelen plateau, the apparent nitrate consumption over the season was observed to be much lower than the silicic acid consumption, implying significant shallow remineralization of N, as evidenced by substantial subsurface ammonium concentrations, reaching up to 2 µM (Mosseri et al., 2008). It is likely that such conditions would also favor a surface ocean development of nitrifying Bacteria and Archaea. Since knowledge about nitrate stable isotope composition is an essential asset to resolve the complex suite of processes that control the oceanic N cycle (Sigman et al., 1999; DiFiore et al., 2006; 2009; Rafter et al., 2013) we analyzed the N and O stable isotope composition of nitrate during the KEOPS 2 expedition (October–November, 2011) to investigate possible imprints of shallow remineralization + nitrification, as well as imprints of enhanced primary production on deep ocean nitrate isotopic composition. This early season KEOPS 2 expedition offered the opportunity to investigate the

seasonal variability of the nitrate isotopic composition, by comparing results with those obtained earlier by others during the late summer KEOPS 1 expedition to the same area (Trull et al., 2008).

The water column was sampled per CTD rosette equipped with 12 L Niskin bottles. The samples for nitrate isotopic composition consisted of a sub-fraction (10 ml) of the filtered seawater collected for nutrient analysis (Acrodisc; 0.2 µm porosity) intended for on-board nitrate + nitrite analysis. These subsamples were kept frozen (-20°C) until analysis in the home-based laboratory. The nitrogen and oxygen isotopic composition of nitrate was determined via the bacterial denitrifier method, using *Pseudomonas aureofaciens* bacteria which reduce nitrate to N_2O (Sigman et al., 2001; Casciotti et al., 2002). We aimed at a final homogenous nitrate content of 20 nmol for samples and reference standards alike (see below). The analytical equipment consisted of a custom-build gas bench connected on-line to a set-up for gas conditioning, which involved elimination of volatile organic carbon compounds, CO_2 and cryogenic focusing of N_2O, GC separation of CO_2 traces from N_2O, a Con-Flo unit and IRMS (Thermo Delta V). For final calculations we used the USGS 32, 34, 35 and IAEA N3 international reference standards (Sigman et al., 2001; Böhlke et al., 2003) and the two-point calibration mode as discussed in Paul et al. (2007) and Casciotti et al. (2002). $\delta^{15}N$ values are reported as $[(^{15}N/^{14}N_{sample})/(^{14}N/^{15}N)_{ref}-1]*1000$, referenced to Air N_2 and $\delta^{18}O$ as $[(^{18}O/^{16}O)_{sample}/(^{18}O/^{16}O)_{ref} - 1]*1000$, referenced to VSMOW. Multiple analyses of USGS and IAEA reference solutions indicate average measurement errors for $\delta^{15}N_{NO3}$ and $\delta^{18}O_{NO3}$ analyses were 0.17‰ and 0.38‰, respectively. We also analyzed 35 duplicate samples from successive CTD casts at same depths yielding median values of the standard deviations being 0.05‰ and 0.28‰ for $\delta^{15}N$ and $\delta^{18}O$, respectively.

The method measures the isotopic composition of NO_3^- plus NO_2^-. In the present study the effect of NO_2^- was neglected since overall nitrite concentrations were small, representing on average <0.5% of the nitrate + nitrite pool (see also DiFiore et al., 2009). However, it has been reported that slightly higher nitrite levels reaching 0.8 % of the nitrite + nitrate pool can result in a slight lowering of the $\delta^{15}N$ and $\delta^{18}O$ values by 0.4 and 0.2‰ on average (Rafter et al., 2013). In general such possible effects are not taken into account (DiFiore et al. 2009; Rafter et al., 2013) and were neither here.

We differentiated 3 regions: (1) Plateau stations located south of the Polar Front, above the shallow plateau and the margin and underlying the bloom plume (stations A3-1, TNS08, TEW4, E4W1, A3-2, E4W2); (2) Polar Front Meander stations in the central part of the basin east of Kerguelen where the bloom had not fully developed yet (stations TNS06, E1, TEW5, TEW6, E3, E4E, E5, IODA-REC); (3) Polar Front and north of Polar Front sites (stations TEW7, TEW8, NPF-L). Average nitrate values in the upper 100m of water column remain high throughout the study period with average values of 26.6 ± 1.9; 26.2 ± 0.9 and 23.1 ± 1.3 µM for Plateau, Meander and PF areas, respectively. With increasing depth, nitrate in general increases to reach maximal values around 37 µM at 500m in Upper Circumpolar Deep waters (UCDW). Concentrations decrease slightly in Lower Circumpolar Deep Waters (around 30 µM) and increase again slightly in bottom waters (around 32 µM).

Profiles of $\delta^{15}N_{NO3}$ mirror the ones of nitrate (Figure 5a,b): High values in surface waters (close to 6.4 ‰) which decrease to 4.9‰ in the NO_3^- maximum and increase slightly to 5‰ till about 2500 m. A slight decrease of $\delta^{15}N_{NO3}$ is noticed in Polar Front bottom waters which also show a slight increase in nitrate concentration. Such values are similar to those observed widely for the deep ocean (see Di-Fiore et al., 2009; Sigman et al., 2000; 2009; Rafter et al., 2013). Although $\delta^{18}O_{NO3}$ values are more scattered, it can be clearly seen that they follow a pattern similar to $\delta^{15}N_{NO3}$, with values up to 6‰ in surface waters, which decrease to <2‰ in the 500 to 1000m depth interval but tend to increase again in deep and bottom waters and stay close to

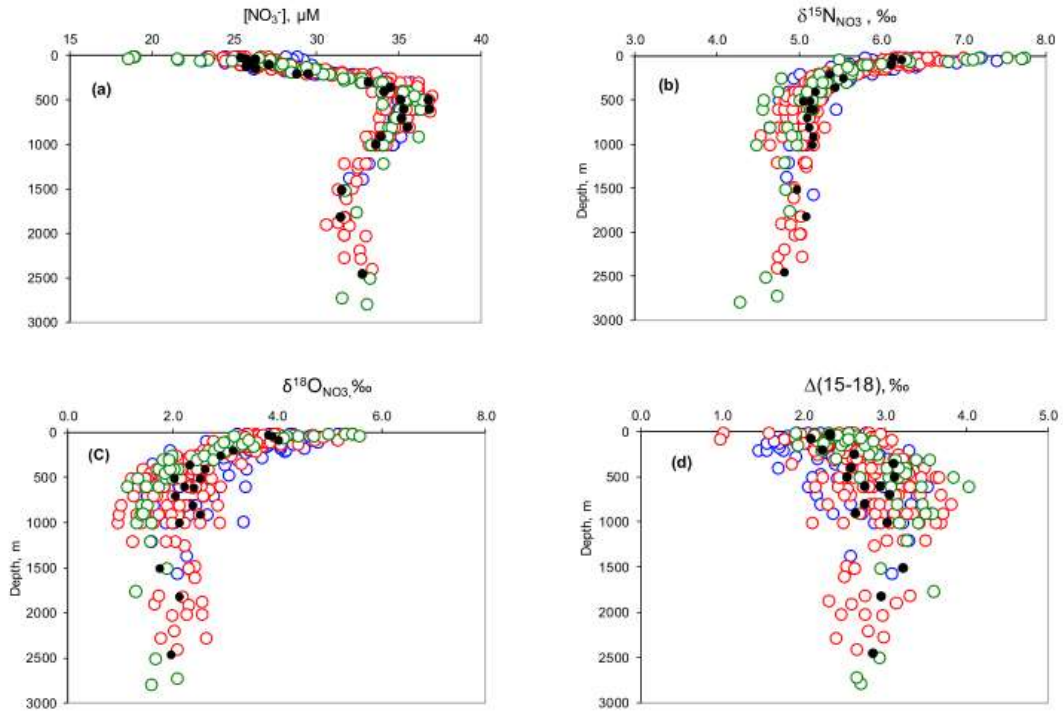

Figure 5: KEOPS 2 expedition. Water column profiles of (a) NO_3- (µM); (b) $\delta^{15}N$-NO_3; (c) $\delta^{18}O$-NO_3, and (d) Δ(15, 18); Complete data set. Blue circles = Plateau stations; Red circles = Meander stations; Green circles = Polar Front and north of PF stations; Filled black circles = Reference station (R-2).

2‰ (Figure 5c). Comparing Plateau and Meander stations we do note that Plateau sites have slightly higher surface water $\delta^{15}N_{NO3}$ values (6.35 ± 0.37 ‰) than Meander sites (6.27 ± 0.21 ‰), as well as slightly enhanced $\delta^{18}O_{NO3}$ values (average $\delta^{18}O_{NO3}$ values are 4.25 ± 0.99 and 3.98 ± 0.54‰, respectively). However, these differences are not significant (p>0.05).

Differences of the $\delta^{15}N$ and $\delta^{18}O$ gradients between deep ocean and surface are generally visualized by plotting the Δ(15,18) values (Figure 5d), which simply represent the difference between $\delta^{15}N$ and $\delta^{18}O$, keeping in mind that for deep waters this $\delta^{15}N_{NO3} - \delta^{18}O_{NO3}$ difference is close to 3‰ (Rafter et al., 2012). From Figure 5d it appears that surface waters have Δ(15,18) values generally <3‰ (range 0.9 - 3‰; average = 2.30 ± 0.5‰), with lowest values observed for Plateau stations (average values in the upper 100m are 2.08 ± 0.66; 2.39 ± 0.44; 2.2.44 ± 0.28 for Plateau, Meander and PF areas, respectively), with Plateau values significantly lower (p<0.05) than PF values. This indicates that surface water $\delta^{18}O$ values have increased more than $\delta^{15}N$ values. In contrast, the sub-surface waters between 250 m and 1250 m show a majority of data points with Δ(15,18) values> 3‰, though values are scattered rather widely. Since uptake of nitrate fractionates $^{15}N/^{14}N$ and $^{18}O/^{16}O$ equally (Granger et al., 2004; Sigman et al., 2005), another process needs to be invoked to explain the low Δ(15,18) values for surface waters. Below we show that these low surface waters Δ(15,18) values (<3‰) can be attributed largely to a partial utilization of the surface water nitrate pool combined with nitrification in the surface and subsurface waters.

Figure 6a,b shows the spatial distribution of the $\delta^{15}N_{NO3}$ and $\delta^{18}O_{NO3}$ signals and nitrate concentration along the W to E and S to N sections. Deep waters (>500m) in the central part of the W to E section, between 72°E and 74°E have $\delta^{15}N_{NO3}$ values close to 5‰, while westward and eastward of this central area, deep waters have slightly lower $\delta^{15}N$ values (Figure 6, top). Lowest $\delta^{15}N_{NO3}$ values are observed in bottom waters (>2000 m) east of 73°E and appear associated with very low temperatures (<1°C). These waters are probably of southerly origin, associated with the Fawn Through Current, transporting cold Antarctic waters of eastern Enderby origin (Park et al., 2008) and possibly also partly with the Deep Western Boundary Current which is part of the deep cyclonic gyre in the Australian – Antarctic Basin (McCartney and Donohue, 2007; Fukamachi et al., 2010).

For the 250 m to 1500 m depth interval at stations on the PFZ side of the PF (east of 74°E) and to a lesser stations close to the plateau margin between 71° and 72°E (Figure 6a) we observe low $\delta^{18}O_{NO3}$ values (<2‰) and high Δ(15,18) values(> 3‰). This feature is probably associated with advection of UCDW as discussed later. The occurrence of these signals at the western and eastern borders of the meander possibly reflects the presence of a cyclonic circulation in the basin which confines the meander, as reported by Park et al. (2014a). Note that the S to N section between approximately 71° and 72°E also intersects the low $\delta^{18}O_{NO3}$ waters (Figure 6b). Below 1500m Δ(15,18) values are close to 3‰, reflecting similar vertical gradients for $\delta^{15}N$ and $\delta^{18}O$.

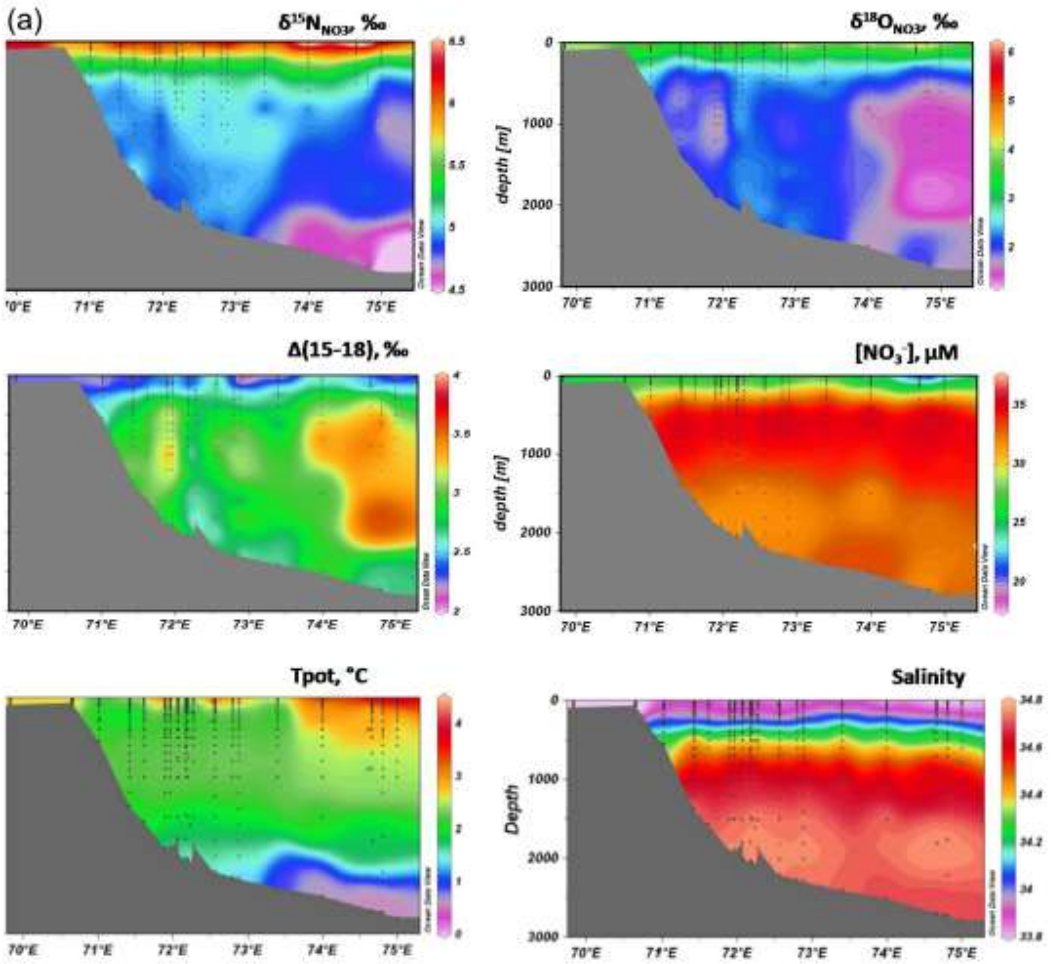

Figure 6a: KEOPS 2. West to east sections of whole water column $\delta^{15}N\text{-}NO_3$ (upper row left), $\delta^{18}O\text{-}NO_3$ (upper row middle), NO_3^- (upper row right), Tpot (lower row left) and Salinity (lower row right), starting on Kerguelen Plateau and crossing the Polar Front Meander. The Polar Front loop is crossed at about 71.3°E and 74°E; (ODV-AWI, R. Schlitzer).

Figure 7 shows the regressions of $\delta^{18}O_{NO3}$ vs. $\delta^{15}N_{NO3}$ for the Plateau, Meander and PF areas. As expected the regression slopes for whole water column are larger than 1 (they vary between 1.4 and 1.5, for PF and Plateau areas, respectively). The black line in Figure 7 reflects the expected regression in case discrimination during nitrate uptake is similar for $^{18}O/^{16}O$ and $^{15}N/^{14}N$ and acts upon a nitrate source reservoir that has a deep water isotopic signature (i.e., $\delta^{15}N_{NO3}$ = 5‰ and $\delta^{18}O_{NO3}$ = 2‰). When focusing on the upper 250m we note that slope values decrease and come close to 1 for the PF area (slope = 1.14), while they are close to 1.3 for Plateau and Meander sites (Figure 7). For all 3 areas, it is clear, however, that data points mostly fall above the expected regression. This condition is also clearly reflected in the Δ(15,18) values which mostly fall below 3‰ for the upper 200m of water column (Figure 5d).

Figure 7 also shows the summer data obtained during KEOPS 1 (Trull et al., 2008) superimposed on the present KEOPS 2 spring data. This comparison is limited to the upper 250 m of the water column, i.e. the depth range analysed during KEOPS 1 (Trull et al., 2008).The summer data overlap tightly with the spring data but also sit above the 1:1 line, defined above, but in contrast to spring, summer shows a slope value close to 1 (0.98).

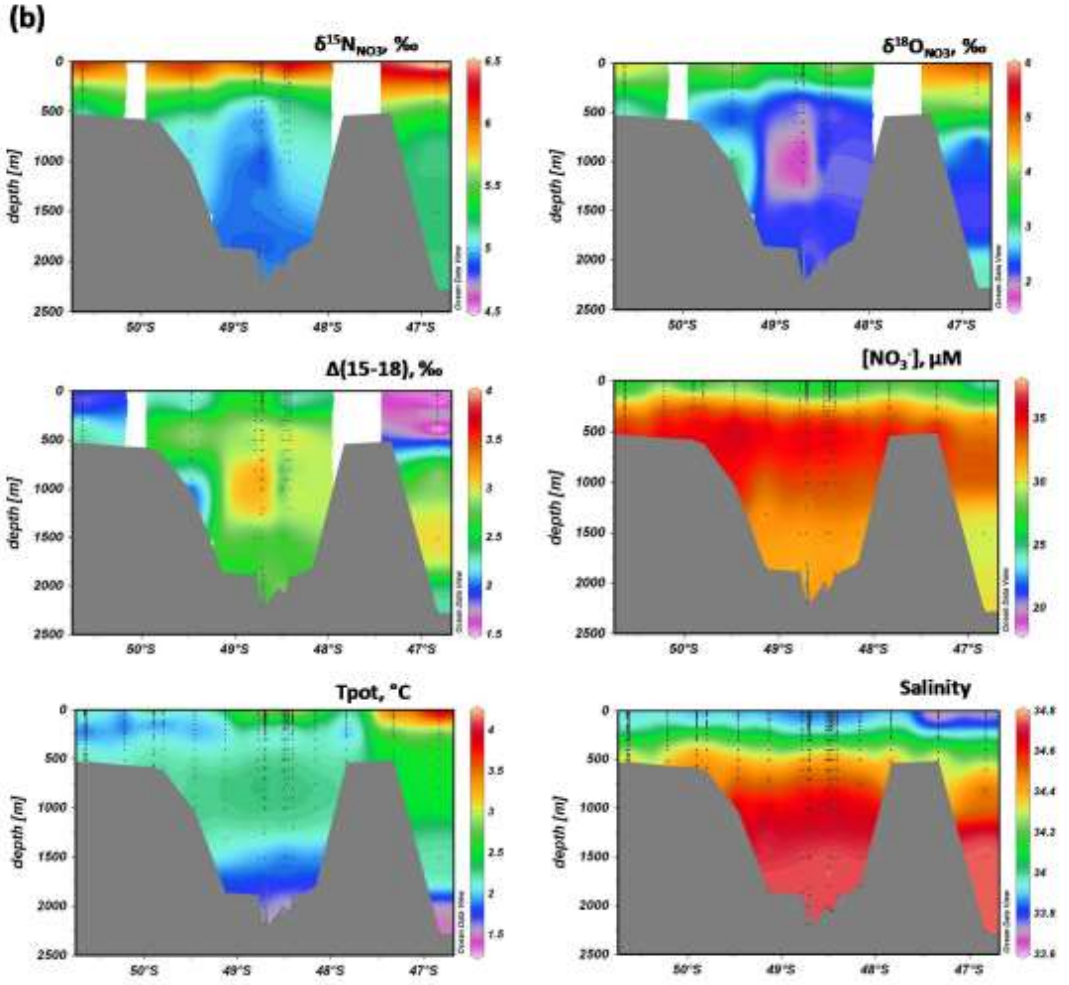

Figure 6b: KEOPS 2. South to North sections along about 72°E of whole water column $\delta^{15}NNO_3$ (upper row left), $\delta^{18}ONO_3$ (upper row middle), NO_3- (upper row right), Tpot (lower row left) and Salinity (lower row right). (ODV-AWI, R. Schlitzer).

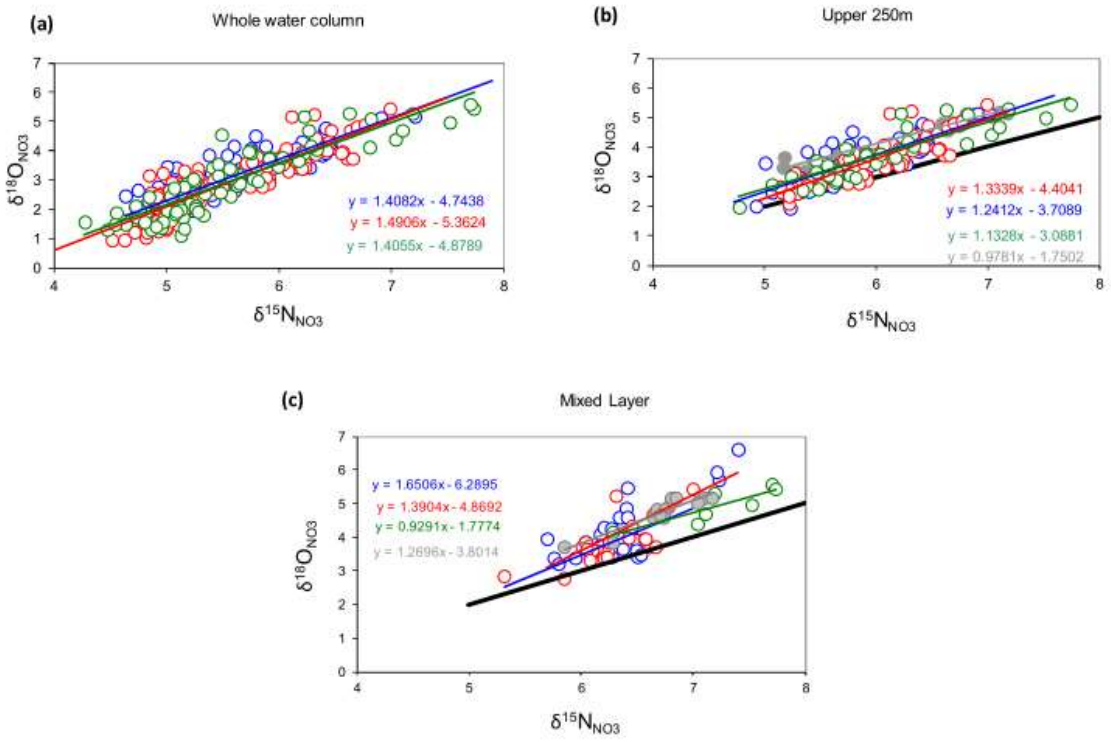

Figure 7: KEOPS 2. Regressions of $\delta^{18}O_{NO3}$ vs. $\delta^{15}N_{NO3}$ for the Plateau, Meander and PF areas.

However, a closer look reveals that the deepest summer samples have slightly more elevated $\delta^{18}O_{NO3}$ values, tilting the regression and thereby decreasing the slope value. These more elevated subsurface $\delta^{18}O_{NO3}$ values may reflect the effect of subsurface nitrification in an area of partial surface nitrate assimilation (Rafter et al., 2013; Sigman et al. 2009). When focusing on the mixed layer depth, the slopes of the $\delta^{18}O_{NO3}$ vs. $\delta^{15}N_{NO3}$ regressions become even steeper for the Plateau (up to 1.65) and Meander areas and for the KEOPS 1 data set (Figure 7), but not for the PF area. Thus, within the upper 250m and even more so in the upper mixed layer, the variations of $\delta^{18}O_{NO3}$ values clearly exceed those for corresponding $\delta^{15}N_{NO3}$ values. Such a condition may result from the remineralization – nitrification of organic nitrogen (Sigman et al., 2009, DiFiore et al., 2009). Also, the absence of a clear differentiation between summer (KEOPS 1) and spring (KEOPS 2) conditions (we would expect to see the summer condition further up the line with higher $\delta^{15}N$ and $\delta^{18}O$ values) is quite puzzling, and may reflect the fact that the nitrate consumed is being largely replenished from remineralization coupled to nitrification, thereby dampening the enrichment of ^{15}N due to uptake (but enhancing the ^{18}O enrichment). The replenishment of nitrate in the mixed layer also is reflected in the mixed layer silicic acid over nitrate depletion ratios which are systematically >> 1 during the time series stations above the Plateau and in the Meander, although $Si(OH)_4/NO_3^-$ uptake ratios are close to 1 (Closset et al., 2014; Cavagna et al., 2015). In fact nitrate contents stay relatively high throughout the growth season and KEOPS 1 summer nitrate values remain generally in excess of 20 µM (Trull et al., 2008), while summer silicic acid concentrations run low to near depletion, despite the $Si(OH)_4/NO_3^-$ uptake

ratio being close to 1 (Mosseri et al., 2008). This is further evidence for significant nitrification in the upper mixed layer. The combined effect of nitrate uptake and nitrification in the euphotic zone will result in decoupling the $\delta^{15}N_{NO3}$ and $\delta^{18}O_{NO3}$ signals, thereby changing (increasing) their average deep ocean offset of 3‰.

We now evaluate the strength of a possible nitrification in the surface layers.

Calculating the temporal evolution of $\delta^{15}N_{NO3}$ and $\delta^{18}O_{NO3}$ in the surface mixed layer

The similarity of the ranges of upper ocean nitrate isotopic compositions during early and late season raises the question whether the Kerguelen system had already reached some steady state condition for nitrogen cycling early in the season, with nitrate consumption being mostly balanced by remineralization combined with nitrification. However, earlier studies, suggest that the evidence for significant euphotic zone nitrification in Southern Ocean surface waters is weak (Olson, 1981; Trull et al., 2008; DiFiore et al., 2009). To resolve this apparent controversy we will estimate the strength of nitrification in the upper mixed layer. We apply a mass balance approach for both, $\delta^{15}N_{NO3}$ and $\delta^{18}O_{NO3}$ in the mixed layer of Plateau and Meander stations where data on temporal evolution are available. We take advantage of the fact that nitrate and ammonium uptake rates were measured during KEOPS 2 (Cavagna et al., 2015) and also that values of isotopic composition of suspended and sinking material are available (Trull et al., 2015; Planchon et al., 2015). Note that the model calculations presented here cover a limited length of growth period (about one month). More complex model calculations describing the evolution nitrification over the full growth season are presented elsewhere (Fripiat et al., 2015).

We take the upper 100 m nitrate conditions observed during the earliest visit to the Plateau and Meander as the initial conditions (i.e. conditions for stations A3-1 and TNS06, respectively). Euphotic zone (0.01% PAR; 57 to 137m deep) integrated nitrate uptake rates reported by Cavagna et al. (2015) do show an increase by some 30% for the Meander region (Stations E1, E3, E4-E and E5; 27 day period). For the Plateau region only two N-uptake profiles (stations E4-W; A3-2) were measured, apart by just 4 days. Nitrate uptake for the Meander sites are on average 12.4 ± 2.2 mmol m^{-2} d^{-1}(n = 4) while for the Plateau sites they are 36 ± 4.7 (n=2). Ammonium uptake rates are 6.6 ± 1.4 mmol m^{-2} d^{-1} (n=4) and 6.2 ± 1.9 (n=2) for Meander and Plateau sites, respectively. Using these average nitrate uptake rates we calculate the nitrate concentrations (called residual nitrate) that would be present in the upper 100 m at the end of the observation period in case uptake is the sole process affecting the nitrate concentration. Nitrate concentrations at stations A3-1 (Plateau) and TNS06 (Meander) were considered to represent the initial conditions, whereas concentrations at stations A3-2 (Plateau) and station E5 (Meander), visited 27 days after A3-1 and TNS06, respectively, represent the conditions at the end of the observation period. Residual nitrate values are slightly (by 6%; Meander) to significantly lower (25%; Plateau) than measured values (see Table 2). The isotopic composition of the residual nitrate is then calculated from the estimated fraction of nitrate remaining, using a discrimination of 5‰ for both $^{15}N/^{14}N$ and $^{18}O/^{16}O$ (Sigman

et al., 1999; DiFiore et al., 2010) and considering that the surface mixed layer operates as a closed system (Rayleigh fractionation applies). The calculated isotopic compositions of the residual nitrate are heavier than the measured ones. The differences between calculated and observed isotopic values are: for $\delta^{15}N$ 0.22‰ and 1.45‰ and for $\delta^{18}O$, 0.10 and 0.98‰ for Meander and Plateau areas, respectively. For the Meander area differences are small (close to the analytical precision) and so the calculated nitrification rate is poorly constrained. For the Plateau area the differences are larger and as a result calculated nitrification combined with nitrate upwelling are better constrained.

The isotope effects associated with nitrification are taken as follows, assuming a steady state between the production and consumption of both ammonium and nitrite (e.g., Fripiat et al., 2014):

For $\delta^{15}N_{NO3}$: Nitrif. $[\delta^{15}N_{PN} - \varepsilon_R + f\ (\varepsilon_{NH4u} - \varepsilon_{AmO}) + y\ (\varepsilon_{NiU} - \varepsilon_{NiO})]$
(6)

For $\delta^{18}O_{NO3}$: Nitrif.$(\delta^{18}O_{H2O} + 1.1)$ (Sigman et al., 2009)
(7)

with Nitrif = the nitrification rate, $\delta^{15}N_{PN}$= the N isotopic composition of suspended material; $\delta^{18}O_{H2O}$ = the oxygen isotopic composition of ambient water; ε_R= the discrimination during remineralization (values); ε_{NH4U} = the isotope discrimination during NH_4 uptake (values); ε_{AMO} = the discrimination during NH_4 oxidation (values); ε_{NiU} = the discrimination during nitrite uptake (values); ε_{NiO} = the discrimination during nitrite oxidation (values); f = the fractional yield of ammonium uptake relative to ammonium oxidation and y = the fractional yield of nitrite uptake relative to nitrite oxidation. Table 2 gives the selected values for the different discrimination factors as taken from the literature.

The theoretical in-situ $\delta^{15}N_{NO3}$ values at the end of the observation period are considered to result from the weighed impact of uptake, nitrification and upwelling and were calculated as follows:

For $\delta^{15}N_{NO3}$

$$\frac{Uptake\left(\delta^{15}N_{NO3} - \varepsilon_{NaU}Lnf\right) + Nitrif\left[\delta^{15}N_{PN} - \varepsilon_R + x\left(\varepsilon_{NH4U} - \varepsilon_{AmO}\right) + y\left(\varepsilon_{NiU} - \varepsilon_{NiO}\right)\right] + Upw\left(\delta^{15}N_{NO3T\min}\right)}{Uptake + Nitrif + Upwelling}$$

(8)

and for $\delta^{18}O_{NO3}$

$$\frac{Uptake\left(\delta^{18}O_{NO3} - \varepsilon_{NaU}Lnf\right) + Nitrif\left(\delta^{18}O_{H2O}\right) + Upw\left(\delta^{18}O_{NO3T\min}\right)}{Uptake + Nitrif + Upwelling} \quad (9)$$

Parameter, Process	$\delta^{18}O$, ‰	ε^{15}‰	ε^{18} ‰	References
$\delta^{18}O$-H_2O	-0.4			Archambeau et al., 1998
Nitrification			1.1	Sigman et al., 2009b
Remineralisation		2		Kendall, 1998; Knapp et al., 2011; Möbius, 2013
NO_3 uptake		5	5	Waser et al., 1998; Granger et al., 2010; DiFiore et al., 2010
NH_4 uptake		5*		Hoch et al., 1992; Fogel & Cifuentes, 1993; Pennock et al., 1996; Waser,et al. 1999
NH_4 oxidation		15		Casciotti et al., 2003; DiFiore et al., 2009
NO_2 oxidation		-12		Buchwald and Casciotti (2010)
NO_2 Uptake		0		Waser et al., 1998

* for low ammonium concentrations (<10 µM)

Table 2: Considered isotopic discrimination factors for model calculations.

With the different ε values = the isotopic discriminations; $\delta^{15}N_{NO3Tmin}$ and $\delta^{18}O_{NO3Tmin}$ = isotopic composition for the subsurface temperature minimum waters (ε and δ values are given in Table 2); f = fraction of remaining nitrate; x = fractional yield of ammonium uptake; y = fractional yield of nitrite uptake; Uptake = nitrate uptake rate; Nitrif = nitrification rate; Upw = rate of vertical advection of nitrate.

The best fit between observed and calculated isotopic compositions is searched using a optimization scheme with nitrification, upwelling from subsurface waters (T_{min}

	[NO3-] µM	$\delta^{15}N_{NO3}$ ‰	$\delta^{18}O_{NO3}$ ‰	Measured Flux mmol/m2/d	Best fit (min - max) mmol/m2/d	Best fit (min - max); fixed upw.[$] mmol/m2/d
Plateau						
Upelling water	29.9	5.76	3.39			
Average condition in upper 100m (A3-1); T0	29.3	5.75	3.61			
Average condition in upper 100m (A3-2); Tend	25.8	6.37	4.59			
NO_3^- uptake				36.5 ± 4.7*		
NH_4^+ uptake				6.2 ± 1.9*		
Calculated: Uptake only (Rayleigh)	*20.2*	*7.61*	*5.48*			
Calculated: Uptake+Upwelling+Nitrification	*25.8***	*6.37*	*4.59*			
Calculated: Nitrification					*18.9 ; (6 - 27)*	*18.9 ; (12 - 22)*
Calculated: NO_3^- upwelling					*4.6 ; (0 - 24)*	*7.4*
Calculated: NO_2^- Uptake					*7 ; (0 - 17)*	*7; (0.2 - 13)*
Polar Front Meander						
Upelling water	31.6	5.32	2.85			
Average condition in upper 100m (TN506); T0	27.4	6.08	3.68			
Average condition in upper 100m (E5); Tend	25.6	6.52	4.26			
NO_3^- uptake				12.4 ± 2.2*		
NH_4^+ uptake				6.6 ± 1.4*		
Calculated: Uptake only (Rayleigh)	*24.0*	*6.73*	*4.33*			
Calculated: Uptake+Upwelling+Nitrification	*25.6***	*6.53*	*4.22*			
Calculated: Nitrification					*1.1 ; (0 - 11)*	*0.7 ; (0 - 4)*
Calculated: NO_3^- upwelling					*4.7 ; (0 - 11)*	*7.4*
Calculated: NO_2^- Uptake					*0*	*0*

* average rates from Cavagna et al. (this issue)

** matching with observed value at T_{end} is imposed

[$] Nitrate upwelling fixed at 7.4 mmol m^{-2} d^{-1}, based on the Ekman pumping velocity in Cambra et al. (this issue)

Table 3: KEOPS 2. Plateau and Meander sites: Observed initial and final conditions of nitrate concentration and isotopic composition; Observed nitrate and ammonium uptake rates (from Cavagna et al., 2015); Calculated nitrification, nitrite uptake, nitrate upwelling rates required to explain the observed nitrate isotopic composition and nitrate concentration at the end of the considered growth period.

waters at 100 to 150 m depth), NH_4^+ oxidation and NO_2^- uptake as adjustable variables. The matching of observed and calculated nitrate draw down and the matching of NH_4^+ oxidation with NO_2^- uptake + nitrification are imposed constraints. The best fit calculations yield nitrification rates of 1.1 ± 2.3 and 18.9 ± 4.3 mmol m^{-2} d^{-1} for Meander and Plateau, respectively (Table 3). Best fit values are 0 and 7 mmol m^{-2} d^{-1} for NO_2^- uptake and 4.7 and 4.6 mmol m^{-2} d^{-1} for NO_3^- upwelling, for Meander and Plateau sites, respectively (Table 3). These latter values are quite similar to the value of 7.4 mmol m^{-2} d^{-1} we calculate, as based on an Ekman pumping velocity of 3 x 10^{-6} m s^{-1} for the studied KEOPS 2 area, reported by Gille et al. (2014), and an average subsurface (150m) NO_3^- concentration of 28.5 µM. In case the NO_3^- upwelling rate is fixed and set equal to the value of 7.4 mmol m^{-2} d^{-1} based on the Ekman pumping velocity, the best fit nitrification rates are slightly smaller but more constrained (see below) with values of 0.7 ± 0.8 and 18.9 ± 2.2 mmol m^{-2} d^{-1}, for Meander and Plateau, respectively.

We performed a sensitivity test to verify the range (minimum – maximum) of nitrification, nitrite uptake and nitrate upwelling rates, taking into account the measurement errors on isotopic compositions (as given in the Methods section) and the observed variability on nitrate and ammonium uptake rates. It appears for the Meander site that the min. – max. range of possible nitrification rates reaches from 0 to 11 mmol m^{-2} d^{-1}, a range which narrows from 0 to 4 mmol m^{-2} d^{-1} in case NO_3^- upwelling is kept fixed. The situation is quite different for the Plateau site where the min. – max. range of nitrification reaches from 6 to 27 mmol m^{-2} d^{-1} which narrows down from 12 to 22 mmol m^{-2} d^{-1} when upwelling is kept fixed. Thus, clearly, for the Plateau site, surface layer nitrification needs to be invoked to explain the observed nitrate isotopic compositions and may represent some 52% of the nitrate uptake. For the Meander site there is evidence for nitrification, but the calculated rate is poorly constrained.

The calculated nitrification rate for the Plateau site significantly exceeds some earlier estimates and which led to the conclusion that nitrification is a rather minor process which accounts for <10% of phytoplankton nitrate uptake in Southern Ocean waters (Olson, 1981; Trull et al., 2008; DiFiore et al., 2009). However, Bianchi et al. (1997) report for the area between Crozet and Kerguelen that nitrification rates in the upper 100m measured during late summer, fall could represent between 10 and 100% of the nitrate requirements. In contrast, high nitrification rates reaching levels similar to the phytoplankton nitrate demand appear to be common for oligotrophic systems (see e.g., Yool et al., 2007; Wankel et al., 2007; Mulholland and Lomas, 2008). Nevertheless, conditions for significant nitrification activity appear to be met in the studied Kerguelen area. For one thing, ammonium concentrations are relatively high, reaching up to 0.5, 0.7 and 0.8 µM within the first 100m for the PF, Meander and Plateau sites, respectively (Figure 3) thus providing the substrate for any bacterial and archaeal ammonium oxidizing activity. Furthermore, nitrite concentrations reach up to 0.33 µM in the upper 100m of water column, again indicating nitrification activity is ongoing there. Archaea do abound in the Southern Ocean (Church et al., 2003) and may exhibit a specific affinity for ammonia similar to the one for diatoms, as

reported for the cultivated marine ammonia oxidizing archeon (*Nitrosopumilus maritimus)* (Martens-Habbena et al., 2009 and Stahl and de la Torre, 2012).

This a priori unexpected importance of nitrification in surface waters of the Kerguelen area also has become evident from a close analysis of the nutrient concentration and isotopic composition changes over the full growth season (integrating results from KEOPS 2 and KEOPS 1; Fripiat et al., 2015). Deep winter vertical mixing imposes high NO_3^- concentration at the onset of the bloom (Figure 8, upper panel). Despite large euphotic layer integrated NO_3^- uptake rates (corresponding to a NO_3^- drawdown of 22 ± 10 µmol L^{-1}), the apparent NO_3^- utilization remains low (6.1 µmol L^{-1}; Figure 8, lower panel).

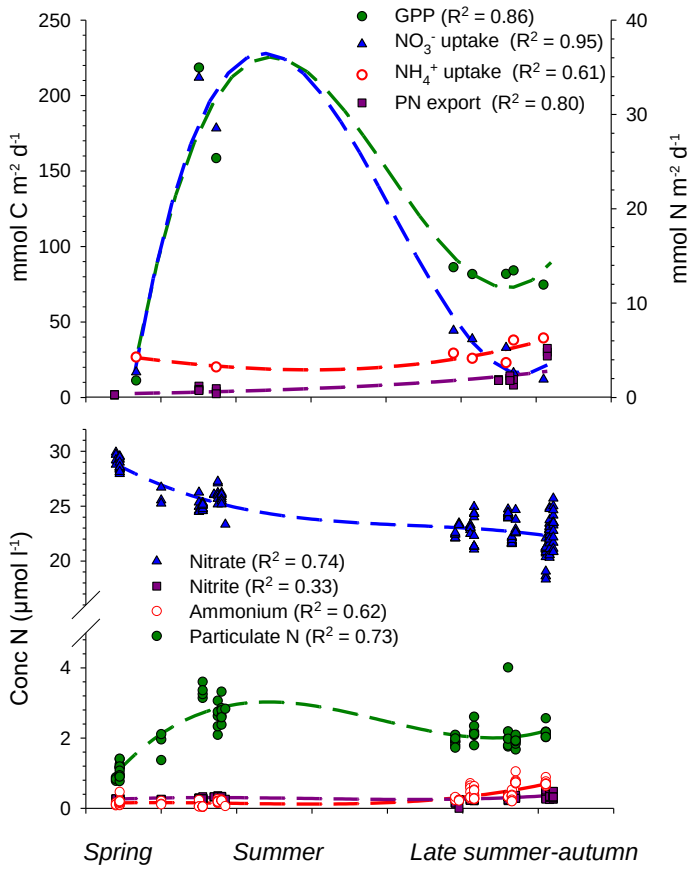

Figure 8: KEOPS 2. Upper panel: Seasonal distribution of euphotic layer integrated gross primary production (GPP; circles; left y-axis), NO_3^- uptake (triangles; right y-axis), $NH4^+$ uptake (empty red circles; right y axis), and PN export (squares; right y-axis). Lower panel: Seasonal distribution of NO_3^- (triangles), PN (circles), NH_4^+ (circles), and NO_2^- (squares) concentrations in the upper mixed layer.

The outcome of a time-dependent single-box model (Fripiat et al., 2015) highlights indeed that nitrification, the microbially mediated process by which ammonium is oxidized to nitrate, is significant in the mixed layer above the Kerguelen Plateau and contributes a large part (~60-80%) of the NO_3^- consumed by the phytoplankton.

Two conditions may explain why the Kerguelen Plateau area appears to be a favorable environment for nitrification: (1) The upper mixed layer depth generally extends deeper than the euphotic layer. The decoupling with depth between NO_3^- assimilation (light-dependent) and nitrification (partly light-inhibited) would allow the nitrifiers within the mixed layer to compete with phytoplankton for the available NH_4^+ pool. It would appear then that NO_3^- is consumed in the upper part of the mixed layer, sustaining a high primary production, and is regenerated in the lower part of the mixed layer where light availability is insufficient to sustain NO_3^- uptake but does not inhibit nitrification; (2) Iron and trace metals are essential for the enzymes involved in the oxidation of NH_4^+ and NO_2^-, as well as in the energy acquisition system of the nitrifiers. A large supply of trace metals (e.g., iron and copper) to the surface waters from enriched deep waters could boost nitrification, either directly, by providing these essential enzyme constituents, or indirectly, via a coupling with an efficient microbial foodweb which continuously supplies NH_4^+, the substrate for nitrification.

Carbon export via the biopump

Total ^{234}Th activities were obtained from 4 L seawater samples collected from 12 L Niskin bottles. Seawater samples were processed for total ^{234}Th activity measurement following the double-spike procedure developed by Pike et al. (2005) and modified by Planchon et al. (2013). Briefly, samples were acidified with nitric acid (pH 2), spiked with ^{230}Th yield tracer, and left for 12 hours equilibration before co-precipitation with MnO_2 (pH 8.5). Co-precipitated samples were filtered on high-purity quartz microfiber filters (QMA, Sartorius; nominal pore size = 1 µm; Ø 25 mm), dried overnight and mounted on nylon filter holders covered with Mylar and Al foil for beta counting. Samples were counted twice on board using a low level beta counter (RISØ, Denmark) and activity measurements were stopped when counting uncertainty was below 2% (RSD). Residual beta activity was measured after a delay of six ^{234}Th half-lives (~6 months) and was subtracted from the gross counts obtained on-board. After background counting, all samples were processed for ^{234}Th recovery using ^{229}Th as a second yield tracer and with a simplified procedure (Planchon et al., 2013). The ^{238}U activity (dpm L^{-1}) was calculated using the following relationship (Owens et al., 2011):

$$^{238}U\ (\pm 0.047) = (0.0786 \pm 0.0045) \times Sal - (0.315 \pm 0.158) \qquad (10)$$

^{234}Th Flux

Export fluxes of ^{234}Th were calculated using a 1D box model which accounts for total ^{234}Th mass balance (Savoye et al., 2006). Fluxes were estimated for the 100 m, 150 m, and 200 m depths. At all stations, ^{234}Th flux was estimated under steady state assumption (SS), i.e. considering constant total ^{234}Th activity over time and neglecting advective and diffusive fluxes of ^{234}Th. For re-visited stations (A3 and E stations), ^{234}Th flux was also estimated under non-steady state assumption (NSS). At A3, the NSS model was applied for the second visit with a time delay of 27.7 days. At E stations, NSS ^{234}Th export flux was estimated when the time delay was greater

than one week (Savoye et al., 2006), which holds for stations E-4E (delay 14.6 days) and E-5 (delay 19.6 days).

In order to check the assumption that physical transport did not impact the ^{234}Th budget, the vertical diffusive flux (Vz) was estimated using the vertical gradient of ^{234}Th activity and a range of vertical diffusivity coefficients (Kz) between 10^{-4} m² s^{-1} and 10^{-5} m² s^{-1} calculated from the Shih model (Park et al., 2014b). The diffuse flux (Vz) estimated at 100,150, and 200 m depth was always below 50 dpm m² d^{-1} and represented a negligible contribution to the particle-associated export flux.

Lateral transport may also impact the ^{234}Th budget (Savoye et al., 2006) especially for stations located downstream of the Kerguelen island. Given the mean residence of surface water parcels over the plateau (2-3 months) (Park et al., 2008) or inside the recirculation feature (0.5-1 month) compared to the mean residence of ^{234}Th (~1 month), lateral contribution was likely minimal.

Particulate ^{234}Th and POC

Suspended particulate matter was collected for particulate ^{234}Th and POC via large-volume (150-1000 L) in-situ filtration systems (Challenger Oceanics and McLane WTS6-1-142LV pumps) equipped with 142 mm diameter filter holders. Two size classes of particles (>53 µm and 1-53 µm) were collected via sequential filtration across a 53 µm mesh nylon screen (SEFAR-PETEX®) and a 1 µm pore size quartz filter (QMA, Sartorius).

After collection, filters were subsampled under clean room conditions with ceramic scissors for the nylon screen and a 25 mm Perspex punch for the QMA filter. For large particles one fourth of the 142 mm nylon screen was used for ^{234}Th and POC analyses. Particles were re-suspended in filtered seawater and collected on 25 mm diameter silver (Ag) filters (1.0 µm porosity). For small particles, 25 mm diameter punches were subsampled from the 142 mm QMA filters. Ag and QMA filters were dried overnight and mounted on nylon filter holders covered with Mylar and Al foil for beta counting. As for total ^{234}Th activity, particulate samples were counted twice on board until the RSD was <2%. The procedure was similar for sediment traps samples. Sediment traps samples were re-suspended in filtered seawater, collected on Ag filters, dried, and mounted on nylon filter holder.

Residual beta activity was measured after six ^{234}Th half-lives (~6 months) and was subtracted from the on-board measured values. Following beta counting, particulate samples (QMA and Ag filters) were dismounted from filters holders and fumed with HCl vapour to remove carbonates. After overnight drying at 50°C samples were packed in silver cups and analyzed with a Flash EA1112 elemental analyzer coupled on-line via a Con-Flo III interface to a Delta V Isotope Ratio Mass Spectrometer (Thermo). Acetanilide standards were used for calibration.

Results of the ^{234}Th and POC export fluxes are shown in Table 4 and Figure 9. Export production in the Fe-fertilized area reveals large spatial variability during the early stages of bloom development with low export found at high productivity sites

located over the central plateau (A3 site) and north of the PF in deep water downstream of the island (F-L site). Highest export was observed south of the permanent meander of the PF (E stations) where a detailed time series was obtained as part of a pseudo-lagrangian study. The comparison with the HNLC reference station (R2) located south of the PF and upstream of the island, indicates that Fe fertilization increased carbon export in all iron fertilized waters during the early stage of the bloom, but to variable degrees. The increase is particularly significant inside the PF meander, but more moderate over the central Kerguelen Plateau and in the northern plume of the Kerguelen bloom. Export efficiencies (ThE) were particularly low at high productivity sites over and off the Plateau (A3 and F-L sites) clearly indicating that biomass was in an accumulation phase rather than in export phase. Spatial variations in natural iron inputs resulted in varied phytoplankton community structures, impacting the potential for carbon export. The high biomass at station A3 over the central plateau was dominated by large-size diatoms, which potentially could sustain higher export than at sites F-L and E sites, but evidence was that this higher export did not occur yet at the time of sampling in early spring. Comparison with late summer POC export obtained during summer 2005 (KEOPS 1) reveals a much smaller carbon export during the early stages of the bloom in spring (KEOPS 2).

Conclusive remarks about Carbon export

During KEOPS 2 (spring season) the POC export fluxes in the Kerguelen area estimated using the ^{234}Th-based approach were low, in general, with average values of 66 to 90 mgC m^{-2} d^{-1} for the plateau area (Figure 9) and a downstream Polar Front meander, as compared to the KEOPS 1 summer results which reached up to 450 mgC m^{-2} d^{-1} above the plateau (Savoye et al., 2008).

Export efficiencies (ratio of POC export over Primary Production) during spring were low as well, reaching only 3% above the Plateau, while they reached more than 10% during summer (KEOPS 1). So clearly, during the initial stage of the seasonal bloom, the export of carbon via the biological pump was not (yet) efficient, and biomass was accumulating in surface waters rather than being exported. Also, a large part of the synthesized biomass was subject to shallow mineralization as evidenced by the magnitude of mixed layer nitrification (see above).

Station	Date	Depth (m)	^{234}Th flux (dpm m^{-2} d^{-1})	C:Th (µmol dpm^{-1})	POC flux (mmol m^{-2} d^{-1})	ThE (%)	EP/NP (%)
R-2	25-oct.	100	412 ± 134	9.2 ± 0.5	3.8 ± 1.2	34	73
R-2	25-oct.	150	448 ± 146	5.6 ± 0.4	2.5 ± 0.8	22	48
R-2	25-oct.	200	449 ± 203	4.1 ± 0.5	1.8 ± 0.9	16	35
A3-1	20-oct.	100	509 ± 127	6.9 ± 1	3.5 ± 0.9		
A3-1	20-oct.	150	666 ± 140	5.8 ± 1	3.9 ± 0.9		
A3-1	20-oct.	200	776 ± 171	4.8 ± 1	3.7 ± 0.9		
A3-2	16-nov.	100	463 ± 151	9.9 ± 0	4.6 ± 1.5	3	3
A3-2	16-nov.	150	829 ± 169	8.6 ± 0	7.1 ± 1.5	5	5
A3-2	16-nov.	200	993 ± 200	3.1 ± 0	3.1 ± 0.6	2	2
A3-2 Trap	15 nov. - 17 nov.	200	506 ± 21	4.5 ± 1.5	2.2 ± 0.7		
A3-2	**20 oct.-16 nov.**	**100**	**736 ± 186**	**9.9 ± 0**	**7.3 ± 1.8**	**5**	**5**
A3-2	**20 oct.-16 nov.**	**150**	**975 ± 209**	**8.6 ± 0**	**8.4 ± 1.8**	**5**	**5**
A3-2	**20 oct.-16 nov.**	**200**	**1202 ± 247**	**3.1 ± 0**	**3.8 ± 0.8**	**2**	**2**
F-L	6-nov.	100	902 ± 117	4.5 ± 0	4.1 ± 0.6	1	2
F-L	6-nov.	150	891 ± 164	4.1 ± 0	3.6 ± 0.8	1	1
F-L	6-nov.	200	973 ± 207	3.1 ± 1	3.0 ± 0.8	1	1
E-1	30-oct.	100	1111 ± 120	10.5 ± 0	11.6 ± 1.3	27	34
E-1	30-oct.	150	1504 ± 158	5.5 ± 0	8.3 ± 0.9	19	24
E-1	30-oct.	200	1665 ± 201	4.7 ± 0	7.7 ± 1.0	18	23
E-1 Trap	29 oct. - 3 nov.	200	881 ± 226	8.6 ± 3.9	7.0 ± 2.3		
E-3	3 nov.	100	1326 ± 110	8.9 ± 0	11.8 ± 1.1	21	32
E-3	3 nov.	150	1742 ± 142	6.2 ± 0	10.8 ± 0.9	19	29
E-3	3 nov.	200	1995 ± 176	4.1 ± 0	8.2 ± 0.8	14	22
E-3 Trap	5 nov. - 9 nov.	200	1129 177	4.0 ± 0.7	4.9 ± 1.5		
E-4E	13 nov.	100	1051 ± 121	5.1 ± 0	5.4 ± 0.7	7	9
E-4E	13 nov.	150	1210 ± 155	3.3 ± 0	4.0 ± 0.5	5	7
E-4E	13 nov.	200	1296 ± 193	4.1 ± 0	5.3 ± 1.0	7	9
E-4E	**30 oct. - 13 nov.**	**100**	**911 ± 242**	**5.1 ± 0**	**4.6 ± 1.3**	**6**	**8**
E-4E	**30 oct. - 13 nov.**	**150**	**726 ± 315**	**3.3 ± 0**	**2.4 ± 1.0**	**3**	**4**
E-4E	**30 oct. - 13 nov.**	**200**	**525 ± 402**	**4.1 ± 0**	**2.1 ± 1.7**	**3**	**4**
E-5	18 nov.	100	1262 ± 116	6.1 ± 0	7.7 ± 0.7	10	14
E-5	18 nov.	150	1671 ± 153	4.2 ± 0	7.0 ± 0.7	9	12
E-5	18 nov.	200	1810 ± 190	3.7 ± 0	6.7 ± 0.8	9	12
E-5 Trap	18 nov. - 19 nov.	200	955 ± 546	2.4 ± 1.0	2.0 ± 1.0		
E-5	**30 oct. - 18 nov.**	**100**	**1383 ± 177**	**6.1 ± 0**	**8.4 ± 1.1**	**11**	**15**
E-5	**30 oct. - 18 nov.**	**150**	**1928 ± 235**	**4.2 ± 0**	**8.1 ± 1.0**	**10**	**14**
E-5	**30 oct. - 18 nov.**	**200**	**2034 ± 299**	**3.7 ± 0**	**7.5 ± 1.2**	**10**	**13**
E-4W	11 nov.	100	1003 ± 124	6.7 ± 0	6.7 ± 0.9	3	3
E-4W	11 nov.	150	1174 ± 168	3.9 ± 0	4.5 ± 0.7	2	2
E-4W	11 nov.	200	1068 ± 208	3.4 ± 0	3.7 ± 0.7	2	2

Table 4: KEOPS 2, ^{234}Th and POC export fluxes and C:Th ratios of sinking particles at 100, 150, and 200 m depth; carbon export efficiency (ThE and EP/NP ratios); (in bold = non-steady state calculations); for station location see Figure 1.

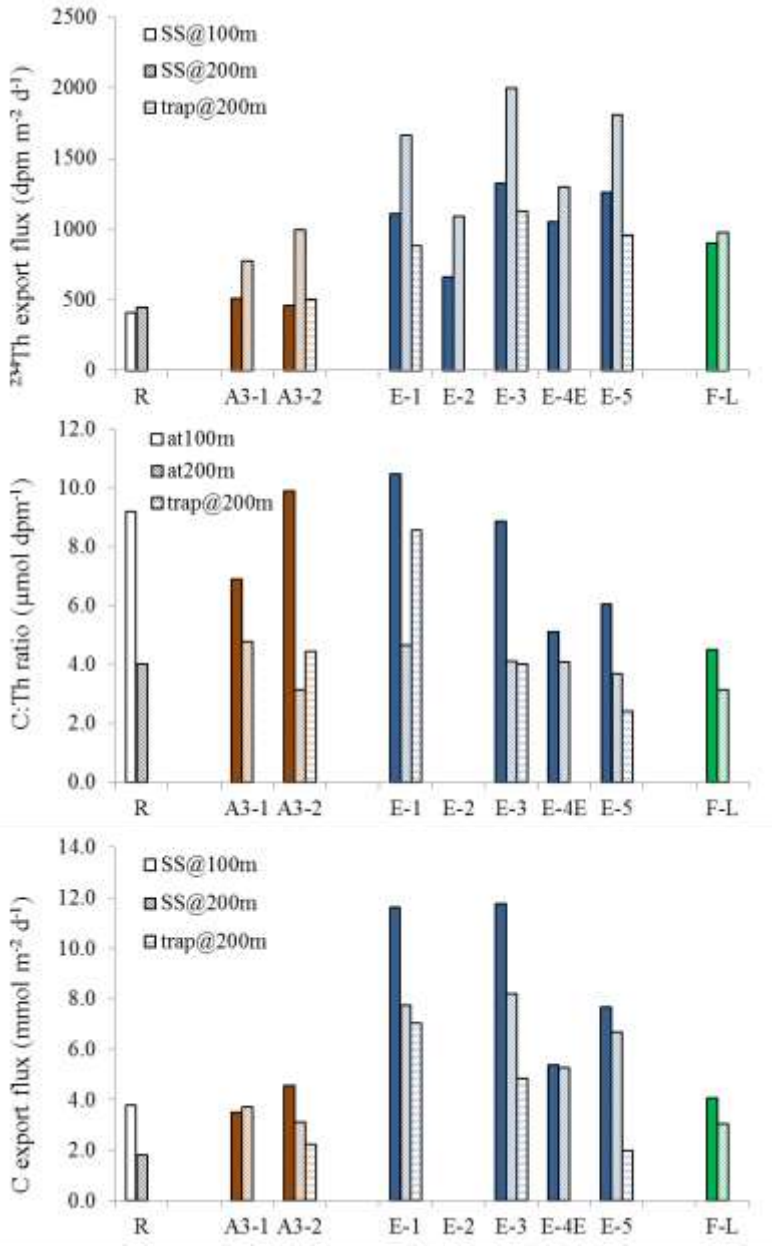

Figure 9: KEOPS 2, Summary results of ^{234}Th export fluxes (dpm m^{-2} d^{-1}), sinking particles C:Th ratios (µmol dpm^{-1}), and POC export fluxes (mmol m^{-2} d^{-1}) obtained at 100 m and 200 m depth and comparison with sediment trap data obtained at 200 m.

Mesopelagic remineralization

Twenty two CTD casts (surface to 500-2000 m) were sampled for particulate barium using a CTD-rosette equipped with 22 10L Niskin bottles. Four to seven L of seawater was filtered onto 47 mm polycarbonate membranes (0.4 µm porosity) under slight overpressure supplied by filtered air (0.4 µm). The filters were rinsed with Milli-Q grade water (<5 mL) to remove sea salt, dried (50°C) and stored in Petri dishes for

later analysis. In the home-based laboratory we performed a total digestion of samples using a tri-acid (0.5 mL HF/1.5 mL HCl/1 mL HNO_3; all Suprapur grade) mixture in closed teflon beakers overnight at 90°C in a clean pressurized room. After evaporation close to dryness samples were re-dissolved into around 13 mL of HNO_3 2%. The solutions were analysed for Ba and other major and minor elements by ICP-QMS (inductively coupled plasma-quadrupole mass spectrometry; X Series 2 ThermoFisher) equipped with a collision cell technology (CCT). To check whether internal standards adequately corrected possible matrix effects, we analysed several certified materials which also served to construct calibration curves. These standards solutions consisted of dilute acid-digested rocks (BHVO, JB-3 and JGB-1), natural riverine water (SLRS-5) and multi-element artificial solution. Based on analyses of these standards, precision accuracy and reproducibility are better than ± 5%. For more details on sample processing and analysis we refer to Cardinal et al. (2001). Among all elements analysed, particular interest went to Ba and Al. The presence of sea-salt was checked by analysing Na and the sea-salt particulate Ba contribution was found negligible. Average detection limits equal 20 ppb for Al and 0.5 ppb for Ba. Detection limits were calculated as three times the standard deviation on the blank. Biogenic barium (hereafter called excess-Ba or Ba_{xs}) was calculated as the difference between total particulate Ba and lithogenic Ba using Al as the lithogenic reference element (Dymond et al., 1992; Taylor and McLennan, 1985). At most sites and depths the biogenic Ba_{xs} represented >95% of total particulate Ba. Lithogenic Ba reached up to 20% of total particulate Ba at some depths in the upper 80-100 m, mainly at station R-2 and stations north of the Polar Front (i.e., TEW-8, F-L and TNS-1). Vertical profiles of Ba_{xs} concentrations are shown in Figure 10, with most profiles showing the characteristic concentration in mesopelagic waters (2100-1000m).

Based on the mesopelagic particulate biogenic Ba inventories which reflect past remineralisation of exported organic detritus and which are correlated with oxygen consumption, we conclude for the shallow Kerguelen Plateau (~500 m depth) that subsurface remineralisation of exported organic carbon is smaller than at deeper sites (Margin; Polar Front Meander; Polar Front) and most carbon exported from the upper mixed layer will eventually accumulate on the seafloor (Figure 11). At sites with a deeper water column (Margin; Polar Front Meander; Polar Front) the remineralisation of exported organic carbon in the upper 400 m is larger than above the Plateau and may even entirely balance POC export when including its effect in the deeper waters (till 800m). In the latter case carbon sequestration efficiency for depths >800 m would be nil.

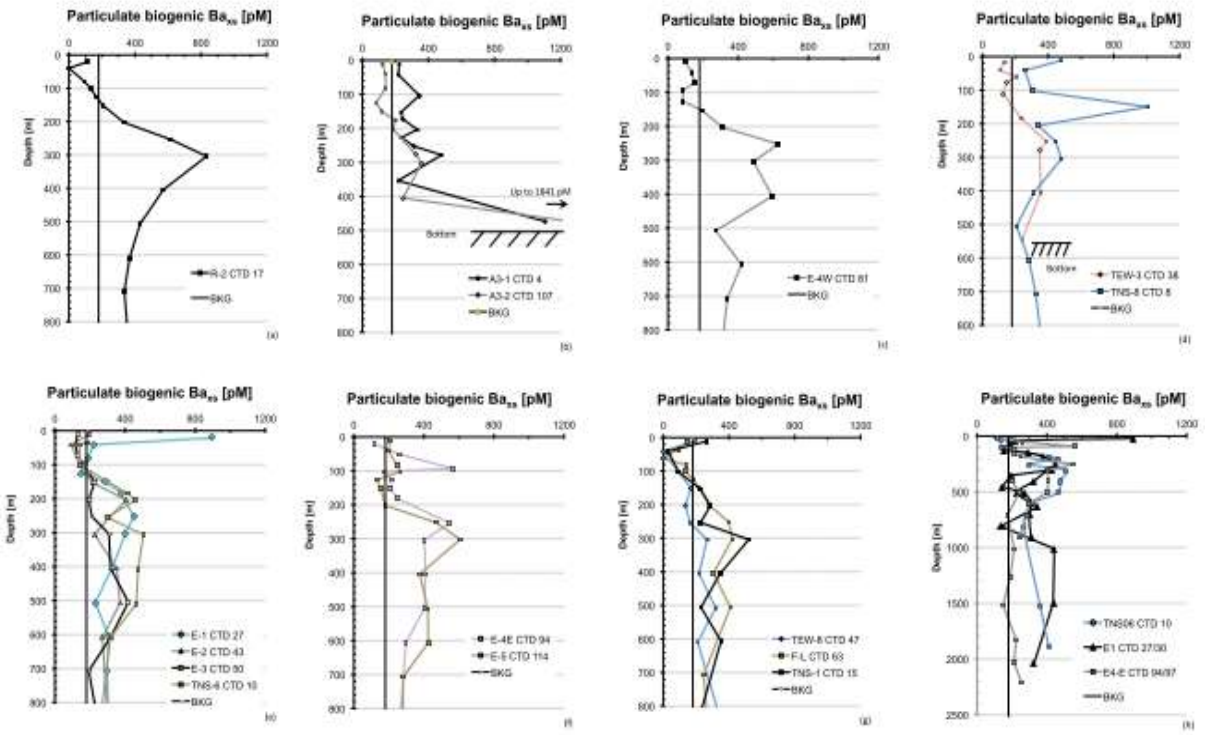

Figure 10: KEOPS 2. Vertical profiles of particulate excess barium (Ba_{xs}) concentrations (pmol L^{-1}).

Comparing the spring (KEOPS 2) and late summer conditions (KEOPS 1) above the Plateau (Figure 12) reveals no significant difference of mesopelagic remineralization efficiency over the season, while magnitude of export and export efficiency of POC in late season largely exceeds the spring values, indicating that about 20% of late season POC export ends up accumulating in the Plateau sediments. These results were published in the KEOPS 2 special issue of Biogeosciences (Jacquet et al., 2015).

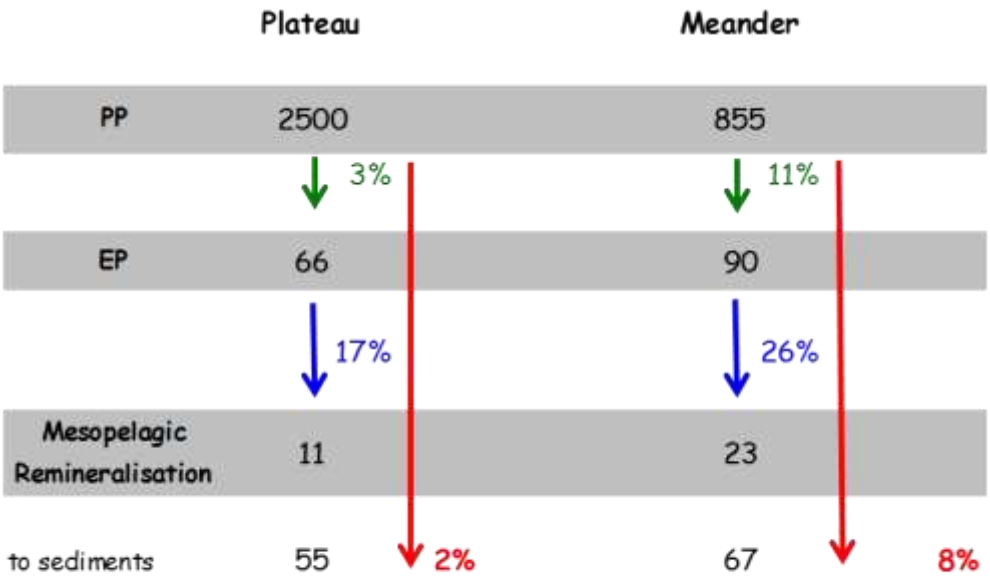

Figure 11: KEOPS 2 expedition, spring 2011. Overview of average carbon fluxes (in mgC m-2 d-1) above the shallow plateau (500 m depth) and in a meander of the Polar Front (2500 m depth). PP = Net primary production; EP = Export production (from ^{234}Th deficit) and mesopelagic remineralization (from particulate excess Ba inventories). Numbers next to arrows give the % of C-flux translocated to and transformed in the deep sea.

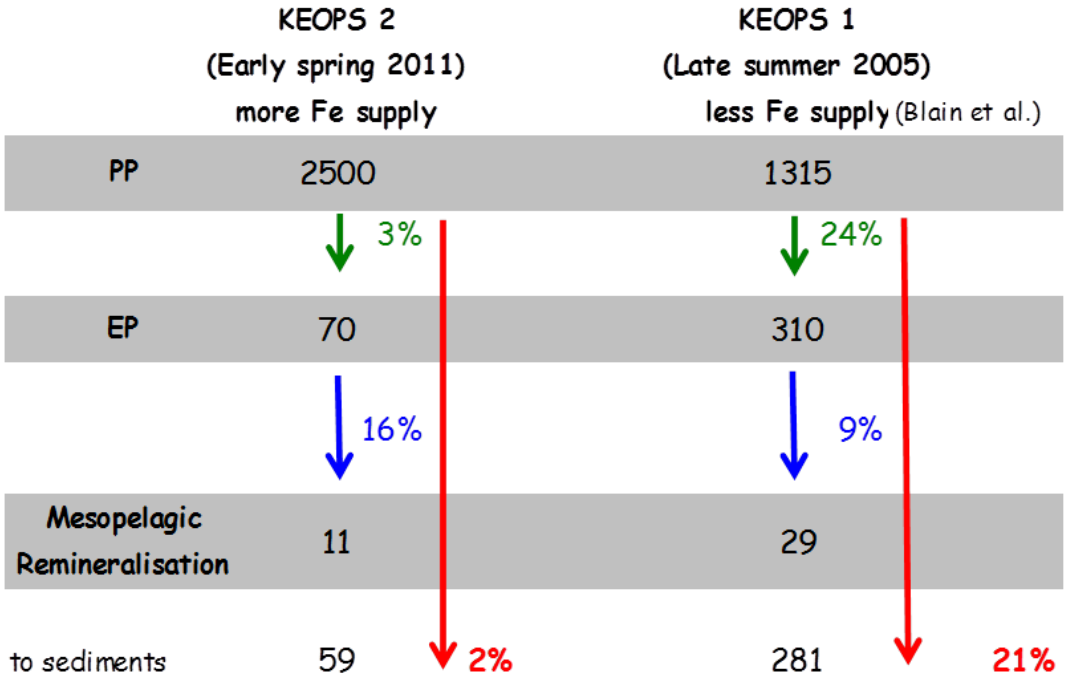

Figure 12: KEOPS 1 & 2 expeditions. Carbon fluxes (mgC m^{-2} d^{-1}) above the shallow (500m) Kerguelen plateau. Comparison of a spring (KEOPS 2) and summer (KEOPS 1) situation. PP = primary production; EP = Export production (from ^{234}Th deficit) and mesopelagic remineralization (from particulate excess Ba inventories). Numbers next to arrows give the % of C-flux translocated to and transformed in the deep sea.

3.1.2. Peer-reviewed publications associated with Topic 1

1. Bowie A.R., F. B. Griffiths, **F. Dehairs** and T.W. Trull, 2011. Oceanography of the subantarctic and polar frontal zones south of Australia during summer: setting for the SAZ-Sense study. *Deep-Sea Research II,* 58, 2059-2070.
2. Bowie A.R., T.W. Trull and **F. Dehairs**, 2011. Estimating the Sensitivity of the Subantarctic Zone to Environmental Change: the SAZ-Sense project. *Deep-Sea Research II*, 58, 2051-2058.
3. **Cavagna A.-J.**, M. Elskens, F.B. Griffiths, **F. Fripiat**, S.H.M. Jacquet, K.J. Westwood and **F. Dehairs**, 2011. Contrasting regimes of production and potential for carbon export in the SAZ and PFZ south of Tasmania. *Deep-Sea Research II,* 58, 2235-2247.
4. **Cavagna A.-J.**, **F. Fripiat**, **F. Dehairs**, D. Wolf-Gladrow, B. Cisewski, N. Savoye, **L. André** and D. Cardinal, 2011. Silicon uptake and supply during a Southern Ocean iron fertilization experiment (EIFEX) tracked by Si-isotopes. *Limnology & Oceanography,* 56(1), 147-160.
5. Dumont I., **V. Schoemann**, F. Masson, S.H.M. Jacquet and S. Becquevort, 2011. Bacterial remineralisation in epipelagic and mesopelagic waters in Sub-Antarctic and Polar frontal zones south of Tasmania. *Deep-Sea Research II,* 58, 2212-2221.
6. **Fripiat F.**, **A.-J. Cavagna**, **F. Dehairs**, S. Speich, **L. André** and D. Cardinal, 2011. Silicic acid pools dynamics in the Antarctic Circumpolar Current inferred from Si-isotopes. *Ocean Sciences,* 8, 533-547.
7. **Fripiat F.**, K. Leblanc, **A.-J. Cavagna**, M. Elskens, L. Armand, **L. André**, **F. Dehairs** and D. Cardinal, 2011. Summer efficient silicon loop despite contrasted diatom Si-affinity across the Polar Front and SubAntarctic Zone. *Marine Ecology Progress Series,* 435, 47-61.
8. **Fripiat F.**, **A.J. Cavagna**, N. Savoye, **F. Dehairs**, **L. André**, and D. Cardinal, 2011. Isotopic constraints on the Si-biogeochemical cycle of the Antarctic Zone. *Marine Chemistry* 123: 11-22.
9. Gonzalez-Davila M., J.M. Santana-Casiano, R.A. Fine, J. Happell, **B. Delille** and S. Speich, 2011. Carbonate system in the water masses of the Southeast Atlantic sector of the Southern Ocean during February and March 2008. *Biogeosciences,* 8, 1401-1413, doi:10.5194/bg-8-1401-2011.
10. Hassler C.S., **V. Schoemann**, C.A.M. Nichols, E.C.V. Butler and P.W. Boyd, 2011. Saccharides enhance iron bioavailability to Southern Ocean phytoplankton. *Proceedings of the National Academy of Sciences*, 108 (3), 1076-1081, 10.1073/pnas.1010963108.
11. Jacquet S.H.M., **F. Dehairs**, I. Dumont, S. Becquevort, **A.-J. Cavagna** and D. Cardinal, 2011. Twilight zone organic carbon remineralisation in the Polar Front Zone and Subantarctic Zone south of Tasmania. *Deep-Sea Research II*, 58, 2222-2234.
12. Jacquet S.H.M, P.J. Lam, T.W. Trull and **F. Dehairs**, 2011. Carbon export production in the Polar Front Zone and Subantarctic Zone south of Tasmania. *Deep-Sea Research II,* 58, 2277-2292.
13. Petrou K., M.A. Doblin, P.J. Ralph, C.S. Hassler, K. Shelly, **V. Schoemann**, S. Wright and R. van den Enden, 2011. Iron-limitation and high light on

phytoplankton populations from the Australian Sub-Antarctic zone (SAZ). *Deep-Sea Research II*, 58, 2200-2211.

14. Quéguiner B., K. Leblanc, V. Cornet-Barthaux, L. Armand, **F. Fripiat** and D. Cardinal, 2011. Using a new fluorescent probe of silicification to measure species-specific activities of diatoms under varying environmental conditions. Global Change: Mankind-Marine Environment Interactions. *Proceedings of the 13th French-Japanese Oceanography Symposium* (Ceccaldi H.-J., Dekeyser I., Girault M., and Stora G., Eds.), Springer Dordrecht, Heidelberg, London, New York, pp. 283-287.
15. **de Brauwere A., F. Fripiat**, D. Cardinal, **A.-J. Cavagna**, **L. André** and **M. Elskens**, 2012. Isotopic model of oceanic silicon cycling: the Kerguelen Plateau case study. *Deep-Sea Research I,* 70, 42-59.
16. **Fripiat F.**, **A.-J. Cavagna**, **F. Dehairs**, **A. de Brauwere**, **L. André** and D. Cardinal, 2012. Processes controlling Si-isotopic composition in the Southern Ocean for an application in paleoceanography. *Biogeosciences,* 9, 2443–2457.
17. Meiners, K.M., **M. Vancoppenolle**, S. Thanassekos, G. S. Dieckmann, D. Thomas, **J.-L. Tison**, K. R. Arrigo, D. Garrison, A. McMinn, D. Lannuzel, P. van der Merwe, K. Swadling, W.O. Smith, I. Melnikov and B. Raymond, 2012. Chlorophyll a in Antarctic sea ice from historical ice core data. *Geophysical Research Letters*, 39, 2012.
18. **Cavagna A.-J.**, **F. Dehairs**, S. Bouillon, V. Woule-Ebongué, F. Planchon, **B. Delille** and I. Bouloubassi, 2013. Water column distribution and carbon isotopic signal of cholesterol, brassicasterol and particulate organic carbon in the Atlantic sector of the Southern Ocean. *Biogeosciences*, 10, 2787-2801, doi: 10.5194/bg-10-2787-2013.
19. **Fripiat F.**, **J.-L Tison**, **L. André**, D. Notz and **B. Delille**, 2013. Biogenic silica recycling in sea ice inferred from Si-isotopes: constraints from winter Arctic first-year sea ice. *Biogeochemistry*, doi:10.1007/s10533-013-9911-8.
20. Planchon F., **A.-J. Cavagna**, D. Cardinal, **L. André** and **F. Dehairs**, 2013. Late summer particulate organic carbon export from mixed layer to mesopelagic twilight zone in Atlantic sector of Southern Ocean. *Biogeosciences,* 10, 803-820.
21. Bakker D.C.E., H.W. Bange, N. Gruber, T. Johannessen, R.C. Upstill-Goodard, A.V. Borges, **B. Delille**, C.R. Löscher, S. W.A. Naqvi., A.M. Omar and M Santana-Casiano, 2014. Air-sea interaction of natural-lived Greenhouse gases (CO2, N2O, CH4) in a changing climate, In: Ocean-Atmosphere interaction of gases and particles (P.S Liss and M.T. Johnson, Eds.), pp113-169, Springer Earth System Sciences, Springer.
22. Closset I., M. Lasbleiz, K. Leblanc, B. Quéguiner, **A.-J. Cavagna**, **M. Elskens, J. Navez** and D. Cardinal, 2014. Seasonal evolution of net and regenerated silica production around a natural Fe-fertilized area in the Southern Ocean estimated with Si isotopic approaches. *Biogeosciences,* 11, 5827-5846.
23. **Fripiat F.**, D.M. Sigman, S.E. Fawcett, P.A. Rafter, M.A. Weigand and **J.-L. Tison**, 2014. New insights into sea ice nitrogen biogeochemical dynamics from nitrogen isotopes. *Global Biogeochemical Cycles*, 28, 115-130, 10.1002/2013GB004729. doi:10.1002/2013GB004729.

24. González M. L., V. Molina, L. Florez-Leiva, L. Oriol, **A. J. Cavagna**, **F. Dehairs**, L. Farias and C. Fernandez, 2014. Nitrogen fixation in the Southern Ocean: a case of study of the Fe-fertilized Kerguelen region (KEOPS II cruise). *Biogeosciences-Discussion,* 11, 17151–17185.
25. **Cavagna A. J.**, **F. Fripiat**, **M. Elskens**, **F. Dehairs**, **P. Mangion**, L. Chirurgien, I. Closset, M. Lasbleiz, L. Flores–Leiva, D. Cardinal, K. Leblanc, C. Fernandez, D. Lefèvre, L. Oriol, S. Blain and B. Quéguiner, 2015. Biological productivity regime and associated N cycling in the vicinity of Kerguelen Island area, Southern Ocean. *Biogeosciences,* 12, 6515-6528.
26. **Dehairs F.**, **F. Fripiat**, **A.-J. Cavagna**, T.W. Trull, C. Fernandez, D. Davies, **A. Roukaerts**, **D. Fonseca Batista**, F. Planchon and **M. Elskens**, 2015. Nitrogen cycling in the Southern Ocean Kerguelen Plateau area: Evidence for significant surface nitrification from nitrate isotopic compositions. *Biogeosciences,* 12, 1459-1482.
27. **Fripiat F.**, **M. Elskens**, T. Trull, S. Blain, **A.-J. Cavagna**, C. Fernandez, **D. Fonseca-Batista**, F. Planchon, P. Raimbault, **A. Roukaerts** and **F. Dehairs**, 2015. Significant mixed layer nitrification in a natural iron-fertilized bloom of the Southern Ocean. *Global Biogeochemical Cycles,* 29, 1929-1943.
28. Laurenceau-Cornec E. C. , T. W. Trull, D. M. Davies, S. G. Bray, J. Doran, F. Planchon, F. Carlotti, M.-P. Jouandet, **A.-J. Cavagna**, A. M. Waite and S. Blain, 2015. The relative importance of phytoplankton aggregates and zooplankton fecal pellets to carbon export: insights from free-drifting sediment trap deployments in naturally iron-fertilised waters near the Kerguelen Plateau. *Biogeosciences*, 12, 1007-1027.
29. Jacquet S. H. M., **F. Dehairs**, D. Lefèvre, **A.-J. Cavagna**, F. Planchon, U. Christaki, L. Monin, **L. André**, I. Closset and D. Cardinal, 2015. Early season mesopelagic carbon remineralization and transfer efficiency in the naturally iron-fertilized Kerguelen area. *Biogeosciences,* 12, 1713-1731. **Moreau S.**, B. Mostajir, S. Bélanger, I.R. Schloss, **M.** Vancoppenolle, S. Demers and G.A. Ferreyra, 2015. Climate change enhances primary production in the western Antarctic Peninsula. *Global Change Biology* 21(6):2191-2205.
30. Pasquer B., N. Metzl, **H. Goosse** and C. Lancelot, 2015. What drives the seasonality of air-sea CO_2 fluxes in the ice-free zone of the Southern Ocean: a 1D coupled physical-biogeochemical model approach. *Marine Chemistry,* 177, 554-565.
31. Planchon F., **D. Ballas**, **A.-J. Cavagna**, A.R. Bowie, D. Davies, T.W. Trull, E. Laurenceau, P. van der Merwe and **F. Dehairs**, 2015. Carbon export in the naturally iron-fertilized Kerguelen area of the Southern Ocean based on the 234Th approach. *Biogeosciences*, 12, 3831-3848.
32. Trull T.W., D. Davies, **F. Dehairs**, **A.-J. Cavagna**, M. Lasbleiz, E.C. Laurenceau-Cornec, F. D'Ovidio, F. Planchon, B. Quéguiner and S. Blain, 2015. Chemometric perspectives on plankton community responses to natural iron fertilisation over and downstream of the Kerguelen Plateau in the Southern Ocean. *Biogeosciences,* 12, 1029-1056, doi:10.5194/bg-12-1029-2015.

33. van der Merwe P., A. Bowie, F. Quéroué, L. Armand, S. Blain, F. Chever, D. Davies, **F. Dehairs**, F. Planchon, G. Sarthou, A.T. Townsend and T.W. Trull, 2015. Sourcing the iron in the naturally-fertilised bloom around the Kerguelen Plateau: particulate trace metal dynamics. *Biogeosciences,* 12, 739–755.
34. **Lemaitre N.**, H. Planquette, F. Planchon, **F. Dehairs**, P. van der Merwe, A. Bowie, T.W. Trull, C. Bollinger, M. Le Goff, E. Grossteffan, 2016. Impact of the natural Fe-fertilization on the magnitude, stoichiometry and efficiency of PN, BSi and PFe export fluxes, *Deep-Sea Research, I,* 117, 11-27.

3.2. TOPIC 2: THE PHYSICAL-BIOLOGICAL CONTROLS OF SEA ICE ON BIOGEOCHEMICAL FLUXES BETWEEN ATMOSPHERE AND OCEAN

3.2.1. Primary production and nutrient cycling in Antarctic pack ice: the SIPEX 2 expedition (Sep.-Nov. 2012)

Sea ice algae can contribute significantly to the total annual primary production in ice-covered waters (Saenz and Arrigo, 2014) and have been suggested to play a key role in feeding pelagic herbivores like krill, especially during winter when food in the water column is scarce (Atkinson et al., 2008; Flores et al., 2012; Kottmeier and Sullivan, 1987; McMinn et al., 2006). Therefore the sea ice environment and sea ice algae are pivotal in structuring Antarctic marine ecosystems (Constable et al., 2014). Primary production (PP) in Antarctic sea ice has a large spatial and temporal variability with maximum carbon uptake rates recorded in land-fast sea ice exceeding 1 g C m^{-2} d^{-1} (Arrigo et al., 1995; Grossi et al., 1987). Measurements of Antarctic PP have focused primarily on land-fast ice in the Ross and Weddell Seas which differs from pack ice as it generally has a larger biomass accumulation (Arrigo and Thomas, 2004) and algae are usually concentrated in the bottom of the sea ice (Ackley and Sullivan, 1994). Available data on PP in Antarctic pack ice shows much lower rates than land-fast ice, with values ranging between 0 and 60 mg C m^{-2} d^{-1} measured in the Antarctic peninsula area (Kottmeier and Sullivan, 1987). Limited data for late spring and summer is available when sea ice production may be highest. Considering the large spatial and temporal variability for the seasonal pack ice, data on primary production remains extremely scarce (McMinn et al., 2006; Meiners et al., 2012). Therefore, observational estimates of primary production for the entire pack ice ecosystem remain highly uncertain, but are urgently needed to evaluate sea ice algal primary production models (Saenz and Arrigo, 2014).

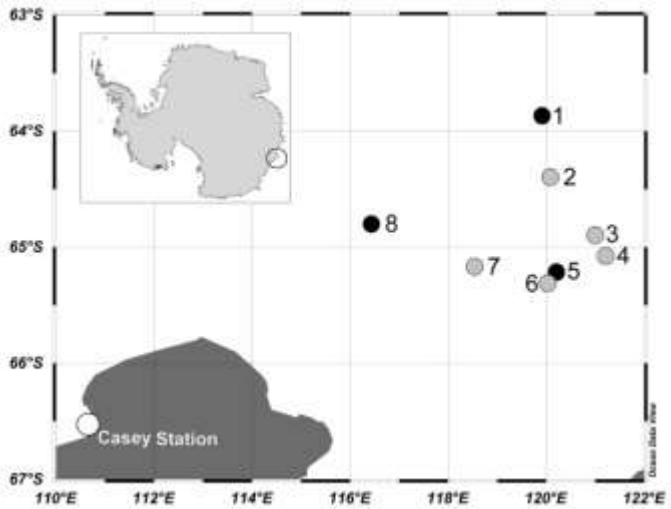

Figure 13: Locations of the ice stations sampled during SIPEX-2. Stations were primary production and nitrogen uptake was measured are shown in black.

To sustain growth algae require nutrients of which nitrogen is one of the main elements. The nitrogen needs of organisms can be satisfied via consumption of different N-substrates (nitrate (NO_3^-), nitrite (NO_2^-), ammonium (NH_4^+) and dissolved

organic nitrogen (DON)) and are recycled through the microbial food web. Several studies report an active nitrogen cycle within sea ice, with high turnover for the fixed nitrogen pools (Cozzi, 2008; Fripiat et al., 2015; Guglielmo et al., 2000; Harrison et al., 1990; Kristiansen et al., 1998; Priscu et al., 1990; Rysgaard et al., 2007). However our understanding of the nitrogen cycle in sea ice is still incomplete due to the difficulties in accessing, sampling and incubating sea ice samples. Rysgaard et al. (2007) found that the presence of anoxic microsites can allow denitrification activity to take place in Artic sea ice while nearby sites can have supersaturated O_2 conditions. More recently Fripiat et al. (2014) showed that based on nitrate isotopic signatures in sea ice, nitrification can be a substantial source of nitrate in the ice as a result of strong remineralisation. Data on assimilation rates of different nitrogen substrates is scarce with only few studies available concerning Antarctic sea ice (Cozzi, 2008; Kristiansen et al., 1992, 1998).

The present study aimed at improving our knowledge of the nitrogen cycle in Antarctic pack ice by measuring *in-situ* uptake rates for carbon, nitrate and ammonium. An incubation method based on ^{13}C-labelled carbon and two ^{15}N-labelled nitrogen substrates ($^{15}NO_3^-$, $^{15}NH_4^+$) was applied to measure C, N uptake in bottom and internal layers of the sea ice cover.

Sampling was carried out during the 2nd Sea Ice Physics and Ecosystems eXperiment cruise (SIPEX-2; Sep.-Nov. 2012) to the East Antarctic sector (63–66°S, 115-125°E) and as a continuation of SIPEX (2007) (Meiners et al., 2016; Worby et al., 2011). Incubation experiments were conducted between 27th Sept – 20th Oct 2012 (austral spring) on board R/V *Aurora Australis* at five pack ice stations (Station 2, 3, 4, 6 and 7, Figure 13). Work on the ice was done in close partnership with the trace metal group and samples were collected on the trace metal site using a trace metal clean ice corer (Lannuzel et al., in press). Only un-deformed sea ice with a thickness of <1.5 m was sampled for this study, encompassing most of the encountered level sea ice (Williams et al., 2014).

During the SIPEX 2 expedition we applied a new field methodology to assess primary production and uptake rates for various nutrient substrates. Two adjacent ice cores (less than 0.2 m apart) were sampled and 3 different incubation depths were selected (Figure 14). Ice and snow conditions at the different sites are reproduced in Figure 15. Each depth was represented by a 0.15 m long section which was cut-out from the core and cut longitudinally to obtain two subsamples per depth serving as initial and final time step. These subsamples were brought back to the ship laboratories for pre-incubation processing (< 1.5 hours).

The ice sections were crushed using an electric ice crusher and transferred to 1 L transparent, acid cleaned (5 % HCl), polycarbonate Nalgene bottles. Stable isotope tracers (0.5-2 ml in Milli-Q grade water) were added to the crushed ice to initial and final bottles. In nitrogen-limited environments, tracer addition can result in elevated uptake rates due to substrate fertilization (Cochlan and Bronk, 2001; Conway et al., 1976). To adjust the tracer additions to achieve a close to 10 % isotope enrichment, ammonium and phosphate concentrations were measured on board. This was done

on an ice core sampled at the same location prior to the incubation experiment. *In situ* nitrate concentrations were estimated based on phosphate concentrations and assuming a 16/1 nitrate/phosphate ratio (Arrigo, 2005). Exact nitrate concentrations were obtained later in the home-based laboratory using an auto-analyzer (QUAATRO Seal Analytical).

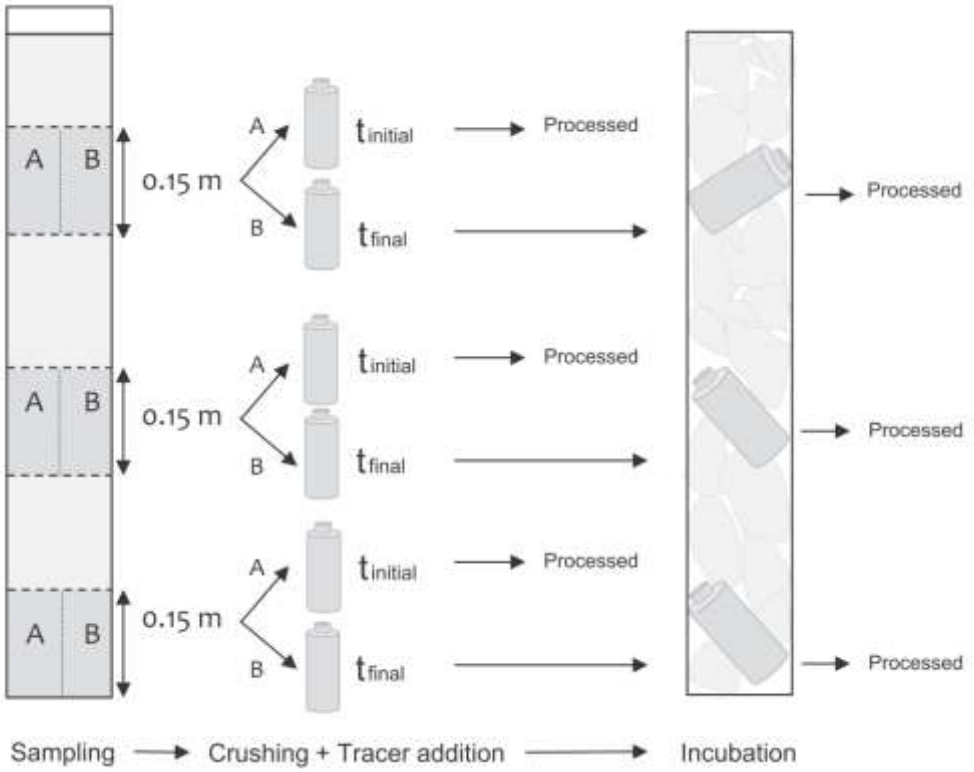

Figure 14: Work scheme for processing ice samples for incubations. Sections of 0.15m were selected and cut out from the ice core and divided longitudinally to obtain two subsamples. The ice was crushed and for each section two bottles were prepared (tinitial and tfinal) and stable isotope tracers added. Bottles serving as tinitial were processed immediately while tfinal bottles were incubated in situ in PMMA cylinders, spaced by pieces of original ice core to reconstruct depth of sampling. After 24 h the bottles were retrieved from the ice and processed in the same manner as tinitial bottles.

Next, the incubation bottles containing the crushed ice samples and tracer solution were shaken well to optimize tracer dispersion. Biological activity for the initial was stopped by adding 200µL saturated $HgCl_2$ solution and the sample was left to melt at room temperature. Meanwhile final bottles were brought back to the ice core site and placed in perspex cylinders. The bottles were spaced with pieces of ice from the original core to reconstruct the original depth of sampling (Figure 15). The cylinders were inserted back in the original ice core holes and left for 24 h incubations. Snow cover was not reconstructed for incubations, but the area that had been cleared from snow was kept as small as possible (approx. 0.5 m^2).

At the end of the incubation the final bottles were retrieved from the ice and treated the same way as the initial bottles. Samples for dissolved inorganic carbon (DIC)

isotopic signatures were collected in 12 ml Exetainers and stored at ambient temperature. Nutrient samples were taken by filtration over 0.2 µm pore size Acrodisc filters and stored at -20°C. Particulate matter was collected by filtration on pre-combusted (450 °C, for 24 hours) GF/F filters (0.7 µm nominal porosity, Whatmann), dried overnight at 50 °C and stored at room temperature (20°C) in the dark in pre-combusted scintillation vials until further processing for isotopic composition at the home-based laboratory.

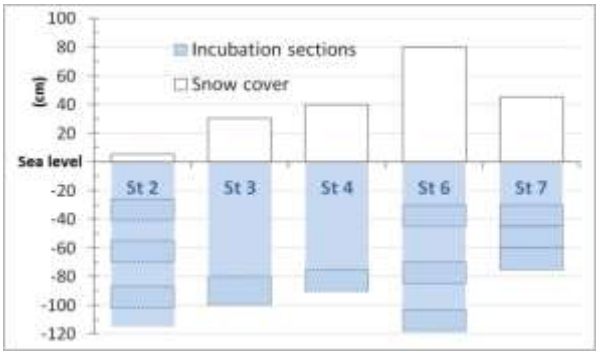

Figure 15: Ice and snow conditions and the different sections incubated at 5 stations during SIPEX 2 in the East Antarctic Sector.

Filters were analysed for particulate organic carbon (POC) and particulate nitrogen (PN) concentrations and their isotopic signatures ^{15}N and ^{13}C using an elemental analyzer – isotope ratio mass spectrometer (EA-IRMS). Uptake rates of C and N were calculated as detailed above in the section on C-assimilation and N-uptake during KEOPS2. Substrate enrichments for nitrate and ammonium were calculated based on *in situ* nitrate or ammonium concentrations and amounts of added tracer.

Sea ice temperature was measured in the field on a dedicated ice core by inserting a temperature probe every 5 cm in hand drilled holes directly after sampling. Bulk salinity of melted ice and chlorophyll α were measured according van der Merwe et al. (2009). Relative brine volumes were calculated based on temperature and salinity measurements following Notz (2005). Calculations for the Rayleigh number (Ra) were done following Notz and Worster (2008) as based on ice temperatures and bulk salinities.

Results show a good reproducibility and a Wilcoxon matched-pairs test confirmed that primary production values for duplicate incubations were not significantly different (p-value = 0.86). Primary production (PP) of the sea ice algae was generally low (Figure 16). At the first ice station (Station 2, 27th Sept), an internal community showed a high PP (1 µmol C L^{-1} d^{-1}), measured in the upper part of the ice (0.33 m below the ice surface). Due to poor weather conditions at Stations 3 and 4, work time on the ice was limited and only the bottom section of the ice cores were incubated while at Station 6 internal PP was low, not exceeding 50 nmol C L^{-1} d^{-1}. Primary production for incubations in the bottom part of the ice were very low (<50 nmol C L^{-1} d^{-1}) at the start of the campaign; 27th Sept – 8th Oct (Stations 2, 3 and 4), followed by

an increase towards the end of the voyage at Stations 6 and 7 (14th and 20th Oct respectively). Rates varied between 150 and 950 nmol C L^{-1} d^{-1} with highest rates observed 0.15-0.30 m above the ice/water interface at Station 7.

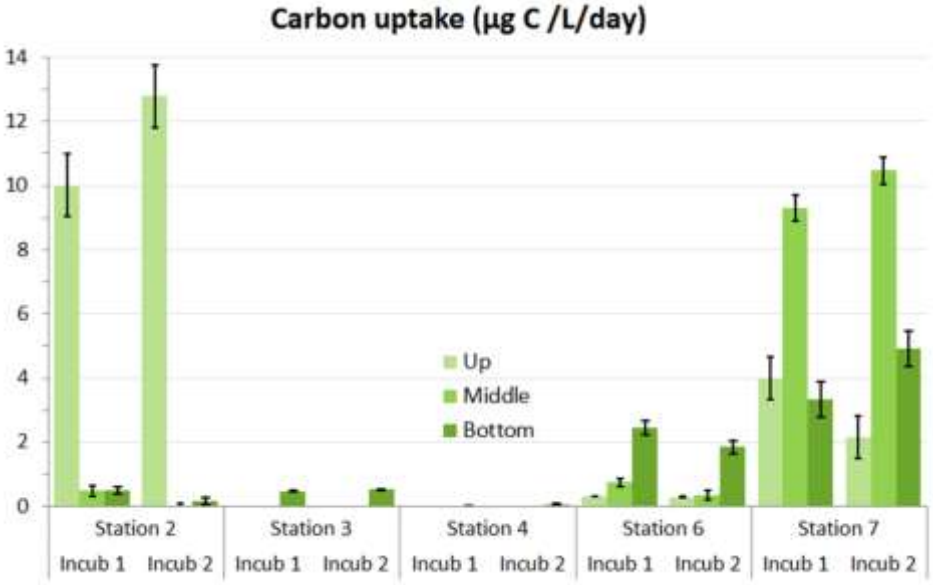

Figure 16: SIPEX 2. Primary production (µg C L^{-1} d^{-1}) was measured in duplicate (incubation 1: $^{15}NO_3^-$ + $H^{13}CO_3^-$, Incubation 2: $^{15}NH_4^+$ + $H^{13}CO_3^-$) and shows good repeatability for all measurements. Error bars are standard deviations from the duplicate incubations.

Depth integrated (rectangular integration over the entire ice thickness) primary production values ranged between <0.19 and 3.5 mg C m^{-2} d^{-1}. The highest PP was observed at Station 2 (6.01 mg C m^{-2} d^{-1}), though this is probably an overestimation because the active internal community was extending over a narrow part of the ice core inducing a bias in the integration approach used. When integrating only over the 0.15 m ice section showing a light green coloration and which was effectively incubated PP values reduce to just below 2 mg C m^{-2} d^{-1}. At Stations 3 and 4, integrated PP was very low due to low rates at the bottom of the ice and the absence of data on internal PP. A gradual temporal increase towards higher PP rates was observed at Stations 6 and 7, reaching an average of 0.91 and 3.33 mg C m^{-2} d^{-1}, respectively.

For nitrogen, nitrate was usually the preferred substrate with exception of the two internal communities (Station 2 and 6). Uptake in the bottom section of Station 6 and all incubated depths at Station 7 showed a clear preference for nitrate (12-35 nmol N L^{-1} d^{-1}) with only minor ammonium uptake (1-3 nmol N L^{-1} d^{-1}) as nitrogen source. The two internal communities at Stations 2 (0.33 m depth) and 6 (0.37 m depth) showed a clear preference for ammonium and uptake rates reached 27 nmol N L^{-1} d^{-1}. At Station 2 nitrate uptake still accounted for roughly 30% of the nitrogen uptake (13.1 nmol N L^{-1} d^{-1}) and for this internal community also PP was high. Station 6 in contrast had only little nitrate uptake and PP.

Results show an increase of primary production over the one month course of the expedition (Figure 16), starting in early spring. Between the first and last sampling station, daylight length increased by approximately 3h. Although we observe an increase in C fixation rates with progress of the season this was moderate and typical for pre-bloom conditions. However, we suspect there was light limitation due to extensive snow cover, which at one station reached up to 80cm (Figure 15). Such thick snow cover would essentially screen off incoming light, considering that a 20cm increase in snow thickness may reduce light transmission by 80% (Arrigo et al., 2003). In contrast it is also observed that bottom communities in sea ice can be extremely shade adapted (Kristiansen et al., 1992).

High snow cover could explain the low primary production rates in early spring during SIPEX-2, possibly reducing and delaying the ice algae bloom. Although primary production in Antarctic pack ice is low it can still contribute significantly to the overall primary production in ice-covered waters. Indeed, since the sea ice phytoplankton production starts early in the season, compared to pelagic production, it is of critical importance for pelagic food webs. If future snowfall on Antarctic sea ice is to increase as models suggest (Hunt et al., 1995), this could not only alter sea ice physics but also the extent and timing of ice algae blooms with potential flow-on effects to higher trophic levels.

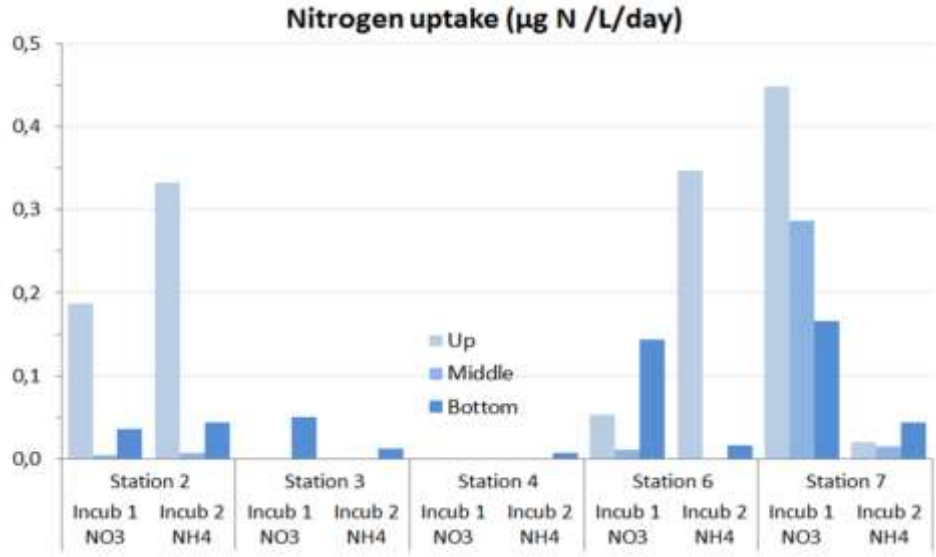

Figure 17: SIPEX 2. Uptake rates for nitrogen (nitrate and ammonium) at 5 stations during in the East Antarctic Sector. Except for some internal communities, nitrate seems the preferred nitrogen source.

The observed nitrogen-uptake preferences suggest the existence of two different regimes: (1) nitrate based 'new' production at the bottom of the ice cover, due to nutrient-replete conditions at the ice-water interface, and characteristic for pre-bloom conditions and (2) sea ice interior primary production supported by regenerated nitrogen sources. Most likely an active microbial loop used detrital matter as a food

source to produce regenerated nitrogen substrates. Based on POC:PN and POC:Chl α ratios a large portion of particulate matter in the ice appeared to be detritus.

Overall we observed a clear preference for nitrate uptake compared to ammonium (Figure 17). Especially at the water/ice interface, nitrate is the main substrate, while high rates for ammonium uptake were observed for some internal communities. The C/N uptake ratio was in most cases larger than the Redfield-ratio, with an average value of 19.4. Such high values have been reported earlier for Antarctic sea ice (Lipizer et al., 2000). Other possible source of nitrogen such as nitrite, Urea and amino acids were not measured.

Nitrate isotopic signatures

Nitrate isotopic signals in the water column showed little variation and were close to deep ocean values ($\delta^{15}N$ = 4.8‰, $\delta^{18}O$ = 2.4‰). However the data does not seem to follow a 1:1 slope but shows a stronger fractionation for oxygen resulting in a steeper slope which indicates that nitrification plays an important role the ice covered water column. In the sea ice, slightly higher values of $\delta^{15}N$ = 5.5‰ were observed at the water-ice interface and which increased to 14‰ in the center and top layers of the ice cores. Increasing $\delta^{15}N$ values coincide with an increase of $\delta^{18}O$ and decrease of nitrate concentration. This suggests that nitrate assimilation or denitrification could be one of the main processes explaining the observed isotopic variations. Segregating these two processes with only the nitrate isotopy tool is difficult, however anoxic conditions and denitrification have been observed in sea ice before (Rysgaard et al., 2008). Further analysis of the data is required to better constrain the processes.

3.2.2. Year-round monitoring of macro-nutrients, S, and C cycling in Antarctic landfast ice: the YROSIAE study (Nov. 2011 – Dec. 2012)

General overview of YROSIAE

YROSIAE (Year Round survey of Ocean-Sea Ice-Atmosphere Exchanges) survey was carried out in McMurdo Sound (Antarctica) from Nov. 2011 to Dec. 2012. YROSIAE aimed at a year-round survey of land-fast sea ice focusing on the study of sea ice physics and biogeochemistry in order to (1) better understand and budget exchanges of energy and matter across the ocean-sea ice-atmosphere interfaces during sea ice growth and decay and (2) quantify their potential impact on fluxes of climate gases (CO_2, DMS, CH_4, N_2O) to the atmosphere and on carbon and nutrients export to the ocean. Survey was carried out nearby Scott Base, the New Zealand permanent Antarctic base located in McMurdo Sound (Ross Sea) in collaboration with T. Haskell (Industrial Research Limited), P. Langhorne (University of Otago) and Antarctica New Zealand. Scott Base is a coastal Antarctic base, with easy access to sea ice and winter-over possibilities. McMurdo Sound is one of the best documented Antarctic Coastal areas, with adequate sea ice cover and sustained biological activity that allow process studies of sea ice biogeochemistry.

The research methodology was highly trans-disciplinary and combined field investigations (partner 2, 5 and 6), and modeling work (partner 4). The sampling

strategy was designed to match modeling constrains. Ice cores, seawater, brines and exported material were collected at regular intervals about 1 km off Cape Evans from Nov. to Dec. 2011 and from Sep. to Dec. 2012 in trace-metal clean conditions.

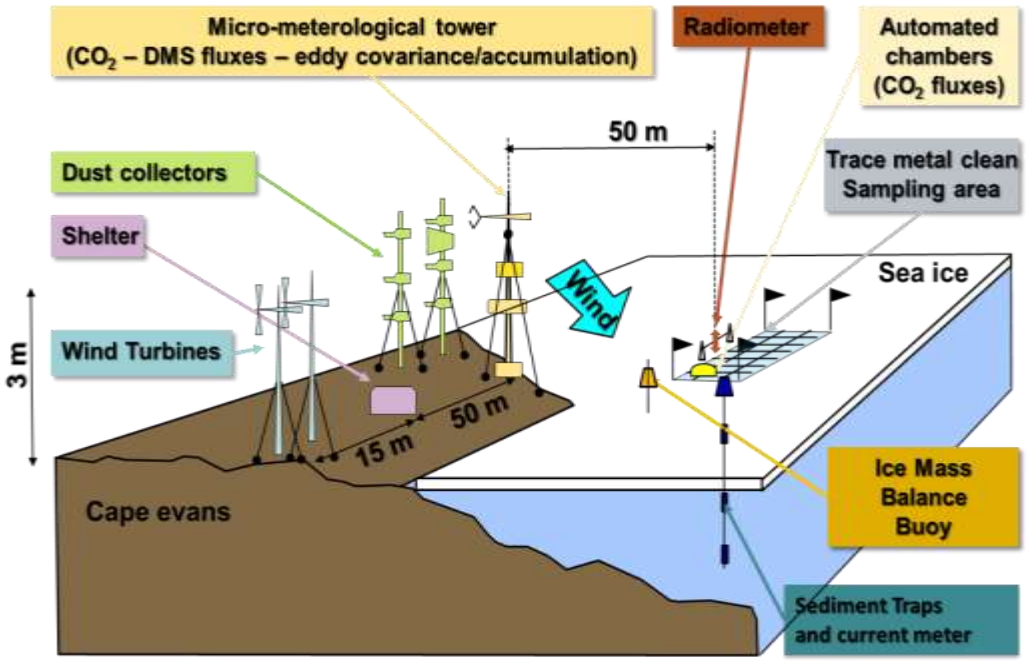

Figure 18: YROSIAE sampling site (1st phase; Nov. 2011 to Sep. 2012). During the 2nd phase (Oct. to Dec. 2012) the shore material was moved onto the newly formed sea ice.

Air-sea ice exchanges were mainly investigated using a tower for micro-meteorological measurements. The tower was equipped for measurement of air-ice CO_2 fluxes by eddy-covariance and DMS fluxes using the gradient flux method (collaboration with T. Papakyriakou, CEOS, University of Manitoba, Canada) together with meteorological and radiation sensors. Power supply of this remote equipment was provided by two wind generators and one methanol fuel-cell. The tower was first deployed from Nov. 2011 to Aug. 2012 on Cape Evans shore to capture fluxes during sea ice decay and early growth (Figure 18). The tower suffered some power and data shortage, but ran satisfactorily from Nov. 2011 to July 2012. The tower was also measuring air temperature and moisture. In September 2012 the tower was moved on the ice, next to the main sampling site to provide robust assessment of fluxes over the ice sampling site, a better wind cover and avoid potential bias from seals respiration. In addition automatic chambers for air-ice CO_2 fluxes were deployed from Nov. 2011 to Dec. 2012 and from Sep. to Dec. 2012. Finally a radiometer for long and short wave coming in and out was also deployed together with the automatic chambers.

Two dust-collecting towers have been set up on Cape Evans Shore from Nov. 2011 to Dec. 2012 (Figure 18) to provide a record of a full suite of trace metal and dust

measurements at different levels above the ground. These will be used to characterize the origin, nature and availability of these compounds that are biologically active in the sea ice. Sea ice ocean exchanges are investigated based on vertical profiles in the water column (down to 30 m) of the parameters described above and carried out synchronously to ice collection. Three sediment traps were deployed from 20 to 70 m deep from Sep. to Dec. 2012 (collaboration with G. Dieckmann, AWI and H. de Baar, NIOZ) to collect particulate organic matter.

Finally, an "Ice-T" ice mass balance buoy was deployed from Sep. to Dec. 2012 (Figure 18) to provide continuous measurements of ice temperature and ice accretion or melting, both at the ice-ocean and the ice-atmosphere interfaces (F. Vivier, LOCEAN, Paris VI). Following the target of Topic 2.1., the sampling strategy was carefully adapted and designed in order to improve our understanding of the key biogeochemical processes to be implemented in the biogeochemical sea ice model (Topic 3, partner 4) and allow its adequate validation for future prognostic applications.

Sea ice conditions

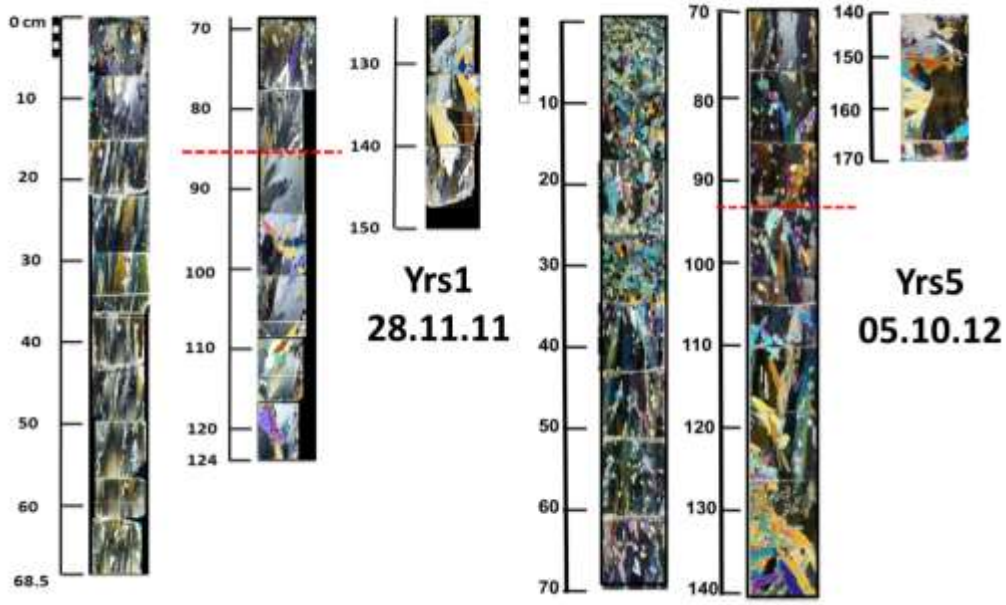

Figure 19: Example of ice textures in Evans Cove landfast sea ice. YRS1 is Station 1 sampled in November 2011 and YRS5 is Station 5, sampled in October 2012. The stippled red line shows the transition from columnar ice to platelet ice. Note the presence of granular ice and probably rafting in the first 30 cm of YRS5.

Sea ice textures are fairly homogeneous from station to station (Figure 19), confirming that we adequately documented a unique time series, with little spatial variability. Apart from apparently more turbulent initial conditions for the build-up of the sea ice cover in 2012 (unusually thick granular ice and potential rafting in the top 30 cm), the sea ice cover always shows columnar ice underlain by platelet ice, with a spatially and temporally repeated transition at about 90 cm. The occurrence of platelet ice in Evans Cove was unexpected from previous studies which suggested

that the area is relatively well protected from Ice Shelf Water intrusion in provenance of the McMurdo ice shelf front. Figure 20 shows the evolution of basic sea ice physical properties as interpolated from discrete profiles from Aug. to Dec. 2012 (a) and as mean ice cover value per station (b) both for Nov.-Dec. 2011 (black squares) and Aug.-Dec. 2012 (black dots). Due to the limited snow cover (few cm) initial surface temperatures are very low. As clearly seen on discrete profiles (Carnat et al., 2014), ice temperatures first warm up in the top half (4 to 5), then in the bottom half (5 to 6), then in the top half again, and becomes near isothermal at the end of the period. Salinity shows a classical C-shaped profile, with a sharp minimum at the columnar-platelet boundary (80-100 cm). Brine volume crosses the 5% permeability threshold throughout the ice cover from Julian day 320 (mid-November). For all physical variables, mean ice cover values at the end of the period are clearly consistent from year to year (Figure 20b).

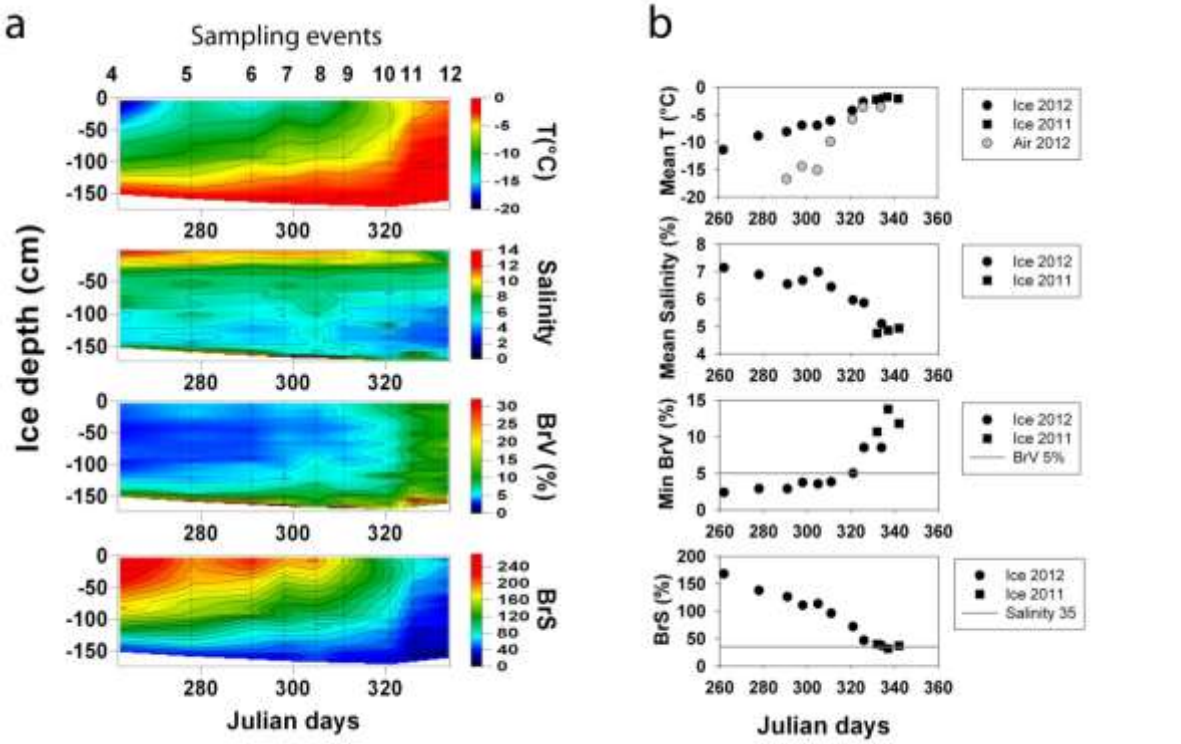

Figure 20: Evolution of sea ice physical properties at Cape Evans. a) interpolation of station profiles from August to December 2012 and b) mean ice cover values for Nov.-Dec. 2011 (black squares) and Aug.–Dec. 2012 (black dots). BrV represent the brine volume and BrS the brine salinity.

Biomass and macro-nutrients cycling

As classically observed in landfast ice, most of the biomass (> 90%) is concentrated in the bottom centimeters in spring as well as strand algal communities attached underneath the ice floe and being directly in contact with seawater (Figure 21), providing a habitat that is both stable and continuously supplied in nutrients. As a comparison, the integrated particulate organic carbon peaks at ~ 4700 mg m^{-2} in November, a value comparable to a productive water column yet contained within a

much smaller volume (tens of meters vs. few centimeters) (Duforet-Gaurier et al., 2010). The increase in biomass follows the increase in solar radiation in spring (Figure 22), and is mainly supported by large-diatom cells (>10µm), followed by flagellates and a minor contribution of dinoflagellates (Carnat et al., 2014).

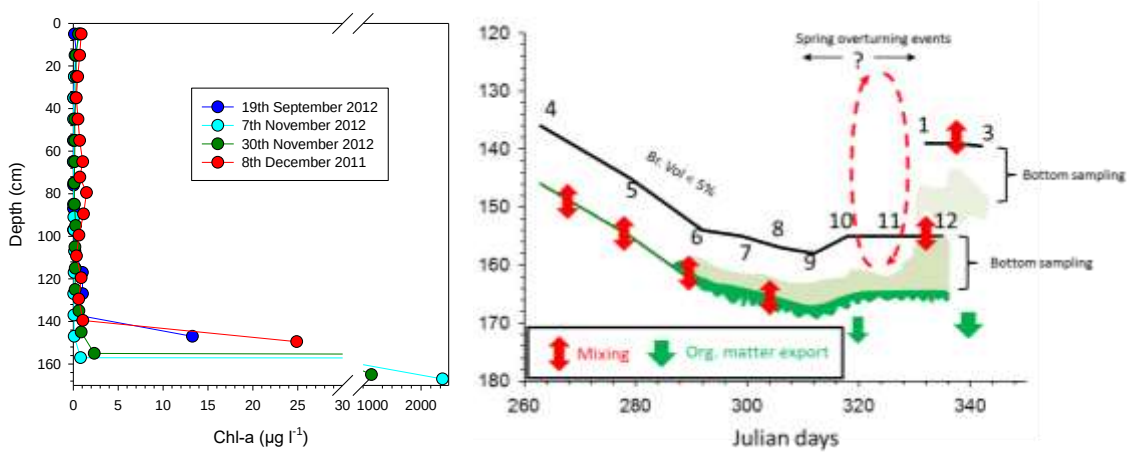

Figure 21: Selected vertical profiles of chl-a (left) and conceptual scheme showing biomass distribution at the bottom of sea ice (right). In the right panel, only the bottom 10 cm are shown with the evolution of sea ice thickness.

Biomass decreases sharply in two steps, first between stations 10 and 11, and second between stations at the end of 2012 and 2011. We believe that the main trigger of this loss in biomass is the bottom melting, destroying the habitat and releasing biomass in the water column (Figures 21 and 22).

Intriguingly, macro-nutrients (nitrate, nitrite, ammonium, phosphate, and silicic acid) are not depleted over the course of the bloom, as expected in aquatic productive ecosystems, but they are accumulated (Figure 22). To reach such concentrations, nutrients must be trapped within sea ice. An initial coupling between brine convection and an excess in assimilation over remineralization is able to build a large trapped pool of organic/biogenic matter (POC, PON, and $bSiO_2$) (between stations 5 and 6). Depending of the spatial (de)coupling between assimilation and remineralization, two scenario can explain such accumulations in nutrients:

(1) Over time the progressive bacterial colonization combined with algal mortality, cell lysis and sloppy feeding, liberate organic matter and promote remineralization, including nitrification (Fripiat et al., 2014, 2015). The resulting transformation of such high concentrations of organic matter into nutrients can explain the nutrient concentrations well above seawater values (Figure 22). At this stage, remineralization could be in excess of assimilation or a tight balance between remineralization and assimilation could be maintained for a given period of time, as long as the environmental conditions are relatively stable. An imbalance toward more assimilation than remineralization at this stage is not possible, since it would deplete the nutrient pool. We believe that brine convection, resulting from a vertical instability

in the brine density distribution when ice is growing was still ongoing at the bottom of the ice until approximately stations 9-10 (Figure 21). Much higher nutrient concentration than that of seawater could be maintained as long as remineralization was a dominant process, outpacing brine convection. However, the shutdown of brine convection at station 9-10 is able to explain the second increase in nutrient concentration, as the product of remineralization is not removed with brine convection and is accumulated within sea ice. The balance between assimilation and remineralization is able to explain the high nitrate $\delta^{15}N$ and $\delta^{18}O$ observed at the bottom of the ice (up to 25‰).

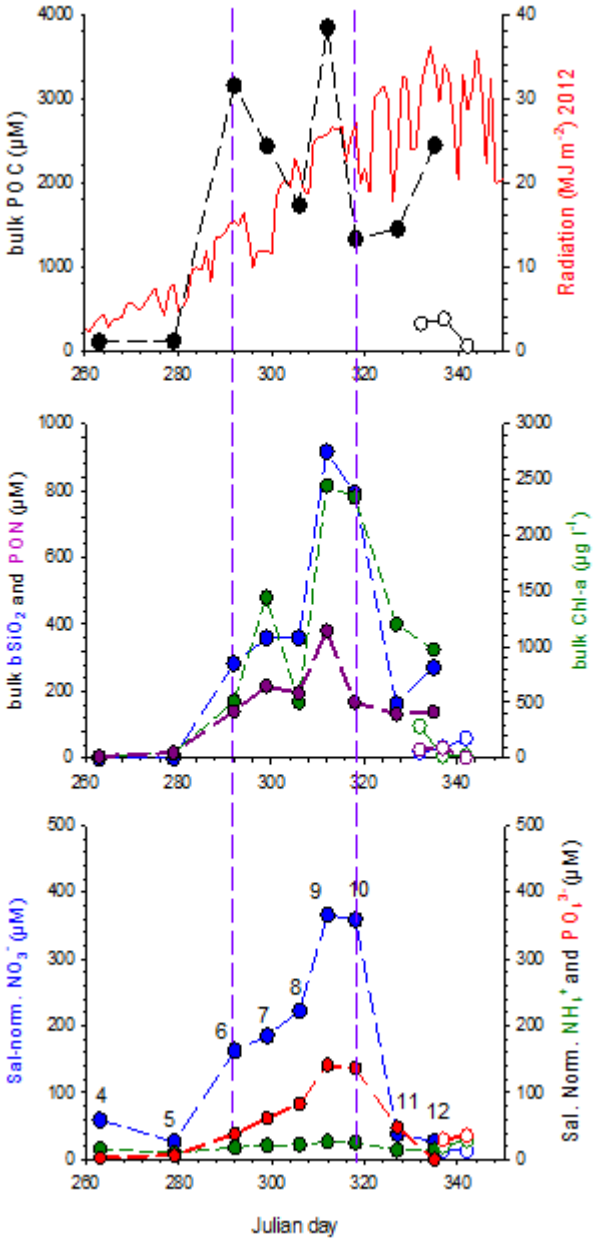

Figure 22: Temporal evolution at the last bottom 10cm of the ice for (upper panel) particulate organic carbon, (mid panel) particulate organic N, chl-a, and biogenic silica, and (lower panel) salinity-normalized nitrate, ammonium, and phosphate. Solar radiation is shown in the upper panel.

Much greater nitrate production (remineralization + nitrification) than consumption (nitrate assimilation) should set the nitrate $\delta^{15}N$ and $\delta^{18}O$ to a value intermediate between newly produced nitrate $\delta^{15}N$ and $\delta^{18}O$ (<12.5 and 1.1‰, respectively) and seawater (5.0 and 2.0 ‰, respectively). Thus, the observed high nitrate $\delta^{15}N$ and $\delta^{18}O$ suggests a balance between nitrate production and consumption, the latter increasing both $\delta^{15}N$ and $\delta^{18}O$ as light-N and O isotopes are preferentially assimilated.

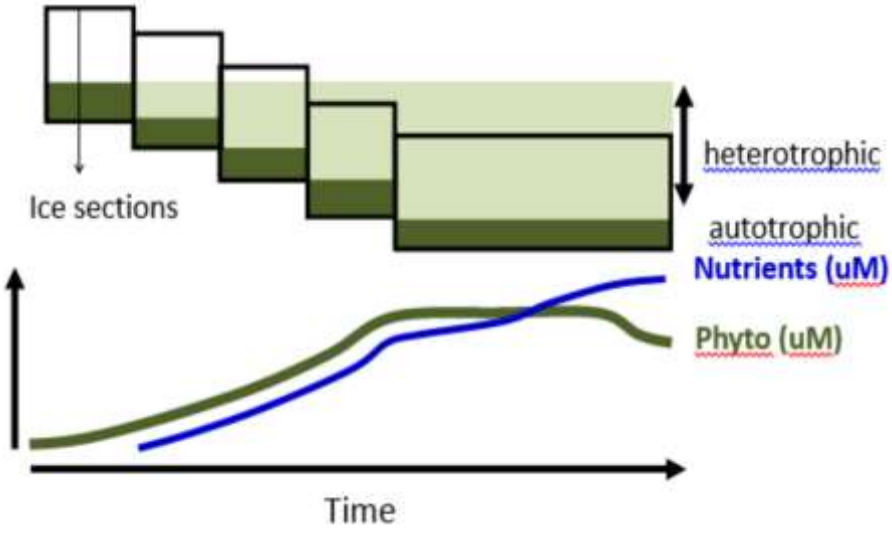

Figure 23: Conceptual scheme showing the growth of sea ice and the sampled bottom ice section (black lined rectangles). At the onset of the bloom, biomass is accumulated at the bottom of sea ice (dark green layer). With the ice growing, this biomass is getting trapped within sea ice, with a switch from autotrophic to heterotrophic growth (light green). At the interface with the ocean, a new autotrophic community is setting place. Overtime, the proportion of heterotrophic layers increases in the sampled ice section (and therefore nutrients increase) and the addition of a new layer of growing algae at each time step increases simultaneously biomass.

(2) The previous scenario implies that both assimilation and remineralization is happening at the same time and location. However, as we sample the last bottom 10cm and biomass accumulation was mainly observed on the last 2-3cm, we cannot rule out a spatial decoupling between assimilation and remineralization (Figure 23). This could imply that the autotrophic growth is mainly occurring at the interface with the ocean. As the ice is growing, this community is getting trapped within the interior of the ice. Harsher conditions and increase in mortality (with the progressive setting of the secondary production) could imply a switch from autotrophic to heterotrophic growth, remineralizing efficiently the large trapped organic matter pool into nutrients. A new community is taking place at the interface with the ocean, implying an increase of biomass with time. As the proportion of the heterotrophic community increase in the sampled ice section (with the ice growth), both biomass and nutrients

progressively increase. Such scenario is more in agreement with NPZD ('Nutrient Phytoplankton Zooplankton Detritus) model as it is difficult to simulate a simultaneous increase in both nutrients and biomass (e.g., as long as there is growing algae, nutrients are depleted), but cannot explain nitrate isotopes as the newly produced nitrate should bear much lower $\delta^{15}N$ and $\delta^{18}O$.

The decrease in nutrients after station 10 can be easily explained, as biomass, with the disappearance of the habitat when the ice is melting (Figures 21 and 22) and the opening of the brine network on the full-thickness of the ice allowing the exchange with both internal nutrients-depleted layers and underlying seawater.

In the following months, we will measure dissolved organic N to have the contribution of dissolved organic matter, as well as finalizing N isotope measurements (particulate and dissolved inorganic N).

DMS and associated compounds

We measured the seasonal and vertical variations of dimethylsulfide (DMS) and its precursor dimethylsulfoniopropionate (DMSP) in sea ice, brine, and under-ice water from station 1 to 3 during the 1st sampling phase and from station 4 to 8 during the 2nd sampling phase. For sea ice, a dedicated ice core was sectioned in 5 cm depth sections and the center part of each section cut into rectangular cuboids. DMS was extracted from the cuboids using the dry-crushing technique (Stefels et al., 2012). In brief, the ice cuboid was weighted and inserted with stainless-steel marbles into an airtight stainless-steel container. The container was then mechanically shaken by fast up and down movements of a homemade crushing device operated with an electric motor. The crushing phase reduced the ice cuboid into a fine ice powder, ensuring a complete release of gas bubbles and brine inclusions from the ice matrix. The container was then hooked up to a traditional purge and trap gas chromatograph system. The gas chromatograph was an Agilent 7890A equipped with a dual flame photometric detector (FPD) and a sulfur-specific DB-1 capillary column. The chromatograph was calibrated using standards prepared from dilution of pure DMS in Milli-Q water. DMSP was measured as DMS after cold alkali cleavage of DMSP into DMS by adding NaOH pellets to the ice powder obtained after crushing and melting overnight.

The bulk sea ice DMS and DMSP concentrations measured (Table 5) are in line with previously reported concentrations in the literature. The results confirm that sea ice is a biome favorable to substantial production of dimethylated sulfur compounds. The maximum DMSP concentration measured in bottom ice during the spring (station 7 – 3865 nM) is the highest ever observed in level Antarctic first-year ice. This is not surprising given the very high biomass observed in bottom ice at station 7(1440 $\mu g.L^{-1}$ of chl-a). DMSP:chl-a ratios are on the other hand relatively small in bottom ice, which is not surprising given that the bottom ice assemblage is largely dominated by diatoms, usually acknowledged as low individual producers of DMSP (Stefels et al., 2007).

Location	Ice Type	Ice Texture[b]	Season	DMSP[c] (nM)	DMS[c] (nM)	Chl *a*[c] (μg/L)	DMS,P[d] sampling Resolution (m)	Reference
Weddell Sea	Pack ice	F+C	Spring	408.9 (4.1–1663.8)	NA	24.8 (3.4–155.7)	0.10 (F.C.)	*Kirst et al.* [1991]
Western Weddell Sea	Pack ice	F+SU+C	Summer	171 (5–2627)	58 (0.5–1430)	5.3 (0.1–28.4)	0.05 (F.C.)	*Tison et al.* [2010]
Bellingshausen Sea	Pack ice	Frozen snow+C	Spring/summer	200 (17–546)	NA	4.6 (0.2–24)	0.15/0.20 (F.C.)	*Turner et al.* [1995]
Prydz Bay	Pack ice	NA	Spring	144 (8–725)	NA	NA	0.10/0.20 (F.C.)	*Curran and Jones* [2000]
Offshore Prydz Bay	Pack ice	NA	Spring	107 (6–787)	NA	4.9 (0.1–41.5)	0.10 (F.C.)	*Trevena et al.* [2000]
Dumont D'Urville Sea	Pack ice	NA	Winter	40 (nd–193)	NA	NA	0.10/0.20 (F.C.)	*Curran et al.* [1998]
Ross Sea	Pack ice	NA	Spring/summer	206.5 (4.4–980.0)	NA	54.4 (1.2–243.3)	0.05/0.20 (B.S.)	*DiTullio et al.* [1998]
Ross Sea	Fast ice	NA	Spring	150.0 (80.9–218.8)	NA	103.7 (38.7–138.5)	0.05/0.20 (B.S.)	*DiTullio et al.* [1998]
Prydz Bay	Fast ice	F+C	Spring/summer	112 (9–1478)	NA	5.6 (0.03–84.8)	0.10 (F.C.)	*Trevena et al.* [2003]
Gerlache inlet	Fast ice	NA	Summer	nd (4.4–450)	NA	(nd–160)	0.10 (F.C.)	*Gambaro et al.* [2004]
Indian sector of SO	Pack/fast ice	NA	Spring	185[e,f] (45–796)	12 (<0.3–75)	NA	0.10 (F.C.)	*Trevena and Jones* [2006]
McMurdo Sound	Fast ice	F+C+P	Spring/summer	87 (<0.3–683)	12 (<0.3–369)	7.6 (0.08–285.4)	0.05 (F.C.)	This study
McMurdo Sound	Fast ice	F+C+P	Winter/spring	76 (<0.3–3865)	7.5 (<0.3–377)	28.4 (0.00–1440.7)	0.05 (F.C.)	This study

[a]Note that the resolution of vertical sampling found in the different studies (0.05, 0.10, and 0.20 m) can affect the reported DMS,P concentrations. Because DMS,P is found in discrete bands within sea ice, the signal can be obscured in case of coarse ice core sectioning. In this study, we report values based on a high vertical sampling resolution (0.05 m). If we had chosen a 0.10–0.20 m vertical sampling resolution, our maximum DMS,P would have been 20–55% lower. Note also that means should not be compared between studies with different sampling strategies. For instance, in *DiTullio et al.* [1998], only the bottom 5–20 cm of ice cores with visible discoloration (and hence important algal biomass) were analyzed, whereas in the other studies referenced in this table, full ice cores were analyzed.
[b]F, frazil ice; C, congelation ice; SU, superimposed ice; P, platelet ice; NA, not available; SO, Southern Ocean.
[c]Mean (range); nd, not determined.
[d]F.C., full core; B.S., bottom sample.
[e]Calculated for ice categories with ice thickness <1.20 m.
[f]Number of cores weighted average.

Table 5: Overview of available Antarctic sea ice DMS,P data sets including the YROSIAE data set.

With the exception of the bottom ice peak and a very localized peak in interior ice (Figure 24), DMSP concentrations are generally small during both sampling phases. This is understandable given the low chl-a concentrations (<2.5 $\mu g.L^{-1}$ of chl-a) (Figure 21) and low percentages of acknowledged high individual DMSP producers (flagellates, dinoflagellates) (Figure 25) observed in most of Evans Cove sea ice layers.

The ice DMS,P cycle at Evans cove during the winter-spring transition of 2012 (2nd sampling phase) is initially driven by ice formation processes. Mixed columnar/platelet ice formation in early May through interactions with ice shelf waters favors the development of strong local DMS,P maxima in interior ice. This is clearly seen in Figure 24 and 26 with a very good correspondence between the depth of the DMS,P maxima and the depth at which the ice texture changes from columnar ice to mixed columnar/platelet ice. First, the formation of platelet crystals incorporates dinoflagellates, usually recognized as individual strong DMSP producers (Stefels et al., 2007) (Figure 25). These dinoflagellates are typically incorporated during the autumnal bloom in the McMurdo Sound, the timing of which corresponded with the formation of the platelet crystals in 2011 and 2012. We suggest platelet crystals could have incorporated the algae via two mechanisms: (1) algae could have become trapped at the base of the ice cover by platelet crystals freezing at the ice-ocean interface by turbulent heat transfer to supercooled McMurdo ice shelf water flowing by, (2) algae could have been transported and incorporated by frazil and/or platelet crystals initially formed at depth in supercooled plumes leaving the McMurdo ice shelf. The absence of loose platelet crystals in the water column in 2011 and 2012, as well as in previous years, is more in favor of growth at the ice-ocean interface.

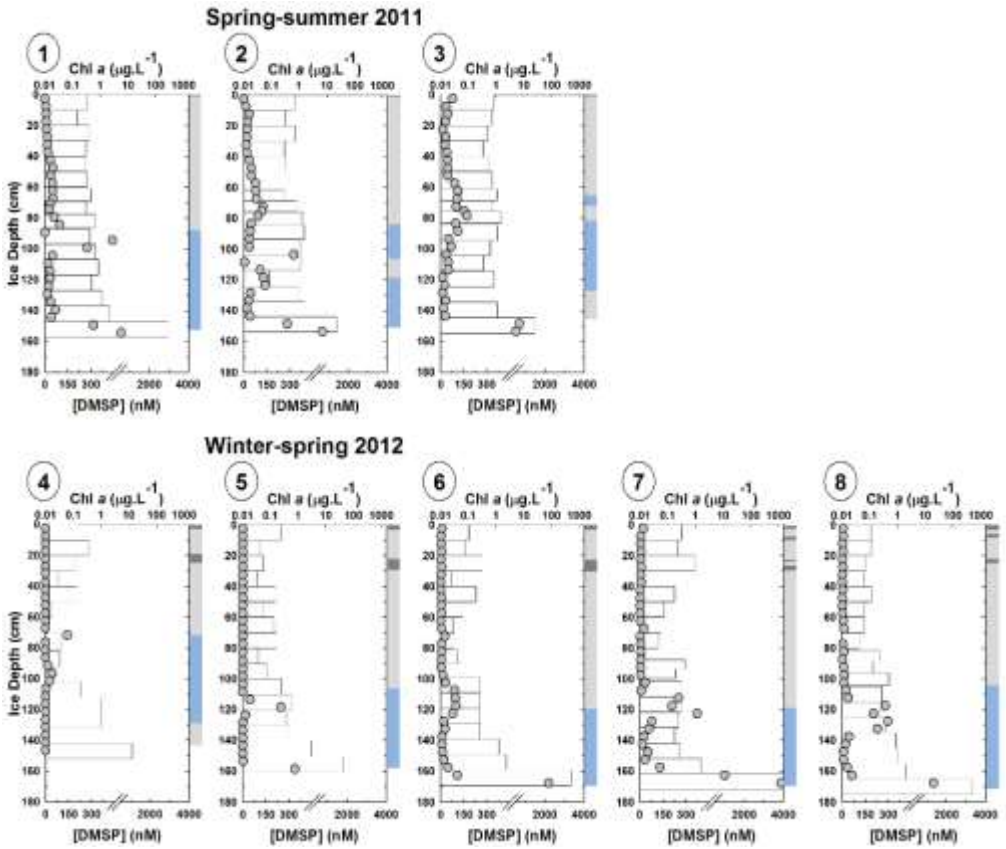

Figure 24: Vertical profiles of DMSP concentrations (gray dots) in the ice during (top) the spring-summer transition (1st sampling phase) in 2011 and (bottom) the winter-spring transition (2nd sampling phase) in 2012. For comparison purposes, chl -a concentrations in ice are reported as horizontal bars. Ice texture is reported as vertical colored bars next to the right y axes. Dark gray is granular ice, light gray is columnar ice, and light blue is mixed columnar/platelet ice.

Second, the formation of platelet ice provides favorable conditions for the production of DMSP by increasing the environmental stresses the interior ice assemblage is exposed to. The transition between columnar and mixed columnar/platelet ice represents a decrease in ice permeability reducing the release of salts through brine convection (i.e. higher osmotic stress – DMSP acting as osmoregulator). Finally, the lower brine inclusions connectivity of the mixed columnar/platelet ice transition constrains the vertical redistribution of DMS,P leading to a local accumulation, similar to what was reported by Tison et al. (2010) in the Weddell Sea. This is to our best knowledge the first evidence of the influence of platelet ice on the DMS,P cycle in sea ice. The processes described above might be of primary importance regionally given the fact that platelet ice and interior ice assemblages of dinoflagellates have been widely reported in the McMurdo Sound, Weddell and Scotia Seas, and Terra Nova Bay.

Following the increase in solar radiation during the winter-spring transition in 2012 (2nd sampling phase) (Figure 22), DMS,P profiles become strongly influenced by the development and decline of a diatom-dominated bloom in bottom ice (Figure 25). We therefore investigate the coupling between chl-a and DMSP in bottom ice (Figure 27). A time lag between algal growth and DMSP production is initially observed. Since this time lag directly follows the dark light transition from winter to spring, we suggest the increase in solar radiation stimulates the synthesis of DMSP by providing the energy required for sulfate uptake and reduction. Further work is needed to test this hypothesis. DMSP then nicely follow the development of the seasonal bloom.

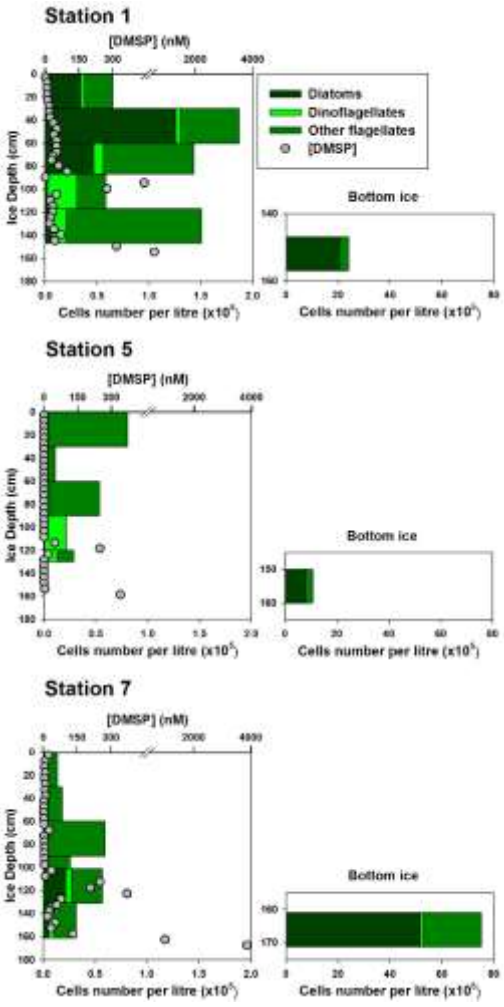

Figure 25: Biomass composition observed at selected depths of three YROSIAE stations. Note the difference in horizontal scale for the bottom ice layers. DMSP profiles are also shown as gray dots for comparison purposes.

During the spring-summer transition in 2011, DMSP is not coupled to chl-a. We believe this trend is attributed to drastic changes in permeability and brine dynamics on warming. This hypothesis is supported by physical and biological observations in ice and under-ice water. Brine convection events are shown to release DMS to the

under-ice water and to redistribute DMSP in interior and surface ice. For instance, a strong brine convection episode likely occurs between station 1 and 2, delivering brine with large diatom cells, DMS, and DMSP to the under-ice water, and replacing brine with seawater containing smaller but more DMSP productive cells. This is supported by the fact that: (1) the ice is permeable and the brine salinity profile unstable at station 1 before becoming stable at station 2, (2) textural features typical of brine drainage (large refrozen vertical tubular drainage structure, inverted funnel-shaped cavities) are observed at station 2, (3) a drastic increase in chl-a, DMS, and DMSP is observed in under-ice water over a very short period of time (5 days) between station 1 and station 2 following a very stable evolution beforehand, (4) the decrease in bottom ice chl-a corresponds to an increase in the percentage of small cells. A strong loss of DMS from sea ice to the under-ice water is also seen between station 2 and 3. A similar coupling is observed for DMSP, although the decrease/increase in bottom ice/under-ice water is less pronounced. This echoes the observations of Tison et al. (2010) in early summer ice from the Weddell Sea and confirms the higher resistance of DMSP to loss via brine convection. Particular DMSP linked to algal cells would mainly remain fixed to the walls of brine channels, whereas DMS present as a solute in the brine would be more easily transported.

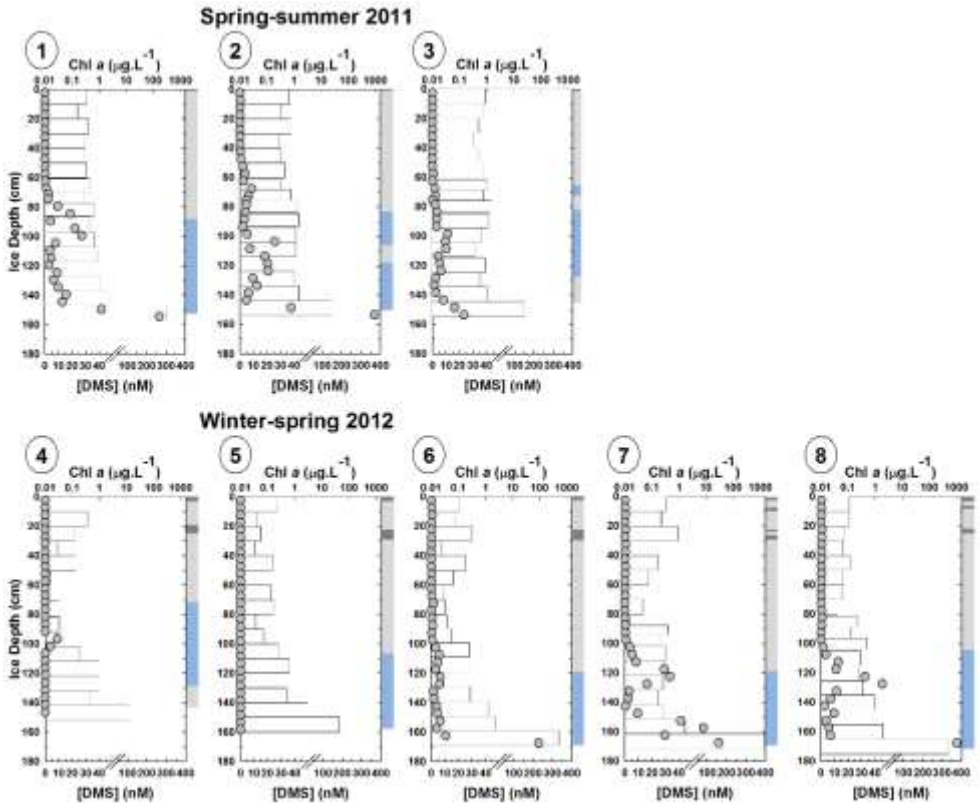

Figure 26: Vertical profiles of DMS concentrations (gray dots) in the ice during (top) the spring-summer transition in 2011 (1st sampling phase) and (bottom) the winter-spring transition in 2012 (2nd sampling phase). For comparison purposes, chl *a* concentrations in ice are reported as horizontal bars. Ice texture is reported as vertical colored bars next to the right y axis. Dark gray is granular ice, light gray is columnar ice, and light blue is mixed columnar/platelet ice.

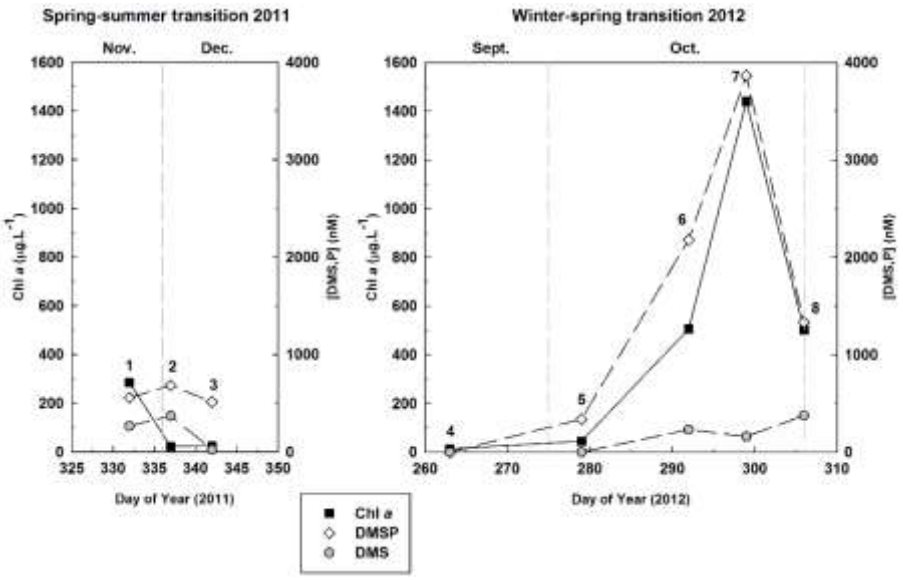

Figure 27: Evolution of DMS (nM), DMSP (nM), and Chl *a* concentrations in bottom ice (5 cm) during the spring-summer transition in 2011(left) and the winter-spring transition in 2012 (right). Each set of dots corresponds to a sampling station, identified by numbers 1 to 8.

We tried to quantify the DMS release through brine drainage looking at the DMS burden in ice at the two last spring-summer stations (2-3). The DMS burden decreases from 29.1 to 6.1 µmol.m^{-2} between station 2 and 3 (5 days), corresponding to a flux of 4.6 µmol.m^{-2}.d^{-1}. Of course, this burden calculated flux does not indicate if the release is directed toward the atmosphere or the under-ice water. Given the drastic increase in under-ice water DMS observed from station 2 to 3 without any significant increase in chl-a, and given the fact that DMS is predominantly located in bottom ice, we believe that a large proportion of the flux is indeed directed toward the under-ice water. It would be interesting in the future to assess the fate of this DMS. Indeed, the strong release of DMS through brine convection would occur before melting when the ice cover is still impeding ocean-atmosphere exchanges. Whether this DMS is quickly loss through transportation to depth and bacterial consumption, or advected to open water at the retreating ice edge will determine the exact impact of strong DMSP production in ice-shelf-influenced fast ice on the regional sulfur atmospheric budget.

Within the YROSIAE framework, we also achieved the first determination of the sulfur natural isotopic composition of DMS and DMSP in natural sea ice. Sulfur natural isotopes are very helpful to trace transport and transformation processes within the sulfur biogeochemical cycle. In 2015, we combined our dry crushing extraction technique of DMS and DMSP with $\delta^{34}S$ determination at the picomole level with GC-MC-ICPMS. This was made possible through an extensive collaboration with Pr. Alon Amrani (Institute of Earth Sciences, Hebrew University of Jerusalem). Sulfur isotopes were measured at specific sea ice depths at multiple YROSIAE stations (3, 4, 6, 8, 9, 11, and 12) but also at two stations (493, 506B) sampled during the AWECS cruise (see section 3.2.3) in winter Weddell Sea pack ice. The overall precision of the

method was 0.5 ‰ (n=6) for the DMS samples, and 0.25 ‰ for the DMSP samples (n=14).

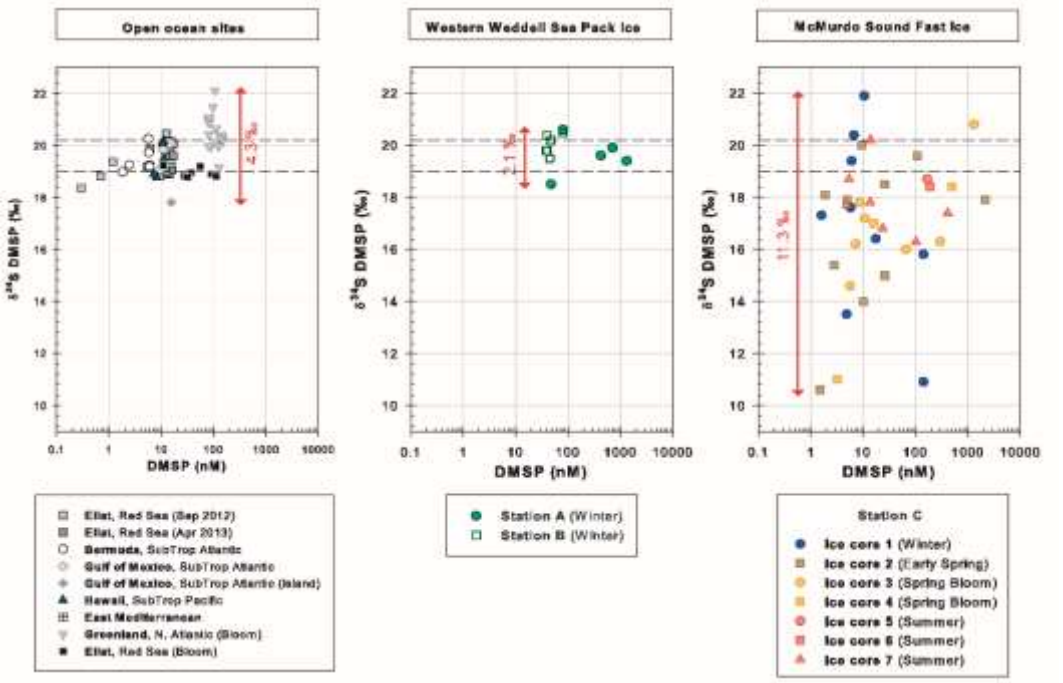

Figure 28: Variability of the $\delta^{34}S$ of DMSP in three different environments: (left) open ocean sites, (middle) Western Weddell Sea Pack Ice, (right) McMurdo Sound Landfast ice. The dashed-line indicates the typical range of values in surface oceanic waters.

$\delta^{34}S$ of sea ice DMSP revealed considerable variability between regions, across seasons, and between sea ice horizons, with values comprised between +10.6 and +21.9‰.

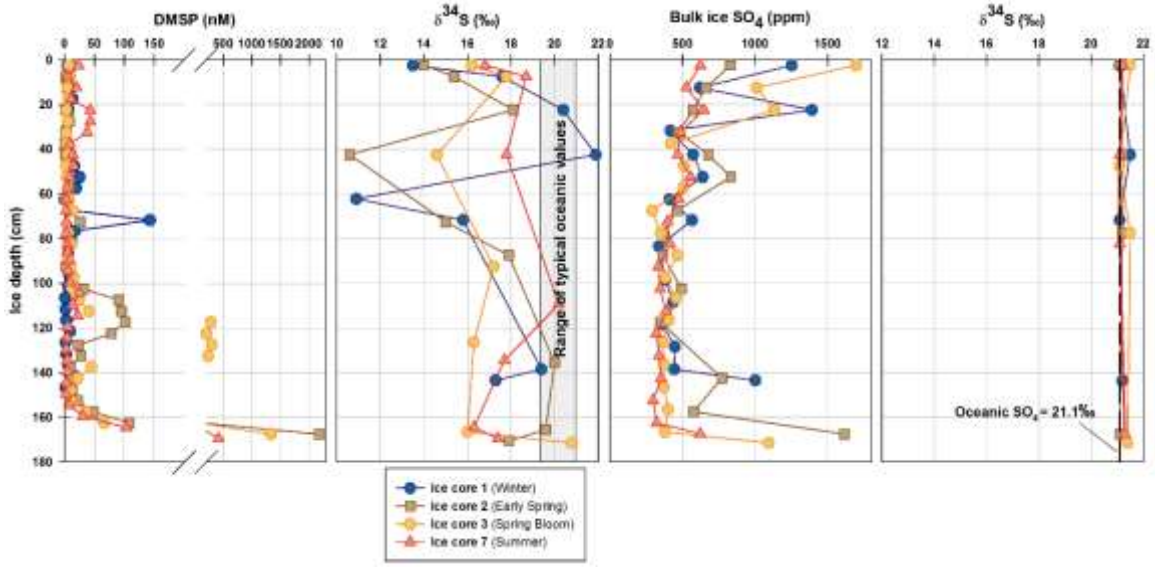

Figure 29: Vertical profiles of sea ice DMSP concentrations and $\delta^{34}S$ (left), compared to vertical profiles of sea ice SO_4 concentrations and $\delta^{34}S$ (right). Ice core 1 corresponds to YROSIAE station 4, ice core 2 to YROSIAE station 6, ice core 3 to YROSIAE station 8, and ice core 7 to YROSIAE station 12.

This variability is remarkable considering the relative sulfur isotopic homogeneity of DMSP in oceanic waters (between +17.8 and +20.3‰) (Figure 28). The variability is considerably higher in the YROSIAE samples (between +10.6 and 21.9‰) than in those collected in the Weddell Sea (between +18.5 and 20.6‰). Most ^{34}S depleted values were mainly observed in surface and interior ice in the winter and early spring (Figure 29).

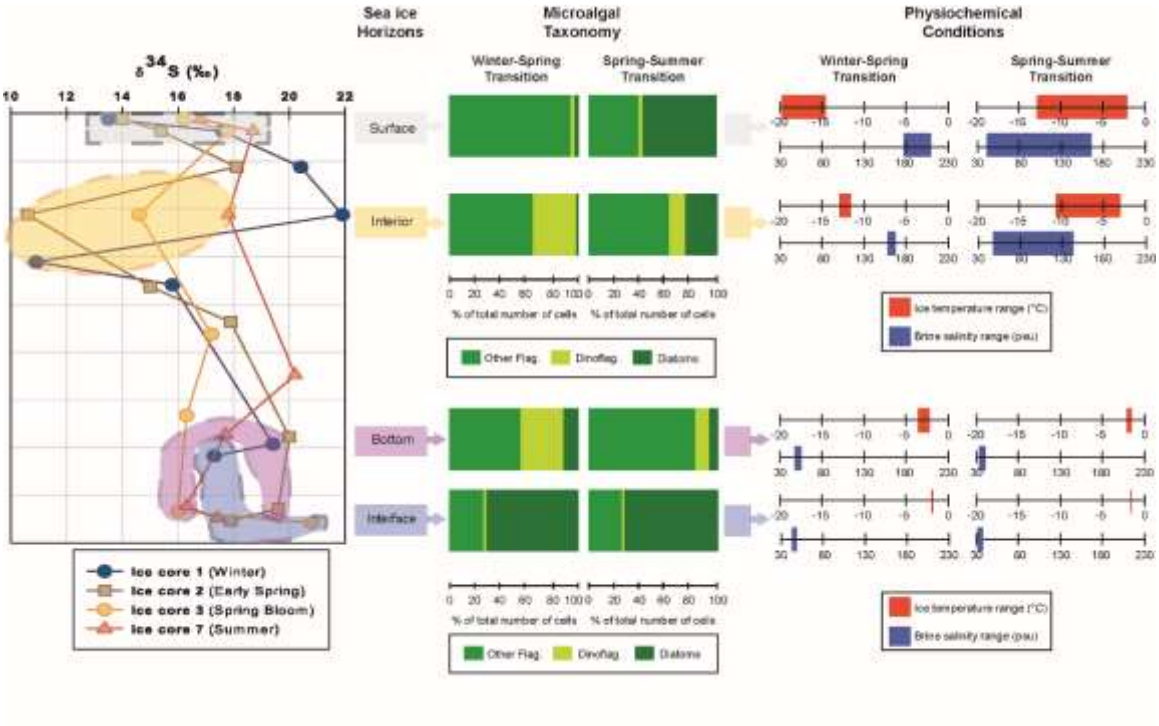

Figure 30: Vertical profiles of the $\delta^{34}S$ of DMSP in 4 YROSIAE cores (left). The taxonomic composition of various depth layers (surface, interior, bottom, ice-ocean interface) for these 4 cores is shown in the middle panel, as well as the ice temperature and brine salinity in the right panel. Ice core 1 corresponds to YROSIAE station 4, ice core 2 to YROSIAE station 6, ice core 3 to YROSIAE station 8, and ice core 7 to YROSIAE station 12.

Based on preliminary results, we hypothesize that there are two possible explanations to the large range of $\delta^{34}S$ values observed in the sea ice samples: (1) an important variability in the $\delta^{34}S$ of the source of S used by sea ice microalgae to synthesize DMSP, (2) very distinct metabolic pathways of DMSP synthesis (and hence distinct isotopic fractionation) in different sympagic microalgal groups, and in different sea ice environmental conditions. The first hypothesis can probably be discarded. SO_4^{2-} is generally admitted as the logical and primary source of S for microalgal metabolism in oceanic waters. This is also very likely the case in the brine habitat, with SO_4^{2-} concentrations in the YROSIAE samples ranging between 214 and 1695 ppm (largely above microalgal requirements at all sampling time and depths). We measured the $\delta^{34}S$ of SO_4^{2-} in the same samples and found remarkable consistency (21±0.1‰), with values similar to the typical isotopic signature of oceanic SO_4^{2-} (Figure 29). The second hypothesis is more interesting but will need further confirmation. We observe a very good correspondence between highly depleted values and dinoflagellates/flagellates dominated assemblages in surface and interior

ice during YROSIAE, in contrast with diatom dominated assemblages in the Weddell Sea samples and YROSIAE bottom ice samples. We also observe that these assemblages correspond to the harsher brine environmental conditions found in the ice cover, both in terms of temperature and salinity (Figure 30). To further test this hypothesis, we will in the next few months submit two cultures of Fragilariopsis cylindrus (diatom – weak DMSP producer) and Phaeocystis Antarctica (haptophytes – strong DMSP producer) to various brine environmental stresses (S, and T) and measure their response in terms of DMSP production and variability in $\delta^{34}S$. These preliminary results are anyway very promising as they suggest that S natural isotopes could represent a very strong tool to study DMSP production processes but also to assess the contribution of various sea ice DMSP producers to the formation of sulfate aerosols and hence regional climate control.

Primary production

We performed ^{13}C-tracer incubations in order to assess net primary production (Figure 31), but from a different location that the main sampling site at cape Evans which is situated closer of Scott base to allow an easier access to the incubation site. Two depths in sea ice were crushed and incubated with a tracer addition consisting of $^{13}HCO_3^-$. Crushed ice was inserted in incubation bottles which were replaced *in situ* during 24h using Plexiglas tubes with a diameter corresponding to the coring device. Not observed on the main sampling site, a loose accumulation of platelet ice was observed underneath sea ice and was likely to be highly productive (colored ice). No strand layer communities are reported and biomass extended deeper within sea ice (4-5cm of colored ice instead of 2-3cm at the main sampling site). The complexity of the sea ice/brine matric presents particular problems to perform incubations and, therefore, the goal of this experiment was to test our incubating protocol.

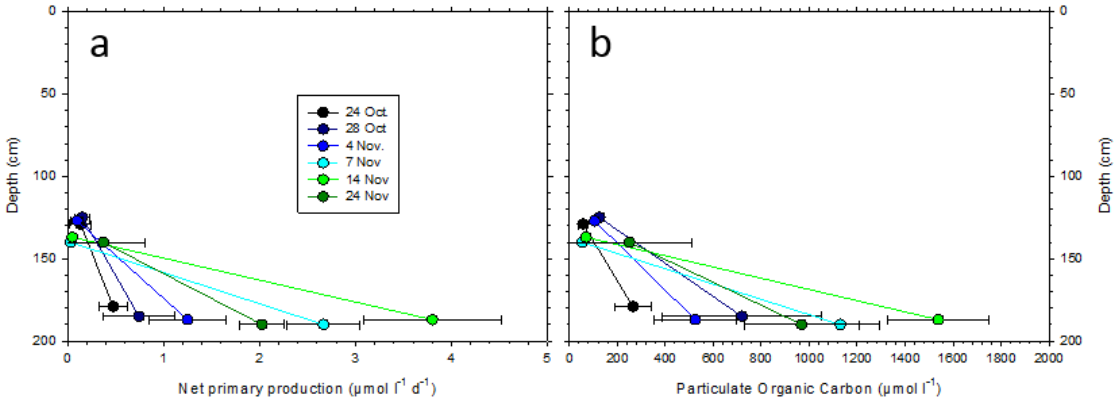

Figure 31: Net primary production (a), and particulate organic carbon (b), at the incubation site in the McMurdo Sound.

What the results shown is that the observed primary production (up to 5 µmol l^{-1} d^{-1}) is not able to reproduce the huge particulate organic matter pool (~ 1000 umol l^{-1}) accumulated in the timeframe of the incubations (~ 1 month).

A tracer-incubation requires (1) to be representative of the in situ community, as well as (2) to ensure a homogenization of the added tracer. Our approach consisting of crushing an ice section should satisfy the first condition. At other hand, the homogenization of tracer is still not guarantee, and could induce a strong underestimation of the net primary production. Sea ice algae tend to growth attached to the ice. The brines with the tracer can be concentrated at the bottom of the incubation bottles and, therefore, not in contact with the whole algal community. In addition, such underestimation could be accentuated with hygroscopic and capillary waters having not been in contact with the tracer.

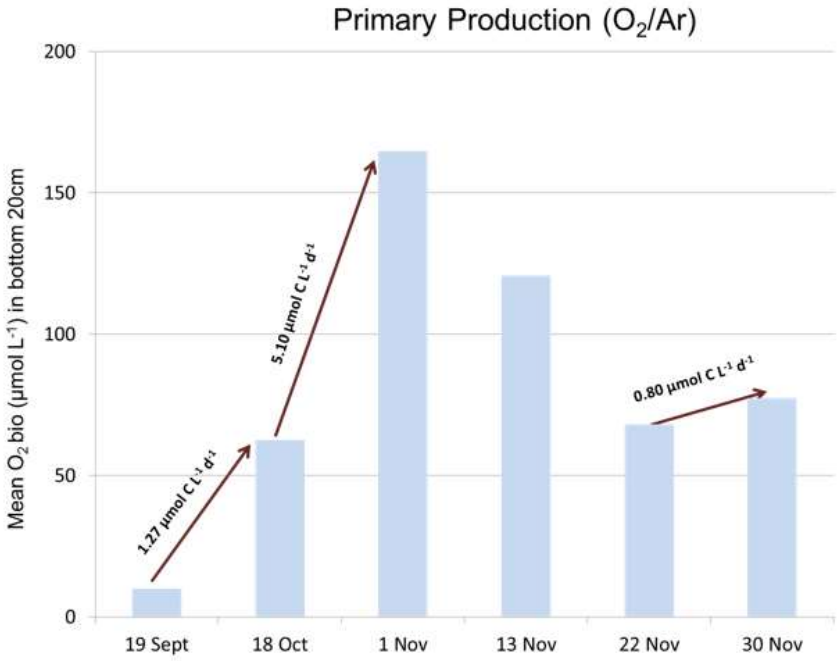

Figure 32: Bottom photosynthetically derived O_2 concentrations and inferred net community production at the main sampling site.

Alternatively, such large accumulation of organic matter could be allochthone and not produced in the porous-bottom consolidated platelet layer in which the incubations were made. If primary production was predominantly occurring in the underlying loose platelet layer, exchanges between the loose and consolidated platelet layers could enrich the latter in organic matter over what is directly produced there.

At the main sampling site, net community production was inferred from vertical O_2:Ar profiles. Photosynthesis accumulates O_2 without affecting Ar concentration. The latter bearing roughly the same solubility and diffusivity than O_2 molecules and will be similarly affected by physical processes. Similar rates are reported than for the incubation site (up to 5 µmol l^{-1}) (Figure 32).

As for the incubation, still much larger organic matter accumulation than expected from estimated production rates was observed in the timeframe given by the observations (3000 µmol l^{-1} in approximately 2 weeks) (Figure 22). As for the incubation site, this could be explained either by a methodological bias or by a predominantly allochthonous origin for the organic matter. No loose platelet layer was observed, but strand communities at the bottom of the ice likely represent a significant share of the newly-produced organic matter and could becoming trapped within sea ice with the ice growth (Figure 23). The latter will be measured with particulate organic carbon, as this community remains stuck at the bottom of the ice upon ice cores retrieval, but not with ice O_2:Ar ratios as this community is laying down in the underlying seawater.

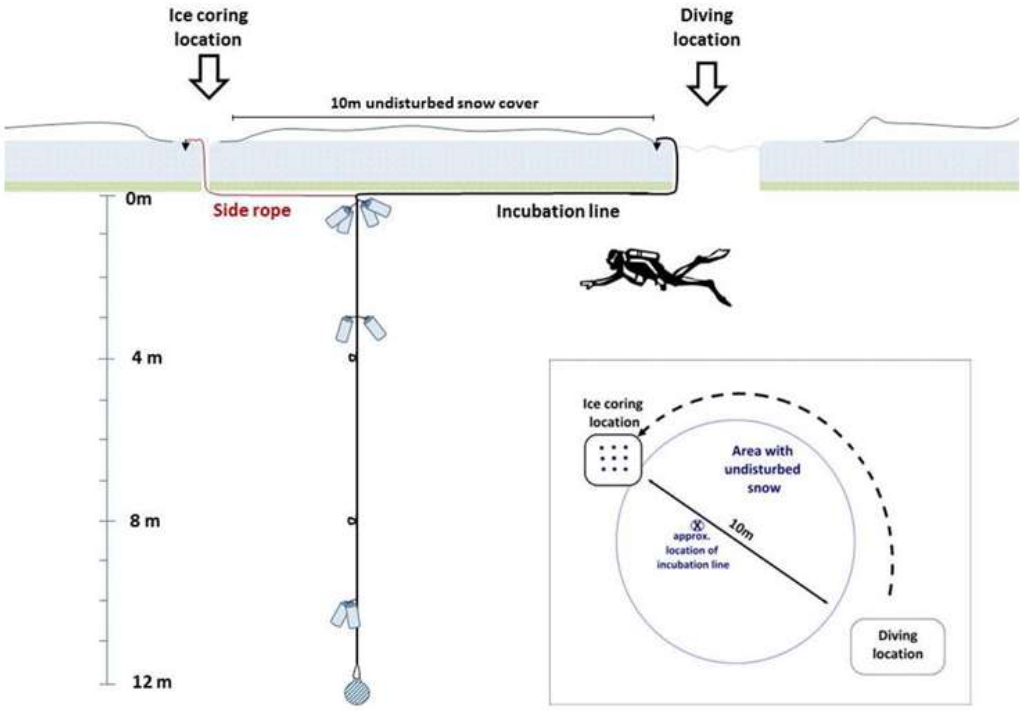

Figure 33: Schematic view of the incubation protocols to assess primary productivity in both bottom ice and underlying seawater at Dumont D'Urville and Davis stations.

To conclude, even if additional test are required (same location, different habitats, …), both methods (O_2:Ar and ^{13}C-incubatons) appear to capture primary productivity and give comparable results. However, the organic matter appears to be mainly allochthone and is formed either in the loose platelet layer underneath the ice floe or in the strand algal community, being progressively trapped within growing sea ice.

To further compare this method and to improve the assessment of sea ice productivity, we collected ice cores for O_2:Ar and performed ^{13}C incubation at the same location (Dumont D'Urville, 2014 and Davis station, 2015), including in the water column following the scheme shown in Figure 33. In addition, an intercomparison between crushed and melted ice sections has been made for the ^{13}C incubation. Such experiments helped improving the incubation protocol.

pCO_2 dynamics within sea ice

The bulk ice pCO_2 profiles as function of ice depth are presented in Figure 34. The pCO_2 ranges from 6 – 810 ppm. The strong pCO_2 gradient between the top and the bottom of the ice observed during early spring collapses dramatically as sea ice warmed.

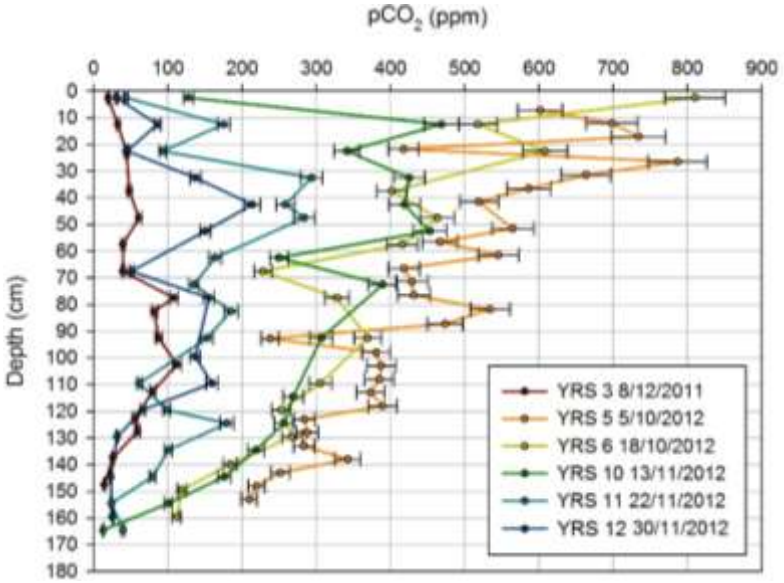

Figure 34: pCO_2 of bulk sea ice using equilibration standard gas of 300 ppm. Error bars show the method precision (5%) (Geilfus et al., 2012).

The surface pCO_2 shifted from a large over-saturation during early spring (October) to a marked under-saturation during summer (November-December). CO_2 over-saturation appeared at stations 5 and 6 in the upper half of the ice. The main pCO_2 shift occurred between stations 6 and 10, decreasing from 810 ppm to 128 ppm at the air-sea ice interface. The pCO_2 decrease diffused over interior ice during the spring-summer transition to reach low values (< ~100 ppm) over the entire ice column by the end of November, at station 3. The bottom pCO_2 remained under-saturated (< 115 ppm and even 45 ppm for station 11, 12, 3) during the study period. This can be related to biological activity since most of the biomass is concentrated in the bottom centimetres.

The evolution of pCO_2 can be divided into 3 stages:

(1) Over-saturation stage: during the winter-spring transition (upper half of stations 5-6): due to cooling, brines concentration (salts, CO_2 and other gases), respiration by bacterial communities, brines expulsion and upward transport occur leading to a potential soruce of atmospheric CO_2.

(2) Surface under-saturation: between stations 6 and 10, the brine volume fraction exceeds 5% in the upper 40 cm of ice (permeability threshold for fluid transport through sea ice (Golden et al., 1998) allowing the pCO_2 to decrease.

(3) Global ice column under-saturation (stations 11, 12, 3) due to melting of pure ice crystals, the brine dilution and opening of the brine network will decrease the pCO_2 on the full ice thickness creating a potential sink of CO_2 in parallel to uptake by sympagic algae growth.

We compared annual dynamics of sea ice pCO_2 with CO_2 fluxes measured by automated accumulation chambers on the field. Air-ice exchanges are driven by the the pCO_2 gradient between the atmosphere and the sea ice brine inclusions near the ice surface. Results confirmed a general trend of brine pCO_2 supersaturation with respect to the atmosphere during the late winter (concentration of DIC in brine and brine expulsion in the brine skim) leading to CO_2 degassing, and undersaturation during the spring (brine dilution and carbon-uptake by autotrophs) leading to

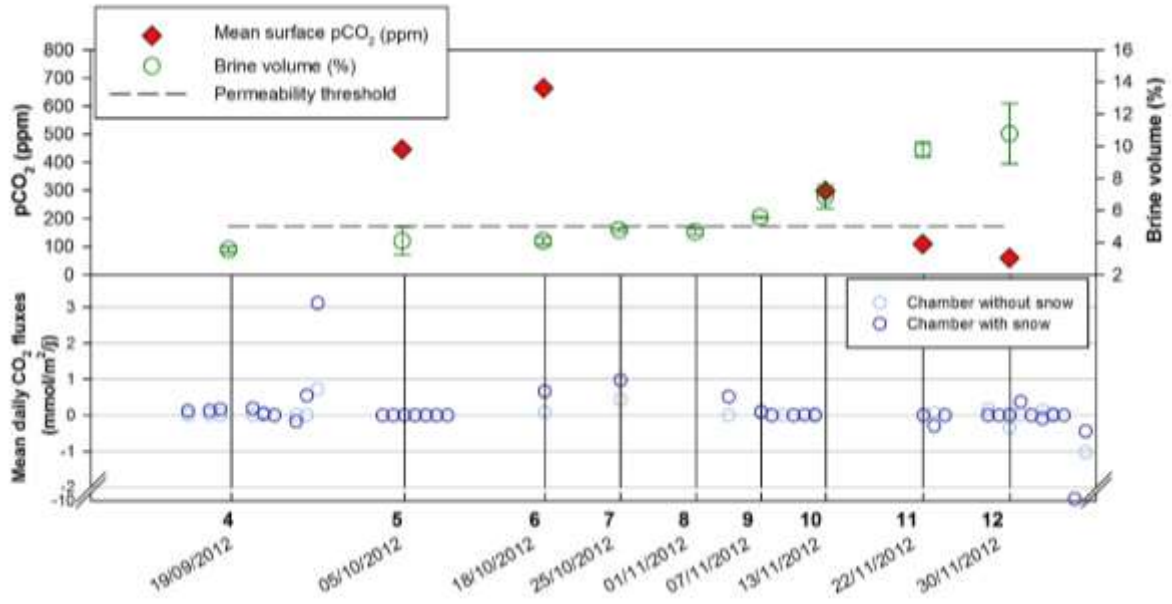

Figure 35: Air-ice CO_2 fluxes related to pCO_2.

atmospheric CO_2 uptake (Figure 35).

However, some variability in the CO_2 fluxes (both in magnitude and sign) could not be explained by variability in sea ice pCO_2 but rather seemed driven by variability in atmospheric conditions and sea ice surface properties. For instance, in late spring, CO_2 fluxes showed a diurnal variability (from CO_2 degassing to uptake) related to atmospheric temperature variations (Figure 36). Short-term atmospheric temperature variations could lead to surface melting and refreezing cycles that could generate short-term fluxes. Furthermore, large and episodic CO_2 fluxes were systematically

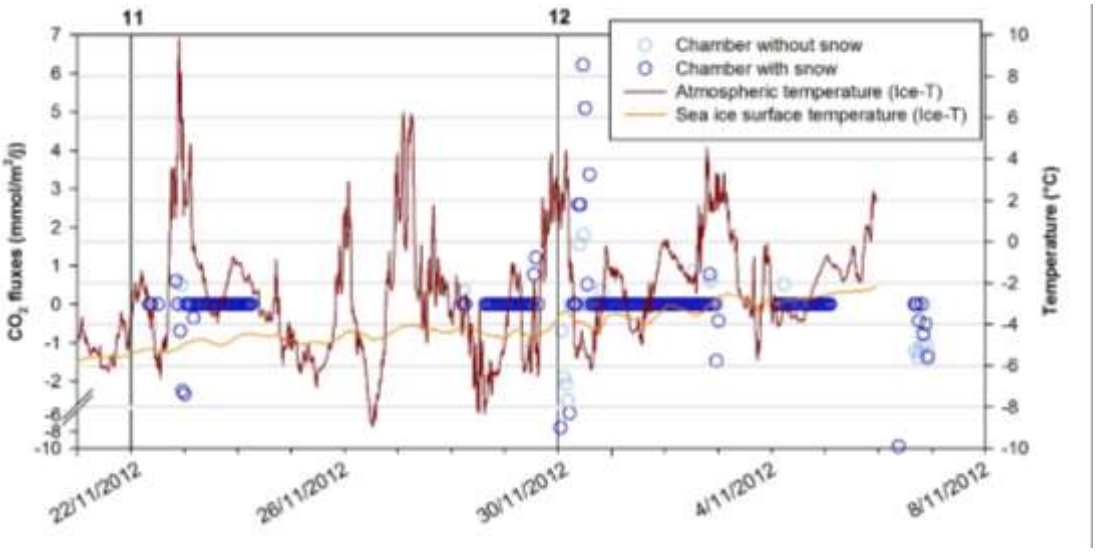

Figure 36: Diurnal variation in air-ice CO_2 exchanges in late spring.

positively correlated with strong wind events that could not only increase the magnitude of the CO_2 flux via pressure pumping (Massman et al., 1997) but also increase the cooling of the surface ice.

Automatic chambers vs eddy-correlation fluxes - We carried out CO_2 fluxes observations using both automatic chambers (AC) and eddy-correlation (EC) techniques on the field. We observed inconsistencies in the ice-atmosphere gas fluxes between both techniques (Figure 37). For example, CO_2 fluxes measured using chambers range from -2,51 à 1,81 mmol m^{-2} d^{-1} at the ice-air interface and -9,76 à 6,22 mmol m^{-2} d^{-1} at the snow-air interface. On the contrary, the minimum and maximum CO_2 fluxes measured using eddy correlation were reported between -70 to 84.4 mmol m^{-2} d^{-1}. We suggest that the large discrepancies might be caused by a heterogeneous EC flux footprint, including open water, leads or ice cracks.

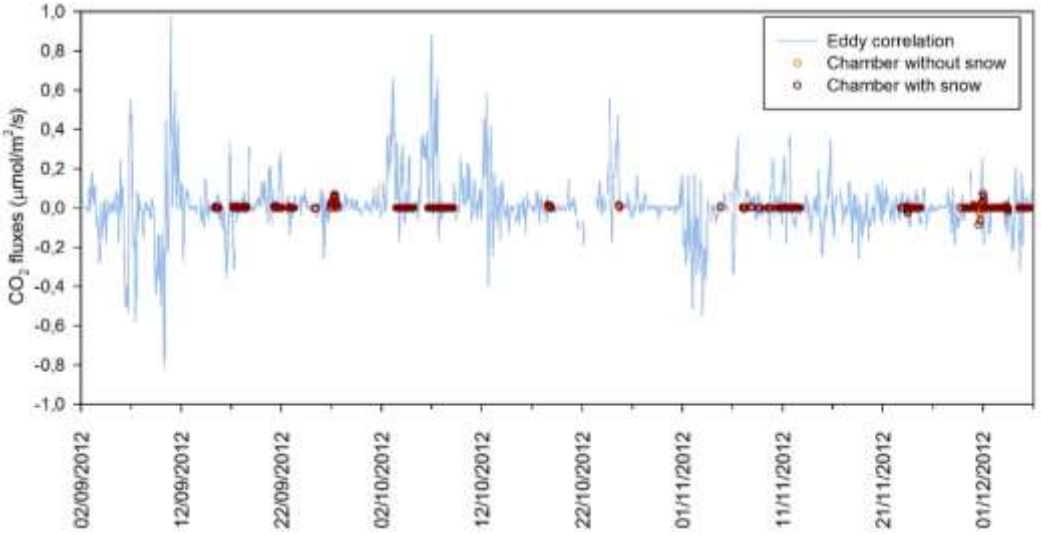

Figure 37: Chamber vs. eddy-correlation CO_2 fluxes.

The role of snow in stocking and releasing gases during strong wind events via wind pumping (Bowling and Massman, 2011) may also explainthe high CO_2 fluxes reported. Eddy correlation measurements of CO_2 fluxes do not reveal a clear transition of summer air-ice CO_2 fluxes from a source to a sink for atmospheric CO_2.

Salinity normalized dissolved inorganic carbon – The dissolved inorganic carbon (DIC) of bulk ice was computed from TA_{bulk} filtered and pH using CO2SYS program for the carbonate system (Lewis et al., 1998). We used CO2 dissociation constants of Goyet and Poisson (1989) and the other constants advocated by Dickson and Goyet (1994). DIC was normalize to a constant salinity of 6, denoted as DIC_6, corresponding to the mean salinity of the ice during this study. This allows us to remove the salinity-related changes (brine rejection, concentration and dilution) and to highlight biogeochemical processes such as biological activity, $CaCO_3$ precipitation and CO_2 exchanges to the atmosphere.

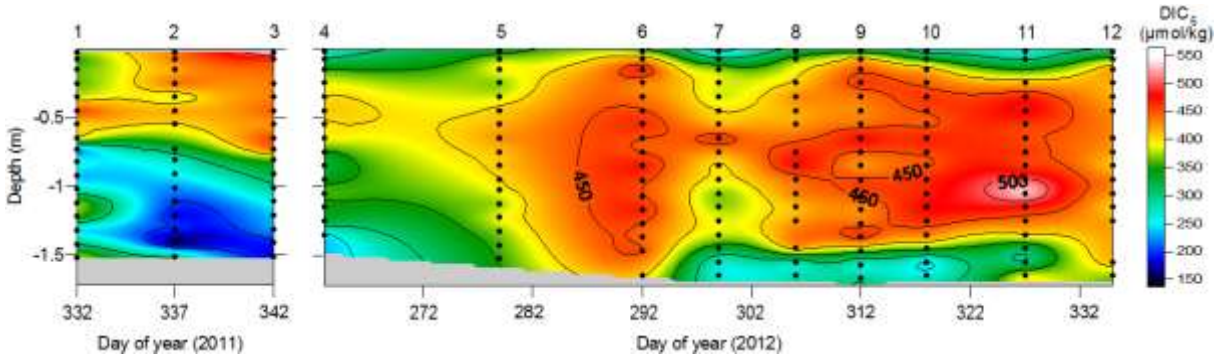

Figure 38: contour plot of DIC_6 during (left) the spring-summer transition in 2011 and (right) the winter-spring transition in 2012. Sampling stations are shown as vertical dotted lines.

DIC_6 varied between 563.2 and 137.9 μmol kg^{-1} (Figure 38). DIC_6 increased gradually from station 4 to 6 during sea ice growth. Bottom and upper ice DIC_6 decreased strongly at station 7, corresponding to a basal peak algal bloom and a surface community development. Then DIC_6 started to increase again to reach a second maximum and stabilized around 450-500 μmol kg-^{1} between station 10 and 11. At the end of the winter-spring transition, DIC_6 decreased over the full ice thickness.

Sea ice is characterized by a typical succession of autotrophic (primary production exceeds bacterial production) and heterotrophic (dominance of bacterial production over algal production) processes. Heterotrophy dominated during low biomass midwinter period (st 4-6), intense autotrophy superimposed during the initial algal bloom (st 7), followed by a heterotrophy-dominated steady state (st 8-11) and finally a late post bloom autotrophy appeared at the end of the spring. Bottom ice is dominated by autotrophy over this period since most of the biomass is concentrated at the ice-water interface. Summer sea ice (year 2011) is divided between a heterotrophic upper ice column and an autotrophic lower ice column (Table 6).

Stations	Chl-a concentrations	Phaeopigment concentrations	DIC	Trophic status
4 - 6	Low	↓	↑	Heterotrophy
7	Basal bloom + surface community	Low	↓	Autotrophy
8-9	Interior ice : ↓ Bottom ice : ↑	↑	↑	Heterotrophy
10 11	Algal bloom	↓	Stabilization at maximum values	
12	↓	Low	↓	Autotrophy

Table 6: Trophic status for the winter-spring transition in 2012 according to biological parameters and DIC evolution.

3.2.3. A winter-time series of Antarctic pack ice biogeochemistry: the AWECS study

A major drawback in previous attempts to pinpoint the annual balance of impact of sea ice on biogeochemical exchanges with the ocean and the atmosphere is the lack of autumn and winter data sets. By default, it is often assumed that sea ice winter biogeochemical activity is restricted by the very low temperatures and light levels. In this section, we use the rare opportunity of the AWECS (Antarctic Winter Ecosystem Climate Study) winter cruise in 2013 to show that this default assumption needs to be revised, especially within the context of a warming world.

General overview of AWECS

The AWECS cruise took place between June 8 and August 12, 2013 in the Weddell Sea (Figure 39a, color dots). The main goal of the expedition was to "understand how the Antarctic sea ice physical environment affects the seasonal and regional dynamics of biogeochemical cycles, with emphasis on winter processes". One of the more specific topics was to gather a suite of physical and biogeochemical parameters at a series of ice stations, in order to decipher winter sea ice biogeochemical dynamics and the control it exerts on the exchange across the atmosphere-ice-ocean interfaces. The RV Polarstern left Cape Town for a southwards transect along the Greenwich meridian, then sailed west towards the Antarctic Peninsula at 68°16 S. The expedition paused for seven days on 17th of July due to medical emergency, then resumed along the Antarctic Peninsula, before heading back North to Punta Arenas (Chile). A total of 11 stations were occupied, for about 12 hours each, to provide a full description of the biogeochemical state of the ice cover. A main meteorological feature of the expedition was the regular alternation of very cold episodes (down to -28°C), with dry southerly wind flow and no clouds, and of very warm episodes (up to -0.5°C) corresponding to fronts and depressions (with high cloud cover and heavy snow fall) travelling eastwards across the Weddell Sea, even relatively close to the Antarctic coast (Figure 39c). This resulted in very contrasted temperature records between stations (Figure 39b), with drastic changes in the sea ice cover properties, as discussed below.

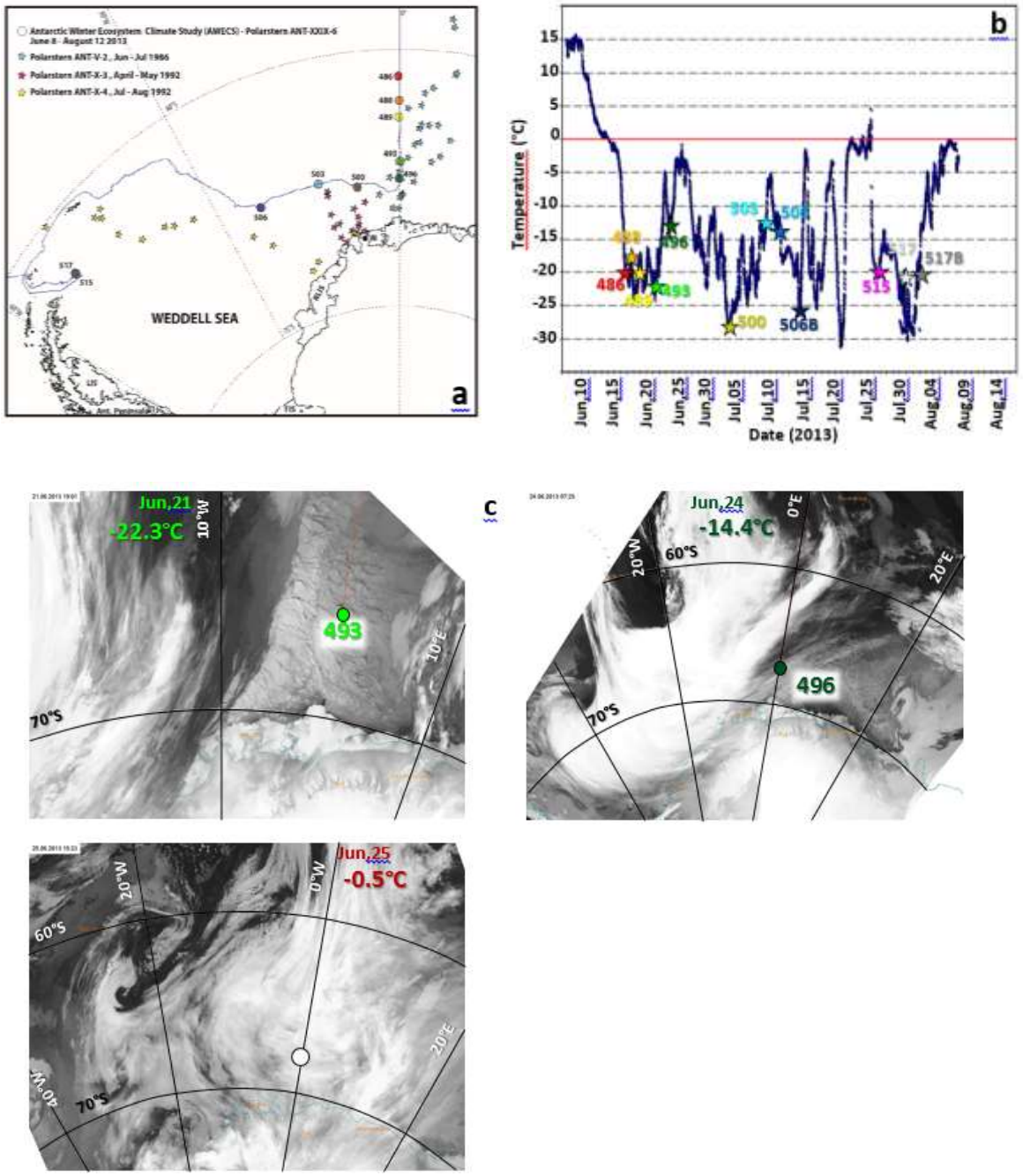

Figure 39: A) Tracks for the 2013, 1986 and 1992 Polarstern winter voyages, with AWECS 2013 Station numbers; B) Air temperatures at 29m height a.s.l. during the AWECS cruise (blue dots) and stations air temperatures at the sampling location (stars) ; C) IR satellite maps (credit: NOAA) on June, 21 (Station 493), June, 24 (Station 496) and June, 25 showing contrasted synoptic regimes (red thin line is the Polarstern track, blue thin lin is the Antarctic coast).

Material and methods - Field sampling

At each of the chosen biogeochemical stations (486 to 517 in Figure 39a) a full suite of physical and biogeochemical parameters has been collected, as summarized in Table 7. In this section, however, we will focus on the basic physico-chemical and biological parameters. To support the discussion on the physical properties, we will

also use the data set from physical transects performed by the ice physics team on board, and therefore briefly expose how these were collected here below.

First, and in accordance with plans from the other AWECS teams, an adequate floe is chosen, and the ship anchored to it so that the trace metal clean biogeochemical sampling site is upwind of the ship (hopefully during the entire running of the ice station) and at a reasonable distance from it (300m to 500m). A 10m by 10 m area is then flagged, in which access will only be permitted to operators wearing clean suits to prevent contamination (Lannuzel et al., 2006). Power is provided by a 5 kVA generator placed 50 meters away from the restricted area and downwind of it. Along the same line lie a table for ice core treatment, ice core storage boxes and the various cargo boxes for transport. First, 5 operators get dressed with Tyvek clean room garments on top of their polar clothes and plastic bags on their shoes. Snow samples are then taken by one of the operators in the central part of the restricted area. Then, a first core is taken along the lower border of the restricted area. A temperature profile is immediately performed along the core. The core is then stored wrapped in -30°C cooling bags within the core storage box, to prevent brine drainage. It will be cut for salinity measurements (5 cm resolution) later onboard the ship. A second "twin core" is collected for "*in situ*" salinity cutting (10 cm resolution) and stored in containers to provide a thorough comparison check of the two techniques (Tison et al., 2008). A sheltering tent is then deployed on top of the two holes that will be used to perform the water sampling at various depths with the help of a non-contaminating peristaltic pump, ensuring limited freezing in the sampling tubes. In the meantime, another team starts the drilling of the "brine sackholes" (Thomas et al., 2010), incomplete holes drilled at two selected depths, designed to collect internal brines in the course of time. The two depths are chosen (based on the temperature profile) so that the shallower one collects brine from the upper impermeable layer (brine volume <5%), and the deeper one from the lower permeable layer. Care is taken not to drill the latter sackholes too deep, to avoid seeping of sea water upward. In order to be able to collect enough brines for the suite of measurements to be performed, 6 sackholes of each depth range are drilled in close vicinity. They are immediately covered with foam corks, to prevent contamination from e.g. blowing snow or other sources. Brine is left to slowly drain for typically a few hours. A second tent is eventually used to protect the operators during the collection of the brines, which is either performed with the help of a syringe or with the peristaltic pump, when the volumes are sufficient. Brines are also circulated in the Sea Ice Equilibrating System (SIES) (dedicated brine hole) which measures the "*in situ*" pCO_2 of the brine using a method derived from underway pCO_2 measurements (Delille, 2006).

As soon as the snow has been sampled, a third team starts the set-up of a series of flux chambers (8 for CO_2 and 1 for VOC) alongside the restricted area. For inter-calibration experiments, 2 kinds of CO_2 chamber systems are used: (1) semi-automated CO_2 chambers initially developed at Hokkaido University for soil CO_2 flux measurements and (2) long-term automatic chambers (Li-8100, LI-COR Biosciences,

USA). Different types of surfaces (on snow, on ice, on slush) are typically investigated, together with ancillary measurements.

TOPICS	MEASUREMENTS
Basic Physico-chemical	Temperature Bulk Salinity Water Stable isotopes Fabrics
Gases	N_2, O_2, Ar, CH_4, N_20 CO_2 (incl. Air fluxes) DMS, DMSP, DMSO, VOC Gas ^{13}C and ^{2}H isotopes Total gas content
Biology	Chla Microbial Foodweb: Targeted enumeration of algae, bacteria, Primary and Bacterial production
Biogeochemistry	Nutrients EPS POC DOC $\delta^{13}C$, $\delta^{30}Si$, $\delta^{15}N$
Trace Metals	Fe, Zn, Mn, Cu, Cd, Ni, Mo, Co, Ba, Al, Pb
Carbonate System	DIC Total Alkalinity (TA) pH $CaCO_3$ crystals (Ikaïte) derived from either optical count and size ranking or TA anomaly

Table 7: Target physical and biogeochemichal parameters at the AWECS sea ice stations.

Finally, a series of 13 supplementary cores are collected in close vicinity to each other (no more than 20 cm apart), in order to collect the material for all the other measurements targeted in Table 7 and to provide the material for some of the experiments to be performed on board. All drillings are performed using a 14 cm diameter electro-polished stainless steel corer or a titanium corer, that have both been tested against contamination for the various trace metals investigated (Lannuzel et al., 2006). Sea ice cores for trace metal determination (1x concentration, 1x isotopes) were also collected using an all-titanium ice corer (Lichtert Industries, Brussels, Belgium) and immediately packed in acid cleaned

plastic bags and stored at -25 °C for further processing at the home laboratory (Université Libre de Bruxelles).

Sea ice thickness, freeboard (height above sea level) and snow depth were measured at 8 representative stations (493, 496, 497, 500, 503, 506, 515 and 517, Figure 39a) during the AWECS cruise. Discrete manual measurements were performed every 5 meters along two crossing transect lines, 100 m long each.

Material and methods - Analytical methods

Temperature: Ice temperature was measured using a calibrated probe (Testo 720). The probe was inserted into 4 mm holes (matching the diameter of the probe), drilled perpendicular to the ice core axis with a depth resolution of 5 cm. Precision of the probe was ±0.1°C. Temperature measurements were completed within 5 minutes after ice core extraction as recommended by Pringle and Ingham (2009).

Bulk salinity: Bulk ice salinity measurements were performed on 5 cm vertical core sections obtained from the ice core that was used for temperature measurements. Salinities were measured with a portable conductimeter (Orion Star Series Meter WP-84TP) on melted ice samples, at room temperature. Each salinity sample was centered on the temperature measurement. The precision was ±0.1.

Thin sections: Continuous ice thin sections (ca. 600 µm thick) were obtained using a microtome (Leica SM2400), following the standard procedure of Langway (1958). The sections were examined and photographed between crossed polarizers on a universal stage system.

Water stable isotopes: Snow, sea ice, brines and water $\delta^{18}O$ and δD were measured at the Alfred Wegener Institute.

Chl-a: For chl-a measurements, a dedicated ice core was sampled continuously at a 10 cm resolution. Samples were melted in the dark, in 0.2 µm filtered seawater (1:4 volume ratio) to avoid osmotic stress. We used 10 and 0.8 µm polycarbonate filters in a sequence in order to distinguish larger microalgae species from the smaller ones. Extractions and calculations were made following the procedure of Arar and Collins (1997).

Cell enumeration, taxa, biomass and DNA extraction: These further detailed biological measurements were performed on cores different from the one used for chl-a (although within 20 cm of each other). Two twin sea ice cores were put into open end PE plastic pipe-bag (Mercamer Oy, Finland) that were sealed immediately after the sampling and kept covered from light until they were transported to the laboratory containers onboard *Polarstern* with temperature set to +4°C. There, they were cut into sections of equivalent depth, using a Fiskars branch saw. Two equivalent sections were then pooled together and crushed to obtain a large enough sample ensuring that the various measurements originate from the same sample. After careful homogenization of the crushed ice it was divided into various melting units and enclosed in 1L plastic containers. In order to avoid organism losses due to

cell lysis caused by rapid changes in salinity during melting (Garrison and Buck, 1986; Kottmeier et al., 1987), a given amount of 0,2 µm filtered sea water (FSW) (Sartorius Sartoban Sterile capsule 300) was added to the crushed ice. The samples were left to melt overnight, as described in Rintala et al. (2014). The melted samples were thoroughly mixed before their volumes were measured in order to deduce the exact volume of sea ice initially collected in each bucket. A dilution factor was then calculated to restore the results at the proper bulk sea ice salinity. All the samples were kept away from light and at +4°C during the melting procedure.

For the live microscopy 800-1,000 ml of live material was concentrated using a 10 µm net of each section. Concentrated live material was examined with inverted light microscope (Leica DMIL) equipped with 12.5x oculars, 10x, 20x 40x objectives. After the live microscopy, a drop of Lugol was added to the 2.5 ml sample in the microscope cuvette to stop the cell movement and a digital camera (Leica DC300F) was used for documentation of the encountered taxa.

Subsamples were also collected into 100-ml brown glass bottles and preserved with acid Lugols' solution and stored in dark at +4°C for quantitative algal cell abundance analysis. Depending on the density of the sample, a volume of 50 mL or 10 ml was settled for 24 h, according to Ütermöhl (1958) and examined with a Leica DM IL, inverted light microscope equipped with 10x oculars and 10x or 40x objectives (Leica Microsystems, Wetzlar, Germany). Large cells and colonies were counted with 100x magnification over an area that covered one half of the cuvette, and the abundance of single celled and small taxa was counted from 50 random fields with 400x magnification. The cell numbers were converted into carbon biomasses (µg C l^{-1}) using species-specific bio-volumes and carbon contents according to Olenina et al. (2006) and Menden-Deuer and Lessard (2000).

For DNA extraction, 500 mL of water or melted sea ice or slush was filtered with 0.2-µm pore-size mixed cellulose ester membrane filters (Whatman, GE Healthcare, United Kingdom) and stored in 2-mL cryovials at -80°C onboard and on shore until further processing. DNA was extracted with PowerSoil® DNA Isolation Kit (MO BIO Laboratories, Inc., Carlsbad, CA, USA) according to the manufacturers' instructions. The approximately 360-bp long 18S rRNA gene fragment V4 (including the variable fragments) was amplified using primers E572F Comeau et al. (2011) and 897R (modified from Hugerth et al., 2014) with attached sample-specific 8-bp-long barcode tags. The PCR amplification was carried out using proof-reading DNA polymerase. The sequencing was done using Illumina MiSeq platform. The processing of reads was carried out by mothur v.1.34.4. (Schloss et al., 2009) using the Kozich et al. (2013) pipeline in http://www.mothur.org/wiki/MiSeq_SOP (accessed 15 November 2015). During the quality filtering primers, barcodes, reads with >8 homopolymers and ambiguous bases were removed. Chimeric reads were identified using UCHIME algorithm (Edgar et al., 2011) within mothur and removed from the dataset. The unique reads were aligned against the recreated SILVA SEED database v119 reference file (http://www.mothur.org/wiki/Silva_reference_files, accessed 15 November 2015). The reads were grouped into OTUs (Operational Taxonomic Units) at 97-% similarity level. OTUs occurring 1–5 times in a sample were removed from

the dataset. The pre cluster command grouped sequences up to 4 bp differences between sequences. Taxonomic assignments were created manually using the NCBI BLAST+ stand-alone v.2.2.31 (downloaded 13 July 2015). Diversity indices, i.e. Simpsons' diversity index, Chao1 and Shannon index, as well as the Venn diagram, were calculated using mothur, and were used to estimate differences between samples.

Material and methods - Derived variables

Several physical variables can usually be derived from the basic ice temperatures and bulk ice salinity measurements.

Theoretical brine salinity and brine volume fraction: were calculated using Cox and Weeks (1983) relationships, neglecting the air volume fraction.

Rayleigh numbers*:* Rayleigh number (Ra) is used as a proxy for gravity drainage (i.e. brine convection). Ra expresses the ratio between the negative buoyancy in the brines and dissipation (Notz and Worster, 2008). At a given depth z within sea ice, Ra is given by:

$$Ra = \frac{g \cdot (h_i - z) \cdot \rho_w . \beta_w . [\sigma(z) - S_w] \cdot \Pi(e_{min})}{\kappa \cdot \eta} \qquad (11)$$

where g is the gravity acceleration g = 9.81 m s^{-2}, $[\sigma(z)\text{-}S_w]$ is the difference between the brine density at the level z and that at the ice-seawater interface, ρ_w is the density of pure water, β_w is the haline expansion coefficient of seawater, with both ρ_w and β_w taken at 0 °C from Fofonoff (1985). $\Pi(e_{min})$ is the effective ice permeability (m²) which is computed using the formula of Freitag (1999) (eq. 2.19, p48) as a function of the minimum brine volume e_{min} between the level z and the ice-ocean interface. For brine volume fraction, we used the equations given in Notz and Worster (2009). The dynamic viscosity and the thermal diffusivity of brine are η = 2.55 10^{-3} kg (m s)$^{-1}$ and κ = 1.2 10^{-7} m s^{-2}, respectively, following Notz and Worster (2008).

It is noteworthy that the formulation of Freitag (1999) for ice permeability was developed for young sea ice (<30 cm), and a more appropriate formula would be the one of Eicken et al. (2004) derived from first-year ice at Barrow. However, we chose to compute permeability using the formulation of Freitag (1999) for consistency and comparison with previous work Notz and Worster (2008).

Material and methods - Modelling

In the discussion section we will compare our sea ice physics observations during AWECS 2013 to those obtained in the few available previous winter cruises in the Weddell Sea (1986, 1992). Along the same lines we will also compare those winter cruises observations to outputs from the NEMO-LIM3 global ocean-sea ice model routinely used in climate studies. The ocean engine of NEMO (Nucleus for European Modelling of the Ocean) is a finite-difference, hydrostatic, free-surface, primitive-equation model Madec and Team (2016). It is coupled to LIM3 (Louvain-la-Neuve

sea Ice Model), a dynamic-thermodynamic sea ice model with a representation of the subgrid-scale distributions of ice thickness, enthalpy and salinity (Vancoppenolle et al., 2009). The explicit inclusion of brine entrapment and drainage makes the sea ice salinity variable both in space and in time. We use version 3.5 of NEMO, with modifications to the sea ice code that include changes in the time stepping and a reformulation of ice-ocean fluxes allowing to track the different contributions to the ice mass, salt and heat balances (Rousset et al., 2015).

In the present application, the model is ORCA1, with a 1° resolution and the simulation runs from 1948 to 2013. Forcings are as follows: Atmospheric forcing fields consist of a combination of NCEP/NCAR daily reanalysis data of surface air temperature and wind speed (Kalnay et al., 1996) with monthly climatologies of relative humidity (Trenberth et al., 1989), cloudiness (Berliand and Strokina, 1980) and precipitation (Large and Yeager, 2004). Continental runoff rates are prescribed from the climatological dataset of Dai and Trenberth (2002). The model has known limitations. For example, in this simulation, it shows too little ice in the austral domain. One should also be aware that the brine volume is the average for 5 classes of ice thickness and that, because they are forced by climatologies, precipitations do not show any trend during the simulation period.

Results – Snow and ice thickness, ice freeboard

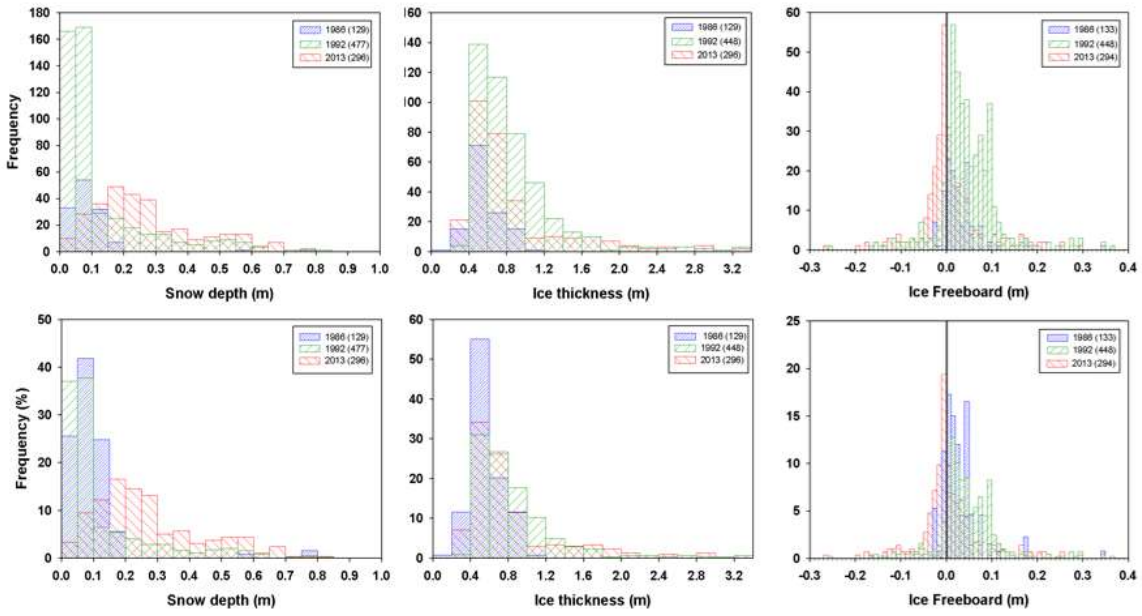

Figure 40: Frequency distribution of observed snow depth (left), ice thickness (middle), and ice freeboard (right) along the AWECS transects (red), compared to data from previous winter cruises in the Weddell Sea: Polarstern ANT V-2 (June-August 1986, blue) and Polarstern ANT X-4 (July-August 1992, green). Top row: absolute counts of samples; Bottom row: percentage of total of samples. Total sample numbers for each group is shown between parentheses. Black vertical line in right pannel underlines the 0m freeboard. ANT V-2 and ANT X-4 data courtesy of AWI (Alfred Wegener Institute) archive and Prof. H. Eicken.

Figure 40 shows the frequency distribution (top: absolute numbers, bottom: %) of observed snow depth, ice thickness and freeboard along the AWECS (2013, red) transects. It is compared to data from the two previous winter cruises in the Weddell Sea: Polarstern ANT V-2 (June-August 1986, blue) and Polarstern ANT X-4 (July-August 1992, green). ANT V-2 and ANT X-4 data are from AWI archives (courtesy of H; Eicken). Probability P-values from Mann-Whitney Rank Sum tests for similarity of median values (non-normal distribution) for snow depth, ice thickness and ice freeboard between the three cruises are given in Table 8. Snow depth distribution is clearly shifted towards higher values in 2013 as compared to the previous cruises, with 1992 and 2013 showing a "tail" of larger values. Trends in ice thickness are less clear, apart from a slight (but significant in terms of median value) increase in 1992 and 2013 as compared to 1986. Positive freeboards clearly dominate the distribution in 1986 and 1992, while it is centered on slightly negative values in 2013. This is a result of the combination of higher snow depth and slightly thinner ice (just not significant in terms of median value) in 2013 than in 1992.

		Snow Depth	Ice Thickness	Ice freeboard	Chla
1986-1992	*Medians*	0.08-0.07	0.52-0.71	0.02-0.04	0.56-0.82
	Probability	0.728	***<0.001***	***<0.001***	***<0.001***
1986-2013	*Medians*	0.08-0.23	0.52-0.66	0.02-0.00	0.56-2.042
	Probability	***<0.001***	***<0.001***	***<0.001***	***<0.001***
1992-2013	*Medians*	0.07-0.23	0.71-0.66	0.04-0.00	0.82-2.042
	Probability	***<0.001***	0.006	***<0.001***	

Table 8: Probability P-values from Mann-Whitney Rank Sum tests for similarity of median values for snow depth, ice thickness, ice freeboard and Chla concentration for the three available winter cruises in the Wedell Sea. Bold italic values indicate highly significant differences.

Results – Ice texture

Figure 41 summarizes the ice textural properties at each biogeochemical station. As previously reported for the Weddell Sea (Lange, 1990; Lange et al., 1989) frazil ice dominates due to the preponderance of turbulent conditions and of the pancake cycle in the region. This is also seen in the signs of rafting (alternation of frazil and columnar layers) visible in some of the cores (489, 500, 506b). Another interesting feature is the regular occurrence of linear brine tubes, generally in the upper 30 cm of the cores (e.g. AW500 left in Figure 41, but also reported at stations 493, 496 and 506b). Along the Antarctic Peninsula the facies differ, with locations of calmer thermodynamic growth of columnar ice (stations 517 and 517b), or influence of coastal processes (thicker ice and platelet ice formation - e.g. 25-40 cm and 105-115 cm- station 515).

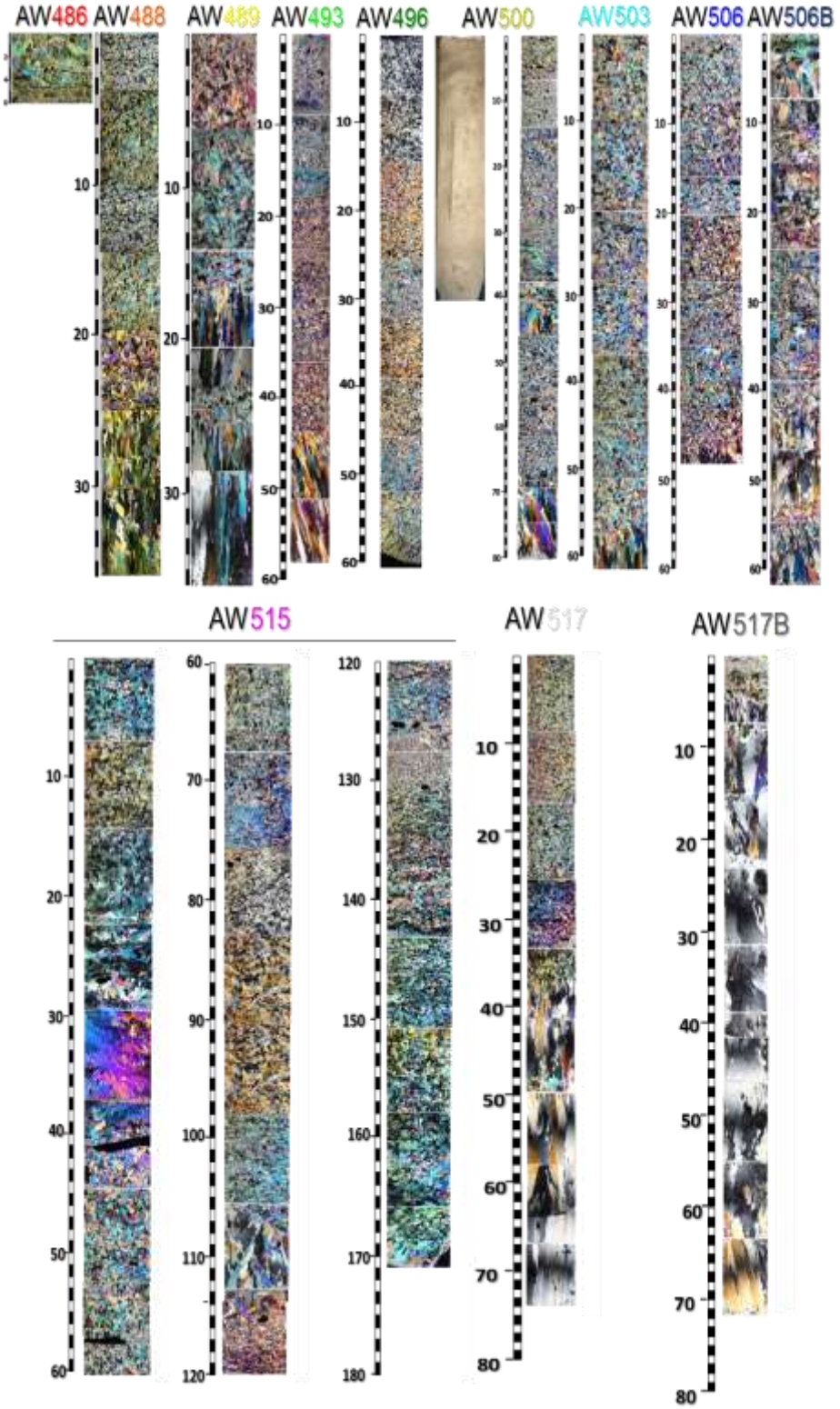

Figure 41: Textural characteristics of the AWECS cores. See Figure 39 for stations location.

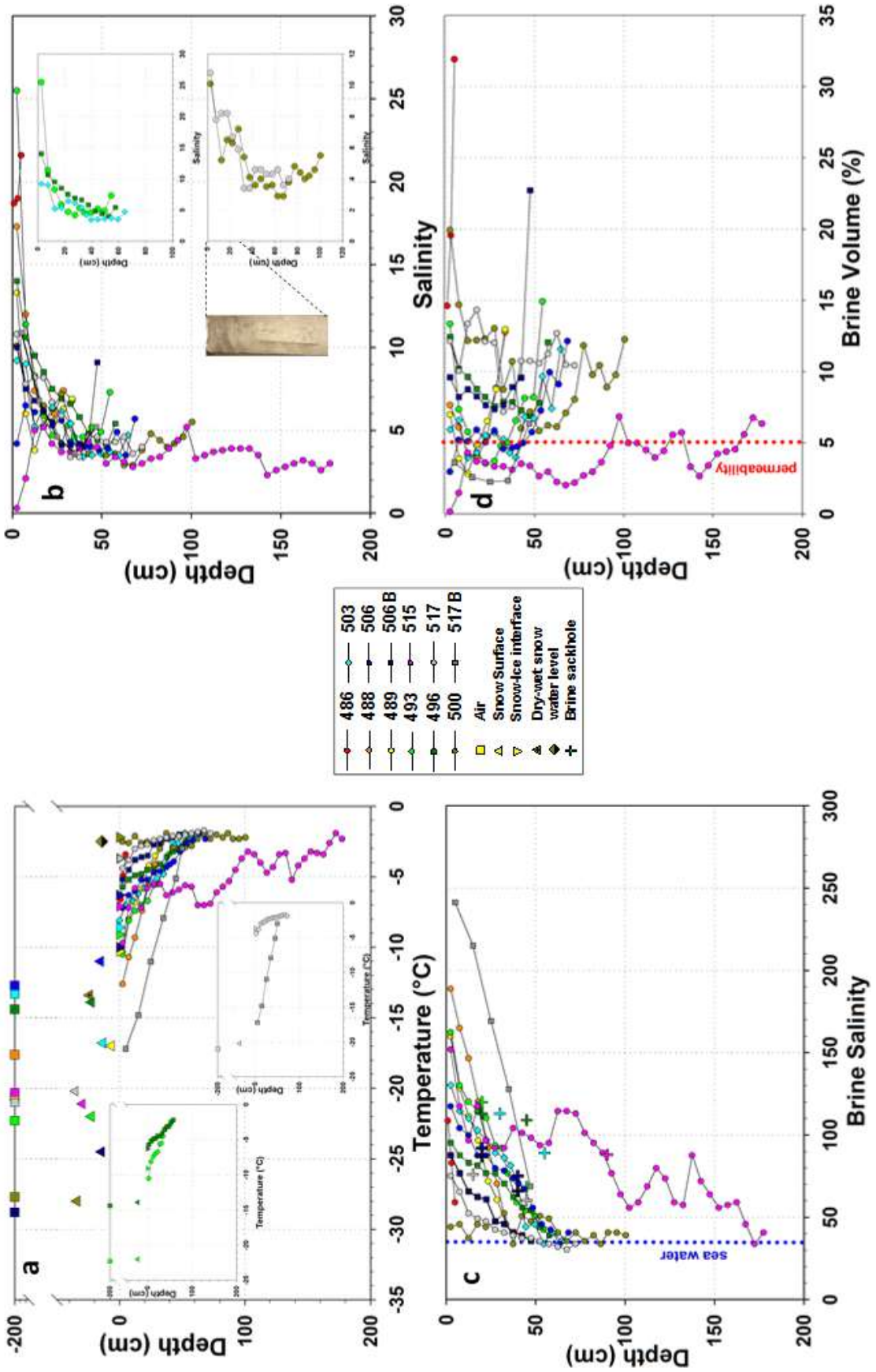

Figure 42: Basic and derived physico-chemical properties of the AWECS ice cores: a) air-snow-ice temperature, b) bulk ice salinity, c) brine salinity (calculated from ice temperature, Petrich and Eicken 2009), d) brine volume (Petrich and Eicken, 2009). Blue dotted line in c) is sea water salinity. Red dotted line in d) is the 5% permeability threshold from Golden et al. (1991).

Results – Ice temperature

Figure 42a summarizes air (squares at 2 meters elevation), snow surface (upwards pointing triangles), snow-ice interface (downwards pointing triangles) and ice (positive depths) temperatures. Complementarily, the figure also shows local snow thickness at the biogeochemistry station (mean of 10 values) and, for the strongly flooded station 500, the limit between dry and wet snow (triangle with cross) and the water level in the snow (2-colors diamond). Large temperature ranges are seen between air, snow and ice. Because of the generally high snow cover, the ice is globally quite warm for this middle of the winter period. This is clearly illustrated by the individual comparison of stations 517 (35.4 cm snow cover) and 517b (same day and same location, no snow cover) in the lower insert of Figure 42a.

Another important controlling factor of ice temperatures is the large range of air temperatures encountered during the voyage, even at a few days interval, as shown by the comparison of stations 493 and 496 with similar snow thickness (upper insert in Figure 42a). Another important consequence of the thicker snow cover is the frequent occurrence of flooding events, sometimes bringing the snow-ice interface temperature (downward pointing triangles) very close to sea water freezing point (e.g. Station 500).

Results – Ice and brine salinity

Bulk ice salinity profiles (Figure 42b) shows a classical C-shaped profile in most cases. Specific features are: a) the very high salinity of the marginal pancake ice at Station 486, b) the surface salinity decrease at stations 506 and 515, c) a relative maximum between 10 and 40 cm depth at stations 493, 496, 503 (upper insert in Figure 42b), 500 and 517 (lower insert in Figure 42b) and d) the generally low salinity and jagged profile at station 515.

Brine salinity, because of the way it is calculated, is the mirror image of the temperature profile, with most values above sea water salinity, apart from the bottom sections.

Results- Brine volumes and Rayleigh numbers

The relative volume of brines in the ice is a crucial parameter since it controls permeability, and therefore exchanges within the sea ice medium and at the interfaces. It is calculated from the ice temperature and the bulk ice salinity. It is recognized (Golden, 2003; Golden et al., 1998) that, for columnar ice, permeability increases by an order of magnitude above a relative brine volume of 5%, which would correspond to a temperature of -5°C for a bulk ice salinity of 5‰, hence the reference to the "law of fives". Because the ice temperatures remained rather warm at AWECS, a high number of stations show a brine volume above the permeability threshold (red dotted line in Figure 42d). Impermeable ice, where it exists, is limited to some internal layers and to the few surface layers with low bulk ice salinity. An obvious exception to these characteristics is the profile at the thicker ice station 515, where brine volumes are generally below or at the permeability threshold.

Rayleigh numbers (Figure 43a) further document potential brine movement in permeable ice. Denser (colder and more saline) brines will initiate convective movement in permeable ice where the density contrast will be high enough to compensate for the effect of dynamic viscosity and thermal diffusivity (see eq. 11). The value of the threshold Rayleigh number is however today still a matter of debate Hunke et al. (2011), ranging from 2 to 10. Rayleigh number profiles should therefore be mainly interpreted in terms of relative values. In Figure 43a, it is clear that only a few stations were susceptible to sustain active convection at the time of sampling: 486, 496, 506b and 517.

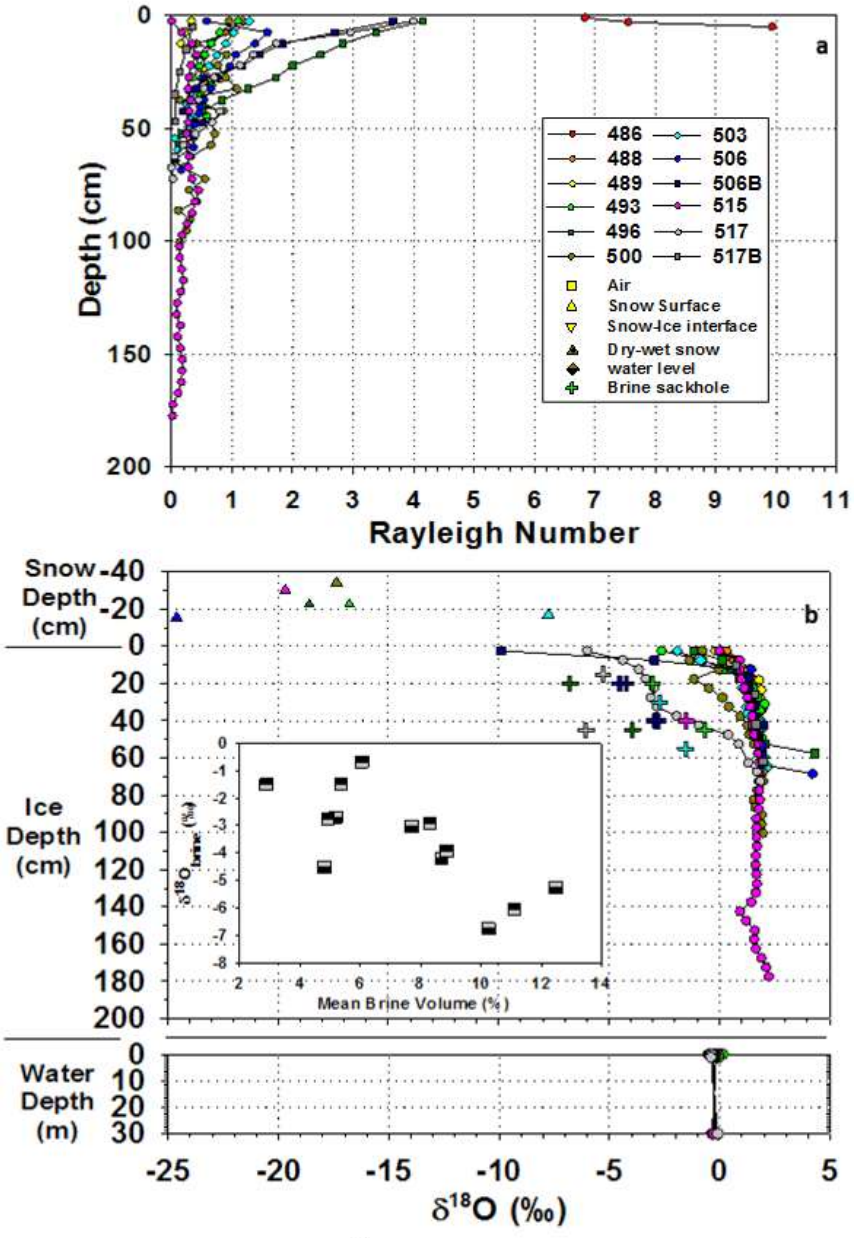

Figure 43: Rayleigh numbers (a) and $\delta^{18}O$ (b) profiles for the AWECS biogeochemical stations. Stations color caption as in Figure 42. Insert in (b) shows the $\delta^{18}O$-brine vs. mean brine volume relationship, where squares with top grey shading are shallow brines and those with bottom grey shading are deep brines. See text for details.

Results – Water stable isotopes - δD and $\delta^{18}O$

Figure 43b shows the $\delta^{18}0$ profiles in snow, ice and waters at the AWECS stations. Co-isotopic diagrams (δD vs. $\delta^{18}O$) are plotted in Figure 44, also for different sub-groups, with associated regression lines and equations. Snow samples show quite negative values (between -8 and -25‰), as expected from the meteoric cycle. Sea water is very close to SMOW with mean values in $\delta^{18}O$ and δD of respectively -0.27 and -2.83‰. Ice samples show steadily increasing $\delta^{18}O$ values with depth (Figure 43b), under the combined effect of snow ice contribution in the surface layers (Jeffries et al., 1994; Jeffries et al., 1997; Lange et al., 1990) and of a decreasing freezing rate downwards (Souchez et al., 1988). In a co-isotopic diagram (Figure 44) Snow samples near-perfectly (r^2= 0.999) align on a regression line with a slope of 7.98, as expected for a Meteoric Water Line. Sea ice samples define a very good (r^2=0.89), regression line with slope of 6.81 (Figure 44, right insert), reasonably close to what would be expected for a freezing slope from a semi-infinite reservoir of constant isotopic signature (theoretical value: 6.98, (Jouzel and Souchez, 1982; Souchez and Jouzel, 1984)). Brine samples very well align (r^2 = 0.99) on a slope of 7.70, with an equation of the regression line remaining unchanged when sea water samples are added to the group. They all show more negative values (between -0.5 and -8 ‰) than the bulk ice from which they were collected (crosses in Figure 43b), and show a global relationship of decreasing $\delta^{18}O$ with increasing brine volume (insert in Figure 43b).

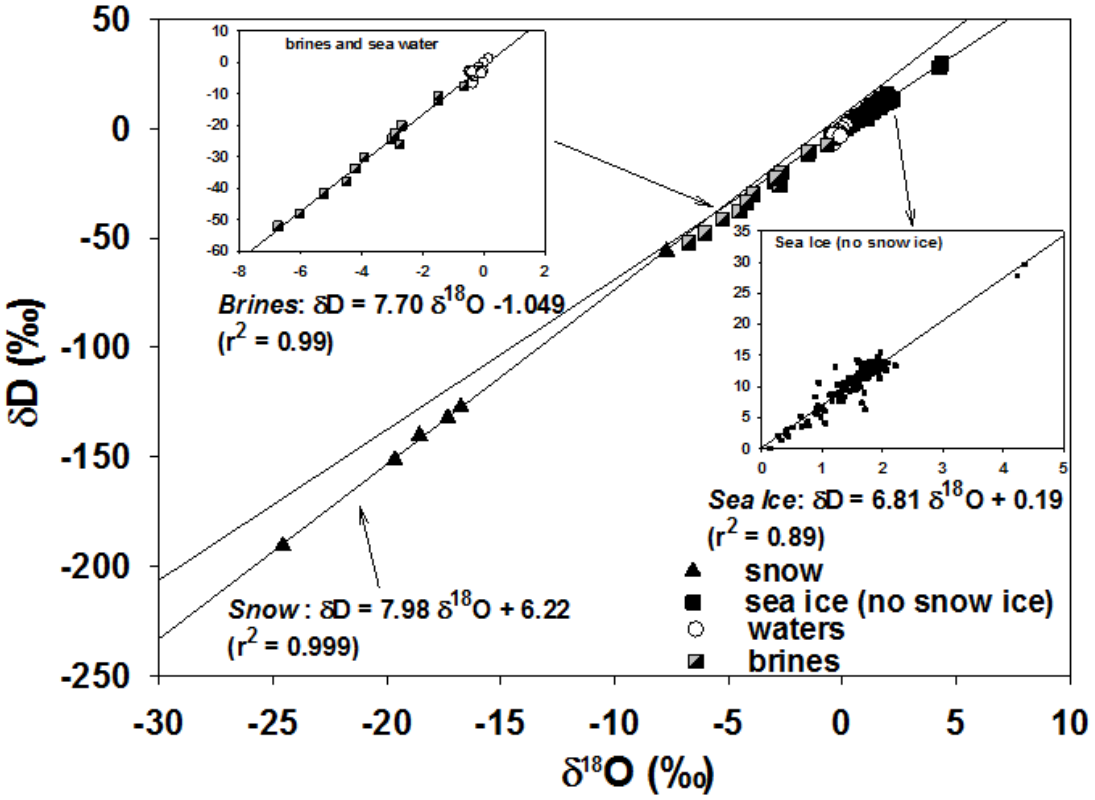

Figure 44: co-isotopic signatures of snow, sea ice, brines and waters at AWECS.

Results – Chlorophyll-*a*

Figure 45 summarizes the results of chl-a analyses at our AWECS stations, together with a few ancillary measurements: brine volume and the permeability limit (red line), air temperature, snow thickness, freeboard and the detection of "brine tubes" (see e.g. core AW500 in Figure 41) in the treated cores. A distinction is made between small (from 0.8 µm to 10 µm, in light green) and large (>10 µm, dark green) autotrophs. Globally, an internal algal community dominates along the Greenwich meridian and in the central Weddell Sea (station 496 is the exception), while a bottom community dominates along the Antarctic Peninsula, where the chl-a levels are also lower. The majority of the chl-a signal comes from the larger organisms, and there is a general trend of increasing chl-a levels from the marginal ice zone towards the Antarctic coast. Generally, also, brine tubes are observed at the stations with the highest chl-a levels.

Results – Biological characteristics at stations 506 and 506b

Because of the very strong contrast in chl-a concentrations at neighboring locations (10-20 m distance) and only 4 days apart at station 506/506b (Figure 45), it has been chosen to document the structure of the algal communities in more details. Figure 46c-d and 46e-f describe the algal speciation at locations 506 and 506b, respectively in terms of number of cells and in terms of biomass (µg C) per liter of melted ice. Figure 46g presents the result of DNA analyses at the two stations, stating the number of Operational Taxonomic Units (OTUs) specific to each location and those common to the two cores. The number of cells is increased by nearly an order of magnitude between the two locations and the biomass by roughly a factor two. While diatoms and dinoflagellates dominate the sympagic population at 506, 506b is overwhelmed by small (<10µm) unident flagellates, with total absence of dinoflagellates. Note, however, that diatoms are still in larger number at 506b than at 506. In terms of biomass, while Dinoflagellates dominate the community at 506, diatoms take over at 506b, increasing their biomass in a given layer from about 75 µg l^{-1}C to up to 400 µg l^{-1}C. Because of their small size, unident flagellates cannot compete with diatoms in terms of biomass, and remain a small fraction of the total. About half of the OTUs detected at location 506b (235 vs. 247) were already present at location 506, but, conversely, the latter presented 164 specific OTUs (not found in 506b- Figure 46g).

Discussion – A dynamic winter sea ice brine system

Our knowledge of winter Antarctic sea ice remains extremely limited, and, based on the intuition of a very cold environment during the winter, it has often been assumed that the sea ice brine system would evolve towards a closed system, with limited biogeochemical activity and exchanges. Results from this AWECS cruise are changing that perspective. As documented in Figure 39 b and c, regular intrusions of large scale synoptic depressions well into the Weddell Sea resulted into a very dynamic air temperature record, with weekly excursions between -30°C and near-zero temperatures (with even slightly positive values near the Antarctic Peninsula).

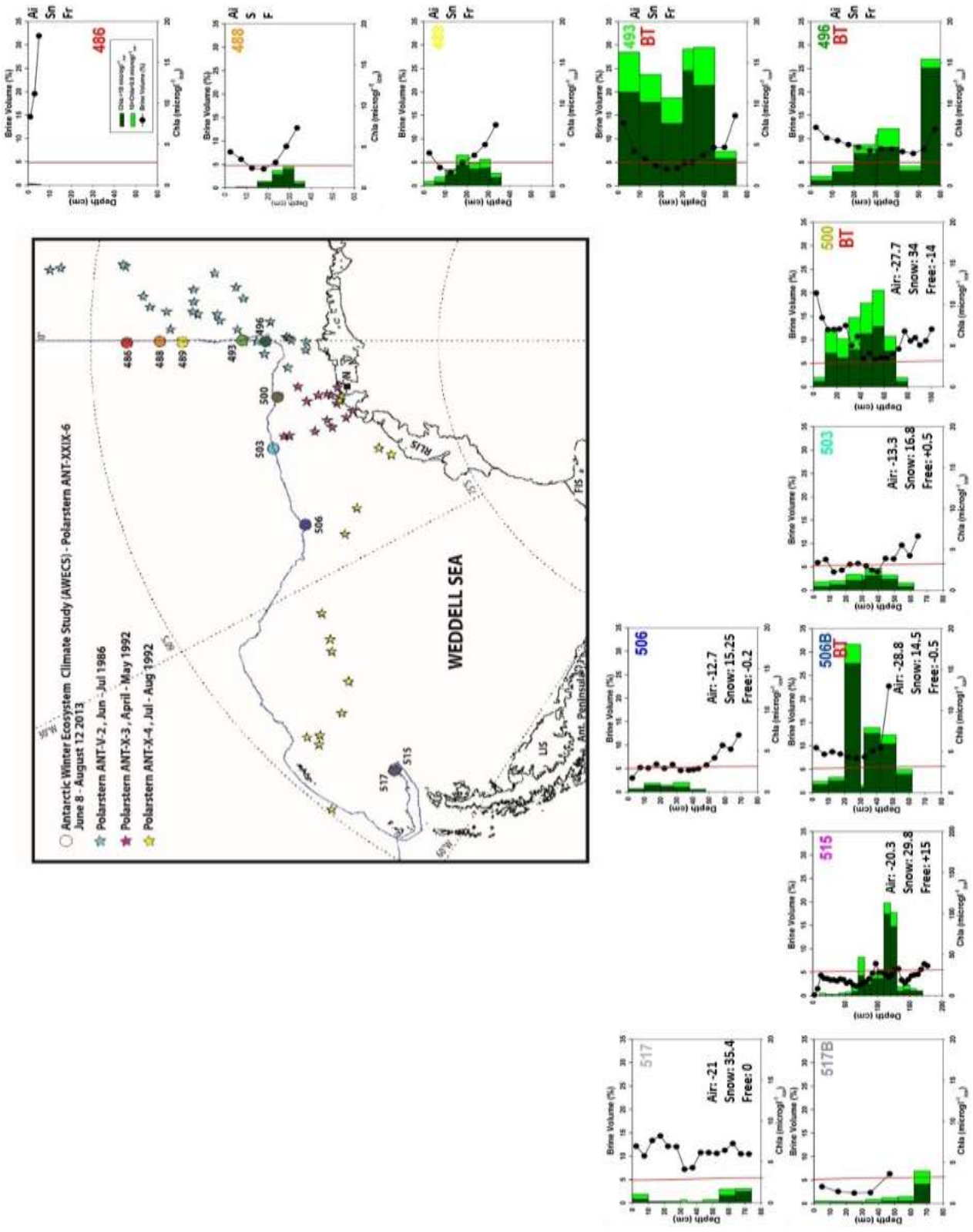

Figure 45: Chl-a concentration in $\mu g.L^{-1}_{ice}$ (> 10 µm size in dark green; between 0.8 and 10 µm size in light green), brine volume (%), air temperature (°C), snow depth (cm), freeboard (cm, negative = flooding) at the AWECS stations. BT refers to the observation of brine tubes in the upper layers of the ice cover (see text for details).

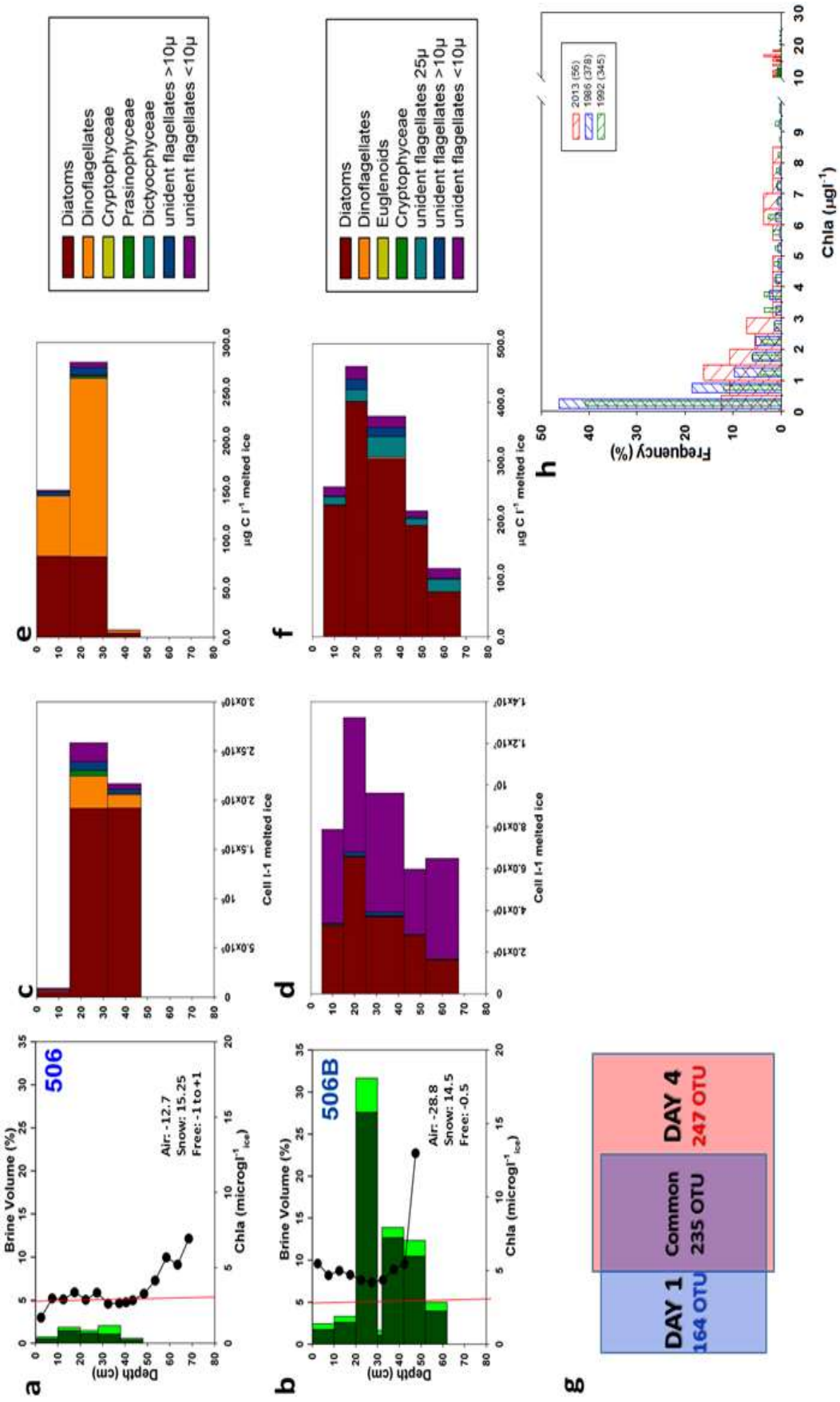

Figure 46: Biological characteristics at Station 506 (a and b are 4 days and 20 m apart) - a,b) Chla (dark green=>10 µm; light green=0.8 to 10 µm) and brine volume (black dots) with red line at permeability threshold of 5%; c,d) number of cells per litre of melted ice; e,f) biomass in µg C L^{-1} of melted ice; g) OTUs for 506 (Day 1) and 506B (Day 4) and h) Frequency distribution (%) of Chla (bins of 0.5 µg L^{-1}) for the 1986 (blue), 1992 (green) and 2013 (red, AWECS) cruises. Note the difference in scales between 41c-41e and 41d-41f.

This in turn contributed to large excursions in the sea ice cover temperature, however with a slight delay and often limited in amplitude due to the insulating role of the generalized snow cover. The latter also favored flooding of the ice cover surface by depressing the snow-ice interface below sea level. The frequency distribution of freeboard records (Figure 40, red bars) indeed shows a slightly negative median value. This resulted in two main consequences: a) the frequent occurrence of a surface snow ice layer some 10 cm thick (with maximum of 30cm to 45 cm at stations 500 and 517 - detected by negative $\delta^{18}O$ values in the profiles of Figure 43b) and b) snow-ice interface temperatures episodically reaching values close to the sea water freezing point (see station 500 in Figure 42a, with a quasi-isothermal ice temperature profile).

Although only station 506 was revisited after a few days (506b), the comparison of their temperature profile (Figure 42a), with similar snow thickness (15.25 cm vs. 14.45 cm), clearly shows large ice temperature excursions within a few days. This suggests that a similar behavior has probably affected the whole sea ice cover in the Weddell Sea in the course of the winter due to the repeated large scale intrusion of cyclonic depressions. The process is in fact similar to what has been described during the SIMBA spring cruise (Nathaniel B. Palmer, Octobre 2007), in monthly regularly investigated "process" stations where regular alternations of dry, cold air of continental origin with wet, warm air of oceanic origin were documented, resulting in similar excursions in ice temperatures (Carnat et al., 2016; Lewis et al., 2011).

A direct consequence of these temperature contrasts is the unusual occurrence of elevated Rayleigh numbers in the upper half of the ice cover at some stations (Figure 43a). Indeed, elevated Rayleigh numbers are usually encountered within the bottom layers of thermodynamically growing sea ice (Notz and Worster, 2009; Zhou et al., 2014), which is actually the case in none of the AWECS stations. High Rayleigh numbers in the upper sea ice cover are rather typical of warming spring sea ice, leading to episodic brine convective events across the whole ice cover (e.g. Zhou et al., 2013). At the SIMBA spring stations, brine movement was documented in the form of "brine tubes", initiating close to the ice cover surface, and sometimes reaching all the way to the bottom (Figures 8 and 11 in Lewis et al., 2011). Brine tubes morphology differs from brine channels. While the latter usually show a funnel-like geometry, with adventitious secondary channels converging towards a central main drainage channel, brine tubes are generally broader linear single features. Brine tubes were observed in several of the AWECS stations (493, 496, 500, 506b - Figures 41), but generally limited to the upper 30-40 cm of the ice cover. We suggest they result (as was the case at the SIMBA process stations) from the combination of flooding and the temperature cycling in the ice. During the cooling phases, surface sea water and brines partly refreeze and see their concentration increase. During the warming phases, these high salinity brines thermodynamically re-adjust, progressively dissolving the ice as they move downwards under gravity. As a result, salts and nutrients are transported downwards, a movement which is sometimes witnessed by a local maximum in salinity at those depth (see inserts of Figure 42b). This process, which can repeat itself several time in the history of the sea ice cover

a given location, together with the globally high brine volumes genereated by the warm ice temperatures (Figure 42d), supporting permeability, turn the sea ice cover into a potentially very dynamic biogeochemical environment.

Stable isotopes data also help in better understanding the dynamic of the winter sea ice brine system during AWECS. Snow samples span a large range of negative values (-8 to -25 ‰), reflecting different temperatures of formation during the precipitation phase of the hydrological cycle. Sea ice, resulting from the freezing of sea water with $\delta^{18}O$ values very close to 0‰ (-0.27‰), is enriched in heavy isotopes and shows increasing positive values downwards due to the effect of the growth rate on the intensity of the fractionation (Eicken, 1998; Souchez et al., 1988). Snow ice, as mentioned before, shows negative values, due to the contribution of snow in various proportions. Brines $\delta^{18}O$ are always more negative than the bulk ice values in the equivalent ice profile. This can only be explained in two ways: a) either it is the remnant signature of the interstitial water of the skeletal layer, later entrapped in the ice, that gets impoverished in stable isotopes while the solid ice gets enriched during growth at the dendritic interface, b) or it is the signature of infiltrated melted snow. The globally inverse relationship between $\delta^{18}O_{brine}$ and the mean brine volume shown in the insert of Figure 43b supports the latter option. Indeed, increasing brine volume during ice warming from internal ice (with positive δ values) melting only, would pull the $\delta^{18}O_{brine}$ values towards less negative values. Co-isotopic stable isotopes values shown in Figure 44 further support option b). In this diagram, snow samples nicely align on a meteoric line of slope close to 8 (7.98). Note that the local sea water displays slightly below that line, probably due to local contribution of sea ice melt from previous summer. Sea ice samples align on a lower slope of 6.81 (lower insert of Figure 44), not very far from the expected freezing slope of 6.98, calculated from the observed sea water values (Jouzel and Souchez, 1982; Souchez and Jouzel, 1984; Souchez et al., 1987). If the brine sample were mainly reflecting the signature of the remnant of interstitial water entrapped during closed system ice growth, they should lie on the same freezing slope. This is not the case since those brine samples are extremely well aligned (r^2=0.99) on a different slope of 7.70. Water samples also lie on that slope (see upper insert of Figure 44), which cross-cuts the meteoric water line at a value of $\delta^{18}O$= -25‰, suggesting that this best fit line materializes a mixing line between sea water and melted winter snow, replacing the original freeze-on signature due to active brine movement within the sea ice cover. This also suggests that snow melting actively contributes to the thermodynamic adjustment of surface brines during warming events.

Discussion – A significant algal community: active or inherited?

The winter chl-a concentration was overall surprisingly high at the AWECS stations, reaching more than 15 µg L^{-1} in several occasions (Figure 45). Concentrations globally increased along the Greenwich meridian towards the Antarctic coast, with a strong contrast both in total concentration and vertical distribution with the Antarctic Peninsula (stations 515, 517, 517b). Ice texture (Figure 41) seems to have played a determining role in this case. Central Weddell Sea samples (486 to 506b) are

predominantly made of granular ice as a result of the pancake cycle in the area (Lange, 1988; 1990). The traditional view is that scavenging processes associated to frazil accumulation in pancake ice is efficient in enriching the internal layers with living material (Garrison et al., 1983; Gradinger and Ikävalko, 1998). On the opposite, columnar ice growth tends to keep the algal community within the bottom layers, as observed for the stations along the Antarctic Peninsula (e.g. 517, 517b), and results in lower chl-a concentrations during the winter. Even in the central Weddell Sea, it appears that intermittent layers of columnar ice are less rich in chl-a (see e.g. 489 round 20 cm depth; 493 bottom, 506b bottom). Note that station 515 is a special case. Its higher thickness (>175 cm) makes it a potential candidate for young second-year ice. Occurrence of platelet ice at two different levels (30-40 cm and 105-115 cm) suggests proximity of an ice shelf along the coast, and large accumulation of compacted frazil of low salinity (Figure 42d) could point to the marginal ice zone of a polynya. This first-year landfast sea ice would have then detached and been entrapped in the newly forming winter ice, promoting it to young second-year ice, having survived one summer. There, record chl-a concentrations are observed, the highest of which (>100 $\mu g l^{-1}$) being located in the platelet ice layer, known as the most productive environment in Antarctic sea ice (Arrigo et al., 1995; Smetacek et al., 1992).

A crucial interrogation is to know if these sympagic communities are passive witnesses of past growth during the early autumnal days of sea ice build-up, or if they are still actively growing at the time of observation. Increasing chl-a concentrations southwards along the Greenwich meridian (486 to 493), suggests that older ice would have had longer time to develop its autumnal sympagic community, although this doesn't rule out that it is still active at the time of sampling. On the other hand, the presence of a chl-a maximum in the recently growing bottom columnar ice at station 517/517b, suggests that the algal population there is contemporaneous and therefore still actively growing. Traditionally again, it is considered that given the very low light levels in the winter, autotrophy should be negligible. A striking contrast in chl-a concentration profiles was observed between stations 506 and 506b that were sampled at the same location (10-20 m apart) at 4 days interval. Station 506b was sampled the last, at a time when the ice was still warm (Figure 42a) and showing high brine volumes (Figure 42d), while the air temperature was switching again towards very low temperatures, a favorable period for surface brine migration downwards in brine tubes. Because of these contrasted properties, these two stations were chosen to document further their biological properties and try to evidence potential algal winter growth (Figure 46).

A first simple question would be to know if the observed very large increase in chl-a concentration could have resulted from active growth during the 4 days interval, or if it is simply the expression of spatial variability of algal outcrops within sea ice (Arrigo et al., 1997; Eicken et al., 1991; Mundy et al. 2005). A very simple calculation would consist in applying a maximum growth potential of 1.5 divisions per day during 4 days to the initial (506) population of diatoms of 1,923,147 cells l^{-1} (Figure 46c). The result of 11,538,882 cells l^{-1} is above the number of diatom cells actually observed at 506b

(6,566,778 cells l^{-1}, Figure 46d), making the hypothesis plausible. However, the main feature of the comparison between cell numbers at 506 and 506b is the outstanding increase in the number of <10 µm unident flagellates, that can in no way be solely explained by similar maximal growth rates (maximum of 332,988 cells l^{-1}. vs. observed of 6,445,465 cells l^{-1}). Further information, can be gained from the relative proportion of common and specific Operational Taxonomic Units at both stations (Figure 46g). 399 OTUs were found at station 506 and 482 OTUs at station 506b, of which 235 were identical. Based on the unweighted Unifrac metric results this difference in OTUs is not significant (p=0.49; UWScore 0.8), meaning that the species composition is not significantly different between the two stations (i.e. at 4 days interval). The contrast could therefore result from spatial patchiness at the time of incorporation and growth However, the weighted Unifrac metric analysis, that also takes into account the relative abundance of taxa encountered within the community, showed a significant difference between the two days (p<0.001; WScore 0.63). This supports the view of active growth and fast division of cells within the 4 days interval. It is worth noting that comparing the two stations in terms of species biomass (in micrograms Carbon per liter of melted ice, Figure 46e-f) the contribution of <10 µm unidents flagellates remains moderate in 506b due to their low specific biomass (per unit cell). On the contrary, the biomass of the larger diatom cells is higher in 506b by nearly an order of magnitude, corroborating the dominance of larger cells in the chl-a signal (Figure 46b, dark green).

In summary, although it is not precluded, active algal growth at the time of sampling cannot be demonstrated by the available data. The strong contrast between stations 506 and 506b could alternatively result from initial environmental patchiness at the time of ice growth (autumn) or from recent invasion of the community due to the flooding process and increased permeability.

The latter is corroborated by the strongly increased brine volume between 506 and 506b, the presence of brine tubes, the explosion of the very small (<10 µm) unident flagellates and the presence of 247 new OTUs at 506b. It would imply that the autotroph community is quite adapted to minimum light levels at this time of the year, which is supported by laboratory PI incubations performed on board (Photosynthesis-irradiance response, J. Rintala, pers. Comm.). Clearly, future work should involve "in-situ" incubation experiments (e.g. Mock, 2002; Mock and Gradinger, 1999; Smith and Herman, 1991; Song et al., 2016) to further document this potentially active photosynthetic activity in the middle of the winter.

Discussion – A changing Antarctic sea ice in the Weddell Sea

Data on winter Antarctic sea ice properties are indeed scarce, and, for the Weddell Sea, only three winter cruises are available, including the AWECS one described in this paper. As pointed out in the description of Figure 40 in the results section, interesting trends however seem to emerge. The 2013 snow thickness distribution is clearly shifted towards higher thickness classes as compared to 1986, a trend that seems to initiate in 1992 already (Figure 40 left, Table 8). While the ice thickness median value is significantly higher in 1992 and 2013 as compared to 1986, no

significant difference is seen between the median values of the last two years. This slight increase in ice thickness could potentially reflect an increase in snow ice formation, as the snow thickness globally increased in the last decades and thin snow ice is generally found at the surface of our AWECS stations (Figures 41). Another consequence of the increase in snow thickness is the shift of the ice freeboard distribution towards slightly negative values, a global freeboard reduction that was also already present in 1992. This in turn means globally warmer ice (in extreme cases, the ice cover becomes isothermal, as in station 500 (Figure 42a)), higher brine volumes and more frequent flooding events with the possibility of brine tubes development in a rapidly changing atmospheric environment. Opening of the brine system and triggering of brine movements should favor an extension of photosynthetic activity later in autumn, or even, light-adaptation permitting, well into the winter. This is what is suggested by the significant trend (Table 8) towards higher chl-a concentration classes, as seen in Figure 46h. These long-term changes in physical sea ice properties and brine dynamics also have a considerable impact on a series of other biogeochemical processes such a CO_2 fluxes to the atmosphere, the DMS,P,O sulfur cycle, the nutrients cycle and regeneration processes, the structure of the bacterial communities a.s.o. These will be described at length in companion papers.

Increasing snow precipitations in the course of the last decades in the eastern Weddell Sea sector has also been recently documented at a coastal continental location. Philippe et al. (2016) reconstructed 250 years of snow accumulation in a 120 m ice core drilled on the Derwael Ice Rise (70°14'44.88" S, 26°20'5.64" E), coastal Dronning Maud Land, East Antarctica. The mean surface mass balance (SMB, net accumulation) for the whole core amounts to 0.47±0.02m water equivalent per year (w.e. a^{-1}). However, the record shows a general increase beginning in the 20^{th} century, particularly marked during the last 50 years (1962-2011), which yield a mean SMB of 0.61 w.e. a^{-1}.

How well are these observed trends in basic sea ice properties represented in present-day global ocean-sea ice models? Figure 47 shows the results of the simulation with the NEMO-LIM3 model described in the methods section, with "snapshots" of snow thickness, mean bulk ice salinity, mean ice temperature and mean brine volume in the Weddell Sea for July 1986, July 1992 and July 2013. Figure 48 compares the June and July 2013 outputs of the model to the mean ice cover values observed at each station. Snow thickness mostly shows coherent values with observations, increasing from negligible at the marginal ice zone to 20-30 cm in the Central Weddell Sea. Our cruise track unfortunately did not penetrate the westerly and most southerly part of the Weddell Sea where the model predicts much higher accumulations (Figure 48, left). Figure 47 shows an overall increase of snow thickness between 1986 and 2013. It is however important to realize that this increase of snow thickness cannot be related to increasing precipitations with time, since the model unfortunately runs with monthly climatologies of precipitation that do not evolve through time. Sea ice dynamics or wind redistribution might therefore be likely candidates for the observed increase in the model.

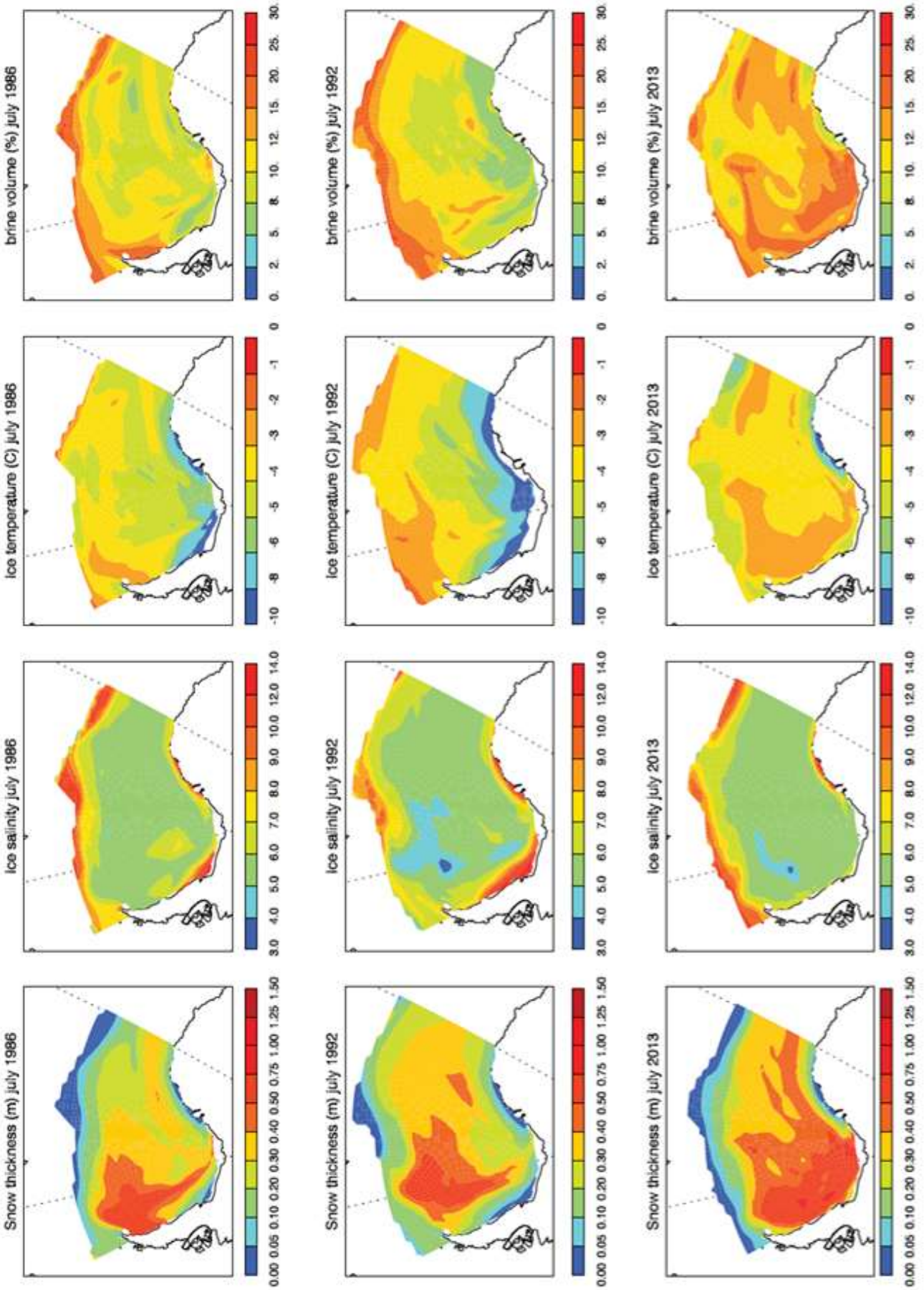

Figure 47: NEMO-LIM3 simulations of Snow thickness, mean bulk ice salinity, mean ice temperature and mean brine volume in the Weddell Sea for a) July 1986 (Polarstern Winter Weddell Sea Project 1986), b) July 1992 (Polarstern ANT X/4) and c) July 2013(Polarstern XXIX).

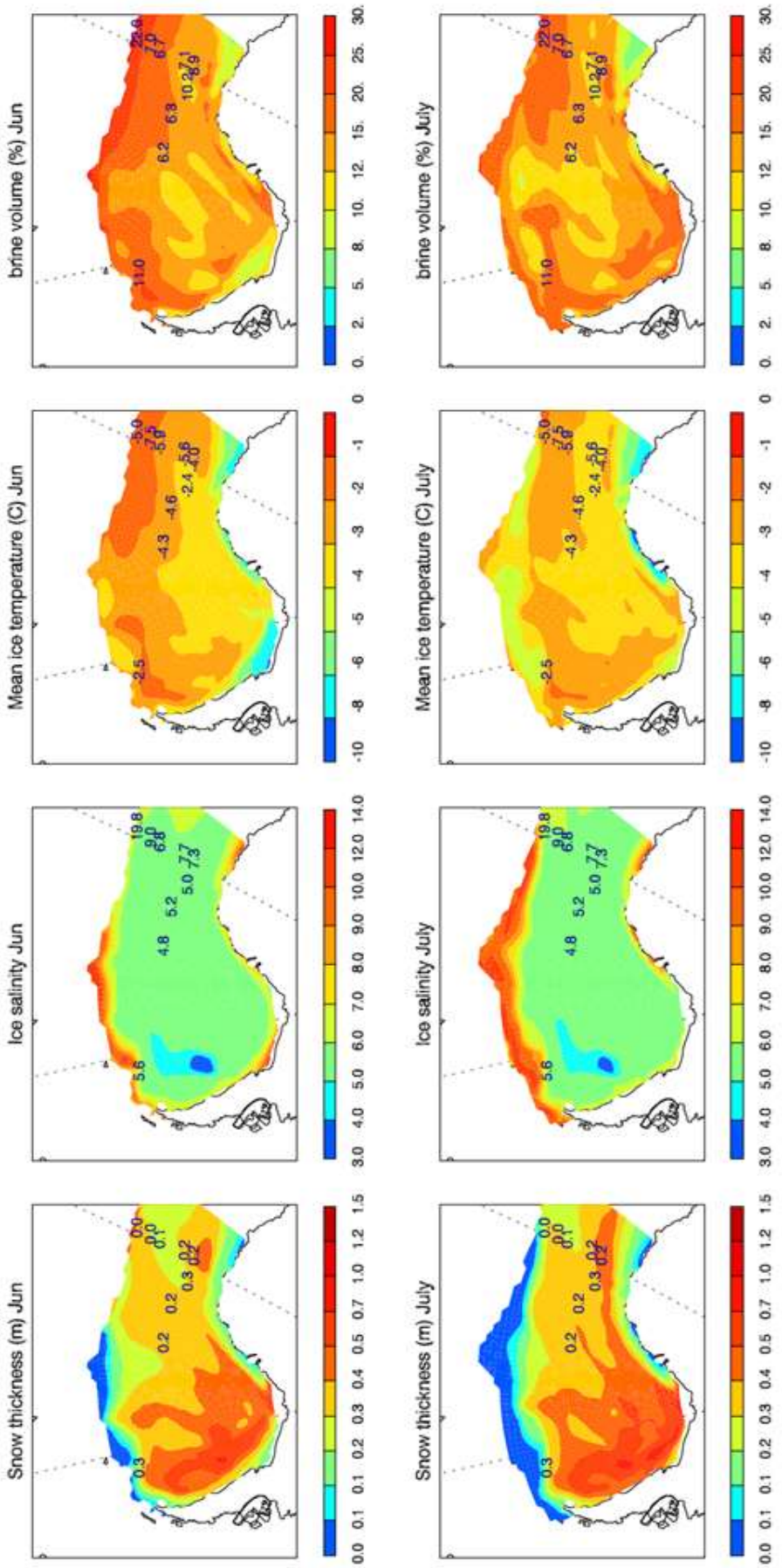

Figure 48: NEMO-LIM3 simulations of snow thickness, mean bulk ice salinity, mean ice temperature and mean brine volume in the Weddell Sea for July 2013 with observations from the AWECS cruise.

More interestingly, however, is that this temporal increase in snow cover with time clearly results in an increase in ice temperature and relative brine volume, as observed (Figure 47). Observed ice salinities are reasonably well simulated, with an increase at the marginal ice zone, and slight underestimation along the Greenwich meridian. The same is true for the mean ice temperature which is this time overestimated along the Greenwich meridian. As a result, brine volume is also overestimated. Since the model coherently translates an increase in snow precipitation in a warmer and more permeable ice cover, accordingly to observations, future modelling work should clearly show more interest in attempting to incorporate daily reanalyzes of those variables linked with the water cycle (relative humidity, cloudiness and precipitation).

3.2.4. Pack ice nutrient compilation

Plants require both light and nutrients to growth. Only the chemicals with the potential to be scarce are considered as nutrients (i.e., dissolved inorganic N, phosphate, silicic acid, and trace metals). In this compilation, we refer only to macro-nutrients (N, P, Si). Both N and P are essential elements to all life, being a structural and functional component of all organisms. At the other hand, silicic acid is predominantly used by diatoms to build their frustules in opal (biogenic silica), with a minor contribution of radiolarians and silicoflagellates.In Antarctic sea ice, previous studies reported only punctual measurements (short term cruises) of macro-nutrients, implying that the overall seasonal and spatial patterns have remained elusive. Sea ice harbors indeed high spatial and temporal variability. To overcome such variability, we compiled most of the currently available macro-nutrient data (nitrate, nitrite, ammonium, phosphate, and silicic acid) in Antarctic pack ice. Data come from peer-reviewed publications, cruise reports, and direct contributions by field-research teams. The location of these studies is shown in Figure 49. This compilation has been done in the framework of the SCOR (Scientific Committee on Oceanic Research) working group BESPII (Biogeochemical Exchange Processes at Sea Ice Interfaces) and the SCAR (Scientific Committee on Oceanic Research) expert group ASPeCT (Antarctic sea ice processes and climate). This dataset consists in 18 cruises, 282 ice cores, 2466 ice sections, and 90 sackholes.

Although that some time periods (e.g., fall and early winter) and locations (e.g., Indian sector of the Southern Ocean) are under-represented in this dataset, clear and contrasted seasonal trends for the different macro-nutrients (N, P, Si) are observed, including in function of depth. In this report, we highlight two overlooked findings from this compilation, opening new research questions. The first one concerns the strong excess in phosphorus in Antarctic pack ice, in comparison to both dissolved inorganic N (Figure 50) and silicic acid (not shown). Over the course of the seasonal spring bloom, nitrate is depleted (as well as silicic acid) but phosphate is accumulated.

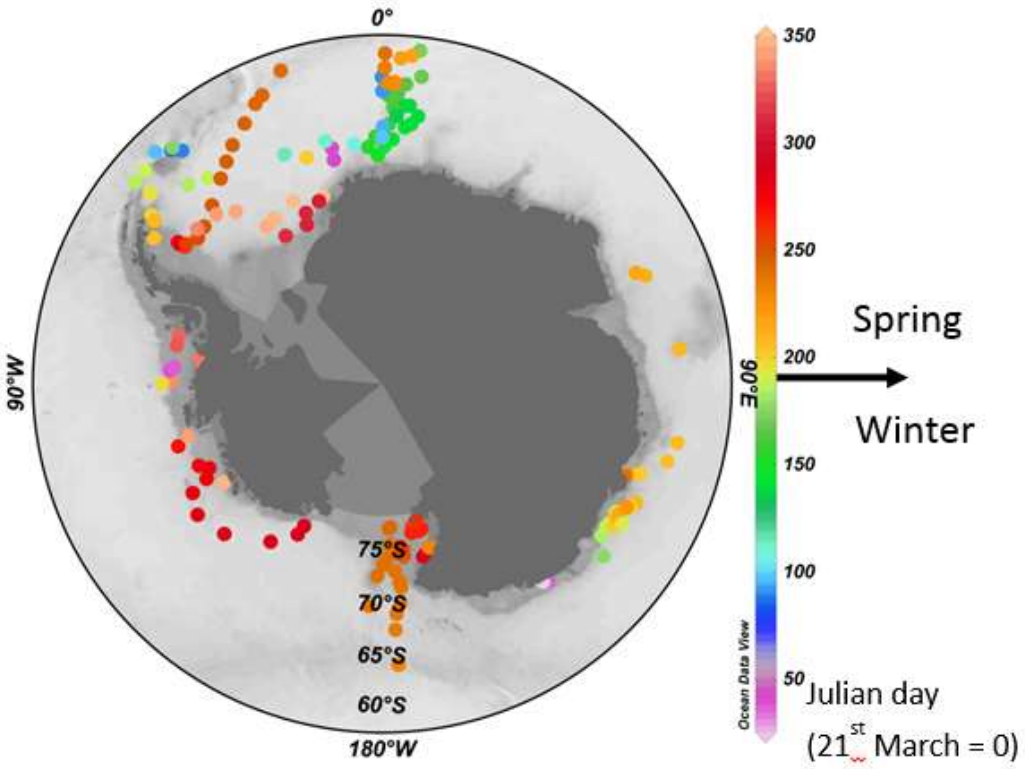

Figure 49: Map showing all the obtained sea ice cores with nutrient data collected around Antarctica. The color of the sampling site refers to Julian day but with the 21st March being the day 0. Pink to green being fall-winter, and orange-red being spring-summer.

In winter, phosphate is likely to be co-precipitated with ikaite (Hu et al., 2014). The latter is formed predominantly at the surface and in the interior of the ice where the lowest and highest temperature and salinity are recorded. The largest depletion is indeed observed in these layers (Figure 50b). The accumulation of phosphorus over seawater values required an external supply. Three processes are able to explain such accumulation:

(1) The growth hypothesis implies that algae allocate differently the ressources to the growth and acquisition (light or nutrients) machinery depending of growth rates (Sterner and Elser, 2002; Klausmeier et al., 2004; Arrigo, 2005). Bloomers should allocate a significant share of the resources into the growth machinery such as ribosomal RNA (enriched in both N and P). Survivalists at the other hand favor the acquisition machinery such as proteins and chlorophyll (enriched in N but not in P). During the sea ice algal bloom, if a mechanism is able to expel the initial excess in nitrogen out of sea ice, then, nutrient assimilation should efficiently trap phosphorus within sea ice (as greater allocation to P-rich biomolecules). The subsequent

remineralization of this P-rich organic matter will enrich the brines in phosphate. Such excess in phosphorus could be further accentuated with the expected switch from bloomers to survivalists over the course of the bloom (preferentially assimilating N over P).

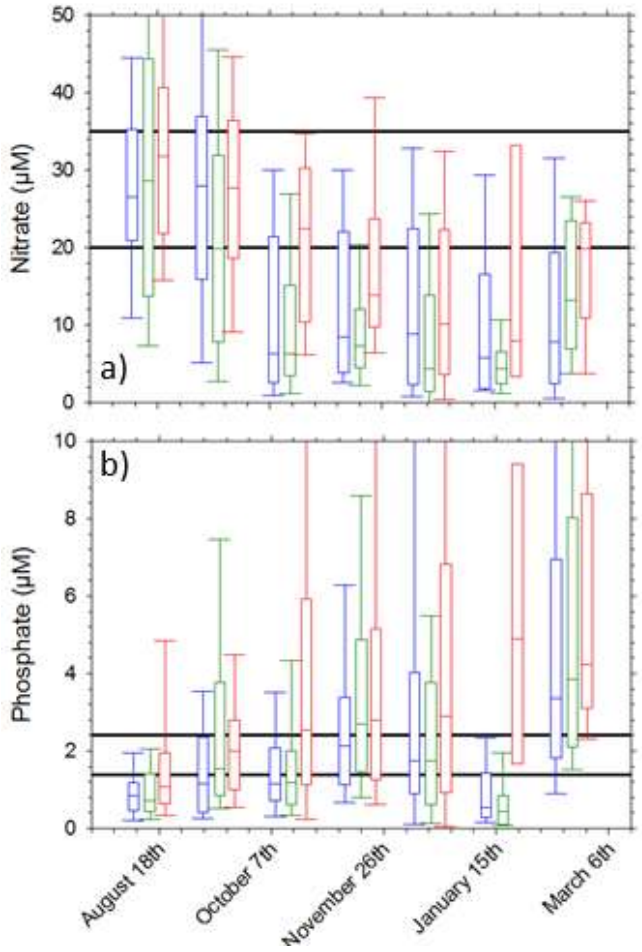

Figure 50: Salinity-normalized concentrations for nitrate (a) and phosphate (b) in Antarctic pack ice. Data have been binned by time-period (~ 1 months) and in function of depth (surface in blue, 0.0 to 0.2 m from the surface; bottom in red, 0.0 to 0.1 m from the bottom; and internal in green). The lines, boxes, and whiskers cover the median, the 25th to 75th, and the 10th and 90th percentiles, respectively.

(2) A large pool of organic matter is trapped within sea ice for weeks to months (Thomas et al., 1998, 2001; Dumont et al., 2009). Such excess of phosphorus can be aslo explained with a preferential remineralization of phosphorus with respect of both N and C, as suggested to occur also in the Ocean (Letscher and Moore, 2015, and references therein).

(3) As further discussed below, the adsorption of phosphate onto metals-organic matter complex can also produce such excess in phosphorus as the nutrient-rich underlying seawater provides a nearly-infinite pool of phosphate for sea ice.

Nutrient adsorption is a well-known process in soils, sediments, and biofilms and is clearly overlooked within sea ice. The comparison between sackhole and bulk melted ice sections could be informative in this regard. In sea ice, the main sorbent is likely to be the large pool of decaying organic matter which is trapped in the tortuosity of the brine network. Organic matter is under-represented within sackholes (Becquevort et al., 2009), likely due to preferential adsorption onto the ice walls, 'filtration' by the brine channel network, and impeded transport by sticky, gelatinous biofilm (Miller et al., 2015), implying that adsorbed nutrients should remain trapped in the sea ice matrix and not collected. We acknowledge that we cannot rule out spatial variability in such comparison as (1) adjacent cores can have dramatically different biogeochemical compositions, and (2) brine collected in the holes integrates the biogeochemical properties of numerous individual brine structures from an undefined volume of ice (over several tens of centimeters). For these reasons, only large differences will be interpreted and only cores from the same cruises will be compared. No clear differences in salinity-normalized concentrations for both nitrate+nitrite and silicic acid are observed between these two sampling techniques (Figure 51). In contrast, higher salinity-normalized concentrations are clearly reported for ammonium and to a lower extent for phosphate in bulk ice sections.

Ammonium adsorption onto organic matter is a well-known process both within soils, sediments, and biofilms. This results from the presence of ionisable functional groups (carboxylic acid and hydroxyl being the most important), conferring a negative net charges to organic matter following deprotonation at the pH typically encountered within sea ice. To be measured in bulk melted ice sections, ammonium has to be desorbed, at least partly. It is likely that the resulting large ammonium dilution, among other processes (changes in the ionic strength, pH, ...), with melting could induce some desorption of this easily exchangeable pool.

To a lower extent, the comparison in phosphate concentrations between sackholes and bulk melted sections also suggest some adsorption within sea ice (Figure 51). Phosphate adsorption is also a well-known process in both soils and sediments. In these environments, the variable charges induced by change in pH are favorable to phosphate adsorption, because surface hydroxyls at the surface of minerals (silicate clays or metal - (oxyhydro) oxides) are readily replaced by phosphate ligands. However, such minerals are not likely to be abundant in Antarctic pack ice, and phosphate do not react with organic matter (likely being the main absorbent within sea ice). However, phosphate does react with Fe and Al associated with organic matter (metal-DOM complexes) (Maranger and Pullin, 2003). The presence of both large quantities of organic matter and trace metals in sea ice should favour this process, as already suggested in Becquevort et al. (2009).

Although that the assimilated nitrate is ultimately transformed to ammonium with remineralization, the latter with the potential to be adsorbed. The exchange with ammonium-poor and phosphate-rich seawater should still be able to build an excess in phosphorus within sea ice. Clearly, studies looking at organic and inorganic matter stoichiometry (C:N:P) will be useful to disentangle between these hypothesis, as well as kinetic adsorption experiments.

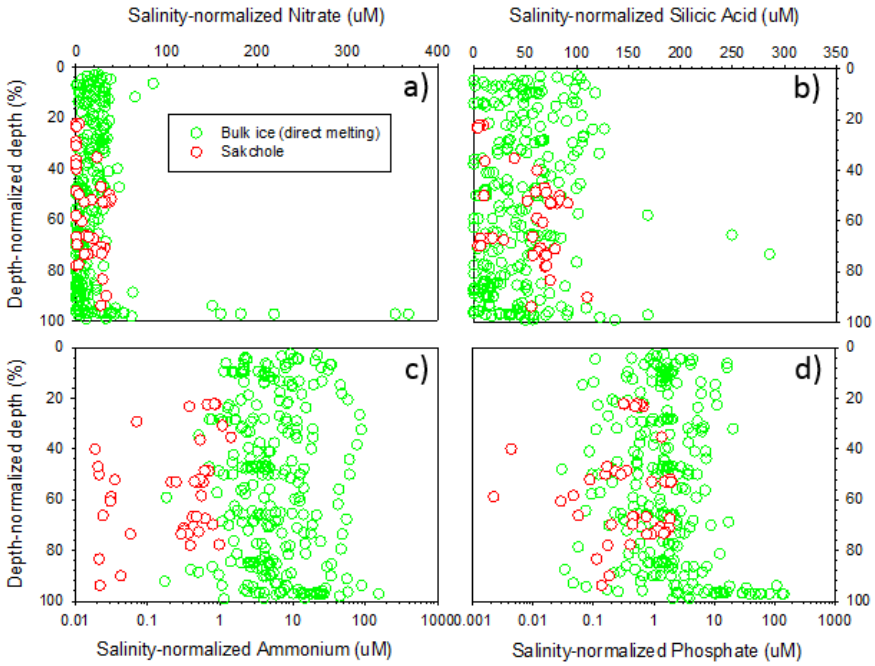

Figure 51: Salinity-normalized concentrations between sackhole (in red) and bulk melted ice sections (in green) from the corresponding cruises. The different panels show for nitrate (a), silicic acid (b), ammonium (c) and phosphate (d).

3.2.5. Trace metals in snow, sea ice, and underlying water

Iron (Fe) is a bio-essential metal with extremely low and therefore bio-limiting concentrations in more than 30% of the oceans, including the Southern Ocean. It has a crucial impact on the biogeochemical cycles of carbon and other elements with ultimate influence on the Earth climate system. Other trace metals, like Mn, Zn, Co and Cu are also required for microorganisms cell metabolism and may be (co-)limiting in those areas. Trace metal inputs from atmospheric dust are known to be generally insignificant in Antarctica. In the case of Fe, previous dissolved and particulate concentration data from East Antarctica and the Weddell Sea pack ice showed that Fe is 10-100 times more concentrated in the sea ice than in underlying seawater and that sea ice melt can deliver up to 70% of the daily Fe supply to the surface waters (Lannuzel et al. 2007, 2008, 2010). According to budget estimates, sea ice accumulated Fe in the Weddell Sea and East Antarctic pack ice would largely be derived from the underlying seawater rather than from atmospheric inputs. Our general objective is to assess the role of sea-ice as a source of bio-essential trace metals and its impact on primary production and on the biological carbon pump. Most of the studies on trace metals in the sea ice so far focused on Antarctic pack ice in

				Fe nM	Al nM	Mn nM	Co pM	Ni nM	Cu nM	Zn nM	Mo nM	Cd pM	Pb pM
SEA ICE	Nov-Dec 2011	Diss	**AVG**	**10.3**	**23.9**	**3.4**	**18.0**	**2.5**	**3.0**	**19.9**	**14.6**	**347**	**59**
			MIN	0.6	5.4	0.6	8.5	0.9	0.5	6.1	9.1	101	10
			MAX	34.4	58.9	19.7	43.4	8.1	11.6	74.3	22.6	1584	182
		Part	**AVG**	**36.0**	**121.5**	**0.9**	**309.2**	**0.7**	**0.6**	**7.5**	**0.1**	**33**	**20**
			MIN	5.7	20.9	0.1	13.7	0.1	0.1	0.2	0.0	1	3
			MAX	135.9	454.2	3.4	1450.8	1.8	2.2	33.2	0.1	332	82
	Sept-Nov 2012	Diss	**AVG**	**7.4**	**21.0**	**2.5**	**17.0**	**1.8**	**1.3**	**9.7**	**19.4**	**343**	**61**
			MIN	0.9	2.2	0.3	6.4	0.8	0.4	1.6	11.8	133	9
			MAX	39.6	72.4	12.5	26.5	5.8	5.1	32.9	34.3	1343	183
		Part	**AVG**	**78.9**	**275.6**	**2.1**	**238.0**	**0.4**	**0.3**	**5.1**	**0.0**	**37**	**28**
			MIN	5.4	14.6	0.0	26.0	0.0	0.0	0.1	0.0	0	2
			MAX	434.4	1905.5	15.7	754.0	1.5	1.3	41.2	0.2	376	88
SNOW	Nov-Dec 2011	Diss	**AVG**	**1766**	**7884**	**60.0**	**601**	**2.5**	**2.3**	**13.3**	**19.6**	**99**	**262**
			MIN	110	900	10.0	109	0.6	0.5	5.1	3.8	17	181
			MAX	2966	14560	89.4	908	3.6	3.3	19.3	44.0	191	381
	Sept-Nov 2012	Diss	**AVG**	**4300**	**12970**	**370**	**1309**	**5.3**	**4.6**	**81.4**	**134.8**	**40**	**370**
			MIN	221	274	60	91	2.7	0.7	6.7	6.1	0	60
			MAX	17751	69430	1310	5648	12.8	17.2	364.9	619.8	91	1310
BRINE	Nov-Dec 2011	Diss	**AVG**	**11.8**	**42.0**	**2.6**	**52.0**	**8.2**	**3.4**	**10.3**	**130.3**	**430**	**206**
			MIN	4.9	22.4	1.9	33.5	6.3	2.1	6.8	105.7	296	122
			MAX	22.5	75.1	4.1	73.1	10.4	5.9	12.1	150.9	643	291
	Sept-Nov 2012	Diss	**AVG**	**13.4**	**6.8**	**8.6**	**103.2**	**12.5**	**3.7**	**17.9**	**130.6**	**1875**	**107**
			MIN	6.2	4.0	6.8	89.6	10.6	3.3	13.2	110.2	1561	41
			MAX	28.7	13.3	11.3	118.9	14.7	4.4	22.6	158.3	2414	284
SEAWATER	Nov-Dec 2011	Diss	**AVG**	**2.1**	**12.8**	**1.2**	**33.5**	**6.4**	**2.0**	**6.6**	**109.5**	**738**	**22**
			MIN	0.9	3.2	1.1	28.3	5.8	1.9	4.7	107.5	699	9
			MAX	4.6	27.4	1.4	40.2	6.6	2.1	9.2	115.6	813	34
	Sept-Nov 2012	Diss	**AVG**	**1.5**	**7.4**	**1.1**	**40.3**	**6.6**	**2.0**	**17.1**	**94.9**	**707**	**22**
			MIN	0.9	4.2	1.0	34.2	6.5	1.7	7.2	85.6	700	13
			MAX	2.0	9.4	1.1	51.7	6.7	2.3	39.7	101.9	725	41

Table 9: Dissolved and particulate trace metals in sea ice, snow, brine and seawater during YROSIAE.

early spring-summer. In the present project, our aim was to investigate land-fast ice during one year around as well as pack ice in winter in Antarctica. Sea ice, brines, snow and under-ice seawater have been collected: (1) in the land-fast ice environment at Cape Evans during the YROSIAE sampling program (Scott Base, McMurdo Sound, Ross Sea, Antarctica) from November 2011 to December 2011 and from August 2012 to December 2012 (2) in the Weddell Sea during the AWECS cruise aboard RV Polarstern from June to August 2013. In order to assess the importance of atmospheric inputs in McMurdo Sound in providing bio-essential trace metals, dust samples were also collected at Cape Evans. Samples were also collected from a sediment trap deployed at 20m depth at Cape Evans.

A method was developed to measure trace metals Mn, Fe, Al, Co, Ni, Cu, Zn, Mo, Cd, Pb in sea ice, snow and seawater by multiple element isotope dilution (Milne et al., 2010). Samples are pre-concentrated by micro-columns filled with the resin Nobias Chelate PA-1 (Hitachi High Technologies, Japan) (Sohrin et al., 2008; Biller et al., 2012). Isotope dilution measurements are done using an Agilent 7700x ICP-MS. The mono-isotopic elements Al, Mn and Co were quantified by means of a detector response factor using as an internal standard the Ni concentration as determined with high accuracy by isotopic dilution. Blanks were low and reproducible. The abovementioned trace metals as well as P, Sc, Ti, V, Cr, Ga, Ge, Sn, Ba, YREE's (Rare earth elements with Yttrium) and Th were quantified in suspended

particulate matter of the sea ice collected during YROSIAE by external calibration using In as internal standard.

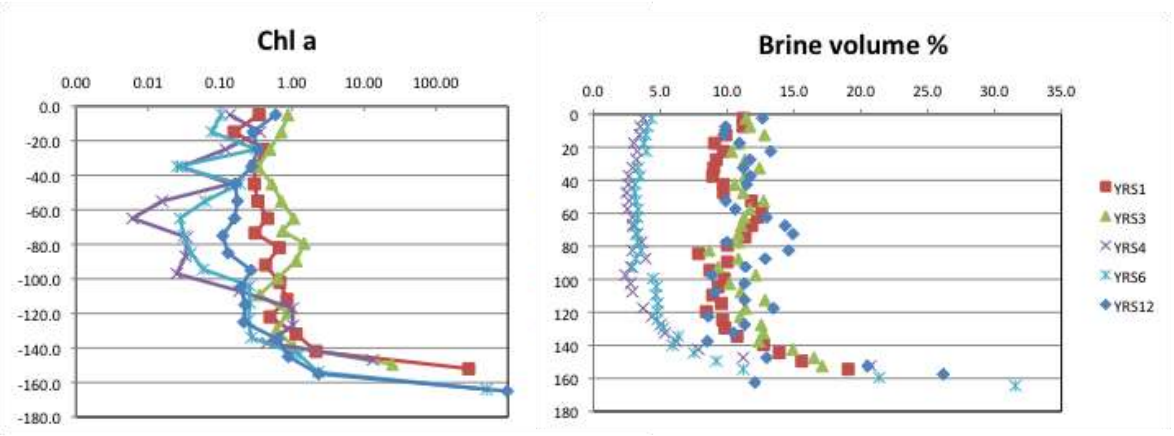

Figure 52: Chl-a, together with Brine volume along the ice cores.

Yrosiae

Trace metals: Results obtained in McMurdo Sound are shown in Table 9. The data are summarized for stations YRS-1 (28/11/11), -3 (8/12/11), -4 (18/9/12), -6 (17/10/12) and -12 (30/11/12). Dissolved trace metals concentrations in snow are one to up to five orders of magnitude higher than the concentrations previously observed in snow from East Antarctica (Lannuzel et al. 2011), showing a much stronger dust input of these metals in McMurdo Sound, confirming findings by De Jong et al. (2013). The trace metal concentrations observed in the snow are extremely variable with highest values being 2 orders of magnitude higher than the lowest ones.

Concentrations of Fe, Al, Mn and Co are much higher in the snow than in the under-ice seawater, whereas concentrations of Cu, Zn, Ni and Pb are similar and the concentrations of Mo and Cd are lower. Similar concentrations of dissolved trace metals were observed in under-ice seawater in Nov-Dec 2011 and in Sept-Nov 2012. Dissolved trace metals in brines were generally higher in 2012 than in 2011, due to a lower brine volume in 2012 (Figure 52). Although dissolved trace metals in sea ice are not significantly different from one year to the other, the particulate sea ice concentrations are higher during Sept-Nov 2012 than during Nov-Dec 2011. This is coinciding with a large difference of the chl-a development, which exhibited much higher concentrations in 2012 than in 2011 (Figure 52).

Lanthanides: From light REE's to heavy REE's, ionic radii become smaller in a systematic way, with gradually changing chemical properties in the marine environment as consequence. REE's have a trivalent oxidation state, with the exception of Ce (III or IV) and Eu (II or III). YREE patterns can be used to identify sources, redox processes, scavenging and (organic) complexation. YREE

concentrations in sea ice particulate matter (summarized in Table 10) were strongly correlated with Al (R>0.9), so we used YREE/Al elemental ratios to draw some general conclusions.

SEA ICE			P	Sc	Ti	V	Cr	Ga	Ge	Y	Sn	Ba	La	Ce	Pr	Nd	Sm	Eu	Gd	Tb	Dy	Ho	Er	Tm	Yb	Lu	Th
			nM	pM	nM	pM	nM	nM	pM	pM	pM	pM	pM	pM	pM	pM	pM	pM	pM	pM	pM	pM	pM	pM	pM	pM	pM
Nov-Dec 2011	SPM	**AVG**	**268**	**59**	**14**	**68**	**1.3**	**0.2**	**16**	**22**	**23**	**266**	**29**	**32**	**3.8**	**12.4**	**2.5**	**0.9**	**2.1**	**0.5**	**1.9**	**0.6**	**1.3**	**0.4**	**1.6**	**0.5**	**15.4**
		MIN	8	14	2	11	0.3	0.0	2	2	7	36	5	3	0.6	1.6	0.3	0.2	0.4	0.1	0.3	0.1	0.3	0.1	0.3	0.2	2.8
		MAX	2197	206	45	289	4.5	0.7	99	93	64	1048	137	119	13.6	46.8	8.7	2.8	6.8	1.7	6.2	1.7	4.3	1.3	6.7	1.4	56.7
Sept-Nov 2012	SPM	**AVG**	**324**	**76**	**23**	**174**	**0.9**	**0.6**	**28**	**43**	**20**	**810**	**48**	**84**	**9.3**	**31.3**	**5.6**	**1.8**	**4.6**	**0.7**	**3.7**	**0.8**	**2.3**	**0.4**	**2.5**	**0.5**	**11.4**
		MIN	2	11	2	13	0.2	0.1	1	2	5	73	1	2	0.3	0.8	0.2	0.1	0.2	0.1	0.1	0.1	0.1	0.1	0.2	0.1	1.4
		MAX	2962	498	149	1013	2.1	2.7	208	244	85	3877	398	710	76.4	258.5	44.2	13.8	34.5	4.7	25.8	4.8	13.3	1.8	12.6	2.3	72.7

Table 10: Particulate P, trace metals (cont.) and YREE in sea ice.

The YREE/Al pattern was normalized to the seawater YREE/Al pattern. For this we used South Atlantic Ocean upper water column YREE values from Hathorne et al. (2015) and Al from Middag et al. (2011). The normalized YREE pattern (note Y between Dy and Ho for reasons of similar ionic radii) reveal an enrichment of LREE's versus HREE's (Figure 53). This is consistent with the notion that heavy REE's are forming stronger compexes (organic or inorganic) in the dissolved phase and are therefore less prone to scavenging than the light REE's (Sholkovitz et al., 1994). A strong Ce enrichment hints at the oxidation of Ce(III) and subsequent scavenging to particles. This Ce anomaly (= Ce / (0.5*La+0.5*Pr)) amounts to 13.8. An Eu anomaly (= Eu / (2/3*Sm + 1/3*Tb) of 1.44 can also be discerned. Eu anomalies are usually associated with high temperature enviroments such as volcanoes and hydrothermal activity (Byrne & Sholkovitz, 1996). To our knowledge there are no submarine hydrothermal vents in McMurdo Sound. It could thus be possible that Eu is simply more susceptible in sea ice to scavenging than its REE neighbours. It should however not be excluded that the Eu anomaly may well be derived from a sedimentary source of volcanic origin. Phonolytic basalt at Mount Erebus is known to exhibit a positive Eu anomaly of 1.31 (Kyle & Rankin, 1976) so this material could explain the Eu anomaly in sea ice particulate matter by ways of transport of wind blown particles from nearby Cape Evans and sediment resuspension of basalt erosion products. For instance, black basaltic particles were observed in abundance on the snow during station YRS-12. Previously, Y-Ho fractionation in seawater was described by Bau et al. (1997) and Nozaki et al. (1997) and was proposed as an indicator of the impact of particles on the distribution of trace metals. This fractionation occurs despite similar ionic radii and can be explained by a different electron configuration of Y, leading to a higher particle affinity for Ho than for Y and thus an enrichment of Y in seawater.

For instance the dissolved Y/Ho ratio for seawater is twice higher than for shale (115 vs. 48). Consequently, Y in particulate matter should be depleted relative to Ho. An Y depletion is what we indeed observe (Figure 54). If we look into detail at the Y/Ho ratios in sea ice particulate matter (Figure 54) we note much lower values than seawater or shale, meaning that Y is strongly depleted. There is also a tendency to increasing ratios with time, during both sampling years. A similar trend is seen in the La/Yb ratios, which can be taken as representative indicator for LREE/HREE

fractionation. Y/Ho and La/Yb seem to be lagging behind in the bottom ice, where chl-a is the highest. The temporal increase of Y/Ho and La/Yb especially in the upper part of the cores indicates increased scavenging of LREE and Y. At the same time, brine channels are opening up and chl-a is picking up in the upper part of the cores (Figure 52). Increases in particulate Ti and Al in the upper part of the cores (not shown) seems to suggest that wind blown dust is percolating into the ice by means of the brine channels becoming more and more interconnected. This means that organic and oxide complexation surfaces increase in the upper part of the ice core, leading to an increased potential for scavenging. The lagging temporal increase in bottom ice of Y/Ho and La/Yb is perhaps due to the dominance of less efficient organic scavenging surfaces as opposed to predominantly Fe and Mn oxyhydroxide scavenging surfaces in the upper part of the cores.

On the whole the YREE results seem to underline the importance of trace metal scavenging in the trace metal cycling and enrichment of sea ice.

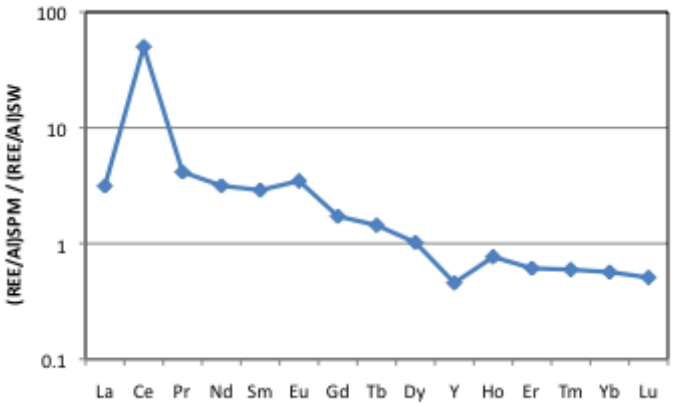

Figure 53: REE pattern of sea ice particulate matter, normalized to Al and seawater.

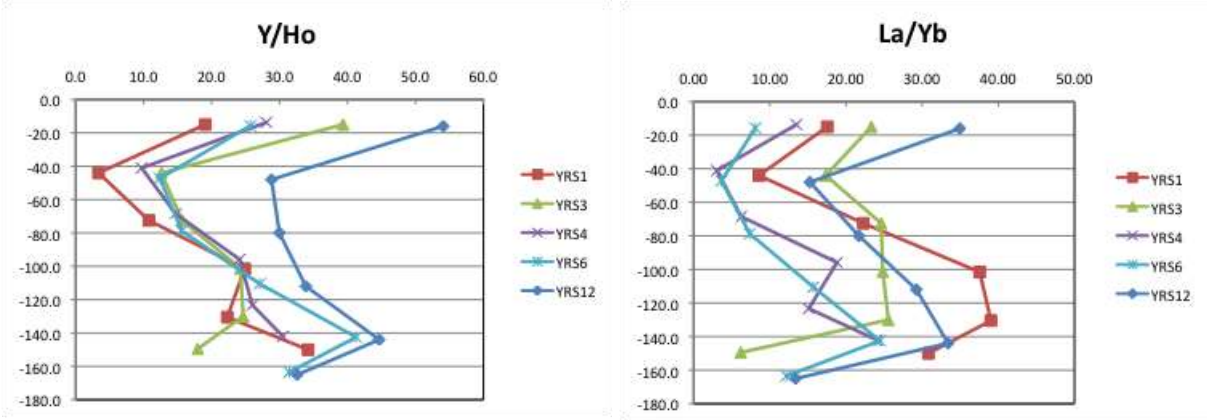

Figure 54: Y/Ho and La/Yb ratios in SPM along the ice cores.

AWECS

The AWECS cruise was a unique opportunity to study sea ice trace metal biogeochemistry and dynamics in the earliest stages of sea ice formation during mid winter. The analytical work is still in progress, but the following important conclusions can be drawn already from the preliminary results.

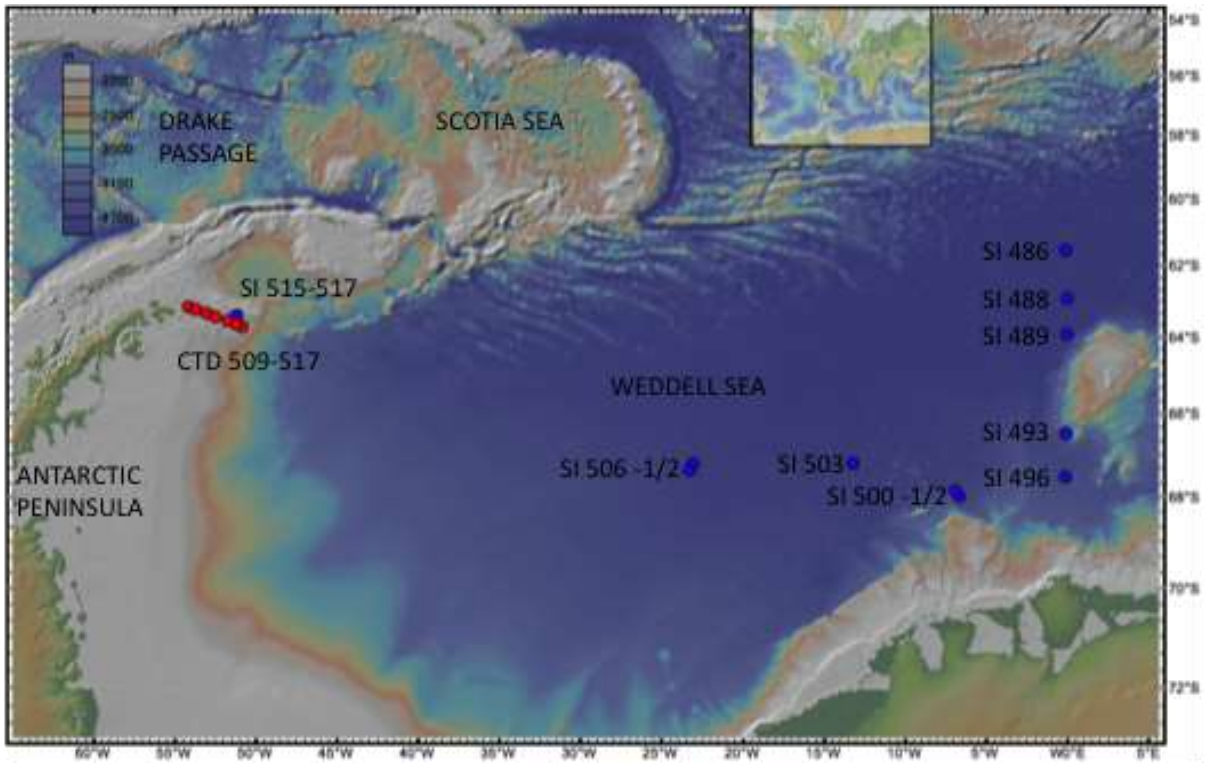

Figure 55: AWECS sea ice stations (blue) and CTD stations (red) which were sampled for trace metals, superimposed on a bathymetric map. Station 486 at the ice edge, the other stations in dense pack ice.

Sea ice – Comparing very young sea ice in the form of pancake ice (St 486) and young ice formed in a lead at St 500 (see Table 11), we can see that in function of increasing ice thickness the trace metal concentrations in the ice increases also. This demonstrates the capacity of sea ice to scavenge and preconcentrate trace metals from the seawater from which it is formed. This is confirmed in an ice growth experiment that was conducted at St 517 (see below).

Unfiltered and dissolved trace metals			Fe	Fe	Ni	Ni	Cu	Cu	Zn	Zn	Mo	Mo	Cd	Cd	Pb	Pb	Al	Al	Mn	Mn	Co	Co
Sea ice	AWECS	Ice thickness	nM	nM	nM	nM	nM	nM	nM	nM	nM	nM	pM	pM	pM	pM	nM	nM	nM	nM	pM	pM
		cm	F	UF	F	UF	F	UF	F	UF	F	UF	F	UF	F	UF	F	UF	F	UF	F	UF
486-SI	Pan cake ice	15	3.5	(841)	4.7	6.4	4.5	13.9	52.3	82.7	74	76	410	437	899	(3081)	43.3	(286)	1.3	5.4	44	(250)
500-YSI1	Young sea ice	6	0.9	10.2	2.6	2.6	1.0	1.3	7.4	8.3	46	46	300	300	56	67	9.6	18.9	0.4	0.5	17	19
500-YSI2	Young sea ice	6	2.1	10.7	3.0	2.8	1.4	1.9	12.1	11.7	52	47	375	327	133	134	30.2	105.2	1.0	1.0	20	20
500-SL	Slush		0.2	2.0	4.0	4.1	1.1	1.2	3.2	3.2	73	74	439	433	13	15	0.6	7.7	0.2	0.2	19	18
503-FF1	Frost flowers		0.4	5.9	11.8	11.9	4.2	4.3	7.5	16.3	117	204	1135	1126	119	108	9.5	15.8	0.5	0.6	50	57
503-FF2	Frost flowers		0.4	6.5	12.5	12.6	4.0	4.2	6.8	8.7	127	176	1210	1205	(104)	72	2.6	7.6	0.6	0.6	52	58

Table 11

We also note the presence of slush (mix of melted snow and seawater) at St 500 due to flooding of the ice floe with seawater. The snow cover consisted of surface layer of

20 cm dry snow, 10 cm wet snow, followed by 14 cm of slush. Trace metal concentrations were generally low in the slush layer, probably due to the mixing of low TM snow with low TM seawater at this remote position in the Weddell Sea (i.e., far away from terrestrial sources of atmospheric dust and sedimentary input). We also report the first TM data for frost flowers. Frost flowers are ice crystals commonly found growing on young sea ice in cold, calm conditions. The ice crystals are similar to hoar frost, and are commonly seen to grow in patches around 3–4 cm in diameter. Frost flowers growing on sea ice have extremely high salinities and concentrations of volatile sea water chemicals and, because of their high surface area, are efficient releasers of these chemicals into the atmosphere. The TM concentrations in frost flowers are comparible with those in brines and especially Cd is high. A role for sea ice bacteria in the biomethylation of heavy metals like Hg,Pb and Cd has been reported before (Ponratz and Heumann, 1999), and sea ice can thus be a source to the atmosphere of volatile monomethylated Cd.

Brines - Brine concentrations (Table 12) collected from sack-holes generally exhibit enhanced concentrations. Taken over time we observe a general increase of the TM content of the brines. This coincides with the cruise track going from very cold regions of the Southeastern Weddell S to the warmer climatology of the Antarctic Peninsula. From colder to warmer conditions, the brine volumes will increase and brine drainage to the underlying seawater will occur, all leading to decreased concentrations. Interestingly, the exception to this trend is St 515 sampled on July 27, 2013 under very cold conditions (air temperature -20°C). The pack ice consisted of second year sea ice (perhaps landfast ice) (Lemke et al., 2014) with typical low bulk ice salinity and low brine volume, hence higher brine concentrations than would be expected for the location.

Unfiltered and dissolved trace metals		Fe	Fe	Ni	Ni	Cu	Cu	Zn	Zn	Mo	Mo	Cd	Cd	Pb	Pb	Al	Al	Mn	Mn	Co	Co
Sea ice brines	AWECS	nM	nM	nM	nM	nM	nM	nM	nM	nM	nM	pM	pM	pM	pM	nM	nM	nM	nM	pM	pM
	depht (cm)	F	UF	F	UF	F	UF	F	UF	F	UF	F	UF	F	UF	F	UF	F	UF	F	UF
496-BR-SH	20	18.6	33.3	18.0	18.1	6.0	6.0	26.1	26.8	71	113	971	960	308	290	1.9	5.4	1.14	1.29	59	63
496-BR-D	45	14.5	28.3	15.3	15.2	5.4	5.2	16.4	16.8	115	179	711	703	196	444	3.0	6.3	0.94	1.03	54	55
503-BR-SH	30	3.8	25.8	18.3	19.2	5.3	5.9	29.2	32.7	133	127	822	880	280	292	1.2	2.3	0.83	1.16	34	39
503-BR-D	55	3.7	17.6	15.1	15.7	4.6	4.9	19.0	20.6	293	157	580	586	126	139	1.6	5.0	0.57	0.77	37	33
506-BR-SH	20	7.5	18.0	14.9	14.9	5.9	5.6	18.3	19.2	248	109	573	583	204	227	2.1	2.3	0.59	0.69	33	33
506-BR-D	40	1.9	3.5	11.3	11.4	3.1	3.1	7.9	8.1	220	166	561	571	40	42	5.3	3.2	0.30	0.32	30	28
506/2-BR-SH	20	2.0	11.9	14.3	14.5	4.3	5.0	26.0	26.7	145	194	679	689	441	165	1.0	2.8	0.41	0.50	33	38
506/2-BR-D	40	0.5	1.4	12.3	12.4	3.2	3.3	10.2	10.9	222	154	626	651	30	24	2.7	3.0	0.20	0.24	31	25
515-BR-D	90	12.3	16.0	8.7	8.8	3.3	4.0	6.0	6.3	102	292	282	294	97	108	2.6	5.0	0.71	0.74	59	58
517-BR-SH	15	2.5	4.3	14.4	14.4	4.4	4.7	25.7	28.0	106	166	2268	2337	73	71	0.9	1.8	2.70	2.78	72	74
517-BR-D	45	1.5	2.4	9.3	9.3	2.7	2.8	14.4	14.8	163	160	1453	1462	25	25	3.8	7.9	1.47	1.51	52	52

Table 12

In the case of Fe the concentrations decrease in both shallow and deep brines with a rate of about 0.4 nM/d DFe and 0.8 nM/d TD-Fe. With an average ice thickness of 0.55 m this would correspond to fluxes of 0.22 µmol/m^2/d DFe and 0.44 µmol/m^2/d TD-Fe. Whether this is an efflux to the underlying seawater or a transfer from the brine solution to the solid ice, is not clear as yet. However we favor the idea of an efflux to the underlying seawater as may be indicated by the enhanced under-ice seawater concentrations at Sts 488 and 493 (see Table 12), which are higher than what would be typical for this region (Klunder et al., 2011). These results seem to suggest that also in winter sea ice is a source for trace metals to the water column, not only during the spring melt.

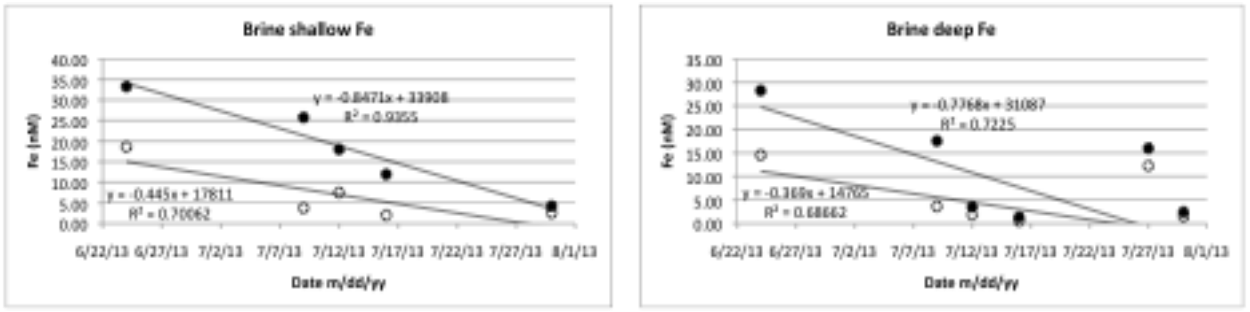

Figure 56: General decrease of Fe concentrations in brine as observed in Weddell Sea basin. Open symbols DFe, closed symbols unfiltered Fe. In the deep brine panel, the data points on July 27, 2013 at St 515 were not taken into account for the linear regression.

Seawater - One depth profile of an off shore transect near the Antarctic Peninsula has been analyzed sofar, notably the one nearest to shore. The goal of this transect is to establish a TM gradient with increasing distance from the continent in order to estimate horizontal and vertical advective and diffusive fluxes into the open ocean. These fluxes will allow to determine and quantify the provenance of high TM concentrations in the sea ice. At St 509, in shallow waters of 244 m depth, high Fe, Mn and Al concentrations point indeed at a continental shelf source for these metals. Enhanced concentrations near the seafloor point at a sedimentary source of these metals, caused by sediment resuspension and diffusion.

Unfiltered and dissolved trace metals		Fe	Fe	Ni	Ni	Cu	Cu	Zn	Zn	Mo	Mo	Cd	Cd	Pb	Pb	Al	Al	Mn	Mn	Co	Co
Seawater	AWECS	nM	nM	nM	nM	nM	nM	nM	nM	nM	nM	pM	pM	pM	pM	nM	nM	nM	nM	pM	pM
	depht (m)	F	UF	F	UF	F	UF	F	UF	F	UF	F	UF	F	UF	F	UF	F	UF	F	UF
488-SW-5m	5	1.6	14.0	6.1	6.2	2.1	2.4	9.5	8.7	120	119	533	536	163	176	2.5	6.9	0.31	0.46	29	30
493-SW-0m	0	3.3	17.6	7.2	7.5	2.3	2.6	16.4	15.1	119	116	695	699	144	182	5.5	28.0	0.54	0.71	51	51
493-SW-1m	1	3.7	12.2	7.0	7.1	2.3	2.5	12.7	12.7	120	118	697	698	127	135	7.8	13.5	0.47	0.53	42	44
509-SW-N22	20	10.1		6.7		2.1		6.3		119		721		52		7.8		2.18		76	
509-SW-N19	50	11.5		6.6		2.0		5.1		118		718		18		13.1		2.25		78	
509-SW-N10	100	21.7		6.7						119		720				17.5		2.39		81	
509-SW-N8	125	25.7		6.7		2.0		5.3		118		717		17		7.9		2.29		79	
509-SW-N6	154	30.9		6.7		2.0		5.4		121		721		24		24.1		2.55		84	
509-SW-N3	214	29.5		6.7		2.1		5.4		121		724		17		21.3		3.62		108	
509-SW-N1 (bottom)	244	23.8		6.7		2.1		6.0		121		732		21		14.1		3.66		110	

Table 13

Ice growth experiment - An ice growth experiment was conducted by drilling a series of holes into the sea ice at station 517, and to sample each refreezing hole at fixed intervals in time. The results suggest a rapid initial growth phase together with a increases of the TM inventory (Fe given as example below). A slow down occurred after 12 h, probably due to a transition from frazil ice accumulation to columnar ice formation. DFe build up continued at a slower pace than initially, but the TD-Fe inventory slightly decreased, probably as a result of a remineralization of particulate Fe to DFe. Probably the build up of Fe in sea ice will continue with the proliferation of sea ice algae.

Unfiltered and dissolved trace metals				Fe	Fe	Ni	Ni	Cu	Cu	Zn	Zn	Mo	Mo	Cd	Cd	Pb	Pb	Al	Al	Mn	Mn	Co	Co
Ice growth experimen		thickness	growth	nM	nM	nM	nM	nM	nM	nM	nM	nM	nM	pM	pM	pM	pM	nM	nM	nM	nM	pM	pM
St 517	ΔT	cm	cm/h	F	UF	F	UF	F	UF	F	UF	F	UF	F	UF	F	UF	F	UF	F	UF	F	UF
t0	0	0																					
ICE EXP t1	6.0	4.5	0.75	1.6	21.0	3.6	3.7	1.7	1.7	22.0	22.9	60	59	486	605	39	43	17.5	49.0	0.49	0.80	29	63
ICE EXP t2	12.0	6	0.25	2.9	36.2	4.6	4.9	1.8	2.4	26.6	30.8	54	51	501	653	158	215	10.7	32.1	1.34	1.85	44	52
ICE EXP t3-top	23.5	10.5	0.39	1.8	16.8	2.0	2.1	1.0	1.2	26.8	27.6	35	35	242	242	126	144	6.5	26.3	0.32	0.44	27	55
ICE EXP t3-bot	23.5			1.8	18.0	1.7	1.7	0.9	1.1	23.8	24.6	27	26	739	743	113	138	12.6	25.2	1.35	1.37	29	40
ICE EXP t4-top	48.0	21.5	0.45	1.7	8.3	2.1	2.2	1.1	1.3	13.3	12.8	36	36	251	244	84	91	9.8	18.3	0.29	0.34	19	25
ICE EXP t4-mid	48.0			0.9	5.7	1.4	1.4	0.5	0.7	6.7	7.0	24	24	244	242	32	37	3.3	7.1	0.30	0.32	14	21
ICE EXP t4-bot	48.0			0.7	11.0	1.6	1.6	1.0	1.3	24.4	25.0	26	25	864	862	37	52	6.7	22.0	1.65	1.66	26	28

Table 14

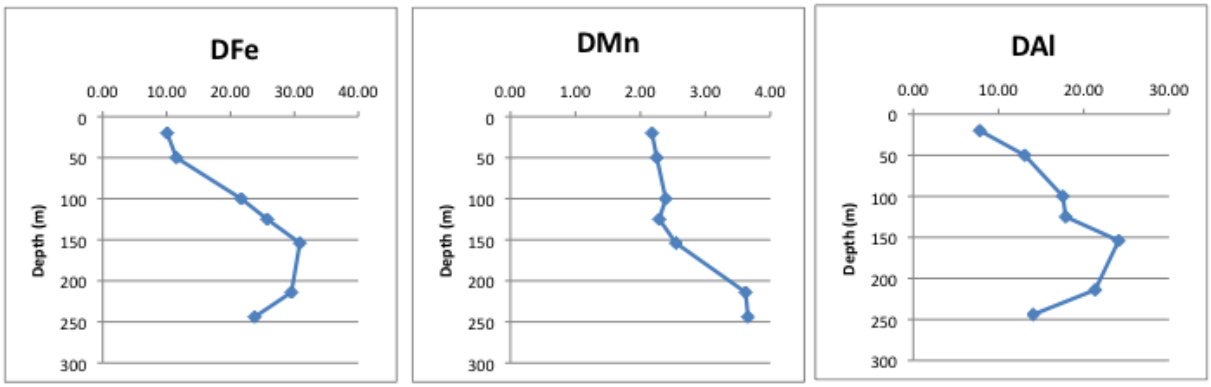

Figure 57: Fe, Mn and Al concentrations at St 509, on the inner continental shelf close to the tip of the Antarctic Peninsula.

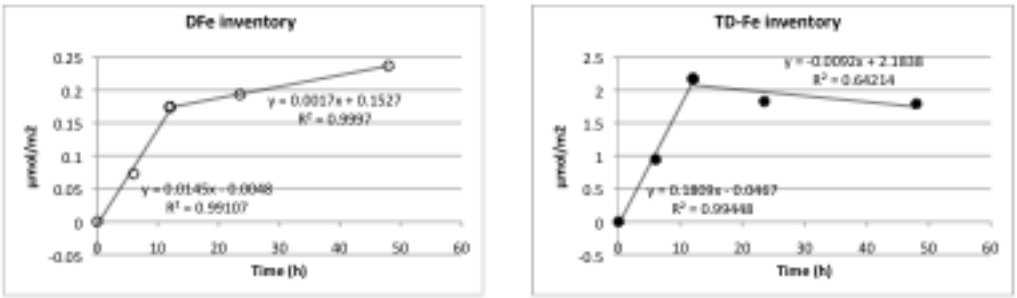

Figure 58: Evolution of the sea ice Fe inventory during an ice growth experiment.

The initial DFe accumulation amounted to 0.35 µmol/m^2/d and slowed down to 0.041 µmol/m^2/d. For TD-Fe this was 4.3 µmol/m^2/d but turned into a slight loss of 0.22 µmol/m^2/d. This means that about 0.18 µmol/m^2/d DFe is lost from the sea ice again while it is forming, probably via brine drainage. This estimate corresponds remarkably well with the one in the brine section above.

3.2.6.Effect of DOC on sea ice biogeochemistry: the INTERICE V artificial sea ice experiment

To investigate and focus on the physical controls of sea ice on biogeochemical fluxes, we participated to the interice V experiment where a controlled cycle of sea ice growth and decay was reproduced from filtered seawater. 4 articles led by members of Bigsouth were published from this experiment (Zhou et al 2014, Moreau et al 2015, Zhou et al. 2016, Kotovitch et al. 2016).

The 19-day experiment took place in the Hamburg Ship Model Basin (www.hsva.de). We used 21 polyethylene experimental mesocosms with a volume of 1.2 m^3 each. Eleven of the mesocosms were filled with 1000 L of seawater from the North Sea (referred hereafter as SW), and the remaining 10 were filled with 900 L of seawater from the North Sea and 100 L of river water (referred hereafter as SWR). The North Sea water was collected on 24 May 2012 (54°7'N 7°54'E near Helgoland) and transported to Hamburg where the mesocosms were filled within 24 h of collection. The river water was collected during spring freshet in mid-May 2012 from River Kiiminkijoki (NW Finland), just before it enters the estuary, stored one week in the cold (4 °C), filtered through 0.2 µm using Durapore 10 inch (Millipore) and Clariflow G 10 inch (Parker) cartridge filters and added to the mesocosms 2 days afterwards.

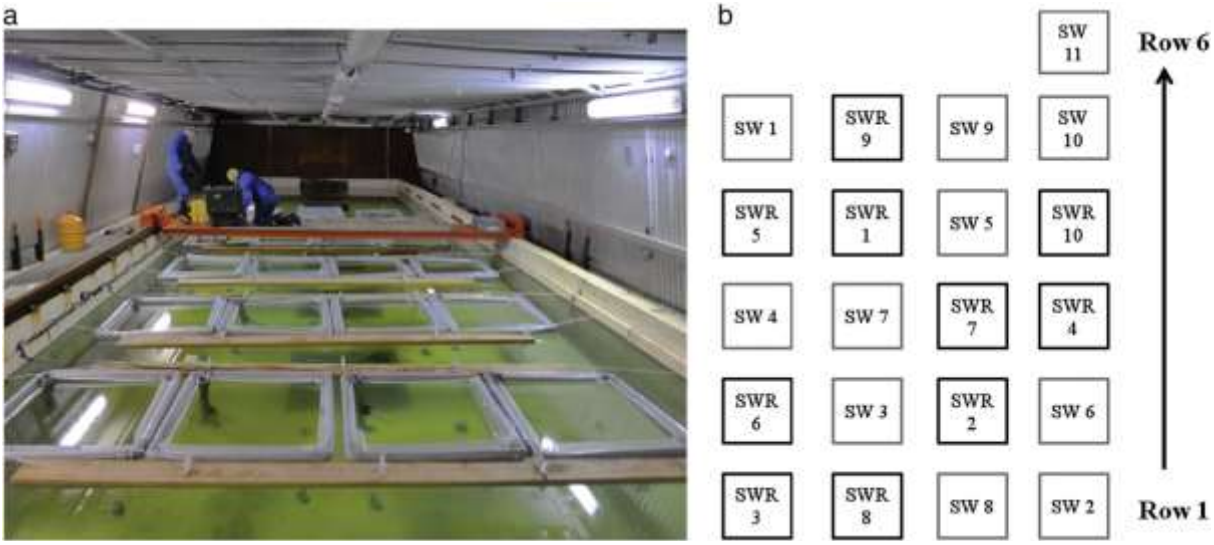

Figure 59: (a) The experimental basin at HSVA, (b) the spatial distribution of the SW and SWR mesocosms. Note that SW11, although sampled, was not included into the data set, because it was reserved for continuous physical measurements.

An overview of the physicals parameters was provided in Zhou et al. (2014). Some of the main observations were that (1) There were no significant differences in the physical parameters of SW and SWR (Figure 60) (2) the incorporation of dissolved compounds (nitrate, nitrite, ammonium, phosphate, silicate, and DOC) into the sea ice was not conservative (relative to salinity) during ice growth. Brine convection clearly influenced the incorporation of the dissolved compounds, since the non-conservative behavior of the dissolved compounds was particularly pronounced in the absence of brine convection. (3) Bacterial activity further regulated nutrient availability in the ice: ammonium and nitrite accumulated as a result of remineralization processes, although bacterial production was too low to induce major changes in DOC concentrations. (4) Different forms of DOC have different properties and hence incorporation efficiencies. In particular, the terrestrially derived DOC from the riverwater was less efficiently incorporated into sea ice than the DOC in the seawater.

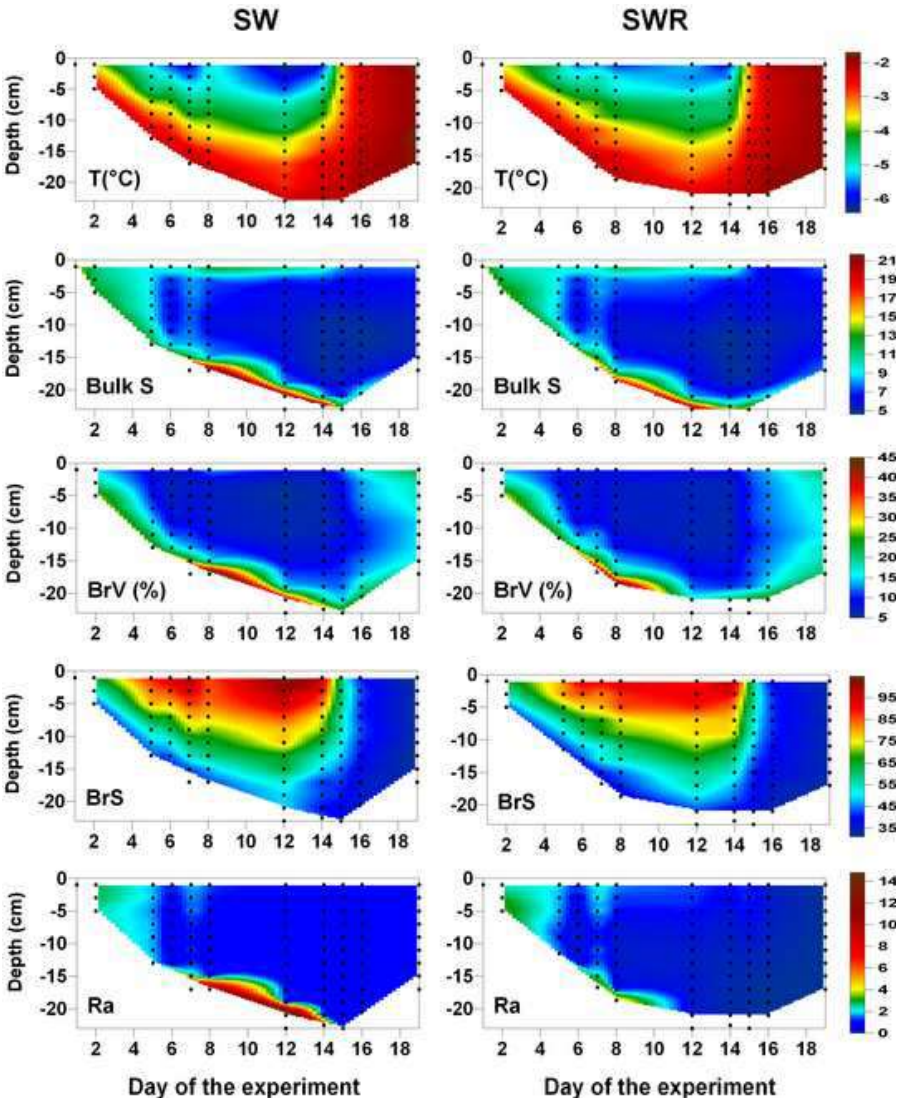

Figure 60: Ice temperature (T), salinity (Bulk S), brine volume fraction (BrV), brine salinity (BrS) and Rayleigh number (Ra) for both SW and SWR mesocosms. Each black dot refers to one data point, the color in between results of interpolation.

Therefore the main factors regulating the distribution of the dissolved compounds within sea ice are clearly a complex interaction of brine dynamics, biological activity and in the case of dissolved organic matter, the physico-chemical properties of the dissolved constituents themselves. Experimental and modelling work has been tightly coupled together and are therefore discussed in the following section "1D modeling of sea ice biogeochemistry.

3.2.7. Peer-reviewed publications associated with Topic 2

1. Brabant F., S. El Amri and **J.-L.Tison**, 2011. A robust approach for the determination of dimethylsulfoxide in sea ice. *Limnology and Oceanography, Methods, 9*, 261-274.
2. Brown K.A., L.A. Miller, C.J. Mundy, T. Papakyriakou, R. François, M. Gosselin, **G. Carnat**, K. Swystun and P.D. Tortell, 2015. Inorganic carbon system dynamics in landfast Arctic sea ice during the early-melt period. *Journal of Geophysical Research-Oceans*, 120, doi: 10.1002/2014JC010620.
3. **Carnat G.**, T. Papakyriakou, N.-X. Geilfus, F. Brabant, **B. Delille**, M. **Vancoppenolle,** G. Gilson, **J. Zhou** and **J.-L. Tison**, 2013. Investigations on physical and textural properties of Arctic first-year sea ice in the Amundsen Gulf, Canada, November 2007–June 2008 (IPY-CFL system study). *Journal of Glaciology*, 57, doi:10.3189/2013JoG12J148.
4. **Carnat G.**, **J. Zhou**, T. Papakyriakou, **B. Delille**, T. Goossens, T. Haskell, **V. Schoemann**, **F. Fripiat**, J.M. Rintala and **J.-L. Tison**, 2014. Physical and biological controls on DMS-P dynamics in ice shelf-influenced fast ice during a winter-spring and a spring-summer transitions. *Journal of Geophysical Research – Oceans*, 119, 2882 – 2905. doi:10.1002/2013JC009381.
5. **Carnat G.**, F. Brabant, I. Dumont, **M. Vancoppenolle**, S.F. Ackley, C. Fritsen, **B. Delille** and **J.-L. Tison**, 2016. Sea-ice algal primary production and nitrogen uptake rates off East Antarctica, *Elementa: Science of the Anthropocene*, 4: 000135, doi: 10.12952/journal.elementa.000135.
6. Crabeck O., **B. Delille**, S. Rysgaard, D.N. Thomas, N.-X. Geilfus, B. Else and **J.-L. Tison**, 2014. First 'in situ' determination of gas transport coefficients (DO2, DAr and DN2) from bulk gas concentration measurements (O2, N2, Ar) in natural sea ice. *Journal of Geophysical Research - Oceans*, 119, 6655-6668, doi: 10.1002/ 2014JC009849.
7. Crabeck O., **B. Delille**, D.N. Thomas., N-X. Geilfus, S. Rysgaard and **J. L. Tison**, 2014. CO2 and CH4 in sea ice from a subarctic fjord under influence of riverine input. *Biogeosciences*, 11:(6525-6538), doi:10.5194/bg-11-6525-2014.
8. Crabeck O., R.J. Galley, **B. Delille,** B. Else, N.-X. Geilfus, M. Lemes, F.P. Des Roches, **J.-L. Tison** and S. Rysgaard, 2015. Imaging air volume fraction in sea ice using non-destructive X-ray tomography. *The Cryosphere - Discussions*, 9, 5203-5251. doi:10.5194/tcd-9-5203-2015.
9. de Jong J., **V. Schoemann**, N. Mattielli, P. Langhorne, T. Haskell and **J.-L. Tison**, 2013. Iron in land-fast sea ice of McMurdo Sound derived from sediment resuspension and wind-blown dust attributes to primary productivity in the Ross Sea. Antarctica, *Marine Chemistry*, 157, 24-40, doi: 10.1016/j.marchem.2013.07.001.

10. de Jong J., S. Stammerjohn, S. Ackley, **J.-L. Tison**, N. Mattielli and **V. Schoemann**, 2015. Sources and fluxes of dissolved iron in the Bellingshausen Sea (West Antarctica): The importance of sea ice, icebergs and the continental margin. *Marine Chemistry*, http:// dx.doi.org/10.1016/j.marchem.2015.08-004.
11. Eronen-Rasimus E., A.-M. Luhtanen, J.-M. Rintala, **B. Delille**, G.S. Dieckmann, A. Karkman and **J.-L. Tison**, submitted to ISME journal. An active bacterial community linked to high chlorophyll-a concentrations in permeable Antarctic winter-pack ice.
12. Fransson A., M. Chierici, L.A. Miller, **G. Carnat**, E. Shadwick, H. Thomas, S. Pineault and T.N. Papakyriakou, 2013. Impact of sea-ice processes on the carbonate system and ocean acidification at the ice-water interface of the Amundsen Gulf, Arctic Ocean. *Journal of Geophysical Research - Oceans*, 118, 1-23, doi: 10.1002/2013JC009164.
13. **Fripiat F.**, **J.-L Tison**, **L. André**, D. Notz and **B. Delille**, 2013. Biogenic silica recycling in sea ice inferred from Si-isotopes: constraints from winter Arctic first-year sea ice. *Biogeochemistry*, doi:10.1007/s10533-013-9911-8.
14. **Fripiat F.**, D.M. Sigman, S.E. Fawcett, P.A. Rafter, M.A. Weigand and **J.-L. Tison**, 2014. New insights into sea ice nitrogen biogeochemical dynamics from nitrogen isotopes. *Global Biogeochemical Cycles*, 28, 115-130, 10.1002/2013GB004729. doi:10.1002/2013GB004729.
15. **Fripiat F.**, **J.-L. Tison, L. André**, D. Notz and **B. Delille**, 2014. Biogenic silica recycling in sea ice inferred from Si-isotopes: Constraints from Arctic winter first-year sea ice. *Biogeochemistry*, *119*(1-3), 25-33. doi: 10.1007/s10533-013-9911-8.
16. **Fripiat, F.**, D.M. Sigman, G.G. Massé and **J.-L. Tison**, 2015. High turnover rates indicated by changes in the fixed N forms and their stable isotopes in Antarctic landfast sea ice. *Journal of Geophysical Research - Oceans*, 120(4), 3079-3097. doi:10.1002/2014JC010583.
17. Geilfus, N. X., **G. Carnat**, T. Papakyriakou, **J.-L.Tison**, B. Else, H. Thomas, E.H. Shadwick and **B. Delille**, 2012. Dynamics of pCO_2 and related air-ice CO_2 fluxes in the Arctic coastal zone (Amundsen Gulf, Beaufort Sea). *Journal of Geophysical Research - Oceans,* 117, C00G10.
18. Geilfus N. X., **B. Delille**, **V. Verbeke** and **J.-L.Tison**, 2012**.** Instruments and methods towards a method for high vertical resolution measurements of the partial pressure of CO_2 within bulk sea ice. *Journal of Glaciology, 58*(208), 287.
19. Geilfus N. X., **G. Carnat**, G.S. Dieckmann, H. Eicken, N. Halden, G. Nehrke, T. Papakyriakou, **J.-L. Tison** and **B. Delille**, 2013. First estimates of the contribution of $CaCO_3$ precipitation to the release of CO_2 to the atmosphere during young sea ice growth. *Journal of Geophysical Research - Oceans,* 118, 1-12.
20. Geilfus N. X., S. Rysgaard, **J.-L. Tison,** S. Ackley, R.J. Galley, L. Miller and **B. Delille**, 2014. Sea ice pCO_2 dynamics and air-ice CO_2 fluxes during the sea ice mass balance in the Antarctic (SIMBA) experiment-Bellingshausen sea, Antarctica. *The Cryosphere*, *8*(6), 2395-2407. doi:10.5194/tc-8-2395-2014.

21. Geilfus N. X., R.J. Galley, O. Crabeck, T. Papakyriakou, J. Landy, **J.-L. Tison** and S. Rysgaard, 2015. Inorganic carbon dynamics of melt pond-covered first year sea ice in the Canadian Arctic. *Biogeosciences*, *12*(6), 2047-2061.
22. Janssens J., K.M. Meiners, **J.-L. Tison**, G. Dieckmann, **B. Delille** and D. Lannuzel, 2016. Incorporation of iron and organic matter into young Antarctic sea ice during its initial growth stages. *Elementa: Science of the Anthropocene*, 4: 000123. doi:10.12952/ journal.elementa.000123.
23. Kaartokallio H., D.H. Søgaard, L. Norman, S. Rysgaard, **J.-L. Tison J.-L**., **B. Delille** and D.N. Thomas, 2013. Short-term variability in bacterial abundance, cell properties, and incorporation of leucine and thymidine in subarctic sea ice. *Aquatic Microbial Ecology*, 71:57-73, doi: 10.3354/ame01667.
24. **Kotovitch M.**, **S. Moreau**, **J. Zhou**, **M. Vancoppenolle**, G.S. Dieckmann, K.-U. Evers, **F. Van der Linden**, D.N. Thomas, **J.-L. Tison** and **B. Delille**, 2016. Air-ice carbon pathways inferred from a sea ice tank experiment. *Elementa Science of the Anthropocene*, 4:112.
25. Kotovitch M., **B. Delille**, **S. Moreau**, **J. Zhou**, **M. Vancoppenolle**, G. Dieckmann, K.-U. Evers, F. Van Der Linden, D.D. Thomas and **J.-L. Tison**, 2016. Air-ice carbon pathways inferred from a sea ice tank experiment. *Elementa: Science of the Anthropocene*, 4: 000112. doi:10.12952/journal.elementa.000112.
26. Lannuzel D., A.R. Bowie, P.C. van der Merwe, A.T. Townsend and **V. Schoemann**, 2011. Distribution of dissolved and particulate metals in Antarctic sea ice. *Marine Chemistry,* 124, 134-146.
27. Lannuzel D., **V. Schoemann**, I. Dumont, M. Content, J. de Jong, **J.-L. Tison**, **B. Delille** and S. Becquevort, 2013. Effect of melting Antarctic sea ice on the fate of microbial communities studied in microcosms. *Polar Biology*, 36:1483-1497, doi:10.1007/s00300-013-1368-7.
28. Lannuzel D, **Vancoppenolle M**, Van der Merwe P, De Jong J, Meiners K, Grotti M, Nishioka J, **Schoemann V** (2016). Iron in sea ice: Review and new insights. Elem Sci Anth 4, 000130, doi: 10.12952/journal.elementa.000130.
29. Lewis M.-J., **J.-L.Tison**, B. Weissling, **B. Delille**, S.F. Ackley, F. Brabant and H. Xie, 2011. Sea ice and snow cover characteristics during the winter-spring transition in the Bellingshausen Sea: an overview of SIMBA 2007. *Deep-Sea Research II,* 58, 1019-1038, doi:10.1016/j.dsr2.2010.10.027.
30. Loose, B., P. Schlosser, D. Ringelberg, D.T. Ho, T. Takahashi, J. Richter-Menge, C.M. Reynolds, W. McGillis and **J.-L. Tison**, 2011. Gas diffusion through columnar laboratory sea ice: implications for mixed-layer ventilation of CO_2 in the seasonal ice zone. *Tellus - Series B - Chemical and Physical Meteorology,* 63(1), 23-39.
31. Marquardt, M., M. Kramer, **G. Carnat** and I. Werner, 2011. Vertical distribution of sympagic meiofauna in sea ice in the Canadian Beaufort Sea. *Polar Biology*, 34, 1887-1900.
32. Meiners, K.M., **M. Vancoppenolle**, S. Thanassekos, G. S. Dieckmann, D. Thomas, **J.-L. Tison**, K. R. Arrigo, D. Garrison, A. McMinn, D. Lannuzel, P. van der Merwe, K. Swadling, W.O. Smith, I. Melnikov and B. Raymond, 2012.

Chlorophyll a in Antarctic sea ice from historical ice core data. *Geophysical Research Letters*, 39, 2012.

33. Middleton C., C. Thomas, A. De Wit and **J.-L. Tison,** 2016. Visualizing brine channel development and convective processes during artificial sea-ice growth using Schlieren optical methods, *Journal of Glaciology*, 62, 1-17. doi:10.1017/jog.2015.1.
34. Miller L.A., **G. Carnat**, B. Else, N. Sutherland and T. Papakyriakou, 2011. Carbonate system evolution at the Arctic Ocean surface during autumn freeze-up. *Journal of Geophysical Research*, 116, C00G04.
35. Miller L. L., **F. Fripiat,** B. Else, J.S. Bowman, K.A. Brown, E.R. Collins, M. Ewert, A.A. Fransson, M. Goselin, D. Lannuzel, K. Meiners, C. Michel, J. Nishioka, D. Nomura, S. Papadimitriou, L.M. Russell, L.L. Sorensen, D. Thomas, D., **J.-L. Tison,** M. van Leeuwe, **M. Vancoppenolle,** E.W. Wolff and **J. Zhou,** 2015. Methods for biogeochemical studies of sea ice: The state of the art, caveats, and recommendations. *Elementa*, *3*, 000038. doi:10.12952/journal.elementa.000038.
36. **Moreau S.**, H. Kaartokallio, **M. Vancoppenolle**, **J. Zhou**, **M. Kotovitch**, G.S. Dieckmann, D.N. Thomas, **J.-L. Tison** and **B. Delille**, 2015. Assessing the O_2 budget under sea ice: An experimental and modelling approach. *Elementa Science of the Anthropocene*, 3:80.
37. Rysgaard S., J. Bendtsen, **B. Delille**, G.S. Dieckmann, R.N. Glud, H. Kennedy, J. Mortensen, S. Papadimitriou, D.L. Thomas and **J.-L. Tison**, 2011. Sea ice contribution to the air-sea CO_2 exchange in the Arctic and Southern Oceans. *Tellus - Series B - Chemical and Physical Meteorology,* 63(5), 823-830.
38. Stefels J., **G. Carnat**, J.W. Dacey, T. Goossens, J.T.M. Elzenga and **J.-L.Tison**, 2012. The analysis of dimethylsulfide and dimethylsulphoniopropionate in sea ice: dry-crushing and melting using stable isotope additions. *Marine Chemistry,* 128-129, 34-43, doi: 10.1016/j.marchem.2011.09.007.
39. Sørensen L. L., B. Jensen, R.N. Glud, D. McGinnis, M.C. Sejr, J. Sievers, D. Søgaard, **J.-L. Tison** and S. Rysgaard, 2014. Parametrization of Atmosphere-Surface exchange of CO_2 over sea ice. *The Cryosphere*, 8 (3), 853-866.
40. **Tison J.-L.**, **B. Delille** and S. Papadimitriou, in press. Gases in Sea Ice, In : Sea Ice, 3rd Edition, Ed. Thomas, D., John Wiley and Sons, Oxford, UK.
41. **Tison J.-L.**, S. Schwegmann, G. Dieckmann, J. Rintala, J. Freitag, **S. Moreau**, **M. Vancoppenolle**, D. Nomura, S. Engberg, L.J. Bloomster, S. Heindrickx, C. Uhlig, A.M. Luhtanen, J. de Jong, J. Janssens, **G. Carnat**, **J. Zhou** and **B. Delille**, submitted. Warming Winter Weddell Sea Ice Pack Triggers Permeability and Biogeochemical Response, *Journal of geophysical research: Ocean.*
42. **Zhou J.**, **B. Delille**, H. Eicken, **M. Vancoppenolle**, F. Brabant, **G. Carnat**, N.-X. Geilfus, T. Papakyriakou, B. Heinesch and **J.-L. Tison**, 2013. Physical and biogeochemical properties in landfast sea ice (Barrow, Alaska): insights on

brine and gas dynamics across seasons. *Journal of Geophysical Research – Oceans*, 118(6):3172-3189.

43. **Zhou J.**, **B. Delille**, H. Kaartokallio, G. Kattner, H. Kuosa, **J.-L. Tison**, R. Autio, G.S. Dieckmann, K.-U Evers, L. Jorgensen et al., 2014. Physical and bacterial controls on inorganic nutrients and dissolved organic carbon during a sea ice growth and decay experiment. *Marine Chemistry*, 166: 59-69.
44. **Zhou J.**, **B. Delille**, F. Brabant and **J.-L. Tison**, 2014. Insights into oxygen transport and net community production in sea ice from oxygen, nitrogen and argon concentrations. *Biogeosciences*, 11, 5007-5020, doi:10.5194/bg-11-5007-2014.
45. **Zhou J.**, **J-L. Tison**, **G. Carnat**, N-X. Geilfus and **B. Delille**, 2014. Physical controls on the storage of methane in landfast sea ice. *The Cryosphere*, 8, 1019-1029, doi:10.5194/tc-8-1019-2014.
46. **Zhou J.**, **M. Kotovitch**, H. Kaartokallio, **S. Moreau**, **J.-L. Tison**, G. Kattner, G. Dieckmann, D.N. Thomas and **B. Delille**, 2016. The impact of dissolved organic carbon and bacterial respiration on pCO_2 in experimental sea ice. *Prog. Oceanogr.*, 141:153-167.
47. **Zhou J.**, M. Kotovitch, H.H. Kaartokallio, **S. Moreau**, **J.-L. Tison**, G.G. Kattner, G. Dieckmann, D.D. Thomas and **B. Delille**, 2016. The impact of dissolved organic carbon and bacterial respiration on pCO2 in experimental sea ice. *Progress in oceanography*, 141, 153-167. doi:10.1016/j.pocean.2015.12.005.

3.3. TOPIC 3: SEA ICE BIOGEOCHEMICAL MODEL AND INTEGRATION IN NEMO-LIM-PISCES

First of all, a review publication was written to describe the state-of-the-art of sea ice biogeochemistry by Vancoppenolle et al. (2013b). In this publication, we reviewed the potential role of sea ice in global biogeochemical cycles concerning: active biological and chemical processes within the sea ice; fluid and gas exchanges at the sea ice interface through an often permeable sea ice cover; and tight physical, biological and chemical interactions between the sea ice, the ocean and the atmosphere (Figure 61).

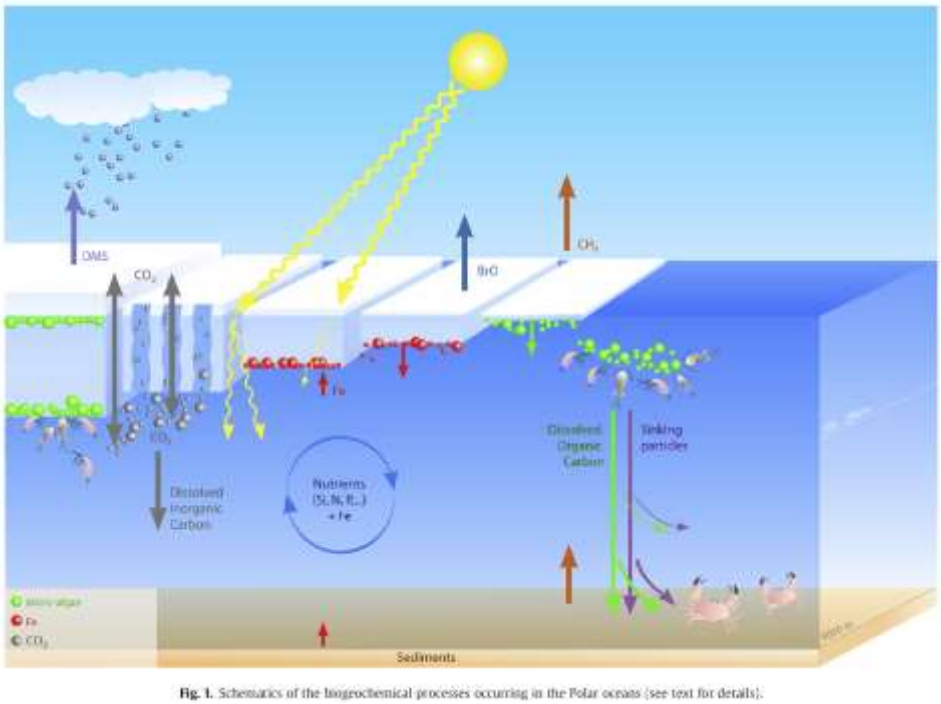

Fig. 1. Schematics of the biogeochemical processes occurring in the Polar oceans (see text for details).

Figure 61: Major biogeochemical processes in the sea ice zone (Vancoppenolle et al, 2013b).

Particularly, we reviewed in details sympagic sea ice primary production; under-ice and ice-edge phytoplankton blooms; the release of iron highly concentrated in sea ice on the iron-limited Southern Ocean; the export of inorganic carbon transport by brine sinking, calcium carbonate precipitation in sea ice, as well as active ice-atmosphere carbon dioxide (CO_2) fluxes; the large production by ice algae of dimethyl-sulfonio-propionate (DMSP), the precursor of sulphate aerosols; the ocean-atmosphere methane (CH_4) fluxes in the Arctic sea ice zone; and the role of sea ice in the springtime atmospheric bromine chemistry. The incorporation of these processes into Earth system models was investigated.

3.3.1. 1D modeling of sea ice biogeochemistry

As a first step of the simulation of gas storage within sea ice, we implemented the transport (including parameterization of gas physics) of dissolved argon, a biogeochemically inert gas, within sea ice into LIM1D using data from an

observational data series at Barrow Point, Alaska (Moreau et al., 2014). The incorporation and transport of dissolved Ar within sea ice and its rejection via gas-enriched brine drainage to the ocean, were modelled following fluid transport equations through sea ice. The nucleation of gas bubbles in sea ice was implemented when Ar is above saturation and when the total partial pressure of all three major atmospheric gases (N_2, O_2 and Ar) is above the brine hydrostatic pressure. The uplift of gas bubbles due to buoyancy was allowed when the brine network is connected with a brine volume above a given threshold. Ice-atmosphere Ar fluxes were formulated as a diffusive process proportional to the differential partial pressure of Ar between brine inclusions and the atmosphere.

Sensitivity analyses suggested that gas bubble nucleation and rise are of most importance to describe gas dynamics within sea ice (Figure 62). Ar dynamics were dominated by uptake, transport by brine dynamics and bubble nucleation in winter and early spring; and by an intense and rapid release of gas bubbles to the atmosphere in spring. Important physical processes driving gas dynamics in sea ice were identified, pointing to the need for further field and experimental studies.

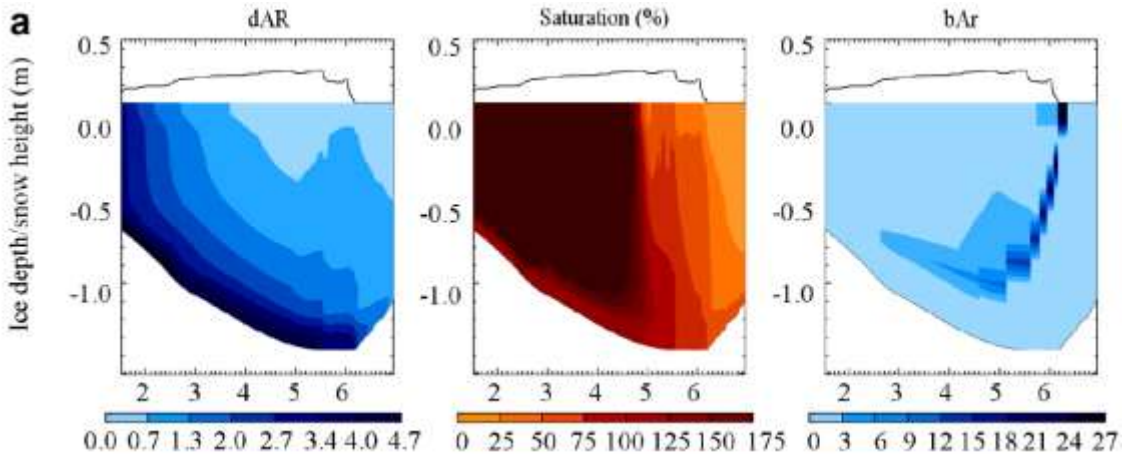

Figure 62: Simulated dissolved Ar, Ar saturation and gaseous Ar in sea ice at Point Barrow, Alaska (Moreau et al, 2014).

Following this research on gas dynamics, Moreau et al. (2015c) included the dynamics of CO_2 and O_2 within sea ice into LIM1D using data from two observational data series: Barrow Point, Alaska, and an ice-growing experiment, INTERICE IV. The ice-ocean fluxes, and vertical transport, of total dissolved inorganic carbon (DIC) and total alkalinity (TA) were represented using fluid transport equations. Carbonate chemistry, the consumption, and release of CO_2 by primary production and respiration, the precipitation and dissolution of ikaite ($CaCO_3$-$6H_2O$) and ice-air CO_2 fluxes, were also included (Figure 63).

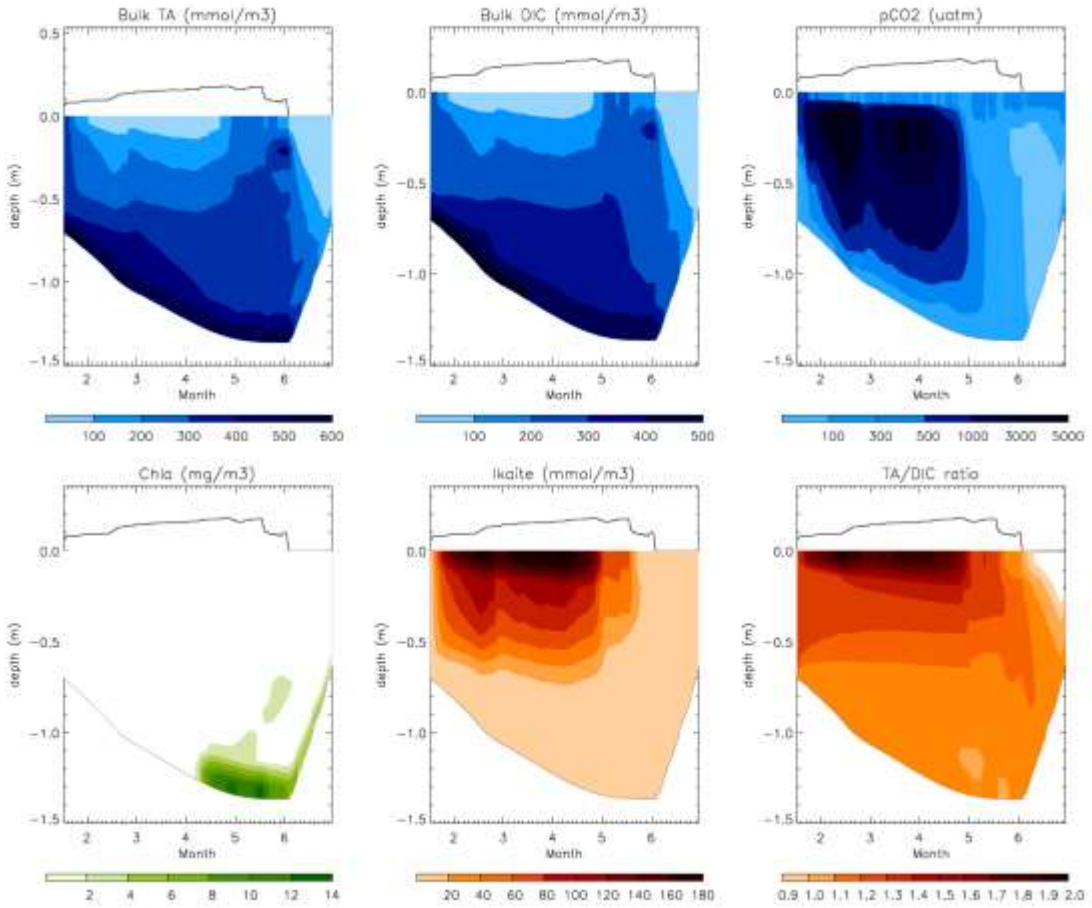

Figure 63: Bulk TA, DIC, sea ice pCO_2, Chl-a, and ikaite concentrations and the TA/DIC ratio in sea ice at Point Barrow, Alaska (Moreau et al, 2015c).

Results showed that the DIC budget is mainly driven by physical processes, whereas brine-air CO_2 fluxes, ikaite formation, and net primary production, are secondary factors (Figure 64). This is a particularly relevant result towards the large scale modelling of sea ice carbon dynamics.

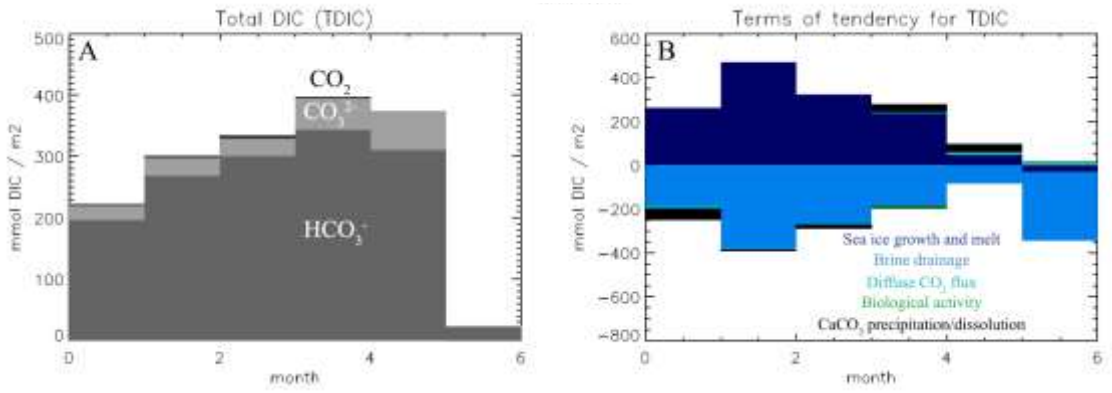

Figure 64: DIC budget in sea ice and driving processes (Moreau et al, 2015c).

In terms of ice-atmosphere CO_2 exchanges, sea ice is a net CO_2 source in winter and a net sink in summer. The formulation of the ice-atmosphere CO_2 flux impacts the simulated near-surface CO_2 partial pressure (pCO_2), but not the DIC budget. Because the simulated ice-atmosphere CO_2 fluxes are limited by DIC stocks, and therefore < 2 mmol m^{-2} d^{-1}, we argue that the observed much larger CO_2 fluxes from eddy covariance retrievals cannot be explained by a sea ice direct source and must involve other processes or other sources of CO_2. Finally, the simulations suggest that near-surface TA/DIC ratios of ~2, sometimes used as an indicator of calcification, would rather suggest outgassing.

The halo-thermodynamic sea ice model LIM1D, including gas physics and sea ice biogeochemistry was further used in three publications in order reporting results from an experimental ice growth experiment: INTERICE V. In a first paper, Moreau et al. (2015a) assessed the O_2 budget in the water under sea ice combining observations and modelling. Modelling was used to discriminate between physical processes, gas-specific transport (i.e., ice-atmosphere gas fluxes and gas bubble buoyancy) and bacterial respiration (BR) and to constrain bacterial growth efficiency (BGE). A module describing the changes of the under-ice water properties, due to brine rejection and temperature-dependent BR, was implemented into LIM1D.

The results showed that BR was the dominant biogeochemical driver of O_2 concentration in the water under ice (in a system without primary producers), followed by gas specific transport (Figure 65). The model suggested that the actual contribution of BR and gas specific transport to the change in seawater O_2 concentration was 37% during ice growth and 48% during melt. BGE in the water under sea ice, as retrieved from the simulated O_2 budget, was found to be between 0.4 and 0.5, which was in line with published BGE values for cold marine waters.

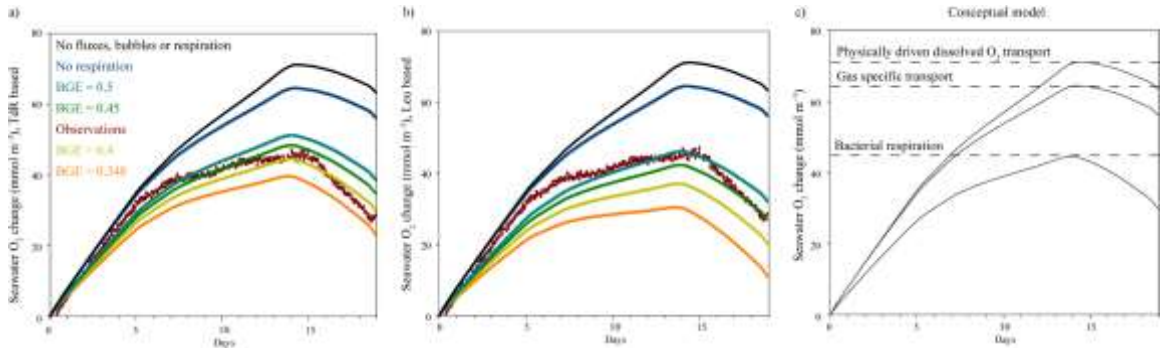

Figure 65: Observed and simulated O_2 dynamics under sea ice (Moreau et al, 2015a).

Given the importance of BR to seawater O_2 in this study, we assumed that bacteria contribute substantially to organic matter consumption and gas fluxes in ice-covered polar oceans. In addition, we proposed a parameterization of polar marine bacterial respiration, based on the strong temperature dependence of bacterial respiration and the high growth efficiency we observed, for further biogeochemical ocean modelling applications, such as regional or large-scale Earth System models.

In a second paper, Kotovitch et al. (2016) observed air-ice CO_2 fluxes from the initial freezing of the sea ice cover until its decay during the INTERICE V experiment at the Hamburg Ship Model Basin. Cooling seawater prior to sea ice formation acted as a sink for atmospheric CO_2, but as soon as the first ice crystals started to form, sea ice turned to a source of CO_2, which lasted throughout the whole ice growth phase. Once ice decay was initiated by warming the atmosphere, the sea ice shifted back again to a sink of CO_2. Direct measurements of outward ice- atmosphere CO_2 fluxes were consistent with the depletion of dissolved inorganic carbon in the upper half of sea ice (Figure 66). Combining measured air-ice CO_2 fluxes with the partial pressure of CO_2 in sea ice, Kotovitch et al. (2016) determined strongly different gas transfer coefficients of CO_2 at the air-ice interface between the growth and the decay phases (from 2.5 to 0.4 mol m^{-2} d^{-1} atm^{-1}). The authors hypothesize the difference in gas transfer coefficients to be due to the transport of bubbles during ice growth, while only diffusion occurs during ice melt.

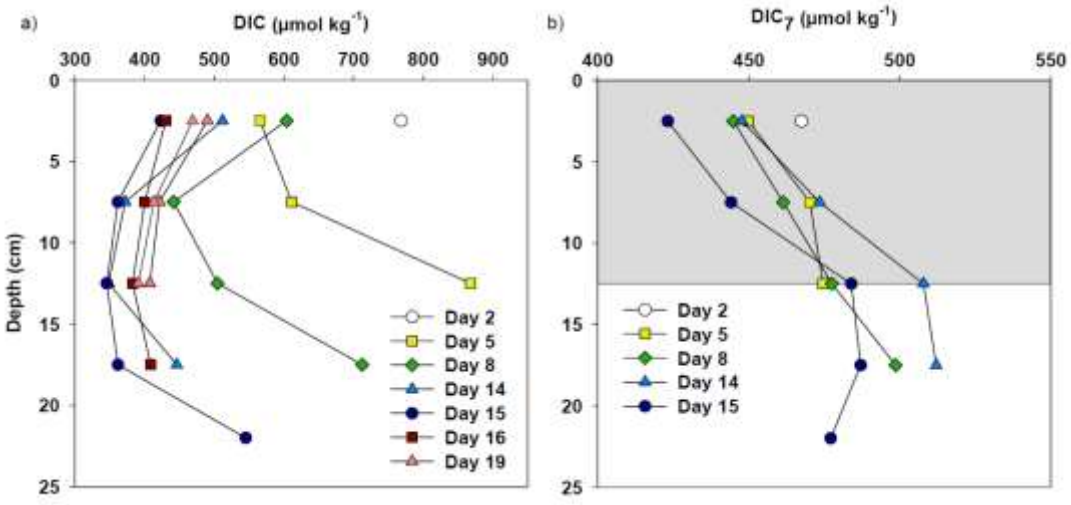

Figure 66: Bulk DIC and normalized DIC (DIC_7) in sea ice. The DIC_7 depletion in the upper part of sea ice is attributed to ice-atmosphere CO_2 fluxes (Kotovich et al., 2016)

To support this hypothesis, Kotovitch et al. (2016) used LIM1D to mimic the observed CO_2 fluxes. With the model, several parameterizations were tested related to processes that potentially affect CO_2 fluxes (e.g. diffusivities, ikaite precipitation) with no account for processes which were not observed or were not significant in the experiment (e.g. frost flowers). The rate of bubble formation was a crucial parameter to reproduce the amplitude of the measured air-ice CO_2 fluxes especially during ice growth (Figure 67). Based on the model results and the experimental difference in transfer coefficients between the growing and melting phases, Kotovitch et al. (2016) argued that bubbles formation and upward transport were crucial drivers of air-ice CO_2 fluxes during ice growth.

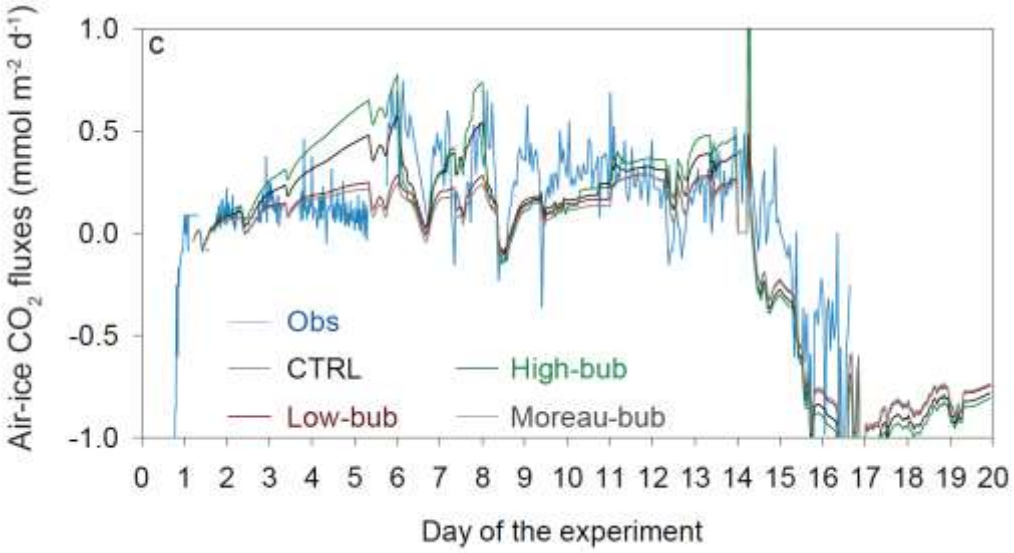

Figure 67: Observed (blue) and simulated ice-atmosphere CO_2 fluxes. Different gas bubbles rates were used to best represent ice-atmosphere CO_2 fluxes (Kotovitch et al., 2016).

In a third paper, Zhou et al. (2016) described the role of dissolved organic carbon (DOC) and bacterial respiration on the partial pressure of carbon dioxide (pCO_2) in sea ice brines during the ice-growing experiment, INTERICE V. The experiment consisted of two series of mesocosms: one was filled with seawater (SW) and the other one with seawater with an addition of filtered humic-rich river water (SWR). The addition of river water increased the DOC concentration of the water from a median of 142 µmol $Lwater^{-1}$ in SW to 249 µmol $Lwater^{-1}$ in SWR. Bacterial respiration in ice was higher in SWR: median bacterial respiration was 25 nmol C L_{ice}^{-1} h^{-1} compared to 10 nmol C L_{ice}^{-1} h^{-1} in SW. pCO_2 in ice was also higher in SWR with a median of 430 ppm compared to 356 ppm in SW (Figure 68).

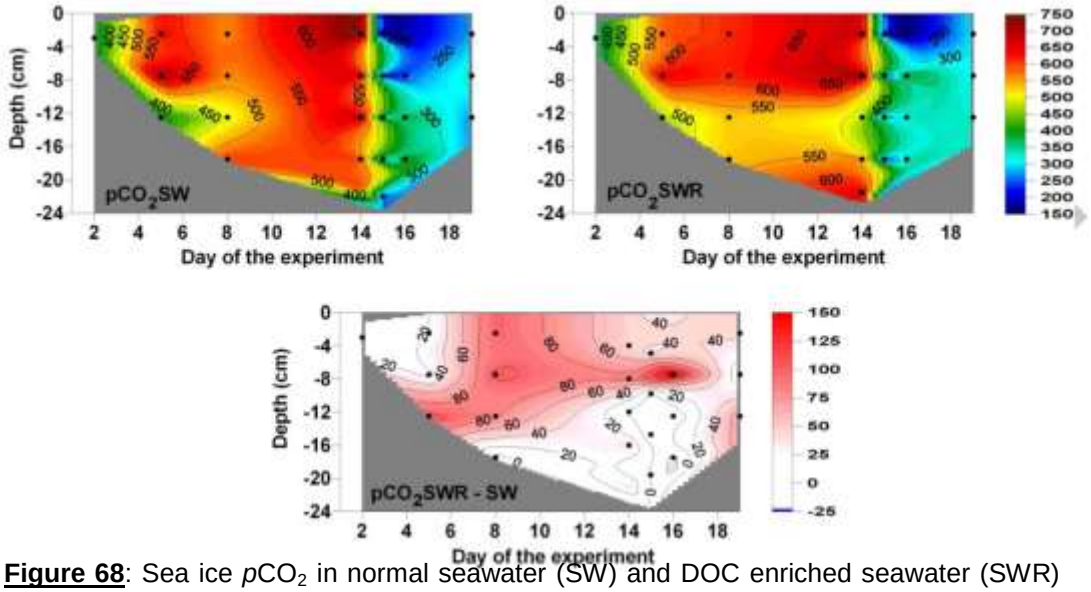

Figure 68: Sea ice pCO_2 in normal seawater (SW) and DOC enriched seawater (SWR) mesocosms during INTERICE V (Zhou et al., 2016).

However, the differences in pCO_2 were larger within the ice interiors than at the surfaces or the bottom layers of the ice, where exchanges at the air-ice and ice-water interfaces might have reduced the differences.

To support their hypothesis that BR was responsible for the higher pCO_2 in sea ice, the authors used LIM1D to simulate the differences of pCO_2 and DIC based on bacterial respiration. The model simulations supported the experimental findings and further suggested that bacterial growth efficiency in the ice might approach 0.15 and 0.2. The authors suggested that the higher pCO_2 in Arctic sea ice brines compared with those from the Antarctic sea ice might be due to an elevated bacterial respiration, sustained by higher riverine DOC loads.

Finally, Vancoppenolle and Tedesco (2015) reviewed the existing sea ice biogeochemical models and how these model can be used to understand and upscale processes, to project them into the future and to study their impacts on other components of the Earth System. They, then, described further the one-dimensional modelling of sea ice algae in LIM1D (Figure 69). In particular, they showed how sea ice physical and biogeochemical processes are typically parameterized and illustrated how this shapes the model seasonality and vertical distribution of sea ice algae.

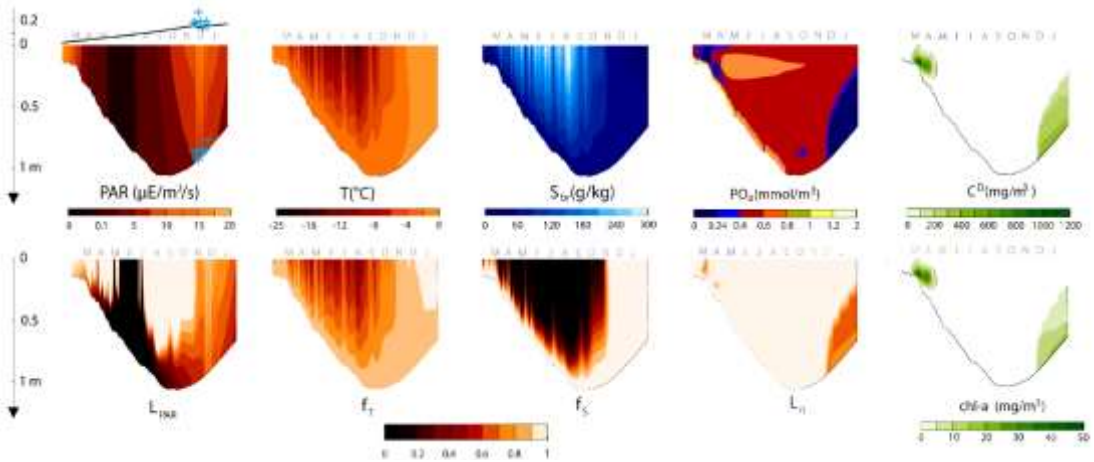

Figure 69: Vertical sea ice distribution of: PAR, temperature, brine salinity, bulk concentration of phosphate, carbon content of ice algae, PAR limitation, temperature inhibition, brine salinity inhibition, nutrients limitation; and bulk Chl-a concentration (Vancoppenolle and Tedesco, 2015).

3.3.2. Biogeochemistry of the sea ice zone

Meiners et al. (2012) used a compilation of sea ice core chl-a data to describe the seasonal, regional and vertical distribution of algal biomass in Southern Ocean pack ice. The Antarctic Sea Ice Processes and Climate – Biology (ASPeCt – Bio) circumpolar dataset, consisting of 1300 ice cores collected during 32 cruises over a period of 25 years, was used. The analyses showed that integrated sea ice chl-a peaks in early spring and late austral summer, which was consistent with theories on

light and nutrient limitation. The results indicated that on a circum-Antarctic scale, surface, internal and bottom sea ice layers contribute equally to integrated biomass (Figure 70), but vertical distribution shows distinct differences among six regions around the continent. The vertical distribution of sea ice algal biomass depends on sea ice thickness, with surface communities most commonly associated with thin ice (<0.4m), and ice of moderate thickness (0.4–1.0 m) having the highest probability of forming bottom communities.

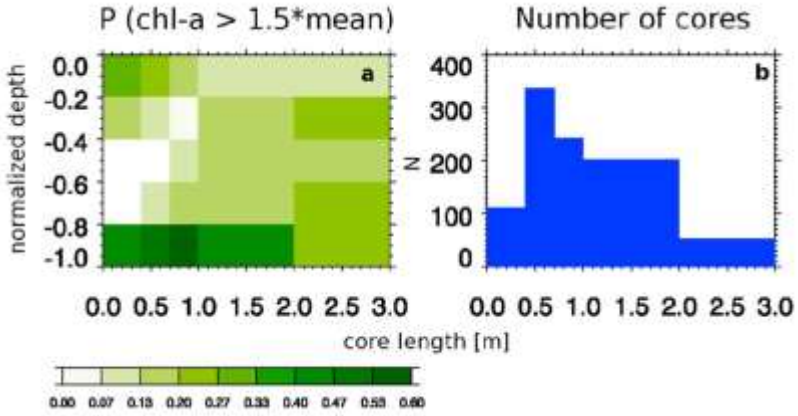

Figure 70: Probability distribution of Chl-a values in Antarctic sea ice (Meiners et al., 2012).

Vancoppenolle et al. (2013a) investigated the future of the net Arctic Ocean primary production (PP) using Coupled Model Inter-comparison Project Phase 5 simulations performed with 11 Earth System Models over 1900–2100. PP is expected to increase over this century, due to less perennial sea ice and more available light, but could decrease depending on changes in nitrate (NO_3^-) supply. Whereas the mean model simulated reasonably well the Arctic-integrated PP (511 TgC yr^{-1}, 1998–2005) and projected a mild 58 TgC yr^{-1} increase by 2080–2099 for the strongest climate change scenario, the 11 models did not agree on the sign of future PP change (Figure 71).

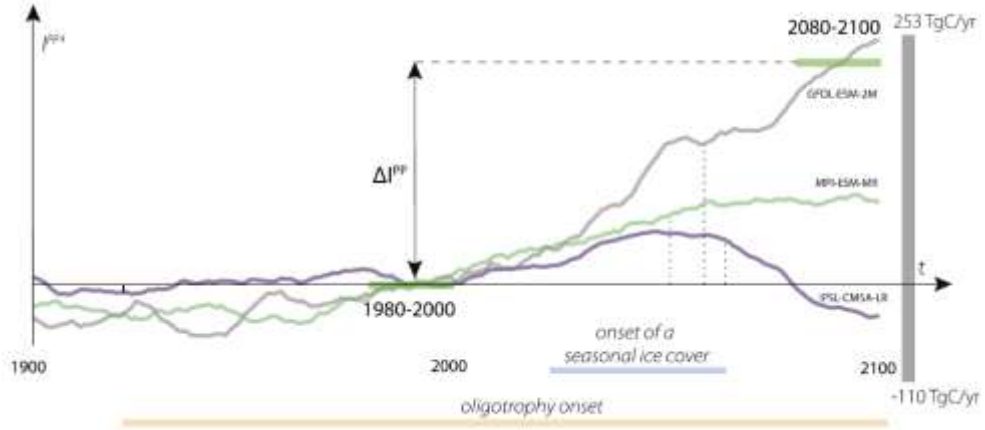

Figure 71: Typical evolution of Arctic Ocean PP anomalies over 1900-2100 from three selected CMIP5 models (Vancoppenolle et al, 2013a).

However, similar mechanisms operated in all models. The perennial ice loss-driven increase in PP was in most models NO_3-limited. The Arctic surface NO_3^- was decreasing over the 21st century (–2.3 ± 1 mmol m^{-3}), associated with shoaling mixed layer and with decreasing NO_3^- in the nearby North Atlantic and Pacific waters. However, the intermodel spread in the degree of NO_3^- limitation was initially high, resulting from >1000 year spin-up simulations. This initial NO_3^- spread, combined with the trend, caused a large variation in the timing of oligotrophy onset—which directly controlled the sign of future PP change. Virtually all models agreed in the open ocean zones on more spatially integrated PP and less PP per unit area. The source of model uncertainty was located in the sea ice zone, where a subtle balance between light and nutrient limitations determined the PP change. Hence, Vancoppenolle et al. (2013a) argued that reducing the uncertainty on present Arctic NO_3^- in the sea ice zone would render Arctic PP projections much more consistent.

3.3.3. Large scale modeling of Southern Ocean biogeochemistry including sea ice

Moreau et al. (2015b) observed the effects of climate change on primary production in the waters west of the Antarctic Peninsula over the last three decades using satellite observations and modelling. Particularly, the study was based on temporal data series of ozone thickness (1972–2010), sea ice concentration (1978–2010), sea-surface temperature (1990–2010), incident irradiance (1988–2010) and satellite-derived chl-a concentration (chl-a, 1997–2010) for the coastal WAP. We first observed that, since 1978, sea ice retreat has been occurring earlier in the season (in March in 1978 and in late October during the 2000s) while the ozone hole is present in early spring (i.e. August to November) since the early 1990s (Figure 72), increasing the intensity of ultraviolet-B radiation (UVBR, 280–320 nm). The WAP waters have also warmed over 1990–2010.

We applied a photosynthesis/photo-inhibition spectral model to satellite-derived data (1997–2010) to compute PP and examine the separate impacts of environmental forcings. The modelled PP rates are in the lower range of previously reported PP rates in the WAP. The annual open water PP in the study area increased from 1997 to 2010 (from 0.73 to 1.03 Tg C yr^{-1}) concomitantly with the increase in the production season length (Figure 73). The coincidence between the earlier sea ice retreat and the presence of the ozone hole increased the exposure to incoming radiation (UVBR, UVAR and PAR) and, thus, increased photo-inhibition during austral spring (September to November) in the study area (from 0.014 to 0.025 Tg C yr^{-1}). This increase in photo-inhibition was minor compared to the overall increase in PP, however. Climate change hence had an overall positive impact on PP in the WAP waters.

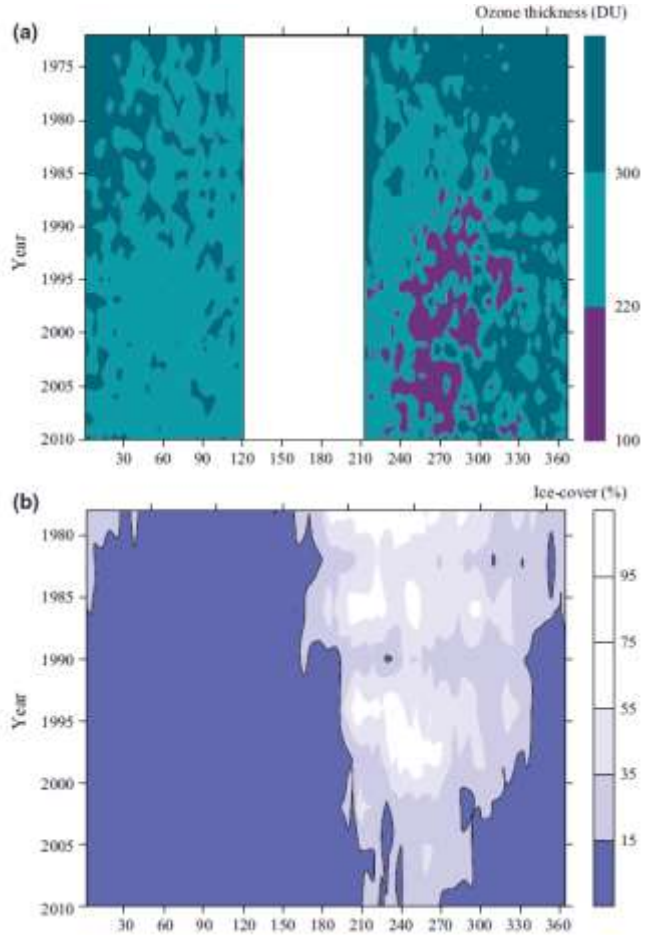

Figure 72: Seasonal variations of the ozone layer thickness and the sea ice concentration for the waters west of the Antarctic Peninsula over the last 3 decades (Moreau et al., 2015b).

Delille et al. (2014) reported first direct measurements of the partial pressure of CO_2 (pCO_2) within Antarctic pack sea ice brines and related CO_2 fluxes across the air-ice interface. The authors reported that, from late winter to summer, brines encased in the ice change from a CO_2 large oversaturation, relative to the atmosphere, to a marked under-saturation while the underlying oceanic waters remains slightly oversaturated. The decrease from winter to summer of pCO_2 in the brines is driven by dilution with melting ice, dissolution of carbonate crystals, and net primary production. As the ice warms, its permeability increases, allowing CO_2 transfer at the air-sea ice interface. The sea ice changes from a transient source to a sink for atmospheric CO_2.

The authors up-scaled these observations to the whole Antarctic sea ice cover using the NEMO-LIM3 large-scale sea ice-ocean and provided first estimates of spring and summer CO_2 uptake from the atmosphere by Antarctic sea ice. Over the spring-summer period, the Antarctic sea ice cover was a net sink of atmospheric CO_2 of 0.029 Pg C, about 58% of the estimated annual uptake from the Southern Ocean (Figure 74). The authors concluded that sea ice contributes significantly to the sink of CO_2 of the Southern Ocean.

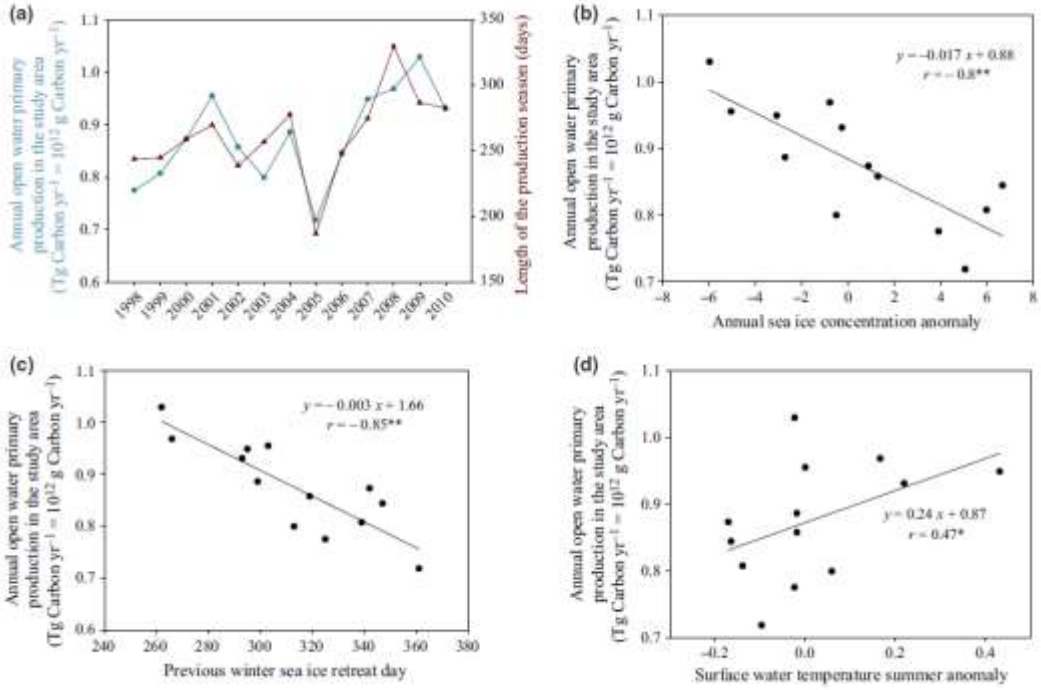

Figure 73: Annual primary production in the WAP waters from 1997 to 2010 compared to the length of the production season, the annual sea ice concentration anomaly, the previous winter sea ice retreat day and the sea surface temperature anomaly (Moreau et al., 2015b).

Finally, the role of sea ice in the carbon cycle was investigated in a large-scale Earth System Models (ESMs): NEMO-LIM (Moreau et al., Submitted). Particularly, we investigated the link between sea ice growth and melt and the ocean dissolved inorganic carbon (DIC) and total alkalinity (TA), generally overlooked during ESM design. We use an ocean general circulation model (NEMO-LIM-PISCES) with sea ice and marine carbon cycle components, forced by atmospheric reanalyses, adding a first-order representation of DIC and TA storage and release in/from sea ice.

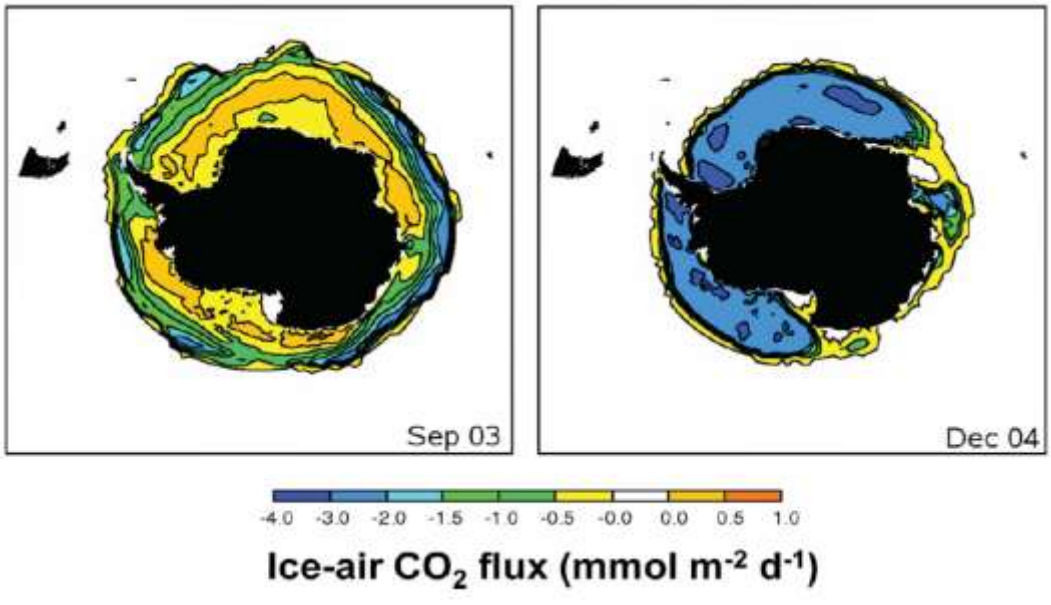

Figure 74: Simulated ice-air CO_2 fluxes during spring (Delille et al., 2014).

Our results suggest that the rejection of DIC during sea ice growth releases several hundreds of Tg C yr^{-1} to the surface ocean, of which only < 2% is exported to depth, leading to a notable but weak redistribution of DIC from lower latitudes towards deep polar basins (Figure 75).

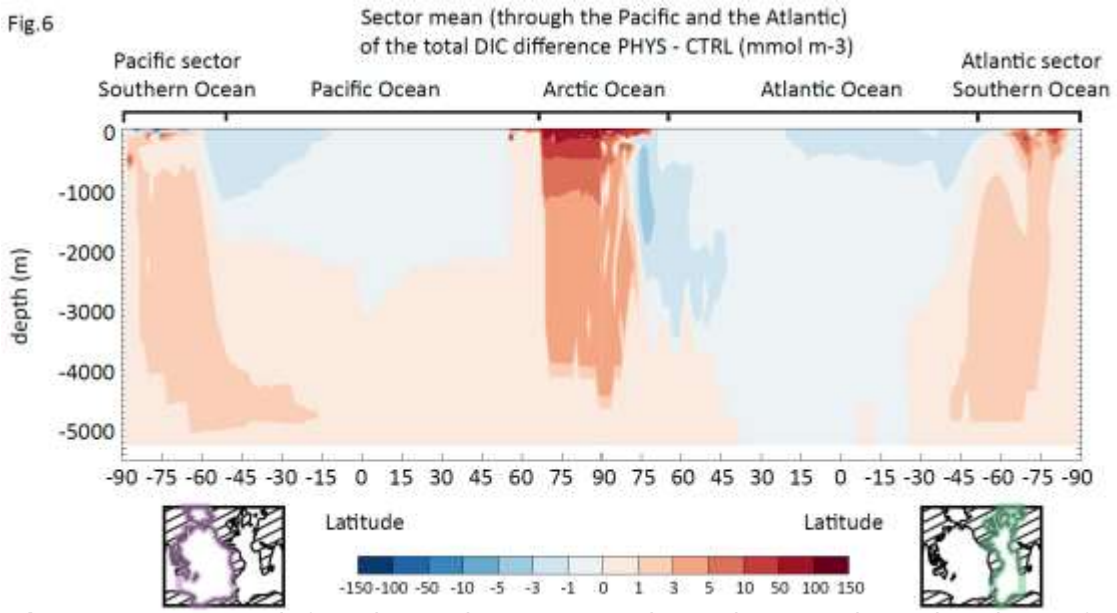

Figure 75: DIC anomaly from the Southern Ocean to the Arctic Ocean due to the release of DIC by brine drainage (Moreau et al., Submitted).

Active carbon processes (i.e. $CaCO_3$ precipitation, ice-atmosphere CO_2 fluxes and net community production) increasing the TA/DIC ratio in sea ice modify ocean-atmosphere CO_2 fluxes by a few Tg C yr^{-1} in the sea ice zone, with specific hemispheric effects (Figure 76).

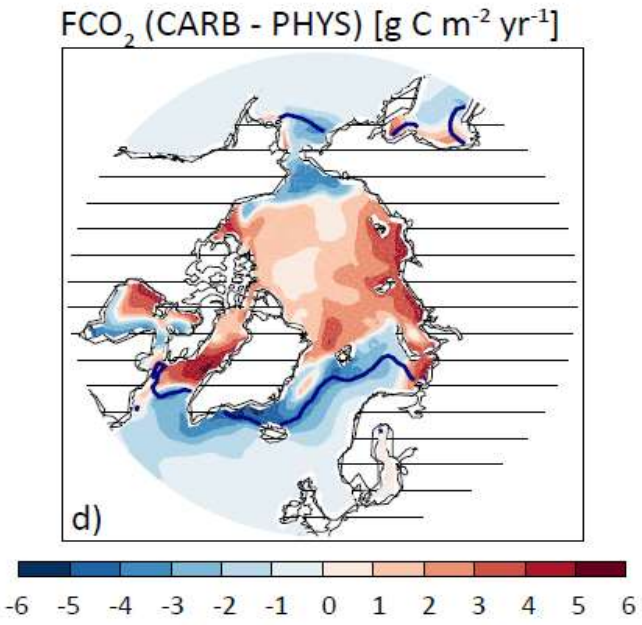

Figure 76: CO_2 fluxes anomaly in the Arctic and Southern Oceans due to active carbon processes in sea ice. (Moreau et al., Submitted).

This decreases the DIC content of the Arctic basin but increases the DIC content of the Southern Ocean (Figure 77). Overall, the DIC content of the Global Ocean increases by 4 Tg C yr^{-1}. The simulated numbers are generally small compared to the present-day global ocean annual CO_2 sink (1.4-2.5 Pg C yr^{-1}). However, sea ice carbon processes seem important at regional scales as they significantly act on the redistribution of DIC within and outside polar basins. The efficiency of carbon export to depth depends on the representation of surface-subsurface exchanges and their relationship with sea ice, and could substantially differ if a higher resolution or a different ocean model was used.

3.3.4. PEER-REVIEWED PUBLICATIONS ASSOCIATED WITH TOPIC 3

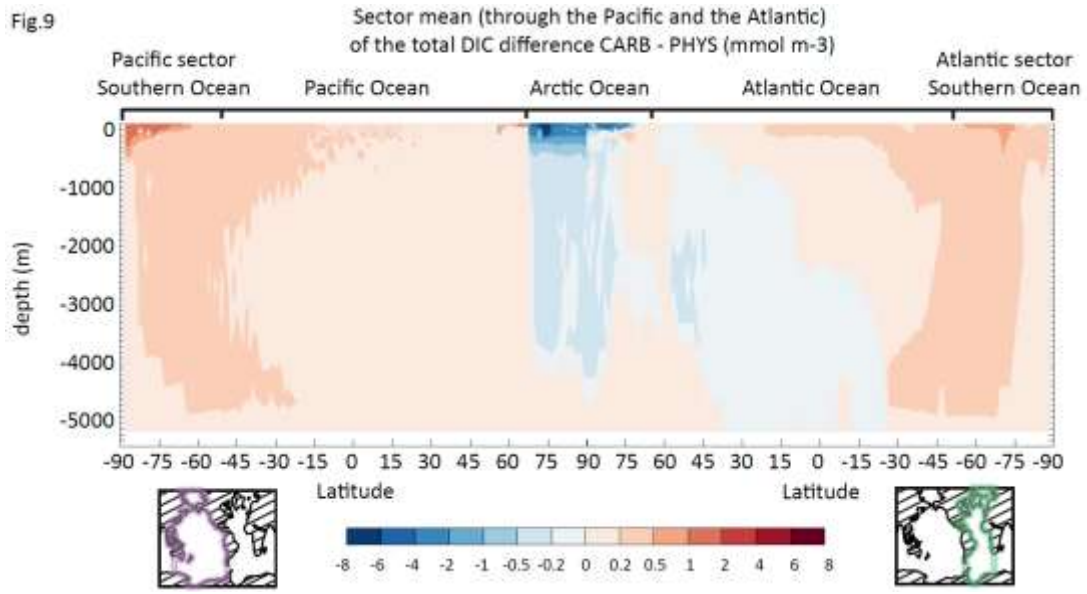

Figure 77: DIC anomaly from the Southern Ocean to the Arctic Ocean due to active carbon processes in sea ice (Moreau et al., Submitted).

1. **Delille B.**, **M. Vancoppenolle**, N.-X. Geilfus , B. Tilbrook, D. Lannuzel, **V. Schoemann**, S. Becquevort, **G. Carnat**, D. Delille, C. Lancelot, L. Chou, G.S. Dieckmann and **J.-L. Tison**, 2014. Southern Ocean CO2 sink: The contribution of the sea ice. *Journal of Geophysical Research: Oceans*, 119, 6340–6355 doi:10.1002/2014JC009941.
2. **Goosse H.** and V. Zunz, 2014. Decadal trends in the Antarctic sea ice extent ultimately controlled by ice-ocean feedback. *The Cryosphere* 8, 453–470. Doi: 10.5194/tc-8-453-2014.
3. **Moreau S.**, **M. Vancoppenolle**, **J. Zhou, J.-L. Tison, B. Delille** and **H. Goosse**, 2014. Modelling argon dynamics in first-year sea ice. *Ocean Modelling*, 73, 1-18. doi:10.1016/j.ocemod.2013.10.004.
4. **Moreau S.**, H.H. Kaartokallio, **M. Vancoppenolle, J. Zhou,** M. Kotovitch, G.S. Dieckmann, D. Thomas, **J.-L. Tison** and **B. Delille**, 2015. Assessing the O2 budget under sea ice: An experimental and modelling approach. *Elementa (Washington, D.C.)*, *3*, 3:000080. doi:10.12952/journal.elementa.000080.

5. **Moreau S.**, B. Mostajir, S. Bélanger, I.R. Schloss, **M.** Vancoppenolle, S. Demers and G.A. Ferreyra, 2015. Climate change enhances primary production in the western Antarctic Peninsula. *Global Change Biology* 21(6):2191-2205.
6. **Moreau S.**, **M. Vancoppenolle, B. Delille, J.-L. Tison, J. Zhou**, M. Kotovitch, D. Thomas, N.-X. Geilfus and **H. Goosse H**, 2015. Drivers of inorganic carbon dynamics in first-year sea ice: A model study. *Journal of Geophysical Research - Oceans*, 120 (1), 471-495, doi: 10.1002/2014JC010388.
7. **Moreau S.**, **M. Vancoppenolle**, L. Bopp, O.O. Aumont, G. Madec, **B. Delille**, **J.-L. Tison,** P.Y.P. Barriat and **H. Goosse**, 2016. Assessment of the sea-ice carbon pump: Insights from a three-dimensional ocean-sea-ice biogeochemical model (NEMO-LIM-PISCES). *Elementa: Science of the Anthropocene*, 4: e000122. doi:10.12952/ journal.elementa.000122.
8. Steiner N., C. Deal, D. Lannuzel, D. Lavoie, F. Massonet, L. Miller, **S. Moreau**, E. Popova, J. Stefels and L. Tedesco, 2016. What sea-ice biogeochemical modellers need from observationalists. *Elementa: Science of the Anthropocene*, 4, doi: 10.12952/journal.elementa.000084.
9. **Vancoppenolle M.**, R. Timmerman, S.F. Ackley, T. Fichefet, **H. Goosse**, P. Heil, J. Lieser, K.C. Leonard, M. Nicolaus, T. Papakyriakou and **J.-L. Tison**, 2011. Assessment of model forcing data sets for large-scale sea ice models in the Southern Ocean. *Deep-Sea Research II, 58*, 1237-1249, doi:10.1016/ j.dsr2.2010.10.039.
10. **Vancoppenolle M.**, L. Bopp, G. Madec, J. Dunne, T. Ilyina, P. R. Halloran and N. Steiner, 2013. Future Arctic Ocean primary productivity from CMIP5 simulations: Uncertain outcome, but consistent mechanisms. *Global Biogeochemical Cycles* 27(3): 605-619.
11. **Vancoppenolle M.**, K. M. Meiners, C. Michel, L. Bopp, F. Brabant, **G. Carnat**, **B. Delille**, D. Lannuzel, G. Madec, **S. Moreau**, **J.-L. Tison** and P. van der Merwe, 2013. Role of sea ice in global biogeochemical cycles: Emerging views and challenges. *Quaternary Science Reviews*, 79:207-230, doi:10.1016/j.quascirev.2013.04.011.

4. CONCLUSIONS AND RECOMMENDATIONS

Open ocean carbon biopump

1. The naturally iron-fertilised Plateau area south-east of Kerguelen sustains a strong seasonal phytoplankton bloom which disperses eastward, channelled by the Polar Front. During early spring primary production above the Plateau exceeds production in the Polar Front Meander eastward of Kerguelen. In general, early spring nitrate uptake rates largely exceed those for ammonium and resulting f-ratios are high.

2. Natural N, O isotopic composition of nitrate during early spring indicates that significant nitrification occurs in the mixed layer, representing a large fraction (up to 50% and more) of the nitrate uptake. This finding is rather unexpected, especially for a nutrient rich system, but confirms earlier suspicions based on the fact that low seasonal nitrate drawdown coincides with large silicate drawdown, despite Si/N uptake ratios of similar magnitude.

3. Carbon export production is relatively more efficient (relative to primary production) at the Polar Front Meander than above the Plateau.

4. Deep water column remineralisation of exported organic matter is proportionally more important for the Polar Front Meander, with a deeper (2500m) water column than in the shallow (500m) Plateau area.

5. Above the Kerguelen Plateau primary production decreases from spring to summer, while export production increases. The fraction of primary production that is exported and may accumulate in the Plateau sediments increases from spring to summer. So, the carbon sequestration efficiency of the system improves with progress of the season. The likely scenario of the seasonal evolution shows an early season increase of phytoplankton biomass in the surface mixed layer, which triggers strong heterotrophic activity and shallow remineralization plus nitrification. Later, during summer carbon export becomes more important.

6. It appears likely that despite higher, trace metal sustained productivities, the plateau systems of the Antarctic and sub-Antarctic islands do not show a proportionally enhanced carbon sequestration efficiency.

Sea Ice Systems

7. We have completed the 3 major field programs aiming at documenting year-round processes in landfast sea ice, early spring and winter processes in pack ice (the latter quite rare, since the previous winter field trip in the Weddell Sea in the winter was in 1992).

8. CO_2 fluxes measured during the Interice V sea ice growth experiment show a coherent pattern of: a) sink for the atmosphere during sea water cooling; b) source for the atmosphere during young sea ice growth and c) sink for the atmosphere during sea ice decay.

9. During Interice V the contrasts in ice pCO_2 between pure sea water and 10% river water enriched sea water is globally related to initial differences in DOC load and contrast in bacterial respiration, but time discrepancies occur.

10. Original first measurements of $\delta^{15}N$ of nitrates, total dissolved nitrogen and particulate nitrogen in sea ice have revealed high levels of regenerated production and nitrification (up to 60%). However, during early spring sea ice algae growth appear to still strongly depend on nitrate uptake (SIPEX results) with higher uptake rates in the top and middle layer of the ice, rather than in the bottom layer. High nitrate uptake in the top layer resulted in significant enrichment of nitrate ^{15}N and ^{18}O.

11. The ^{13}C, ^{15}N isotope enrichment methodology developed for assessment of in-situ, within ice primary productivity and N-uptake proves to be reliable and reproducible.

12. We have also shown from $\delta^{30}Si$ measurements in sea ice that physical processes do not fractionate the silicon isotopic composition, suggesting that all changes can then be attributed to biogeochemical processes.

13. The year-round survey of the basic physical properties of McMurdo Sound landfast sea ice during YROSIAE shows a classical transition from impermeable winter sea ice (to the exception of the very bottom layer) to a fully permeable ice cover at the end of the summer. A high frequency temperature and salinity record in the month of November 2012, shows a transition period marked by large diurnal oscillations of the Ra number, witnessing repeated brine convection events.

14. Original N_2O measurements in sea ice brines during YROSIAE show large increases (>60 nmoles per litre of brine) detected in late winter-early spring, synchronous with high pCO_2 levels (>4000 ppmV), suggesting sustained respiration during the winter and active microbial processes which fits the picture of considerable regenerated primary production from the ^{15}N measurements.

15. Preliminary results from the AWECS cruise definitively breaks down the view of a biogeochemically "frozen" Weddell Sea ice in the winter.

16. Winter sea ice sustains considerable biological stocks and activities throughout, despite the reduced amount of available PAR.

17. Winter sea ice sustains a non-negligible sea ice source for the CO_2 fluxes to the atmosphere.

18. Building of the snow cover and alternation of contrasted weather conditions (cyclonic activities) switch the sea ice from permeable to impermeable, inducing favourable conditions for brine transport and biological activity in a relatively warm sea ice cover.

19. Most of the winter Weddell Sea is characterized by the development of an internal algal community, while on the western stretch along the peninsula it develops a more "classical" bottom community in a columnar-dominated sea ice texture.

20. Second-year ice along the Peninsula also shows internal communities, with strong signs of degradation by-products in potentially partly anaerobic conditions.

21. Winter sea ice shows considerable amounts of both DMSP and DMS. When the sea ice is impermeable, profiles are similar, while most of the DMS is lost in permeable ice.

22. Clear relationships between DMSP and chl-a exist, although complex, with contrasting DMSP/chl-a ratios, depending on the species present (e.g. coccoïds vs. diatoms).

23. Weddell Sea chl-a profiles show a secondary maximum in bottom waters, a possible sign of Deep Water production (or fast export from sea ice ??)

24. Arctic distribution of iron in sea ice is very different from its Antarctic counterpart, with a maximum in the upper layers, in relationship with the inputs sources (continental rivers and aerosols vs. deep waters upwelling).

25. The incorporation of sea ice tracers in a global Earth System Model significantly modifies the modelled carbon cycle. Surface DIC, TA and pCO_2 are modified, resulting in a modification of ocean-atmosphere CO_2 fluxes. The Arctic Ocean is a stronger CO_2 sink when using this configuration. The role of ice growth and ice melt areas, hence of sea ice transport, explains much of the observed changes. This may have an effect on the export of DIC to the deeper layers of the Oceans.

5. POLICY SUPPORT

Frank Dehairs, Jean-Louis Tison, Hugues Goosse, Bruno Delille, François Fripiat, are members of the National Belgian Committee on Antarctica, that is actively involved in international organisations of advise and management of the Antarctic system (Scientific Committee of Antarctic Rsearch; Antarctic Treaty Consultative Meeting; Committee for Environmental Protection; Convention for the Conservation of Antarctic Resources; European Polar Board)

Hugues Goosse is co-author of the update performed by the ACCE (Antarctic Climate Change and the Environment) in December 2012, see Turner J., N. Barrand, T. Bracegirdle, P. Convey, D. Hodgson, M. Jarvis, A. Jenkins, G. Marshall, H. Roscoe, J. Shanklin, J. French, H. Goosse, M. Guglielmin, J. Gutt, S. Jacobs, C. Kennicutt, V. Masson-Delmotte, P. Mayewski, F, Navarro, S. Robinson, T. Scambos, M. Sparrow, K. Speer, C. Summerhayes, D. Thompson, A. Klepikov, 2014. Antarctic Climate Change and the Environment – An Update, *Polar Record*, 50, 237-259.

Hugues Goosse is contributing author of the IPCC AR5, in charge in particular of the future changes in the sea ice cover and in the Southern Ocean.

François Fripiat, Jean-Louis Tison, Bruno Delille, Jiayun Zhou, Martin Vancoppenolle and Sebastien Moreau are members of the SCOR BEPS II sea ice biogeochemistry group.

The reports issued by these working groups are important elements for the scientific basis of any decision making related to future climate changes.

6. DISSEMINATION AND VALORISATION

Networks

BIGSOUTH network became endorsed (July 8th, 2013) by the IMBER Scientific Steering Committee.

The BIGSOUTH network is associated with the Antarctic Climate and Ecosystem - Cooperative Research Center (ACE-CRC; Australia).

Outreach activities (selection)

Dehairs F. and C. Lancelot, Le rôle de l'océan Austral dans le cycle du carbone, L'océanologie en Antarctique, Collège de Belgique, Namur, sept. 20, 2011.

Tison, J.-L. and F. Pattyn, La Glaciologie en Antarctique: la banquise et la calotte glaciaire, des acteurs climatiques multiples, Collège de Belgique, Namur, octobre 4, 2011.

October 30, 2013: Interview with journalist Johan Lambrechts, about the achievements of the BIGSOUTH network. The text of the interview is intended for a general public brochure about 'Climate' that will be published by BELSPO during 2014.

Websites

In September 2013 we developed a website for the BIGSOUTH project (www.bigsouth.be). Since then 222 people from 28 different countries (with 67% new visitors) visited the website (e.g., USA, Australia, China, Brazil, …). The website has now been archived.

Other websites associated with BIGSOUTH individual field projects are still active:

http://www.mio.univ-amu.fr/~queguiner/KEOPS_2.html

http://yrosiae.blogspot.be/?view=classic

http://awecs.blogspot.be/2013

http://seaice.acecrc.org.au/sipex2012/

Publications

The BIGSOUTH team has published over 100 peer-reviewed international papers during the course of the project (see publication list below).

7. PUBLICATIONS

7.1. PAPERS

2011

1. Bowie A.R., F. B. Griffiths, **F. Dehairs** and T.W. Trull, 2011. Oceanography of the subantarctic and polar frontal zones south of Australia during summer: setting for the SAZ-Sense study. *Deep-Sea Research II,* 58, 2059-2070.
2. Bowie A.R., T.W. Trull and **F. Dehairs**, 2011. Estimating the Sensitivity of the Subantarctic Zone to Environmental Change: the SAZ-Sense project. *Deep-Sea Research II*, 58, 2051-2058.
3. Brabant F., S. El Amri and **J.-L.Tison**, 2011. A robust approach for the determination of dimethylsulfoxide in sea ice. *Limnology and Oceanography, Methods, 9*, 261-274.
4. **Cavagna A.-J.**, M. Elskens, F.B. Griffiths, **F. Fripiat**, S.H.M. Jacquet, K.J. Westwood and **F. Dehairs**, 2011. Contrasting regimes of production and potential for carbon export in the SAZ and PFZ south of Tasmania. *Deep-Sea Research II,* 58, 2235-2247.
5. **Cavagna A.-J.**, **F. Fripiat**, **F. Dehairs**, D. Wolf-Gladrow, B. Cisewski, N. Savoye, **L. André** and D. Cardinal, 2011. Silicon uptake and supply during a Southern Ocean iron fertilization experiment (EIFEX) tracked by Si-isotopes. *Limnology & Oceanography,* 56(1), 147-160.
6. Dumont I., **V. Schoemann**, F. Masson, S.H.M. Jacquet and S. Becquevort, 2011. Bacterial remineralisation in epipelagic and mesopelagic waters in Sub-Antarctic and Polar frontal zones south of Tasmania. *Deep-Sea Research II,* 58, 2212-2221.
7. **Fripiat F.**, **A.-J. Cavagna**, **F. Dehairs**, S. Speich, **L. André** and D. Cardinal, 2011. Silicic acid pools dynamics in the Antarctic Circumpolar Current inferred from Si-isotopes. *Ocean Sciences,* 8, 533-547.
8. **Fripiat F.**, K. Leblanc, **A.-J. Cavagna**, M. Elskens, L. Armand, **L. André**, **F. Dehairs** and D. Cardinal, 2011. Summer efficient silicon loop despite contrasted diatom Si-affinity across the Polar Front and SubAntarctic Zone. *Marine Ecology Progress Series,* 435, 47-61.
9. **Fripiat F.**, **A.J. Cavagna**, N. Savoye, **F. Dehairs**, **L. André**, and D. Cardinal, 2011. Isotopic constraints on the Si-biogeochemical cycle of the Antarctic Zone. *Marine Chemistry* 123: 11-22.
10. Gonzalez-Davila M., J.M. Santana-Casiano, R.A. Fine, J. Happell, **B. Delille** and S. Speich, 2011. Carbonate system in the water masses of the Southeast Atlantic sector of the Southern Ocean during February and March 2008. *Biogeosciences,* 8, 1401-1413, doi:10.5194/bg-8-1401-2011.
11. Hassler C.S., **V. Schoemann**, C.A.M. Nichols, E.C.V. Butler and P.W. Boyd, 2011. Saccharides enhance iron bioavailability to Southern Ocean phytoplankton. *Proceedings of the National Academy of Sciences*, 108 (3), 1076-1081, 10.1073/pnas.1010963108.
12. Jacquet S.H.M., **F. Dehairs**, I. Dumont, S. Becquevort, **A.-J. Cavagna** and D. Cardinal, 2011. Twilight zone organic carbon remineralisation in the Polar

Front Zone and Subantarctic Zone south of Tasmania. *Deep-Sea Research II*, 58, 2222-2234.

13. Jacquet S.H.M, P.J. Lam, T.W. Trull and **F. Dehairs**, 2011. Carbon export production in the Polar Front Zone and Subantarctic Zone south of Tasmania. *Deep-Sea Research II,* 58, 2277-2292*.*

14. Lannuzel D., A. Bowie, T. Remenyi, P. Lam, A. Townsend, E. Ibisanmi, E. Butler, T. Wagener and **V. Schoemann**, 2011. Distributions of dissolved and particulate iron in the sub-Antarctic and Polar Frontal Southern Ocean (Australian sector). *Deep-Sea Research II,* 58, 2094-2112.
15. Lannuzel D., A.R. Bowie, P.C. van der Merwe, A.T. Townsend and **V. Schoemann**, 2011. Distribution of dissolved and particulate metals in Antarctic sea ice. *Marine Chemistry,* 124, 134-146.
16. Lewis M.-J., **J.-L.Tison**, B. Weissling, **B. Delille**, S.F. Ackley, F. Brabant and H. Xie, 2011. Sea ice and snow cover characteristics during the winter-spring transition in the Bellingshausen Sea: an overview of SIMBA 2007. *Deep-Sea Research II,* 58, 1019-1038, doi:10.1016/j.dsr2.2010.10.027.
17. Loose, B., P. Schlosser, D. Ringelberg, D.T. Ho, T. Takahashi, J. Richter-Menge, C.M. Reynolds, W. McGillis and **J.-L. Tison**, 2011. Gas diffusion through columnar laboratory sea ice: implications for mixed-layer ventilation of CO_2 in the seasonal ice zone. *Tellus - Series B - Chemical and Physical Meteorology,* 63(1), 23-39.
18. Marquardt, M., M. Kramer, **G. Carnat** and I. Werner, 2011. Vertical distribution of sympagic meiofauna in sea ice in the Canadian Beaufort Sea. *Polar Biology*, 34, 1887-1900.
19. Miller L.A., **G. Carnat**, B. Else, N. Sutherland and T. Papakyriakou, 2011. Carbonate system evolution at the Arctic Ocean surface during autumn freeze-up. *Journal of Geophysical Research*, 116, C00G04.
20. Petrou K., M.A. Doblin, P.J. Ralph, C.S. Hassler, K. Shelly, **V. Schoemann**, S. Wright and R. van den Enden, 2011. Iron-limitation and high light on phytoplankton populations from the Australian Sub-Antarctic zone (SAZ). *Deep-Sea Research II*, 58, 2200-2211.
21. Quéguiner B., K. Leblanc, V. Cornet-Barthaux, L. Armand, **F. Fripiat** and D. Cardinal, 2011. Using a new fluorescent probe of silicification to measure species-specific activities of diatoms under varying environmental conditions. Global Change: Mankind-Marine Environment Interactions. *Proceedings of the 13th French-Japanese Oceanography Symposium* (Ceccaldi H.-J., Dekeyser I., Girault M., and Stora G., Eds.), Springer Dordrecht, Heidelberg, London, New York, pp. 283-287.
22. Rysgaard S., J. Bendtsen, **B. Delille**, G.S. Dieckmann, R.N. Glud, H. Kennedy, J. Mortensen, S. Papadimitriou, D.L. Thomas and **J.-L. Tison**, 2011. Sea ice contribution to the air-sea CO_2 exchange in the Arctic and Southern Oceans. *Tellus - Series B - Chemical and Physical Meteorology,* 63(5), 823-830.
23. **Vancoppenolle M.**, R. Timmerman, S.F. Ackley, T. Fichefet, **H. Goosse**, P. Heil, J. Lieser, K.C. Leonard, M. Nicolaus, T. Papakyriakou and **J.-L. Tison**, 2011. Assessment of model forcing data sets for large-scale sea ice models in

the Southern Ocean. *Deep-Sea Research II, 58*, 1237-1249, doi:10.1016/ j.dsr2.2010.10.039.

2012

24. de Brauwere A., **F. Fripiat**, D. Cardinal, **A.-J. Cavagna**, **L. André** and M. Elskens, 2012. Isotopic model of oceanic silicon cycling: the Kerguelen Plateau case study. *Deep-Sea Research I,* 70, 42-59.
25. de Jong J., **V. Schoemann**, D. Lannuzel, H. de Baar and **J.-L. Tison**, 2012. Natural iron fertilization of the Atlantic Southern Ocean by continental shelf sources of the Antarctic Peninsula. *Journal of Geophysical Research - Oceans*, 117, G01029, doi:10.1029/2011JG001679.
26. **Fripiat F.**, **A.-J. Cavagna**, **F. Dehairs**, A. de Brauwere, **L. André** and D. Cardinal, 2012. Processes controlling Si-isotopic composition in the Southern Ocean for an application in paleoceanography. *Biogeosciences,* 9, 2443–2457.
27. Geilfus, N. X., **G. Carnat**, T. Papakyriakou, **J.-L.Tison**, B. Else, H. Thomas, E.H. Shadwick and **B. Delille**, 2012. Dynamics of pCO_2 and related air-ice CO_2 fluxes in the Arctic coastal zone (Amundsen Gulf, Beaufort Sea). *Journal of Geophysical Research - Oceans,* 117, C00G10.
28. Geilfus N. X., **B. Delille**, **V. Verbeke** and **J.-L.Tison**, 2012**.** Instruments and methods towards a method for high vertical resolution measurements of the partial pressure of CO_2 within bulk sea ice. *Journal of Glaciology, 58*(208), 287.
29. Hassler C.S., **V. Schoemann**, M. Boyé, A. Tagliabue, M. Rozmarynowycz and R.M.L. McKay, 2012. Iron availability in the Southern Ocean. *Oceanography and Marine Biology: An Annual Review,* 50, 1-64.
30. Meiners, K.M., **M. Vancoppenolle**, S. Thanassekos, G. S. Dieckmann, D. Thomas, **J.-L. Tison**, K. R. Arrigo, D. Garrison, A. McMinn, D. Lannuzel, P. van der Merwe, K. Swadling, W.O. Smith, I. Melnikov and B. Raymond, 2012. Chlorophyll a in Antarctic sea ice from historical ice core data. *Geophysical Research Letters*, 39, 2012.
31. Stefels J., **G. Carnat**, J.W. Dacey, T. Goossens, J.T.M. Elzenga and **J.-L.Tison**, 2012. The analysis of dimethylsulfide and dimethylsulphoniopropionate in sea ice: dry-crushing and melting using stable isotope additions. *Marine Chemistry,* 128-129, 34-43, doi: 10.1016/j.marchem.2011.09.007.
32. Thomas H., E. Shadwick, **F. Dehairs**, B. Lansard, A. Mucci , J. Navez, Y. Gratton, F. Prowe, M. Chierici, A. Fransson, T. Papakyriakou, E. Sternberg, L. Miller and C. Monnin, 2012. Barium and Carbon fluxes in the Canadian Arctic Archipelago. *Journal of Geophysical Research*-Oceans, 116, C00G08, doi:10.1029/2011JC007120.
33. Vogt, M., C., O'Brien, J. Peloquin, **V. Schoemann**, E. Breton, M. Estrada, J. Gibson, D. Karentz, M.A. Van Leeuwe, J. Stefels, C. Widdicombe and L. Peperzak, 2012. Global marine plankton functional type biomass distributions: Phaeocystis spp. *Earth System Science Data* 4 (1), 107-120.

2013

34. **Carnat G.**, T. Papakyriakou, N.-X. Geilfus, F. Brabant, **B. Delille**, M. **Vancoppenolle,** G. Gilson, **J. Zhou** and **J.-L. Tison**, 2013. Investigations on physical and textural properties of Arctic first-year sea ice in the Amundsen Gulf, Canada, November 2007–June 2008 (IPY-CFL system study). *Journal of Glaciology*, 57, doi:10.3189/2013JoG12J148.
35. **Cavagna A.-J.**, **F. Dehairs**, S. Bouillon, V. Woule-Ebongué, F. Planchon, **B. Delille** and I. Bouloubassi, 2013. Water column distribution and carbon isotopic signal of cholesterol, brassicasterol and particulate organic carbon in the Atlantic sector of the Southern Ocean. *Biogeosciences*, 10, 2787-2801, doi: 10.5194/bg-10-2787-2013.
36. de Jong J., **V. Schoemann**, N. Mattielli, P. Langhorne, T. Haskell and **J.-L. Tison**, 2013. Iron in land-fast sea ice of McMurdo Sound derived from sediment resuspension and wind-blown dust attributes to primary productivity in the Ross Sea. Antarctica, *Marine Chemistry*, 157, 24-40, doi: 10.1016/j.marchem.2013.07.001.
37. Fransson A., M. Chierici, L.A. Miller, **G. Carnat**, E. Shadwick, H. Thomas, S. Pineault and T.N. Papakyriakou, 2013. Impact of sea-ice processes on the carbonate system and ocean acidification at the ice-water interface of the Amundsen Gulf, Arctic Ocean. *Journal of Geophysical Research - Oceans*, 118, 1-23, doi: 10.1002/2013JC009164.
38. **Fripiat F.**, **J.-L Tison**, **L. André**, D. Notz and **B. Delille**, 2013. Biogenic silica recycling in sea ice inferred from Si-isotopes: constraints from winter Arctic first-year sea ice. *Biogeochemistry*, doi:10.1007/s10533-013-9911-8.
39. Geilfus N. X., **G. Carnat**, G.S. Dieckmann, H. Eicken, N. Halden, G. Nehrke, T. Papakyriakou, **J.-L. Tison** and **B. Delille**, 2013. First estimates of the contribution of $CaCO_3$ precipitation to the release of CO_2 to the atmosphere during young sea ice growth. *Journal of Geophysical Research - Oceans,* 118, 1-12.
40. Gledhill M., C.S. Hassler and **V. Schoemann**, 2013. The environmental bioinorganic chemistry of aquatic microbial organisms. *Frontiers in Microbiology*, 4, 100. doi: 10.3389/fmicb.2013.00100.
41. Kaartokallio H., D.H. Søgaard, L. Norman, S. Rysgaard, **J.-L. Tison J.-L**., **B. Delille** and D.N. Thomas, 2013. Short-term variability in bacterial abundance, cell properties, and incorporation of leucine and thymidine in subarctic sea ice. *Aquatic Microbial Ecology*, 71:57-73, doi: 10.3354/ame01667.
42. Lannuzel D., **V. Schoemann**, I. Dumont, M. Content, J. de Jong, **J.-L. Tison**, **B. Delille** and S. Becquevort, 2013. Effect of melting Antarctic sea ice on the fate of microbial communities studied in microcosms. *Polar Biology*, 36:1483-1497, doi:10.1007/s00300-013-1368-7.
43. Planchon F., **A.-J. Cavagna**, D. Cardinal, **L. André** and **F. Dehairs**, 2013. Late summer particulate organic carbon export from mixed layer to mesopelagic twilight zone in Atlantic sector of Southern Ocean. *Biogeosciences,* 10, 803-820.
44. **Vancoppenolle M.**, L. Bopp, G. Madec, J. Dunne, T. Ilyina, P. R. Halloran and N. Steiner, 2013. Future Arctic Ocean primary productivity from CMIP5

simulations: Uncertain outcome, but consistent mechanisms. *Global Biogeochemical Cycles* 27(3): 605-619.

45. **Vancoppenolle M.**, K. M. Meiners, C. Michel, L. Bopp, F. Brabant, **G. Carnat**, **B. Delille**, D. Lannuzel, G. Madec, **S. Moreau**, **J.-L. Tison** and P. van der Merwe, 2013. Role of sea ice in global biogeochemical cycles: Emerging views and challenges. *Quaternary Science Reviews*, 79:207-230, doi:10.1016/j.quascirev.2013.04.011.
46. **Vancoppenolle M.**, D. Notz, F. Viviers, **J.-L. Tison**, **B. Delille**, **G. Carnat**, **J. Zhou**, F. Jardon, P. Griewank and A. Lourenço, 2013. Technical Note: On the use of the mushy-layer Rayleigh number for the interpretation of sea-ice core data. *The Cryosphere Discussions*, 7 (4), 3209-3230.
47. **Zhou J.**, **B. Delille**, H. Eicken, **M. Vancoppenolle**, F. Brabant, **G. Carnat**, N.-X. Geilfus, T. Papakyriakou, B. Heinesch and **J.-L. Tison**, 2013. Physical and biogeochemical properties in landfast sea ice (Barrow, Alaska): insights on brine and gas dynamics across seasons. *Journal of Geophysical Research – Oceans*, 118(6):3172-3189.

2014

48. Bakker D.C.E., H.W. Bange, N. Gruber, T. Johannessen, R.C. Upstill-Goodard, A.V. Borges, **B. Delille**, C.R. Löscher, S. W.A. Naqvi., A.M. Omar and M Santana-Casiano, 2014. Air-sea interaction of natural-lived Greenhouse gases (CO2, N2O, CH4) in a changing climate, In: Ocean-Atmosphere interaction of gases and particles (P.S Liss and M.T. Johnson, Eds.), pp113-169, Springer Earth System Sciences, Springer.
49. **Carnat G.**, **J. Zhou**, T. Papakyriakou, **B. Delille**, T. Goossens, T. Haskell, **V. Schoemann**, **F. Fripiat**, J.M. Rintala and **J.-L. Tison**, 2014. Physical and biological controls on DMS-P dynamics in ice shelf-influenced fast ice during a winter-spring and a spring-summer transitions. *Journal of Geophysical Research – Oceans*, 119, 2882 – 2905. doi:10.1002/2013JC009381.
50. Closset I., M. Lasbleiz, K. Leblanc, B. Quéguiner, **A.-J. Cavagna**, M. Elskens, J. Navez and D. Cardinal, 2014. Seasonal evolution of net and regenerated silica production around a natural Fe-fertilized area in the Southern Ocean estimated with Si isotopic approaches. *Biogeosciences,* 11, 5827-5846.
51. Crabeck O., **B. Delille**, S. Rysgaard, D.N. Thomas, N.-X. Geilfus, B. Else and **J.-L. Tison**, 2014. First 'in situ' determination of gas transport coefficients (DO2, DAr and DN2) from bulk gas concentration measurements (O2, N2, Ar) in natural sea ice. *Journal of Geophysical Research - Oceans*, 119, 6655-6668, doi: 10.1002/ 2014JC009849.
52. Crabeck O., **B. Delille**, D.N. Thomas., N-X. Geilfus, S. Rysgaard and **J. L. Tison**, 2014. CO2 and CH4 in sea ice from a subarctic fjord under influence of riverine input. *Biogeosciences*, 11:(6525-6538), doi:10.5194/bg-11-6525-2014.
53. **Delille B.**, **M. Vancoppenolle**, N.-X. Geilfus , B. Tilbrook, D. Lannuzel, **V. Schoemann**, S. Becquevort, **G. Carnat**, D. Delille, C. Lancelot, L. Chou, G.S. Dieckmann and **J.-L. Tison**, 2014. Southern Ocean CO2 sink: The contribution of the sea ice. *Journal of Geophysical Research: Oceans*, 119, 6340–6355 doi:10.1002/2014JC009941.

54. Dierckx M., M.M. Peternell, C. Schroeder and **J.-L. Tison**, 2014. Influence of pre-existing microstructure on mechanical properties of marine ice during compression experiments. *Journal of Glaciology*, 60 (221).
55. **Fripiat F.**, D.M. Sigman, S.E. Fawcett, P.A. Rafter, M.A. Weigand and **J.-L. Tison**, 2014. New insights into sea ice nitrogen biogeochemical dynamics from nitrogen isotopes. *Global Biogeochemical Cycles*, 28, 115-130, 10.1002/2013GB004729. doi:10.1002/2013GB004729.
56. **Fripiat F.**, **J.-L. Tison, L. André**, D. Notz and **B. Delille**, 2014. Biogenic silica recycling in sea ice inferred from Si-isotopes: Constraints from Arctic winter first-year sea ice. *Biogeochemistry*, *119*(1-3), 25-33. doi: 10.1007/s10533-013-9911-8.
57. Garbe C.S., A. Rutgersson, J. Boutin, **B. Delille**, C.W. Fairall, N. Gruber, J. Hare, D. Ho, M. Johnson, G. de Leeuw, P.D. Nightingale, H. Pettersson, Jacek Piskozub, E. Sahlee, W.-T. Tsai, B. Ward, D.K. Woolf and C.J. Zappa, 2014. Transfer across the air-sea interface, In Ocean-Atmosphere interaction of gases and particles (P.S Liss and M.T. Johnson, Eds), pp55-112, Springer Earth System Sciences, Springer.
58. Geilfus N. X., S. Rysgaard, **J.-L. Tison,** S. Ackley, R.J. Galley, L. Miller and **B. Delille**, 2014. Sea ice pCO_2 dynamics and air-ice CO_2 fluxes during the sea ice mass balance in the Antarctic (SIMBA) experiment-Bellingshausen sea, Antarctica. *The Cryosphere*, *8*(6), 2395-2407. doi:10.5194/tc-8-2395-2014.
59. González M. L., V. Molina, L. Florez-Leiva, L. Oriol, **A. J. Cavagna**, **F. Dehairs**, L. Farias and C. Fernandez, 2014. Nitrogen fixation in the Southern Ocean: a case of study of the Fe-fertilized Kerguelen region (KEOPS II cruise). *Biogeosciences-Discussion,* 11, 17151–17185.
60. **Goosse H.** and V. Zunz, 2014. Decadal trends in the Antarctic sea ice extent ultimately controlled by ice-ocean feedback. *The Cryosphere* 8, 453–470. Doi: 10.5194/tc-8-453-2014.
61. Hassler CS, Norman L, Nichols CAM, Clementson LA, Robinson C, **Schoemann V**, Watson RJ, Doblin MA (2014). Iron associated with exopolymeric substances is highly bioavailable to oceanic phytoplankton. Mar Chem 173, 136-147.
62. Jardon F., F. Vivier, **M. Vancoppenolle**, A. Lourenco, P. Bouruet-Aubertot and Y. Cuypers, 2014. Full-depth desalination of warm sea ice. *Journal of Geophysical Research - Oceans*, 118:435–447.
63. Laurenceau-Cornec E. C. , T. W. Trull, D. M. Davies, S. G. Bray, J. Doran, F. Planchon, F. Carlotti, M.-P. Jouandet, **A.-J. Cavagna**, A. M. Waite and S. Blain, 2014. The relative importance of phytoplankton aggregates and zooplankton fecal pellets to carbon export: insights from free-drifting sediment trap deployments in naturally iron-fertilised waters near the Kerguelen Plateau, *Biogeosciences*, 12, 1007-1027.
64. **Moreau S.**, **M. Vancoppenolle**, **J. Zhou, J.-L. Tison, B. Delille** and **H. Goosse**, 2014. Modelling argon dynamics in first-year sea ice. *Ocean Modelling*, 73, 1-18. doi:10.1016/j.ocemod.2013.10.004.

65. Rijkenberg MJA, Middag R, Laan P, Gerringa LJA, Van Aken HM, **Schoemann V**, De Jong JTM, Hein JW De Baar HJW (2014). The distribution of dissolved iron in the West Atlantic Ocean. PloS One 9 (6), e101323.
66. Sørensen L. L., B. Jensen, R.N. Glud, D. McGinnis, M.C. Sejr, J. Sievers, D. Søgaard, **J.-L. Tison** and S. Rysgaard, 2014. Parametrization of Atmosphere-Surface exchange of CO_2 over sea ice. *The Cryosphere*, 8 (3), 853-866.
67. Turner J., N. Barrand, T. Bracegirdle, P. Convey, D. Hodgson, M. Jarvis, A. Jenkins, G. Marshall, H. Roscoe, J. Shanklin, J. French, **H. Goosse**, M. Guglielmin, J. Gutt, S. Jacobs, C. Kennicutt, V. Masson-Delmotte, P. Mayewski, F, Navarro, S. Robinson, T. Scambos, M. Sparrow, K. Speer, C. Summerhayes, D. Thompson and A. Klepikov, 2014. Antarctic Climate Change and the Environment – An Update. *Polar Record*, 50, 237-259.
68. **Zhou J.**, **B. Delille**, H. Kaartokallio, G. Kattner, H. Kuosa, **J-L. Tison**, R. Autio, G. S. Dieckmann, K-U. Evers, L. Jørgensen, H. Kennedy, M. Kotovitch, A-M. Luhtanen, C. A. Stedmon and D. N. Thomas, 2014. Physical and bacterial controls on inorganic nutrients and dissolved organic carbon during a sea ice growth and decay experiment. *Marine Chemistry*, 166, 59-69, doi:10.1016/j.marchem.2014.09.013.
69. **Zhou J.**, **B. Delille**, F. Brabant and **J.-L. Tison**, 2014. Insights into oxygen transport and net community production in sea ice from oxygen, nitrogen and argon concentrations. *Biogeosciences*, 11, 5007-5020, doi:10.5194/bg-11-5007-2014.
70. **Zhou J.**, **J-L. Tison**, **G. Carnat**, N-X. Geilfus and **B. Delille**, 2014. Physical controls on the storage of methane in landfast sea ice. *The Cryosphere*, 8, 1019-1029, doi:10.5194/tc-8-1019-2014.

2015

71. Brown K.A., L.A. Miller, C.J. Mundy, T. Papakyriakou, R. François, M. Gosselin, **G. Carnat**, K. Swystun and P.D. Tortell, 2015. Inorganic carbon system dynamics in landfast Arctic sea ice during the early-melt period. *Journal of Geophysical Research-Oceans*, 120, doi: 10.1002/2014JC010620.
72. **Cavagna A. J.**, **F. Fripiat**, M. Elskens, **F. Dehairs**, P. Mangion, L. Chirurgien, I. Closset, M. Lasbleiz, L. Flores–Leiva, D. Cardinal, K. Leblanc, C. Fernandez, D. Lefèvre, L. Oriol, S. Blain and B. Quéguiner, 2015. Biological productivity regime and associated N cycling in the vicinity of Kerguelen Island area, Southern Ocean. *Biogeosciences,* 12, 6515-6528.
73. Crabeck O., R.J. Galley, **B. Delille,** B. Else, N.-X. Geilfus, M. Lemes, F.P. Des Roches, **J.-L. Tison** and S. Rysgaard, 2015. Imaging air volume fraction in sea ice using non-destructive X-ray tomography. *The Cryosphere - Discussions*, 9, 5203-5251. doi:10.5194/tcd-9-5203-2015.
74. **Dehairs F.**, **F. Fripiat**, **A.-J. Cavagna**, T.W. Trull, C. Fernandez, D. Davies, **A. Roukaerts**, D. Fonseca Batista, F. Planchon and M. Elskens, 2015. Nitrogen cycling in the Southern Ocean Kerguelen Plateau area: Evidence for significant surface nitrification from nitrate isotopic compositions. *Biogeosciences,* 12, 1459-1482.

75. de Jong J., S. Stammerjohn, S. Ackley, **J.-L. Tison**, N. Mattielli and **V. Schoemann**, 2015. Sources and fluxes of dissolved iron in the Bellingshausen Sea (West Antarctica): The importance of sea ice, icebergs and the continental margin. *Marine Chemistry*, http:// dx.doi.org/10.1016/j.marchem.2015.08-004.
76. **Fripiat F.**, M. Elskens, T. Trull, S. Blain, **A.-J. Cavagna**, C. Fernandez, D. Fonseca-Batista, F. Planchon, P. Raimbault, **A. Roukaerts** and **F. Dehairs**, 2015. Significant mixed layer nitrification in a natural iron-fertilized bloom of the Southern Ocean. *Global Biogeochemical Cycles,* 29, 1929-1943.
77. **Fripiat, F.**, D.M. Sigman, G.G. Massé and **J.-L. Tison**, 2015. High turnover rates indicated by changes in the fixed N forms and their stable isotopes in Antarctic landfast sea ice. *Journal of Geophysical Research - Oceans*, 120(4), 3079-3097. doi:10.1002/2014JC010583.
78. Geilfus N. X., R.J. Galley, O. Crabeck, T. Papakyriakou, J. Landy, **J.-L. Tison** and S. Rysgaard, 2015. Inorganic carbon dynamics of melt pond-covered first year sea ice in the Canadian Arctic. *Biogeosciences*, *12*(6), 2047-2061.
79. Gerringa LJA, Rijkenberg MJA, **Schoemann V**, Laan P, De Baar HJW (2015). Organic complexation of iron in the West Atlantic Ocean. Mar Chem 177, 434-446.
80. Jacquet S. H. M., **F. Dehairs**, D. Lefèvre, **A.-J. Cavagna**, F. Planchon, U. Christaki, L. Monin, **L. André**, I. Closset and D. Cardinal, 2015. Early season mesopelagic carbon remineralization and transfer efficiency in the naturally iron-fertilized Kerguelen area. *Biogeosciences,* 12, 1713-1731.
81. Laurenceau-Cornec E. C. , T. W. Trull, D. M. Davies, S. G. Bray, J. Doran, F. Planchon, F. Carlotti, M.-P. Jouandet, **A.-J. Cavagna**, A. M. Waite and S. Blain, 2015. The relative importance of phytoplankton aggregates and zooplankton fecal pellets to carbon export: insights from free-drifting sediment trap deployments in naturally iron-fertilised waters near the Kerguelen Plateau. *Biogeosciences*, 12, 1007-1027.
82. Miller L. L., **F. Fripiat,** B. Else, J.S. Bowman, K.A. Brown, E.R. Collins, M. Ewert, A.A. Fransson, M. Goselin, D. Lannuzel, K. Meiners, C. Michel, J. Nishioka, D. Nomura, S. Papadimitriou, L.M. Russell, L.L. Sorensen, D. Thomas, D., **J.-L. Tison,** M. van Leeuwe, **M. Vancoppenolle,** E.W. Wolff and **J. Zhou,** 2015. Methods for biogeochemical studies of sea ice: The state of the art, caveats, and recommendations. *Elementa*, *3*, 000038. doi:10.12952/journal.elementa.000038.
83. **Moreau S.**, H.H. Kaartokallio, **M. Vancoppenolle, J. Zhou,** M. Kotovitch, G.S. Dieckmann, D. Thomas, **J.-L. Tison** and **B. Delille**, 2015. Assessing the O2 budget under sea ice: An experimental and modelling approach. *Elementa (Washington, D.C.)*, *3*, 3:000080. doi:10.12952/journal.elementa.000080.
84. **Moreau S.**, B. Mostajir, S. Bélanger, I.R. Schloss, **M.** Vancoppenolle, S. Demers and G.A. Ferreyra, 2015. Climate change enhances primary production in the western Antarctic Peninsula. *Global Change Biology* 21(6):2191-2205.
85. **Moreau S.**, **M. Vancoppenolle, B. Delille, J.-L. Tison, J. Zhou**, M. Kotovitch, D. Thomas, N.-X. Geilfus and **H. Goosse H**, 2015. Drivers of inorganic carbon

dynamics in first-year sea ice: A model study. *Journal of Geophysical Research - Oceans*, 120 (1), 471-495, doi: 10.1002/2014JC010388.

86. Pasquer B., N. Metzl, **H. Goosse** and C. Lancelot, 2015. What drives the seasonality of air-sea CO_2 fluxes in the ice-free zone of the Southern Ocean: a 1D coupled physical-biogeochemical model approach. *Marine Chemistry,* 177, 554-565.
87. Planchon F., D. Ballas, **A.-J. Cavagna**, A.R. Bowie, D. Davies, T.W. Trull, E. Laurenceau, P. van der Merwe and **F. Dehairs**, 2015. Carbon export in the naturally iron-fertilized Kerguelen area of the Southern Ocean based on the 234Th approach. *Biogeosciences*, 12, 3831-3848.
88. Trull T.W., D. Davies, **F. Dehairs**, **A.-J. Cavagna**, M. Lasbleiz, E.C. Laurenceau-Cornec, F. D'Ovidio, F. Planchon, B. Quéguiner and S. Blain, 2015. Chemometric perspectives on plankton community responses to natural iron fertilisation over and downstream of the Kerguelen Plateau in the Southern Ocean. *Biogeosciences,* 12, 1029-1056, doi:10.5194/bg-12-1029-2015.
89. van der Merwe P., A. Bowie, F. Quéroué, L. Armand, S. Blain, F. Chever, D. Davies, **F. Dehairs**, F. Planchon, G. Sarthou, A.T. Townsend and T.W. Trull, 2015. Sourcing the iron in the naturally-fertilised bloom around the Kerguelen Plateau: particulate trace metal dynamics. *Biogeosciences,* 12, 739–755.

2016

90. **Carnat G.**, F. Brabant, I. Dumont, **M. Vancoppenolle**, S.F. Ackley, C. Fritsen, **B. Delille** and **J.-L. Tison**, 2016. Sea-ice algal primary production and nitrogen uptake rates off East Antarctica, *Elementa: Science of the Anthropocene*, 4: 000135, doi: 10.12952/journal.elementa.000135.
91. Janssens J., K.M. Meiners, **J.-L. Tison**, G. Dieckmann, **B. Delille** and D. Lannuzel, 2016. Incorporation of iron and organic matter into young Antarctic sea ice during its initial growth stages. *Elementa: Science of the Anthropocene*, 4: 000123. doi:10.12952/ journal.elementa.000123.
92. Jutras M. M., **M. Vancoppenolle**, A.A. Lourenço, F.F. Vivier, **G. Carnat**, G. Madec, C. Rousset and **J.-L. Tison**, 2016. Thermodynamics of slush and snow–ice formation in the Antarctic sea-ice zone. *Deep-sea research. Part 2. Topical studies in oceanography*, 131, 75-83. doi:10.1016/j.dsr2.2016.03.008.
93. Kotovitch M., **B. Delille**, **S. Moreau**, **J. Zhou**, **M. Vancoppenolle**, G. Dieckmann, K.-U. Evers, F. Van Der Linden, D.D. Thomas and **J.-L. Tison**, 2016. Air-ice carbon pathways inferred from a sea ice tank experiment. *Elementa: Science of the Anthropocene*, 4: 000112. doi:10.12952/journal.elementa.000112.
94. Lannuzel D, **Vancoppenolle M**, Van der Merwe P, De Jong J, Meiners K, Grotti M, Nishioka J, **Schoemann V** (2016). Iron in sea ice: Review and new insights. Elem Sci Anth 4, 000130, doi: 10.12952/journal.elementa.000130.
95. **Lemaitre N.**, H. Planquette, F. Planchon, **F. Dehairs**, P. van der Merwe, A. Bowie, T.W. Trull, C. Bollinger, M. Le Goff, E. Grossteffan, 2016. Impact of the natural Fe-fertilization on the magnitude, stoichiometry and efficiency of PN, BSi and PFe export fluxes, *Deep-Sea Research, I,* 117, 11-27.

96. Middleton C., C. Thomas, A. De Wit and **J.-L. Tison,** 2016. Visualizing brine channel development and convective processes during artificial sea-ice growth using Schlieren optical methods, *Journal of Glaciology*, 62, 1-17. doi:10.1017/jog.2015.1.
97. **Moreau S.**, **M. Vancoppenolle**, L. Bopp, O.O. Aumont, G. Madec, **B. Delille**, **J.-L. Tison,** P.Y.P. Barriat and **H. Goosse**, 2016. Assessment of the sea-ice carbon pump: Insights from a three-dimensional ocean-sea-ice biogeochemical model (NEMO-LIM-PISCES). *Elementa: Science of the Anthropocene*, 4: e000122. doi:10.12952/ journal.elementa.000122.
98. **Roukaerts A.**, **A.-J. Cavagna**, **F. Fripiat**, D. Lannuzel, K. Meiners and **F. Dehairs**, 2016. Sea-ice algal primary production and nitrogen uptake rates off East Antarctica. *Deep-Sea Research II*, 131, 140-149.
99. Steiner N., C. Deal, D. Lannuzel, D. Lavoie, F. Massonet, L. Miller, **S. Moreau**, E. Popova, J. Stefels and L. Tedesco, 2016. What sea-ice biogeochemical modellers need from observationalists. *Elementa: Science of the Anthropocene*, 4, doi: 10.12952/journal.elementa.000084.
100. **Tison J.-L.**, **B. Delille** and S. Papadimitriou, in press. Gases in Sea Ice, In : Sea Ice, 3rd Edition, Ed. Thomas, D., John Wiley and Sons, Oxford, UK.
101. **Tison J.-L.**, S. Schwegmann, G. Dieckmann, J. Rintala, J. Freitag, **S. Moreau**, **M. Vancoppenolle**, D. Nomura, S. Engberg, L.J. Bloomster, S. Heindrickx, C. Uhlig, A.M. Luhtanen, J. de Jong, J. Janssens, **G. Carnat**, **J. Zhou** and **B. Delille**, submitted. Warming Winter Weddell Sea Ice Pack Triggers Permeability and Biogeochemical Response, *Journal of geophysical research: Ocean.*
102. **Zhou J.**, M. Kotovitch, H.H. Kaartokallio, **S. Moreau**, **J.-L. Tison**, G.G. Kattner, G. Dieckmann, D.D. Thomas and **B. Delille**, 2016. The impact of dissolved organic carbon and bacterial respiration on pCO2 in experimental sea ice. *Progress in oceanography*, 141, 153-167. doi:10.1016/j.pocean.2015.12.005.

7.2. SYMPOSIA AND WORKSHOPS

2010

1. **Carnat G.**, F. Brabant, **J.-L. Tison**, **B. Delille**, N.X. Geilfus, G. Gilson, M. Levasseur and T. Papakyriakou, 2010. A comparative study of DMS,P dynamics in Arctic and Antarctic sea ice. *International Glaciological Society Symposium on Sea Ice in a Changing Environment*, Tromso, Norway. Talk.
2. **Carnat G.**, F. Brabant, J. Stefels, M. Levasseur, T. Papakyriakou, **B. Delille**, N.X. Geilfus, G. Gilson, T. Goossens and **J.-L. Tison**, 2010. DMS, P, O : the contribution of the marine cryosphere. *5th International Symposium on Biological and Environmental Chemistry of DMS(P) an Related Compounds*, Goa, India. Invited Talk.

3. **Carnat G.**, N.X Geilfus, G. Nehrke, **J.-L. Tison**, T. Papakyriakou, N. Halden, **J.-L. Tison** and **B. Delille**, 2010. First estimation of the contribution of $CaCO_3$ precipitation to the release of CO_2 to the atmosphere during young sea ice growth. *Arctic Net Annual Meeting*, Ottawa, Canada. Poster.
4. **Delille B., M. Vancoppenolle**, B. Tilbrook, D. Lannuzel, **V. Schoemann**, S. Becquevort, N.-X. Geilfus, **G. Carnat**, A. V. Borges, D. Delille, C. Lancelot, L. Chou, G. S. Dieckmann and **J.-L. Tison**, 2010. Air-sea ice CO_2 fluxes: a tentative upscaling. *Eos Trans. AGU* 91(26), Ocean Sci. Meet. Suppl., Abstract CO35C-03.
5. **Delille B.** and the BASICS team, 2010. Oceanic CO_2 sink: the contribution of the marine cryosphere. *EGU 2010*, Vienna, Austria. Talk.
6. Galindo V., M. Levasseur, M. Scarratt, C.J. Mundy, M. Gosselin, T. Papakyriakou, Y. Gratton, M. Lizotte, **G. Carnat** and S. Michaud, 2010. Influence of a rapid shift in UV and PAR radiation on the production of dimethylsulfoniopropionate (DMSP) and dimethylsulfoxide (DMSO) by ice algae and phytoplankton during the spring ice melt period in the Arctic. *Arctic Net Annual Meeting*, Ottawa, Canada. Poster.
7. Geilfus N.X, **J.-L. Tison**, **G. Carnat**, B. Else, A.V. Borges, H. Thomas, E. Shadwick and **B. Delille**, 2010. Air-ice CO_2 fluxes and pCO_2 dynamics in the Arctic coastal area (Amundsen Gulf, Canada). *EGU 2010*, Vienna, Austria. Poster.
8. Heinesch B., **J.-L. Tison**, **G. Carnat**, H. Eicken, N.X. Xavier, T. Goossens, T. Papakyriakou, M. Yerneaux and **B. Delille**, 2010. Micrometeorological survey of air-sea ice CO_2 fluxes in Arctic coastal waters. *EGU 2010*, Vienna, Austria. Poster.
9. Lannuzel D., **V. Schoemann**, P. Van Der Merwe, A. Townsend and A.R. Bowie, 2010. Dissolved and Particulate Metals Distribution in Antarctic Sea Ice and their Role in Tracing Iron Sources. *Eos Trans. AGU*, 91(26), Ocean Sci. Meet. Suppl., Abstract CO13A-05.
10. Rysgaard S., J. Bendtsen, **B. Delille**, G.S. Dieckmann, R.N. Glud, H. Kennedy, J. Mortensen, S. Papadimitriou, D. Thomas and **J.-L. Tison**, 2010**.** Sea ice contribution to the air-sea CO2 exchange in the Arctic and Southern oceans. *Sea Ice Workshop,* Nuuk, Greenland, paper writing.
11. **Tison J.-L.** and the BASICS team, 2010. Sea ice Biogeochemistry and the Climate: Where do we stand and where to go? *International Glaciological Society Symposium on Sea Ice in a Changing Environment*, Tromso, Norway. Talk.

2011

12. de Brauwere A., **F. Fripiat**, **A.-J. Cavagna**, D. Cardinal and M. Elskens, 2011. Isotopic model of oceanic silicon cycling: The Kerguelen Plateau case study. *3rd GEOTRACES data/model synergy workshop*, Barcelona, Spain.
13. Dehairs F., S. Jacquet, **F. Fripiat**, D. Cardinal, M. Hoppema, C. Jeandel, J. Navez, **A.-J. Cavagna**, S. Speich, M. Boyé, E. Fahrbach, S. Blain, M. Rutgers van der Loeff, H. de Baar and S. Rintoul, 2011. Differential retention of dissolved barium and silicon in the Atlantic, Indian and Australian sectors of the Southern Ocean. *43rd Intl. Liège Colloquium on Ocean Dynamics "Traces & Tracers"*, Liège, Belgium.
14. Delille B., N.-X. Geilfus, **M. Vancoppenolle**, B. Tilbrook, D. Lannuzel, **V. Schoemann**, S. Becquevort, **G. Carnat**, A.V. Borges, F. Deleu, D. Delille, C. Lancelot, L. Chou, G.S. Dieckmann, B. Heinesch, M. Aubinet, F. Brabant, H. Eicken, T. Papakyriakou, **J. Zhou** and **J.-L. Tison**, 2011. Overview of CO2 dynamics within sea ice. *MBI Workshop 6: Ocean Ecologies and Their Physical Habitats in a Changing Climate*, Columbus, OH, USA. Invited talk.
15. **Fripiat F.**, D.M. Sigman and J.L. Tison, 2011. Nitrogen and silicon isotopic signatures in the sea ice and surface waters of polars oceans: Implications for modern and past biogeochemical cycles. *SOLAS/COST workshop on Sea-Ice Biogeochemistry and Interactions with the Atmosphere*, Royal Netherlands Academy of Arts and Sciences, Amsterdam, The Netherlands.
16. Gonzalez-Davila M., J.M. Santana-Casiano, R.A. Fine, J. Happell, **B. Delille** and S. Speich, 2011. Carbonate system buffering in the water masses of the Southwest Atlantic sector of the Southern Ocean during February-March 2008, 2011. *43rd International Liège Colloquium on Ocean Dynamics*, Liège, Belgium. Talk.
17. Norman L., **V. Schoemann**, M. Doblin, R. Watson, L. Clementson and C. Hassler, 2011. The response of natural phytoplankton communities to iron from different sources. *AMSA2011, Crossing Boundaries*, Freemantle, Australia. Poster.
18. Rijkenberg M.J.A., L.J.A. Gerringa, P. Laan, **V. Schoemann**, R. Middag, S.M.A.C., L. Salt, H.M. Van Aken, J.T.M. de Jong and H.J.W. de Baar, 2011. GEOTRACES: Dissolved Fe in the Western Atlantic Ocean: distribution, sources, sinks and cycling. *Goldschmidt Conference*, Prague, Czech Republic. Talk.
19. Rijkenberg, M.J.A., L.J.A. Gerringa, P. Laan, **V. Schoemann**, R. Middag, S.M.A.C., L. Salt, H.M. Van Aken, J.T.M. de Jong and H.J.W. de Baar, 2011. Dissolved Fe in the Western Atlantic Ocean: distribution, sources, sinks and cycling. *43rd International Liège Colloquium on Ocean Dynamics*, Liège, Belgium. Talk.
20. **Schoemann V.**, J.T.M. de Jong, D. Lannuzel, **B. Dellile**, L. Chou, S. Becquevort and **J.-L. Tison**, 2011. Fe isotopes: a tool to trace biological processes in Antarctic sea ice. *43rd International Liège Colloquium on Ocean Dynamics*, Liège, Belgium, Belgium. Poster.

21. **Schoemann V.**, 2011. Sea ice as a source of bioavailable iron. *COST meeting of Working group 1 & 3 "Sea-ice biogeochemistry and interactions with the atmosphere",* Amsterdam, The Netherlands. Invited talk.
22. **Schoemann V**., 2011. Sea ice as a source of Fe for phytoplankton. *Royal NIOZ seminar series*, Texel, The Netherlands. Talk.
23. **Tison J.-L.**, **J. Zhou**, D.L. Thomas, S. Rysgaard, H. Eicken, O. Crabeck, F. Deleu and **B. Delille**, 2011. Gas transport processes in sea ice: How convection and diffusion processes might affect biological imprints, a challenge for modellers. *EGU General Assembly Conference Abstracts* p. 11390.
24. **Tison J.-L.**, 2011. Biogenic Gases in Sea Ice: from complex measurements to simple models…Wishful Thinking? *Gordon Research Seminars - Contributing to the Understanding of Complex Polar Marine Systems*, Ventura, USA. Invited talk.
25. **Tison J.-L.**, 2011. Biogenic Gases in Sea Ice: from complex measurements to simple models…Wishful Thinking? *CEOS, Clayton H. Riddell Seminar Series*, Winnipeg, Canada. Invited talk.
26. **Tison J.-L.**, 2011. Modelling biogenic gases concentrations and fluxes in sea ice: Wishful thinking? *SOLAS/COST Workshop on Sea Ice Biogeochemistry*, Amsterdam, The Netherlands. Invited talk.
27. **Tison J.-L.**, 2011. Modelling biogenic gases concentrations and fluxes in sea ice: Whishful thinking? *MBI, Mathematical Biosciences Institute, Workshop: Ocean Ecologies and their physical habitats in a changing climate*, Columbus, Ohio. Invited talk.
28. **Tison J.-L.**, 2011. Theme 4: Improved budgets for aboundless organic and inorganic carbon cycle: A global perspective – "A hitchiker's guide for a boundless cycle: The sea ice carbon pump". *IGBP, Global Carbon Project, Workshop: Exploring Knowledge Gaps along the Global Carbon Route*, Rochefort, Belgium. Invited talk.
29. Tisnérat-Laborde N., **B. Delille**, M. Gonzalez-Davila, J. M. Santana-Casiano, L. Bordier, C. Hatté, C. Moreau, M. Paterne, M. Boyé and S. Speich. Evolution of dissolved inorganic radiocarbon in the eastern Atlantic sector of the Southern Ocean. *43rd International Liège Colloquium on Ocean Dynamics*, Liège, Belgium. Talk.
30. **Zhou J.**, **J.-L. Tison**, H. Eicken, C. Petrich, N.-X. Geilfus, F. Brabant, **G. Carnat**, T. Papakyriakou, B. Heinesch, R. Laing and **B. Delille**, 2011. Dynamic processes in sea ice captured by the temporal evolution of its biogeochemical properties. *VLIZ Young Scientist Day*, Brugge, Belgium. Talk.
31. **Zhou J.**, **J.-L. Tison**, H. Eicken, C. Petrich, N.-X. Geilfus, F. Brabant, **G. Carnat**, T. Papakyriakou, B. Heinesch, R. Laing and **B. Delille**, 2011. A multidisciplinary approach to understanding the sea ice system: implications on gas. *Gordon Research Seminars - Contributing to the Understanding of Complex Polar Marine Systems*, Ventura, USA. Talk.
32. **Zhou J.**, **J.-L. Tison**, H. Eicken, C. Petrich, N.-X. Geilfus, F. Brabant, **G. Carnat**, T. Papakyriakou, B. Heinesch, R. Laing and **B. Delille**, 2011. Temporal evolution of biogeochemical properties of landfast sea ice at Barrow

(Alaska). *Gordon Research Conferences - Exploring Complex Systems in Polar Marine Science*, Ventura, USA. Poster.

2012

33. **Cavagna A.-J.**, **F. Dehairs**, B. Quéguiner, C. Fernandez and D. Lefèvre, 2012. Regimes of production and potential for carbon export in naturally iron-fertilized waters in the Southern Ocean. *ASLO Meeting 2012*, Lake Biwa, Japan.
34. **Cavagna A.-J.**, B. Quéguiner, F. Planchon, M. Elskens, **F. Dehairs**, 2012. Primary production and C-export during KEOPS 2. *Post-cruise Workshop*, Centre Océanologique de Banyuls, Banyuls, France. Talk.
35. de Baar, H., M. Rijkenberg, L. Gerringa, R. Middag, M. van Hulten, P. Laan, **V. Schoemann**, J. de Jong, A. Sterl, H. van Aken, 2012. Contrasting Biogeochemical Cycling of Iron and Aluminium along the GEOTRACES West Atlantic Section. Montreal, Canada. Talk.
36. de Brauwere, A., C. Jeandel, F. Lacan, P. Van Beek, C. Venchiuratti and **F. Fripiat**, 2012. Putting the pieces together: A multi-tracer model to quantitatively identify the major processes related to the fertilized bloom on the Kerguelen Plateau (Southern Ocean). *AGU fall meeting*, San Francisco. Talk.
37. **Dehairs F.**, T. Trull, C. Fernandez and D. Davies, 2012. KEOPS 2 results for $\delta^{15}N\text{-}NO_3$, $\delta^{18}O\text{-}NO_3$. *Post-cruise Workshop*, Centre Océanologique de Banyuls, Banyuls, France. Talk.
38. **Delille B.**, N.-X.Geilfus, **M. Vancoppenolle**, B. Tilbrook, D. Lannuzel, **V. Schoemann**, S. Becquevort, **G. Carnat**, A.V. Borges, D. Delille, C. Lancelot, L. Chou, G.S. Dieckmann, B. Heinesch, M. Aubinet, F. Brabant, H. Eicken, T. Papakyriakou, M. Yernaux and **J.-L. Tison**, 2012. CO_2 dynamics and related air-ice exchanges in sea ice. *Workshop COST - sea ice biogeochemistry*, Amsterdam. Talk.
39. **Fripiat F.**, 2012. Silicon isotopic signatures in the Southern Ocean: Implication for modern and past biogeochemical cycles. *Seminar at EPOC*, Université de Bordeaux, Talence, France. Talk.
40. **Fripiat F.**, 2012. Isotopic study of nitrogen and silicon cycling in the Southern Ocean (Sea Ice and Antarctic Zone). *Seminar at LOCEAN*, Université Pierre & Marie Curie, Paris. Talk.
41. **Fripiat F.**, **A.-J. Cavagna**, **F. Dehairs**, **L. André** and D. Cardinal, 2012. Silicon isotopic constraints on the Southern Ocean Si-biogeochemical cycle. *IBIS workshop*, Antwerp, Belgium. Talk.
42. **Fripiat F.**, **A.-J. Cavagna**, **F. Dehairs**, S. Speich, **L. André** and D. Cardinal, 2012. Silicon pool dynamics and biogenic silica export in the Antarctic Circumpolar Current inferred from Si-isotopes. *43rd Intl. Liège Colloquium on Ocean dynamics "Traces & Tracers"*, Liège, Belgium. Talk.
43. **Fripiat F.**, D.M. Sigman and J.-L.Tison, 2012. Nitrate ($\delta^{15}N$) isotopic distribution in Antarctic Sea Ice. *Goldschmidt Conference*, Montreal, Canada.
44. Hassler C., L. Norman, R. Watson, M. Doblin, C. Nichols, G. McTainsh, L. Clementson, **V. Schoemann**, 2012. Impact of various iron sources to Tasman

Sea phytoplankton: From bioavailability to community shift. *Ocean Sciences Meeting*, Salt Lake City, Utah, USA. Poster.

45. Jacquet S.H.M., **F. Dehairs**, **A.J. Cavagna**, F. Planchon, I. Closset and D. Cardinal, 2012. Seasonal variability of mesopelagic organic carbon remineralization in the naturally iron-fertilized Kerguelen area (Southern Ocean). *ASLO Meeting*, New Orleans.
46. Meiners K. M., **M. Vancoppenolle** and S. Thanassekos, 2012. Chl-a in Antarctic sea ice from historical ice core data. *SCAR science conference*, Portland, Oregon. Talk.
47. **Moreau S.**, **M. Vancoppenolle**, **J. Zhou**, **J.-L. Tison**, **B. Delille** and **H. Goosse**., 2012. Modeling Argon dynamics in first-year sea-ice. *SCAR science conference*, Portland, Oregon. Talk.
48. Planchon F., D. Ballas, **A.-J. Cavagna**, T. Trull, D. Davis, A. Bowie, P. Van Der Merwe, **F. Dehairs**, 2012. Carbon export during KEOPS 2 using the ^{234}Th proxy. *Post-cruise Workshop*, Centre Océanologique de Banyuls, Banyuls, France. Talk.
49. **Schoemann V.**, 2012. Sea ice as a source of bioavailable iron. *Symposium Iron in the Oceans*, Texel, The Netherlands. Invited talk.
50. **Schoemann V.**, D. Lannuzel, **B. Delille**, H. de Baar and **J.-L. Tison**, 2012. Sea ice as a source of bioavailable iron. *SOLAS Open Science Conference*, *Cle Elum*, WA, USA. Invited talk.
51. **Schoemann V.**, J.T.M. de Jong, D. Lannuzel, **B. Dellile**, L. Chou, S. Becquevort, N. Mattielli, H. de Baar and **J.-L. Tison**, 2012**.** Iron stable isotopes: a tool to trace biological processes in Antarctic sea ice. *SOLAS Open Science Conference*, *Cle Elum*, WA, USA. Poster.
52. **Schoemann V.**, J.T.M. de Jong, D. Lannuzel, **B. Dellile**, L. Chou, S. Becquevort, N. Mattielli, H. de Baar and **J.-L. Tison**, 2012. Iron isotopes in Antarctic sea ice. *GEOTRACES Workshop – Stable isotopes of biologically important trace metals*, London, UK. Poster.
53. Tedesco L., **M. Vancoppenolle**, and M. Vicchi, 2012. LIM1D-BFM-SI: A new advanced model of the sea ice ecosystem. *IPY-2012 : From knowledge to action*, Montreal, Canada. Poster.
54. **Tison J.-L.**, **J. Zhou**, D. Thomas, S. Rysgaard, H. Eicken, O. Crabeck, F. Deleu and **B. Delille**, 2012. Gas transport in sea ice: How convection and diffusion processes might affect biological imprints…A challenge for modellers. *EGU 2012*, Vienna, Austria. Invited talk.
55. **Vancoppenolle M.** and **H. Goosse**, 2012. Modelling sea ice biogeochemistry. *SCOR-WG Sea Ice Proxy workshop*, Montréal. Invited talk.
56. **Zhou J.**, **S. Moreau**, **M. Vancoppenolle**, **B. Delille**, **H. Goosse** and **J.-L. Tison**, 2012. Gas migration in sea ice: from observations to modelling. *SOLAS Open Science Conference*, Cle Elum, USA. Talk.

2013

57. **Carnat G.**, **J. Zhou**, **B. Delille**, T. Papakyriakou, **M. Vancoppenolle**, T. Goossens and **J.-L. Tison**, 2013. Scenario of DMS(P) evolution in landfast

sea ice over an annual cycle of ice growth (Cape Evans, Antarctica). *Gordon Research Conference Polar Marine Sciences*, Ventura, USA. Poster.

58. **Cavagna A.-J.**, B. Quéguiner, F. Planchon, S.H.M. Jacquet, I. Closset and **F. Dehairs**, 2013. Production regime and potential for carbon export in the naturally iron fertilized Kerguelen area (Southern Ocean). *ASLO Meeting New Orleans*.
59. **Cavagna A.-J.**, **F. Dehairs**, S.H.M. Jacquet and F. Planchon, 2013. Gaining information on C-sequestration efficiency using a production / export / remineralisation toolbox: the S.O. naturally Fe-fertilized areas study-case. *45th International Liège Colloquium, Primary Production in the Ocean: From the Synoptic to the Global Scale*, Liège, Belgium.
60. de Brauwere A., C. Jeandel, F. Lacan, P. Van Beek, C. Venchiuratti and **F. Fripiat**, 2013. Putting the pieces together: A multi-tracer model to quantitatively identify the major processes related to the fertilized bloom on the Kerguelen Plateau (Southern Ocean). *ASLO meeting*, New Orleans, United States of America.
61. **Dehairs F.**, T. Trull, C. Fernandez, D. Davies, **A.-J. Cavagna** and A.E. Piniella, 2013. Nitrate isotopic composition in the Kerguelen area (Southern Ocean) during KEOPS 2. *ASLO Meeting*, New Orleans, USA.
62. **Delille B**., 2013. From the release of CH_4 by sub-sea permafrost to the oceanic sink of CO_2: the role of sea ice in the fate of greenhouse gases in polar oceans. *Gordon Research Conferences – Polar Marine Science: Contributing to the Understanding of Complex Polar Marine Systems*, Ventura, USA. Invited talk.
63. **Fripiat F.**, D.M. Sigman and **J.-L. Tison**, 2013. Nitrogen Isotopic distribution in Antarctic Sea Ice. *Gordon conference on Polar Ocean*, Ventura, USA.
64. Geilfus N.-X., **J.-L. Tison**, **G. Carnat**, T. Papakyriakou, S. Rysgaard and **B. Delille**, 2013. Role of the arctic sea ice to the CO_2 exchange during the last IPY. *Gordon Research Conferences – Polar Marine Science: Contributing to the Understanding of Complex Polar Marine Systems*, Ventura, USA. Poster.
65. Jacquet S.H.M., S. Chifflet, **A.J. Cavagna**, **F. Dehairs**, L. Monin and D. Lannuzel, 2013. Distribution of dissolved and particulate barium in Antarctic sea ice. *ASLO Meeting*, New Orleans.
66. Jacquet S.H.M., **F. Dehairs**, **A.J. Cavagna**, F. Planchon, I. Closset and D. Cardinal, 2013. Seasonal variability of mesopelagic organic carbon remineralization in the naturally iron-fertilized Kerguelen area (Southern Ocean). *ASLO Meeting*, New Orleans.
67. Meiners K. M., **M. Vancoppenolle**, S. Thanassekos, G. S. Dieckmann, D. Thomas, **J.-L. Tison**, K. R. Arrigo, D. Garrison, A. McMinn, D. Lannuzel, P. van der Merwe, K. Swadling, W.O. Smith, I. Melnikov and B. Raymond, 2013. Chlorophyll a in Antarctic sea ice from historical ice core data. *45th Liege Colloquium on Ocean Dynamics*. Talk.
68. **Moreau S.**, **M. Vancoppenolle**, **J. Zhou**, **J.L. Tison**, **B. Delille** and **H. Goosse**, 2013. Modeling gas dynamics in first-year sea ice. *Gordon Research Conferences – Polar Marine Science: Contributing to the Understanding of Complex Polar Marine Systems*, Ventura, USA. Poster.

69. **Roukaerts A.**, 2013. Nutrient uptake and primary production in the east Antarctic sea ice zone (SIPEX II). *Gordon Research Conference*, USA.
70. **Roukaerts A.**, **A.-J. Cavagna** and **F. Dehairs**, 2013. Carbon and Nitrogen uptake rates in the East Antarctic sea-ice zone, (SIPEX II preliminary results). *45th International Liège Colloquium, Primary Production in the Ocean: From the Synoptic to the Global Scale*, Liège, Belgium.
71. **Schoemann V.**, 2013. Sea ice as a source of bioavavailable Fe to the Southern Ocean. *FNRS contact group "Geochemistry" workshop day*, Brussels, Belgium. Talk.
72. **Tison J.-L.**, **J. Zhou**, O. Crabeck and **B. Delille**, 2013. Oxygen dynamics in spring first year sea ice, Kapissilit, Greenland: implications for oxygen fluxes to the ocean and net primary production estimates. *Gordon Research Conferences – Polar Marine Science: Contributing to the Understanding of Complex Polar Marine Systems*, Ventura, USA. Poster.
73. **Vancoppenolle M.**, 2013. Linking Ecological Responses and Models from Contemporary Observations: introduction to the session. *Gordon Research Conference on Polar Marine Ecosystems*, Ventura, CA. Invited talk.
74. **Vancoppenolle M.**, L. Bopp, G. Madec, J. Dunne, T. Ilyina, P.R. Halloran and N. Steiner, 2013. Future arctic primary productivity from CMIP5 simulations: Uncertain outcome, but consistent mechanisms. *Chantier Arctique Francais*. Poster.
75. **Vancoppenolle M.**, L. Bopp, G. Madec, J. Dunne, T. Ilyina, P.R. Halloran and N. Steiner, 2013. Future arctic primary productivity from CMIP5 simulations: Uncertain outcome, but consistent mechanisms. *European Geosciences Union*, Vienna. Talk.
76. **Vancoppenolle M.**, L. Bopp, G. Madec, J. Dunne, T. Ilyina, P.R. Halloran and N. Steiner, 2013. Future arctic primary productivity from cmip5 simulations: Uncertain outcome, but consistent mechanisms. *45th Liege Colloquium on Ocean Dynamics*. Talk.

2014

77. **Carnat G.**, **J. Zhou**, T. Papakyriakou, **B. Delille**, T. Goossens, T. Haskell, **V. Schoemann** and **J-L Tison**, 2014. Biological and physical controls on DMS, P dynamics in ice-shelf-influenced fast ice. *International Symposium on Sea Ice in a Changing Environment, International Glaciological Society*, Hobart, Australia. Talk.
78. **Cavagna A.-J.**, K. Westwood, **A. Roukaerts**, D. Lannuzel, K. Meiners, **F. Fripiat** and **F. Dehairs**, 2014. Primary Production SIPEX 2 field tests: ^{14}C and ^{13}C-methods comparison. *International Symposium on Sea Ice in a Changing Environment*, Hobart Australia. Talk.
79. **Dehairs F.**, T. Trull, **A.-J. Cavagna**, F. Planchon and **F. Fripiat**, 2014. Nitrate isotopic composition in the Kerguelen area (Southern Ocean). *Ocean Sciences 2014*, Honolulu, Hawaii.
80. **Delille B.**, T. Haskell, W. Champenois, **B. Heinesch**, **J. Zhou**, **V. Schoemann**, **G. Carnat**, **F. Fripiat**, T. Goossens, **S. Moreau**, **M. Vancoppenolle**, F. Vivier, A. Lourenço and **J.-L. Tison**, 2014. Year-round

survey of Ocean-Sea Ice-Air Exchanges – the YROSIAE survey. *International Symposium on Sea Ice in a Changing Environment, International Glaciological Society*, Hobart, Australia. Poster.

81. **Fripiat F.**, D.M. Sigman and **J.-L. Tison**, 2014. Nitrogen biogeochemical dynamics in Antarctic pack ice as reflected in the nitrogen isotopes. *International Symposium on Sea Ice in a Changing Environment, International Glaciological Society*, Hobart, Australia. Poster.
82. **Goosse H.**, 2014. The influence of ice-ocean feedbacks on the variability and predictability of sea ice. *Advances in Climate Theory*, Brussels, Belgium. Invited talk.
83. **Goosse H.**, 2014. How can we improve the prediction of decadal trends in Antarctic sea ice extent? *International workshop on polar-lower latitude linkages and their role in weather and climate prediction*, Barcelona, Spain. Talk.
84. **Goosse H.**, V. Zunz and **S. Moreau**, 2014. Decadal trends in the Antarctic sea ice extent ultimately controled by ice-ocean feedback. *SCAR biennal conference*, Auckland, New Zealand. Poster.
85. Jacquet S.H.M., S. Chifflet, **A.J. Cavagna**, **F. Dehairs**, L. Monin and D. Lannuzel, 2014. Distribution of dissolved and particulate barium in Antarctic sea ice. *Ocean Sciences,* Honolulu, Hawaii. *International Symposium on Sea Ice in a Changing Environment, International Glaciological Society*, Hobart, Australia. Poster.
86. Janssens J., **B. Delille**, **J.-L. Tison**, D. Lannuzel, K.M. Meiners and G. Dieckmann, 2014. Investigating iron and organic matter incorporation in growing sea ice.
87. **Lemaitre N.**, F. Planchon, H. Planquette, A. Bowie, T. Trull and **F. Dehairs**, 2014. Biogenic silica (BSi) and trace elements (TE), Fe, Zn, Cu, Cd, Mn, Co, P, surface export fluxes near Kerguelen Island, Southern Ocean (KEOPS2). *Ocean Sciences 2014*, Honolulu, Hawaii.
88. Middleton C.A., C. Thomas, D.M. Escala, A. De Wit and **J.-L. Tison**, 2014. Experimental observations of the transport of brine and dissolved gases in sea ice. *European Geosciences Union, General Assembly 2014*, Vienna, Austria.
89. **Moreau S.**, **M. Vancoppenolle**, L. Bopp, **B. Delille**, **J.-L.Tison** and **H. Goosse**, 2014. The role of sea ice DIC and TA boundary conditions on the cycling of carbon in a global blue-white-green ocean modeling system. *SCAR biennal conference*, Auckland, New Zealand. Talk.
90. **Moreau S.**, **M. Vancoppenolle**, L. Bopp, **B. Delille**, **J.-L.Tison** and **H. Goosse**, 2014. The role of sea ice DIC and TA boundary conditions on the cycling of carbon in a global blue-white-green ocean modeling system. *Canadian Meteorological and Oceanography Society Congress in Rimouski*, Qc, Canada. Talk.
91. **Moreau S.**, **M. Vancoppenolle**, **J.-L.Tison**, **B. Delille** and **H. Goosse**, 2014. Modeling CO_2 dynamics in first-year sea ice. *International Symposium on Sea Ice in a changing environment*, Hobart, Tasmania, Australia. Poster.
92. Nomura D., **B. Delille**, G.S. Dieckmann, **J.-L. Tison**, K.M. Meiners, M.A. Granskog and T. Tamura, 2014. Sea ice CO2 flux in the Southern Ocean

during mid-winter and early spring. *International Symposium on Sea Ice in a Changing Environment, International Glaciological Society*, Hobart, Australia.

93. Nomura D., A. Ooki, G.S. Dieckmann, E. Damm, K.M. Meiners, **B. Delille**, **J.-L. Tison** and T. Tamura, 2014. Bromoforme emission over Antarctic Sea Ice. *International Symposium on Sea Ice in a Changing Environment, International Glaciological Society*, Hobart, Australia. Poster.

94. Planchon F., **D. Ballas**, **A.-J. Cavagna**, T. Trull and **F. Dehairs**, 2014. Fe fertilization and carbon export production: the natural laboratory of the Kerguelen Island, Southern Ocean. *Ocean Sciences* 2014, Honolulu, Hawaii.

95. **Roukaerts A.**, **A.-J. Cavagna**, **F. Dehairs**, **F. Fripiat**, D. Lannuzel and K. Meiners, 2014. Nutrient uptake rates and primary production in East Antarctic sea-ice (SIPEX II results). *International Symposium on Sea Ice in a Changing Environment*, Hobart, Australia.

96. Roukaerts A., **A.-J. Cavagna** and **F. Dehairs**, 2014. Nitrate isotopic signatures ($\delta^{15}N\text{-}NO_3$ and $\delta^{18}O\text{-}NO_3$) in East Antarctic sea-ice and the underlying water column (SIPEX II results). *International Symposium on Sea Ice in a Changing Environment*, Hobart, Australia.

97. Sapart C.J., **J. Zhou**, H. Niemann, T. Röckmann, **B. Delille**, C. van der Veen and **J.-L. Tison**, 2014. Using stable isotopes to unravel the role of sea-ice in the methane cycle. *International Symposium on Sea Ice in a Changing Environment, International Glaciological Society*, Hobart, Australia. Talk.

98. **Schoemann V.**, J.T.M. de Jong, **J.-L. Tison**, T. Haskell, H. de Baar, W. Champenois, **J. Zhou**, **G. Carnat**, **F. Fripiat**, T. Goossens and **B. Delille**, 2014. Land-fast sea ice as a source of bio-essential trace metals for primary productivity in the McMurdo Sound (Ross Sea, Antarctica). *International Symposium on Sea Ice in a Changing Environment, International Glaciological Society*, Hobart, Australia. Poster.

99. **Tison J.-L.**, **B. Delille**, G. Dieckmann, J. de Jong, J. Janssens, J. Rintala, A.M. Luhtanen, N. Gussone, C. Uhlig, D. Nomura, **V. Schoemann**, **J. Zhou**, **G. Carnat** and **F. Fripiat**, 2014. Snow Cover and Short-term Synoptic Events Drive Biogeochemical Dynamics in Winter Weddell Sea Pack Ice (AWECS cruise - June to August 2013). *International Symposium on Sea Ice in a Changing Environment, International Glaciological Society*, Hobart, Australia. Talk.

100. **Tison J.-L.**, 2014. Climate significant gases in sea ice: bridging the air-ocean interfaces. *Québec-Ocean Seminars*, Université Laval. Invited talk.

101. **Tison J.-L.**, **B. Delille**, G. Dieckmann, J. de Jong, J. Janssens, J. Rintala, A. Luhtanen, N. Gussone, C. Uhlig, D. Nomura, **V. Schoemann**, **J. Zhou**, **G. Carnat** and **F. Fripiat**, 2014. Snow cover and short-term synoptic events drive biogeochemical dynamics in winter Weddell Sea pack ice (AWECS cruise - June to August 2013). *European Geosciences Union, General Assembly 2014*, Vienna, Austria. Talk.

102. Uhlig C., **J.-L. Tison**, J. Rintala, **G. Carnat**, G. Dieckmann, **B. Delille** and E. Damm, 2014. Dimethyl sulfide and dimethylsulfoniopropionate profiles in sea ice during winter in the Weddell Sea. *International Symposium on Sea*

Ice in a Changing Environment, International Glaciological Society, Hobart, Australia. Poster.

103. **Vancoppenolle M.**, K. Meiners, **S. Moreau**, L. Bopp and G. Madec, 2014. Sea Ice and Biological Productivity of the Polar Oceans. *GIS-COOC symposium*, Wimereux, France. Invited talk.
104. **Zhou J.**, **B. Delille**, F. Brabant and **J.-L. Tison**, 2014. On the use of O_2/Ar and O_2/N_2 to estimate the biological carbon uptake in landfast sea ice. *International Symposium on Sea Ice in a Changing Environment, International Glaciological Society*, Hobart, Australia.
105. **Zhou J.**, **B. Delille**, **J.-L. Tison**, R. Autio, G. Dieckmann, K.U. Evers, L. Jorgenesen, H. Kaartokallio, G. Kattner, H. Kennedy, M. Kotovitch, H. Kuosa, A.-M. Luhtanen, C.A. Stedmon and D.N. Thomas, 2014. Factors driving pCO_2 dynamics in sea ice during a large-scale ice tank experiment. *International Symposium on Sea Ice in a Changing Environment, International Glaciological Society*, Hobart, Australia.

2015

106. Crabeck O., R. Galley, B. Else, N.-X. Geilfus, K. Campbell, W. Boone, **J.-L. Tison**, **B. Delille** and S. Rysgaard, 2015. Imaging air filled porosity in sea ice cover: Implication for sea ice permeability and gas exchange at the ice-atmosphere interface. *Gordon Research Conference on Polar Marine Science*, Lucca, Italy.
107. **Delille B.**, M. Kotovitch, F. Van Der Linden, D. Nomura, W. Champenois, B. Heinesch, N-X Geilfus, **J. Zhou** and **J.-L. Tison**, 2015. How snow affects air-sea ice CO2 fluxes? *Gordon Research Conference on Polar Marine Science*, Lucca, Italy.
108. **Fripiat F.**, **M. Elskens**, T.W. Trull, S. Blain, **A.-J. Cavagna**, C. Fernandez, **D. Fonseca-Batista**, F. Planchon, **A. Roukaerts** and **F. Dehairs**, 2015. Significant mixed layer nitrification in a natural iron-fertilized bloom of the Southern Ocean. *Gordon Research Conference on Polar Marine Science*, Lucca, Italy.
109. **Goosse H.**, 2015. Towards a coupled re-analysis in the Southern Ocean covering the last centuries. *Workshop on Large-scale climate variability in Antarctica and the Southern Ocean over decades to centuries, and links to extra-polar climate,* La Jolla, California, USA. Talk.
110. **Goosse H.**, 2015. Estimating and understanding trends in Antarctic sea ice extent using data assimilation. *TITAN project meeting*, Edinburg (Great Britain). Talk.
111. Kotovitch M., **S.Moreau**, **J. Zhou**, **J.-L. Tison**, F. Van Der Linden, K.-U. Evers, D. Thomas and **B.Delille**, 2015. Measurements of air-ice CO_2 fluxes over artificial sea ice emphasize the role of bubbles in gas transport. *Gordon Research Conference on Polar Marine Science*, Lucca, Italy.
112. Luhtanen A.-M., D. Bamford, J. de Jong, G. Dieckmann, **B. Delille**, H. Oksanen, **J.-L. Tison** and J.-M. Rintala, 2015. Isolation of cultivable viruses from Antarctic wintertime sea ice. *Gordon Research Conference on Polar Marine Science*, Lucca, Italy.

113. Middleton C.A., C. Thomas, D.M. Escala, **J.-L. Tison** and A. de Wit, 2015. Imaging the evolution of brine transport in experimentally grown quasi-two-dimensional sea ice. *Procedia IUTAM*, 15, 95-100.
114. **Moreau S.**, **M. Vancoppenolle**, **B. Delille**, M. Kotovitch, **J.-L. Tison** and **H. Goosse**, 2015. The role of sea ice in the carbon cycle of Polar Seas: 1D to 3D modeling. *SOLAS conference*, Kiel, Germany. Poster.
115. **Moreau S., M. Vancoppenolle**, **B. Delille**, **J.-L. Tison**, M. Kotovitch and **H. Goosse**, 2015. The role of sea ice in the carbon cycle of Polar Seas: 1D to 3D modeling. *Goldschmidt Conference*, Prague, Czech Republic. Talk.
116. **Moreau S.**, **M. Vancoppenolle**, **B. Delille**, **J.-L. Tison**, **J. Zhou**, M. Kotovitch, D. Thomas, N.-X. Geilfus and **H. Goosse**, 2015. The role of sea ice in the carbon cycle of Polar Seas: 1D to 3D modelling. *International Liège Colloquium on Marine Environmental Monitoring, Modelling and Prediction*, Liège, Belgium. Poster.
117. **Moreau S.**, **M. Vancoppenolle**, **B. Delille**, **J.-L. Tison**, **J. Zhou**, M. Kotovitch, D. Thomas, N.-X. Geilfus and **H. Goosse**, 2015. Drivers of inorganic carbon dynamics in first-year sea ice: A model study. *European Geosciences Union (EGU) conference*, Vienna, April. Talk.
118. Nomura D., **B. Delille**, G.S. Dieckmann, M.A. Granskog, **J.-L. Tison**, K.M. Meiners, A. Fransson, K.I. Oshima and T. Tamura, 2015. Mid-winter survey of sea ice biogeochemistry in polar oceans. *Goldschmidt Conference*, Prague, Czech Republic. Talk.
119. Rintala J.-M., A.-M. Luhtanen, S. Enberg, R. Autio, J. Blomster, J. de Jong, J. Jannsens, N. Gussone, C. Uhlig, D. Nomura, **B. Delille**, **J.-.L Tison** and G. Dieckmann, 2015. Photosynthesis-irradiance response curves revealed active sympagic communities in the Weddell Sea Winter, 2013. *Gordon Research Conference on Polar Marine Science*, Lucca, Italy.
120. **Roukaerts A.**, **J. Zhou**, **F. Fripiat**, **J.-L. Tison** and **F. Dehairs**, 2015. Missing carbon source or methodological bias? *Goldschmidt Conference*, Prague, Czech Republic. Talk.
121. Sanial V., P. Van Beek, B. Lansard, M. Souhaut, E. Kestenare, **F. Dehairs**, S. Jacquet, F. d'Ovidio, M. Zhou and S. Blain, 2015. What have we learned from Ra isotopes about the natural iron fertilization offshore from the Crozet and Kerguelen islands? *Goldschmidt Conference*, Prague, Czech Republic. Talk.
122. **Tison J.-L.**, 2015. The cryosphere between the cracks, does it matter? *Gordon Research Conference on Polar Marine Science*, Lucca, Italy. Invited talk.
123. Uhlig C., **J.-L. Tison**, J.-M. Rintala, J. Blomster, **G. Carnat**, G. Dieckmann, A.-.M. Luthanen, **B. Delille** and E. Damm, 2015. Blue sky and green bugs–How physical parameters and algal speciation influence DMSP and DMS profiles in Antarctic winter sea ice. *Gordon Research Conference on Polar Marine Science*, Lucca, Italy.
124. **Vancoppenolle M.**, **S. Moreau**, L. Bopp, G. Madec, **B. Delille**, **J.-L. Tison** and D. Lannuzel, 2015. Sea ice marine biogeochemical cycles : Large-

scale processes. *Goldschmidt Conference*, Prague, Czech Republic. Invited talk.

125. **Vancoppenolle M.**, 2015. Sea ice and the carbon cycle. *Conference on the Mathematics of sea ice*, Vancouver, BC, Canada. Invited talk.

2016

126. **Carnat G.**, W. Said-Ahmad, **F. Fripiat**, **J.-L. Tison** and A. Amrani, 2016. Sulfur isotope variability of DMS,P production by Antarctic sea ice microbial communities. *Goldschmidt Conference*, Yokohama, Japan. Talk.

127. **Carnat G.**, W. Said-Ahmad, **F. Fripiat**, **J.-L. Tison** and A. Amrani, 2016. Sulfur isotope variability of DMS,P production by Antarctic sea ice microbial communities. *AGU Fall meeting*, San Francisco, USA. Invited talk.

128. **Delille B.**, 2016. Highly productive, yet heterotrophic, and still pumping CO2 from the atmosphere: A land fast ice paradigm? *International Symposium on Polar Environmental Change and Public Governance*, Wuhan, China. Talk.

129. **Deman F.,** 2016. A time series study during spring transition in the fast ice at Davis station, Antarctica: preliminary results, *International Symposium on Polar Environmental Change and Public Governance*, Wuhan, China. Talk.

130. **Kotovitch M.,** 2016. Sea ice - Source or sink for nitrous oxide, *International Symposium on Polar Environmental Change and Public Governance,* Wuhan, China. Talk.

7.3. MASTER AND PHD THESES

PhD Theses:

Finalized

- **Cavagna, Anne-Julie:** (2011)
  The biological pump in the Southern Ocean: three case studies, three stable isotope tools, Vrije Universiteit Brussel
- **Brabant, Frédéric**: (2012)
  Physical and biogeochemical controls on the DMS,P,O cycle in sea ice, Université Libre de Bruxelles
- **Zhou, Jiayun**: (2014)
  The physical and biological controls on the distribution of gases and solutes in sea ice from ice growth to ice decay, Université Libre de Bruxelles
- **Carnat, Gauthier**: (2014)
  Towards an understanding of the physical and biological controls on the cycling of dimethylsulfide (DMS) in Arctic and Antarctic sea ice, Université Libre de Bruxelles
- **Lemaitre Nolwenn:** (2016)
  Multi-proxy approach (^{234}Th, Ba_{xs}) of export and remineralization fluxes of carbon and biogenic elements associated with the oceanic biological pump, Vrije Universiteit Brussel and Université de Bretagne Occidentale

Ongoing

- **Wittek, Boris**: (2016-)
  Influence of seasonal environmental stresses in sea ice on the production and emission of dimethylsulfide by microbial communities, Université Libre de Bruxelles
- **Jacques, Caroline**: (2016-)
  Using isotopes to understand the role of sea ice in the biogeochemical cycles of the main greenhouse gases, Université Libre de Bruxelles
- **Roukaerts, Arnout: (**submission by the end of 2016)
  Primary production and nutrient cycling in Antarctic sea-ice and open waters, Vrije Universiteit Brussel.
- **Florian, Deman**: (2016-)
  Study of the N-cycle in the Antarctic sea ice: Significance of N2O production and relative role of nitrification-denitrification, co-tutelle Vrije universiteit Brussel – Université de Liège

Master Thesis (ULB):

Finalized

- **Gilson, Gaëlle**: (2010)
  Composition en DMS et composes soufrés associés de la glace de mer annuelle arctique en Mer de Beaufort (CFL, Canada) et implication pour les flux de DMS vers l'atmosphère
- **Willame, Alan** : (2010)
  Premières mesures à haute résolution de la concentration en dioxyde de carbone dans la glace de mer : un exemple arctique, la mission Barrow (Janvier-Juin 2009) – implications pour les flux de CO_2 en régions polaires
- **Zhou, Jiayun** : (2010)
  Evolution des propriétés biogéochimiques des glaces de mer annuelles côtières (Barrow, Alaska) : implications pour la productivité primaire et les flux de gaz à effet climatique
- **Crabeck, Odile** : (2011)
  Etudes des processus physico-chimiques affectant la teneur et la composition des glaces de mer de Gothabsfjord (Nuuk, Groenland) et relations avec les flux de CO_2 à l'interface glace-air
- **Deleu, France :** (2011)
  Etudes des propriétés physico-chimiques des glaces de mer artificielles de l'expérience européenne INTERICE IV et relations entre concentrations en CO_2 dans la glace et flux glace-air de CO_2
- **De Potter, Kristell :** (2012)
  Etude des compositions en dioxyde de carbone dans la glace de banquise antarctique de la mer de Bellingshausen : implications pour les puits et les sources atmosphériques et océaniques
- **Herzet, Sophie** : (2012)

Etude des compositions en O_2, N_2, Ar, CH_4, dans les glaces de banquise Antarctique de la mer de Bellingshausen (Mission Simba 2007) : implications pour la productivité primaire nette

- **Courtois, Cindy :** (2013)
  Etude de l'influence des mécanismes de formation de la banquise côtière de la plate-forme de glace Roi Baudouin sur la production de gaz biogénique à effet climatique
- **Driane, Vanessa :** (2014)
  Etude de l'évolution temporelle de la chl *a*, O_2, Ar, N_2 dans la glace de mer à Cape Evans (Ross Island Antarctica) : implications sur la production primaire nette
- **Rottier, Arnaud :** (2014)
  Etude de la production de gaz à effets climatiques antagonistes (DMS, CH_4) par la banquise arctique via la dégradation de DMSP
- **De Pierpont, Gaëlle** : (2016)
  Compréhension et quantification de certains processus de désalinisation : étude expérimentale des rejets de la saumure lors de la formation de la glace de mer
- **Declercq, Maxime** : (2016)
  Nitrogen cycle inferred from N and O isotopes in a changing Arctic Ocean
- **Estievenart, Barbara:** (2016)
  Dynamique du CO_2 dans la glace de mer hivernale en Mer de Weddell (Antarctique)
- **Françoise, Damien :** (2016)
  Profils et flux d'oxyde nitreux N_2O dans la glace de mer hivernale en mer de Weddell

Ongoing

- **Lemmers, Benoît :** (2016-)
  Le rôle du couvert de glace sur le cycle du méthane
- **Diricq, Malcolm :** (2016-)
  Production de composés soufrés dans la glace de mer par des algues de l'Antarctique en réponse à des variations de stress environnementaux dans les saumures : le cas *Fragilariopsis cylindrus*
- **Oppitz, Gwenaël :** (2016-)
  Production de composés soufrés dans la glace de mer par des algues de l'Antarctique en réponse à des variations de stress environnementaux dans les saumures : le cas Phaeocystis antarctica

Master Thesis (VUB)

- **Ballas Dyonisis :** (2012)
  Carbon export flux by the biological pump in the Kerguelen Island area (KEOPS 2).
- **Laurila, Mirka:** (2013)
  Understanding the differential behavior of barium and silicic acid in the Southern Ocean.

8. ACKNOWLEDGEMENTS

We are grateful to the following Antarctic administrations which provided access to research vessels, ice stations and logistic support:

- Australian Antarctic Division, Kingston, Tasmania
- Institut Polaire Français, Paul Emile Victor, Plouzané, France
- Alfred Wegener Institute, Bremerhaven, Germany
- Antarctica New Zealand, Christchurch, New Zealand

9. REFERENCES

-Aminot A., and R. Kérouel, 2007. Dosage automatique des nutriments dans les eaux marines: méthodes en flux continu. Ed. Ifremer, 2007.

-Amrani A., W. Said-Ahmad, Y. Shaked and R.P. Kiene, 2013. Sulfur isotope homogeneity of oceanic DMSP and DMS. *PNAS*, doi: 10.1073/pnas.1312956110.

-Arar E. and G. B. Collins, 1997. Method 445.0 In vitro determination of Chlorophyll a and Pheophytin a in marine and freshwater algae by fluorescence. *Rep.*, 22 pp, U.S. Environmental Protection Agency Washington D.C.

-Archambeau A.-S., C. Pierre, A. Poisson and B. Schauer, 1998. Distributions of oxygen and carbon stable isotopes and CFC-12 in the water masses of the Southern Ocean at 30°E from South Africa to Antarctica: results of the CIVA1 cruise. *J. Mar. Syst.*, 17, 25-38.

-Arrigo K.R., 2005. Marine microorganisms and global nutrient cycles. *Nature* 437, 349–355. http://dx.doi.org/10.1038/nature04159.

-Arrigo K. R., D. N. Dieckmann, M. Gosselin, D. H. Robinson, C. H. Fritsen and C. W. Sullivan, 1995. High resolution study of the platelet ice ecosystem in McMurdo Sound, Antarctica: biomass, nutrient, and production profiles within a dense bloom. *Marine Ecology Progress Series*, *127*, 255-268.

-Arrigo K.R., D.H. Robinson, R.B. Dunbar, A.R. Laventer and M.P. Lizotte, 2003. Physical control of chlorophyll a, POC, and TPN distributions in the pack ice of the Ross Sea, Antarctica. *Journal of Geophysical Research*, 108.

-Arrigo K. R., D. L. Worthen, M. P. Lizotte, P. Dixon and D. N. Dieckmann, 1997. Primary production in Antarctic sea ice. *Science*, *276*(5311), 394-397, doi:10.1126/science.276.5311.394.

-Atkinson A., V. Siegel, E.A. Pakhomov, P. Rothery, V. Loeb, R.M. Ross, L.B. Quetin, K. Schmidt, P. Fretwell, E.J. Murphy, G.A. Tarling and A.H. Fleming, 2008. Oceanic circumpolar habitats of Antarctic krill. *Mar. Ecol. Prog. Ser.* 362: 1–23.

-Assur A., 1958. Composition of sea ice and its tensile strength. *Arct. Sea Ice*, 106-138.

-Bau M., P. Möller and P. Dulski, 1997. Yttrium and lanthanides in eastern Mediterranean seawater and their fractionation during redox-cycling. *Marine Chemistry*, 56: 123-131.

-Becquevort S. I. Dumont, J.-L. Tison, D. Lannuzel, M.L. Sauvée, L. Chou and V. Schoemann, 2009. Biogeochemistry and microbial community composition in sea ice and underlying seawater off East Antarctica during early spring. *Polar Biology*, 32:879-895.

-Berliand M. E. and T. G. Strokina, 1980. Global distribution of the total amount of clouds. *Rep.*, 71 pp, Leningrad, Russia.

-Bianchi M., F. Feliatra, P. Tréguer, M.-A. Vincedeau and J. Morvan, 1997. Nitrification rates, ammonium and nitrate distribution in upper layers of the water column and in sediments of the Indian sector of the Southern Ocean. *Deep-Sea Research Part II*, 44, 1017-1032.

-Biller D. and K.W. Bruland, 2012. Analysis of Mn, Fe, Co, Ni, Cu, Zn, Cd, and Pb in seawater using the Nobias-chelate PA1 resin and magnetic sector inductively coupled plasma mass spectrometry (ICP-MS). *Mar. Chem.,* 130-131, 12–20.

-Böhlke J., S. Mroczkowski and T.B. Coplen, 2003. Oxygen isotopes in nitrate: New reference materials for ^{18}O:^{17}O:^{16}O measurements and observations on nitrate-water equilibrations. *Rapid Comm. Mass Sp.*, 17, 1835-1846.

-Bowling D.R. and W.J.Massman, 2011. Persistent wind-induced enhancement of diffusive CO_2 transport in a mountain forest snowpack. *J. Geophys. Res.*, 116(G4), G04006.

-Bronk D.A., P.M. Glibert and B.B. Ward, 1994. Nitrogen uptake, dissolved organic nitrogen release, and new production. *Science*, 265, 1843-1846.

-Buchwald C. and K.L. Casciotti, 2010. Oxygen isotopic fractionation and exchange during bacterial nitrite oxidation. *Limnol. Oceanogr.*, 55, 1064-1074.

-Byrne R.H and E.R. Sholkovitz, 1996. Marine chemistry and geochemistry of the lanthanides. In: Handbook on the physics and chemistry of rare earths Vol. 23 (Gschneidner KG and Eyring L, eds.). Elsevier North Holland, pp497-593.

-Cardinal D., F. Dehairs, T. Cattaldo and L. André, 2001. Constraints on export and advection in the Subantarctic and Polar Front Zones, south of Australia from the geochemistry of suspended particles. *J. Geophys. Res. - Oceans,* 106, 31,637.

-Carnat G., J. Zhou, T. Papakyriakou, B. Delille, T. Goossens, T. Haskell, V. Schoemann, F. Fripiat, J.M. Rintala and J.-L. Tison, 2014. Physical and biological controls on DMS-P dynamics in ice shelf-influenced fast ice during a winter-spring and a spring-summer transitions. *Journal of Geophysical Research – Oceans*, 119, 2882-2905.

-Carnat G., F. Brabant, I. Dumont, M. Vancoppenolle, S. F. Ackley, C. Fritsen, B. Delille and J. L. Tison, 2016. Influence of short-term synoptic events and snow depth on DMS, DMSP, and DMSO dynamics in Antarctic spring sea ice. *ELEMENTA: Science of the Anthropocene*, *4*(000135), doi:10.12952/journal.elementa.000135.

-Casciotti K.L., D.M. Sigman, M.G. Hastings, J.K. Böhlke and A. Hilkert, 2002. Measurement of the oxygen isotopic composition of nitrate in seawater and freshwater using the denitrifier method. *Anal. Chem.*, 74, 4905-4912.

-Cavagna A.J., F. Fripiat, M. Elskens, P. Mangion, L. Chirurgien, I. Closset, M. Lasbleiz, L. Flores–Leiva, D. Cardinal, K. Leblanc, C. Fernandez, D. Lefèvre, L. Oriol, S. Blain, B. Quéguiner and F. Dehairs, 2015. Biological productivity regime and associated N cycling in the vicinity of Kerguelen Island area, Southern Ocean, *Biogeosciences,* 12, 6515-6528.

-Church M.J., E.F. DeLong, H.W. Ducklow, M.B. Karner, C.M. Preston and D.M. Karl, 2003. Abundance and distribution of planktonic Archaea and Bacteria in the waters west of the Antarctic Peninsula. *Limnol. Oceanogr.*, 48, 1893-1902.

-Closset I., M. Lasbleiz, K. Leblanc, B. Quéguiner, A.-J. Cavagna, M. Elskens, J. Navez and D. Cardinal, 2014. Seasonal evolution of net and regenerated silica production around a natural Fe-fertilized area in the Southern Ocean estimated from Si isotopic approaches. Biogeosciences, 11, 5827-5846.

-Cochlan W.P. and D.A. Bronk, 2001. Nitrogen uptake kinetics in the Ross Sea, Antarctica. *Deep Res. II-Top. Stud. Oceanogr.*, 48, 4127–4153. http://dx.doi.org/10.1016/S0967-0645(01)00083-2.

-Comeau A. M., W. K. W. Li, J.-E. Tremblay, E. C. Carmack and C. Lovejoy, 2011. Arctic Ocean microbial community structure before and after the 2007 record sea ice minimum. *PLoS One*, *6*(11), e27492.

-Conway H.L., P.J. Harrison and C.O. Davis, 1976. Marine diatoms grown in chemostats under silicate or ammonium limitation. II. Transient response of Skeletonema costatum to a single addition of the limiting nutrient. *Mar. Biol.*, 35, 187–199. http://dx.doi.org/10.1007/BF00390940.

-Cozzi S., 2008. High-resolution trends of nutrients, DOM and nitrogen uptake in the annual sea ice at Terra Nova Bay, Ross Sea.

-Cox G. F. N. and W. F. Weeks, 1983. Equations for determining the gas and brine volumes in sea-ice samples. *J. Glaciol.*, *29*(102), 306-316.

-Dai A. and K. E. Trenberth, 2002. Estimates of freshwater discharge from continents: Latitudinal and seasonal variations. *Journal of Hydrometeorology*, *3*, 660-686.

-Damm E., E. Helmke, S. Thoms, U. Schauer, E. Nöthig, K. Bakker and R. P. Kiene, 2010. Methane production in aerobic oligotrophic surface water in the central Arctic Ocean. *Biogeosciences*, *7*(3), 1099-1108.

-De Jong J.T.M., V. Schoemann, N. Maricq, N. Mattielli, P. Langhorne, T. Haskell and J.-L. Tison, 2013. Iron in land-fast sea ice of McMurdo Sound derived from sediment resuspension and wind-blown dust contributes to primary productivity in the Ross Sea, Antarctica. *Mar. Chem.*, 157, 24-40.

-Delille B. 2006. Inorganic carbon dynamics and air-ice-sea CO_2 fluxes in the open and coastal waters of the Southern Ocean, Université de Liège.

-Dieckmann G. S., M. Spindler, M.A. Lange, S.F. Ackley and H. Eicken, 1991. Antarctic sea ice: a habitat for the foraminifer *Neogloboquadrina pachyderma. J. of Foraminiferal Res.*, 21, 182-189.

-DiFiore P.J., D.M. Sigman and R.B. Dunbar, 2009. Upper ocean nitrogen fluxes in the Polar Antarctic Zone: constraints from the nitrogen and oxygen isotopes of nitrate. *Geochem., Geophys. Geosyst.*, 10, doi:10.1029/2009GC002468.

-DiFiore P.J., D.M. Sigman, T.W. Trull, M.J. Lourey, K. Karsh, G. Cane and R. Ho, 2006. Nitrogen isotope constraints on subantarctic biogeochemistry. *J. Geophys. Res.*, 111, C08016, doi:10.1029/2005JC003216.

-Dugdale R.C. and J.J. Goering, 1967. Uptake of new and regenerated forms of nitrogen in primary productivity. *Limnology and Oceanography*, 196-205.

-Dymond J.R., E. Suess and M. Lyle, 1992. Barium in deep-sea sediment: a geochemical proxy for paleoproductivity. *Paleoceanography*, 7, 163–181.

-Edgar R. C., B. J. Haas, J. C. Clemente, C. Quince and R. Knight, 2011. UCHIME improves sensitivity and speed of chimera detection. *Bioinformatics*, *27*(16), 2194-2200, doi:10.1093/bioinformatics/btr381.

-Eicken H., 1998. Deriving modes and rates of ice growth in the Weddell Sea from microstructural, salinity and stable-isotope data. *Antarctic sea ice: physical processes, interactions and variability*, 74, 89-122.

-Eicken H., T. C. Grenfell, D. K. Perovich, J. A. Richter-Menge and K. Frey, 2004. Hydraulic controls of summer Arctic pack ice albedo. *Journal of Geophysical Research*, 109(C08007), doi:10.1029/2003JC001989.

-Eicken H., M. A. Lange and D. N. Dieckmann, 1991. Spatial variability of sea-ice properties in the Northwestern Weddell Sea. *Journal of Geophysical Research*, *96*(C6), 10603-10615.

-Elskens M., W. Baeyens, N.N. Brion, S. De Galan, L. Goeyens and A. de Brauwere, 2005. Reliability of N flux rates estimated from ^{15}N enrichment and dilution experiments in aquatic systems. *Global Biogeochemical Cycles*, 19, GB4028, doi:10.1029/2004GB002332.

-Eppley R .W. and B.J. Peterson, 1979. Particulate organic matter flux and planktonic new production in the deep ocean. *Nature*, 282, 677-680.

-Flores H., A. Atkinson, et al., 2012. Impact of climate change on Antarctic krill. *Mar. Ecol. Prog. Ser.*, 458, 1–19. http://dx.doi.org/10.3354/meps09831.

-Fofonoff N. P., 1985. Physical properties of seawater: A new salinity scale and equation of state for seawater. *Journal of Geophysical Research*, *90*(C2), 3332-3342.

-Fogel M.L. and L.A. Cifuentes, 1993. Isotope fractionation during primary production. In: Organic Geochemistry, edited by Engel, M.H., and Macko, S.A, Plenum Press, N.Y., 73-98.

-Freitag J., 1999. Untersuchungen zur Hydrologie des arktischen Meereises-Konsequenzen für den kleinskaligen Stofftransport. *Ber. Polarforsch./Rep. Pol. Res.*, *325*.

-Fripiat F., M. Elskens, T. Trull, S. Blain, A.-J. Cavagna, C. Fernandez, D. Fonseca-Batista, F. Planchon, P. Raimbault, A. Roukaerts, and F. Dehairs, 2015. Significant mixed layer nitrification in a natural iron-fertilized bloom of the Southern Ocean, *Global Biogeochemical Cycles,* 29, 1929-1943

-Fuhrman J.A. and F. Azam, 1980. Bacterioplankton secondary production estimates for coastal waters of British Columbia, Antarctica, and California. *Appl. Environ. Microbiol*. 39:1085–1095.

-Fuhrman J.A. and F. Azam, 1982. Thymidine incorporation as a measure of heterotrophic bacterioplankton production in marine surface waters: Evaluation and field results. *Mar*. *Biol*., 66:109–120.

-Fukamachi Y., S.R. Rintoul, J.A. Church, S. Aoki, S. Sokolov, M.A. Rosenberg and M. Wakatsuchi, 2010. Strong export of Antarctic bottom water east of the Kerguelen Plateau. *Nat. Geosci.*, 3, 327–331.

-Garrison D. L., S. F. Ackley and K. R. Buck, 1983. A physical mechanism for establishing algal population in frazil ice. *Nature*, *306*, 363-365.

-Garrison D. L. and K. R. Buck, 1986. Organism losses during ice melting: A serious bias in sea ice commulity studies. *Polar Biology*, *6*(4), 237-239.

-Geilfus N.-X., B. Delille, V. Verbeke and J.-L. Tison, 2012. Towards a method for high vertical resolution measurements of the partial pressure of CO_2 within bulk sea ice. *J. Glaciol*, 58(208), 287-300.

-Geilfus N.-X., G. Carnat, G.S. Dieckmann, N. Halden, G. Nehrke, T. Papakyriakou, J.-L. Tison and B. Delille, 2013. First estimates of the contribution of $CaCO_3$ precipitation to the release of CO_2 to the atmosphere during young sea ice growth. *Journal of Geophysical Research – Oceans*, 118 (1-12).

-Gille S. T., M.M. Carranza, R. Cambra and R. Morrow, 2014. Wind-induced upwelling in the Kerguelen Plateau Region. *Biogeosciences Discuss.*, 11, 8373–8397, doi:10.5194/bgd-11-8373-2014.

-Golden K. M., 2003. Critical behavior of transport in sea ice. *Physica B: Condensed Matter*, *338*(1–4), 274-283.

-Golden K. M., S. F. Ackley and V. Lytle, 1998. The Percolation Phase Transition in Sea Ice. *Science*, *282*, 2238-2240.

-Goyet C. and A. Poisson, 1989. New determination of carbonic acid dissociation constants in seawater as a function of temperature and salinity. *Deep Sea Research*, 36: 1635-1654.

-Gradinger R. R. and J. Ikävalko, 1998. Organism incorporation into newly forming Arctic sea ice in the Greenland Sea. *Journal of Phytoplancton Research*, *20*(5), 871-886.

-Granger J., D.M. Sigman, J.A. Needoba and P.J. Harrison, 2004. Coupled nitrogen and oxygen isotope fractionation of nitrate during assimilation by cultures of marine phytoplankton. *Limnol. Oceanogr.*, 49, 1763–1773.

-Guglielmo L., G.C. Carrada, G. Catalano, A. Dell'Anno, M. Fabiano, L. Lazzara, O. Mangoni, A. Pusceddu and V. Saggiomo, 2000. Structural and functional properties of sympagic communities in the annual sea ice at Terra Nova Bay (Ross Sea, Antarctica). *Polar Biol.*, 23, 137–146. http://dx.doi.org/10.1007/s003000050019.

-Harrison W.G., G.F. Cota and R.E.H. Smith, 1990. Nitrogen-utilization in ice algal communities of Barrow Strait, Northwest-Territories, Canada. *Mar. Ecol. Prog.Ser.*, 67, 275–283.

-Hathorne E.C., T. Stichel, B. Brück and M. Frank, 2015. Rare earth element distribution in the Atlantic sector of the Southern Ocean: The balance between particle scavenging and vertical supply. *Mar. Chem.*, 177, 157–171.

-Henley W.J., 1993. Measurement and interpretation of photosynthetic and dial changes. *J. Phycol.*, 29:729-739.

-Hoch M. P., M.L. Fogel and D.L. Kirchman, 1992. Isotope fractionation associated with ammonium uptake by a marine bacterium. *Limnol. Oceanogr.*, 37, 1447–1459.

-Holmes R.H., A. Aminot, R. Kérouel, B.A. Hooker and B.J. Peterson, 1999. A simple and precise method for measuring ammonium in marine and freshwater ecosystems. *Canadian Fisheries and Aquatic Sciences*, 56(10), 1801-1808.

-Hugerth L. W., E. E. Muller, Y. O. Hu, L. A. Lebrun, H. Roume, D. Lundin, P. Wilmes and A. F. Andersson, 2014. Systematic design of 18S rRNA gene primers for determining eukaryotic diversity in microbial consortia. *PLoS One*, *9*(4), e95567.

-Hunke E. C., D. Notz, A. K. Turner and M. Vancoppenolle, 2011. The multiphase physics of sea ice: a review for model developers. *The Cryosphere*, *5*(4), 989-1009, doi:10.5194/tc-5-989-2011.

-Hunt B.G., H.B. Gordon and H.L. Davies, 1995. Impact of the greenhouse effect on sea ice characteristics and snow accumulation in the polar regions. *Int. J. Climatol.*, 15, 3–23.

-Jacquet S. H. M., F. Dehairs, D. Lefèvre, A.-J. Cavagna, F. Planchon, U. Christaki, L. Monin, L. André, I. Closset and D. Cardinal, 2015. Early season mesopelagic carbon remineralization and transfer efficiency in the naturally iron-fertilized Kerguelen area. *Biogeosciences,* 12, 1713-1731.

-Jeffries M. O., R. A. Shaw, K. Morris, A. L. Veazey and H. R. Krouse, 1994. Crystal structure, stable isotopes (d18O) and development of sea ice in the Ross, Amundsen and Bellingshausen Seas, Antarctica. *Journal of Geophysical Research*, *99*(C1), 985-995.

-Jeffries M. O., A. P. Worby, K. Morris and W. F. Weeks, 1997. Seasonal variations in the properties and structural composition of sea ice and snow cover in the Bellingshausen and Amundsen Seas, Antarctica. *Journal of Glaciology*, *43*(143), 138-151.

-Jouzel J. and R. Souchez, 1982. Melting-refreezing at the glacier sole and the isotopic composition of the ice. *J. Glaciol.*, *28*(98), 35-42.

-Kalnay E., et al., 1996. The NCEP/NCAR 40-Year Reanalysis Project. *Bulletin of the American Meteorological Society*, *77*(3), 437-471.

-Karl D. M., L. Beversdorf, K. M. Bjorkman, M. J. Church, A. Martinez and E. F. DeLong, 2008. Aerobic production of methane in the sea. *Nat. Geosci*., *1*(7), 473-478.

-Kendall C., 1998. Tracing nitrogen sources and cycling in catchments. In: Isotope Tracers in Catchment Hydrology, edited by: Kendall, C., and McDonnell, J. J., Elsevier, 519–576.

-Kiene R. P. and L. J. Linn, 2000. Distribution and turnover of dissolved DMSP and its relationship with bacterial production and dimethylsulfide in the Gulf of Mexico. *Limnology and Oceanography*, *45*, (4), 849–861, 2000.

-Klunder M.B., P. Laan, R. Middag, H.J.W. De Baar and J. Van Ooijen, 2011. Dissolved iron in the Southern Ocean (Atlantic sector). *Deep-Sea Res II*, 58, 2678–2694.

-Kottmeier S.T. and C.W. Sullivan, 1987. Late winter primary production and bacterial production in sea ice and seawater west of the Antarctic Peninsula. *Mar. Ecol.Prog. Ser.*, 36, 287–298.

-Kottmeier S.T and C.W. Sullivan, 1988. Sea-ice microbial communities 9. Effects of temperature and salinity on rates of metabolism and growth of autotrophs and heterotrophs. *Polar Biol.,* 8:293-304.

-Kottmeier S. T., S. M. Grossi and C. W. Sullivan, 1987. Sea ice microbial communities (SIMCO).VIII. Bacterial production in the annual sea ice of Mc Murdo Sound, Antarctica. *Mar. Ecol. Prog. Ser.*, *35*, 175-186.

-Kozich J. J., S. L. Westcott, N. T. Baxter, S. K. Highlander and P. D. Schloss, 2013. Development of a Dual-Index Sequencing Strategy and Curation Pipeline for Analyzing Amplicon Sequence Data on the MiSeq Illumina Sequencing Platform. *Appl. Environ. Microbiol.*, *79*(17), 5112-5120, doi:10.1128/aem.01043-13.

-Kristiansen S., T. Farbrot, H. Kuosa, S. Myklestad and C.H.V. Quillfeldt, 1998. Nitrogen uptake in the infiltration community, an ice algal community in Antarctic pack ice. *Polar Biol.*, 19, 307–315.

-Kristiansen S., E.E. Syvertsen and T. Farbrot, 1992. Nitrogen uptake in the Weddell Sea during late winter and spring. *Polar Biology*, 12, 245-251.

-Kyle P.R.and P.C. Rankin, 1976. Rare earth element geochemistry of Late Cenozoic alkaline lavas of the McMurdo Volcanic Group, Antarctica. *Geochim. Cosmochim. Acta*, 40, 1497-1507.

-Lange M. A., 1988. Basic properties of Antarctic sea ice as revealed by textural analysis of ice cores. *Ann. Glaciol.*, *10*, 95-101.

-Lange M. A., 1990. Development and physical properties of sea ice in the Weddell Sea, Antarctica. In Sea Ice Properties and Processes, *Monograph Rep. 90-1*, 22-40 pp, CRRELL.

-Lange M. A., S. F. Ackley, P. Wadhams, G. S. Dieckmann and H. Eicken, 1989 Development of sea ice in the Weddell Sea, Antarctica. *Ann. Glaciol.*, *12*, 92-96.

-Lange M. A., P. Schlosser, S. F. Ackley, P. Wadhams and G. S. Dieckmann, 1990. ^{18}O concentrations in sea ice of the Weddell Sea, Antarctica. *Journal of Glaciology*, *36*(124), 315-323.

-Langway C. C. J., 1958. Ice fabrics and the Universal stage. *Rep.*, 16 pp, CRREL Technical Report, 62.

-Lannuzel D., A.R. Bowie, P.C. Van der Merwe, A.T. Townsend and V. Schoemann, 2011. Distribution of dissolved and particulate metals in Antarctic sea ice. *Mar. Chem.*, 124, 134-146.

-Lannuzel D., J. de Jong, V. Schoemann, A. Trevena, J.-L. Tison and L. Chou, 2006. Development of a sampling and flow injection analysis technique for iron determination in the sea ice environment. *Analytica Chimica Acta*, *556*(2), 476-483.

-Lannuzel D., V. Schoemann, J. de Jong, J.-L. Tison and L. Chou, 2007. Distribution and biogeochemical behaviour of iron in the East Antarctic sea ice. *Mar. Chem.*, 106: 18-32.

-Lannuzel D., V. Schoemann, J. de Jong, L. Chou, B. Delille, S. Becquevort and J.-L. Tison, 2008. Iron study during a time series in the western Weddell pack ice. *Marine Chemistry*, 108: 85-95.

-Lannuzel D., V. Schoemann, J. de Jong, B. Pasquer, P. van der Merwe, F. Masson, J.-L. Tison and A. Bowie, 2010. Distribution of dissolved iron in Antarctic sea ice: Spatial, seasonal, and inter-annual variability. *J. Geophys. Res.*, 115 (3), G03022.

-Large W. G. and S. G. Yeager, 2004. Diurnal to decadal global forcing for ocean and sea ice models: The data sets and flux climatologies. *Rep.*, 112 pp, NCAR, Boulder, Colorado.

-Laws E., E. Sakshaug, M. Babin, Y. Dandonneau, P. Falkowski, R. Geider, L. Legendre, A. Morel, M. Sondergaard, M. Takahashi and P.J. Williams, 2002. Photosynthesis and Primary productivity in marine ecosystems: Practical aspects and application of techniques. *Joint Global Ocean Flux Study – JGOFS* – Report No. 36.

-Lemke P. et al., 2014. The Expedition of the Research Vessel "Polarstern" to the Antarctic in 2013 (ANT-XXIX/6). Berichte zur Polar- und Meeresforschung 679, 159.

-Lewis E., D. Wallace and L.J. Allison, 1998. Program developed for CO_2 system calculations. *Tennesse*.

-Lewis M. J., J.-L. Tison, B. Weissling, B. Delille, S. Ackley, F. Brabant and H. Xie, 2011. Sea ice and snow cover characteristics during the winter–spring transition in the Bellingshausen Sea: an overview of SIMBA 2007. *Deep Sea Research Part II: Topical Studies in Oceanography*, *58*(9), 1019-1038.

-Lipizer M., O. Mangoni, G. Catalano and V. Saggiomo, 2000. Phytoplankton uptake of ^{15}N and ^{14}C in the Ross Sea during austral spring 1994. *Polar Biology*, 23, 495-502.

-Lipschultz F., S.C. Wofsy, B.B. Ward, L.A. Codispoti, G. Friedrich and J.W. Elkins, 1991. Bacterial transformations of inorganic nitrogen in the oxygen-deficient waters of the Eastern Tropical South Pacific Ocean. *Deep-Sea Research Part II*, 37(10), 1513-1541.

-Madec G. and N. Team, 2016. NEMO Ocean Engine version 3.6 stable. *Rep. ISSN N° 1288-1619*, 406 pp, Institut Pierre-Simon Laplace, Paris, France.

-Martens-Habbena W., P.M. Berube, H. Urakawa, J.R. de la Torre and D.A. Sath, 2009. Ammonia oxidation kinetics determine niche separation of nitrifying Archaea and Bacteria. *Nature*, 461, 976–979, 2009.

-Massman W.J., R.A. Sommerfeld, A.R. Mosier, K.F. Zeller, T.J. Hehn and S.G. Rochelle, 1997. A model investigation of turbulence-driven pressure-pumping effects on the rate of diffusion of CO_2, N_2O, and CH_4 through layered snowpacks. *J. Geophys.Res.*, 102(97).

-McCartney M. S. and K.A. Donohue, 2007. A deep cyclonic gyre in the Australian–Antarctic Basin. *Prog. Oceanogr.*, 75, 675–750.

-McMinn A., K.G. Ryan, P.J. Ralph and A. Pankowski, 2006. Spring sea ice photosynthesis, primary productivity and biomass distribution in eastern Antarctica, 2002–2004. *Mar. Biol.*, 151, 985–995. http://dx.doi.org/10.1007/s00227-006-0533-8.

-Meiners K.M., K. Golden, P. Heil, J.L. Lieser, R. Massom, B. Meyer and G.D. Williams, 2016. SIPEX-2, a study of sea ice physical, biogeochemical and ecosystem processes off East Antarctica during spring 2012. *Deep Sea Res. Part II Top. Stud.Oceanogr.*, 131, 1–6. http://dx.doi.org/10.1016/j.dsr2.2016.06.010.

-Meiners K.M., M. Vancoppenolle, S. Thanassekos, G.S. Dieckmann, D.N. Thomas, J.-L. Tison, K.R. Arrigo, D.L. Garrison, A. McMinn, D. Lannuzel, P. Van Der Merwe, K.M. Swadling, W.O. Smith, I. Melnikov and B. Raymond, 2012. Chlorophyll-a in Antarctic sea ice from historical ice core data. *Geophys. Res. Lett.*, 39. http://dx.doi.org/10.1029/2012gl053478, L21602.

-Menden-Deuer S. and E. J. Lessard, 2000. Carbon to volume relationships for dinoflagellates, diatoms and other protist plankton. *Limnology and Oceanography*, *45*(3), 569-579.

-Middag R., C. Van Slooten, H.J.W. de Baar and P. Laan, 2011. Dissolved aluminium in the Southern Ocean. *Deep-Sea Res II*, 58, 2647–2660.

-Milne A., W. Landing, M. Bizimis and P. Morton, 2010. Determination of Mn, Fe, Co, Ni, Cu, Zn, Cd and Pb in seawater using high resolution magnetic sector inductively coupled mass spectrometry (HR-ICP-MS). *Anal. Chim. Acta*., 665: 200–207.

-Möbius J., 2013: Isotope fractionation during nitrogen remineralization (ammonification): Implications for nitrogen isotope biogeochemistry. *Geochim. Cosmochim. Ac.*, 105, 422-432.

-Mock T., 2002. In situ primary production in young Antartic sea ice, *Hydrobiologia*. *470*, 127-132.

-Mock T. and R. R. Gradinger, 1999. Determination of Arctic ice algal production with a new in situ incubation technique. *Marine Ecology Progress series*, *177*, 15-26.

-Moran J. J., E. J. Beal, J. M. Vrentas, V. J. Orphan, K. H. Freeman and C. H. House, 2008. Methyl sulfides as intermediates in the anaerobic oxidation of methane. *Environmental Microbiology*, *10*, (1), 162–173.

-Mosseri J., B. Quéguiner, L. Armand and V. Cornet-Barthaux, 2008. Impact of iron on silicon utilization by diatoms in the Southern Ocean: a case study of Si/N cycle decoupling in a naturally iron enriched area. *Deep Sea Research Part 2*, 55, 801-819.

-Mundy C. J., D. G. Barber and C. Michel, 2005. Variability of snow and ice thermal, physical and optical properties pertinent to sea ice algae biomass during Spring. *Journal of marine Systems*, *58*, 107-120.

-Nomura D., H. Yoshikawa-Inoue and T. Toyota, 2006. The effect of sea-ice growth on air-sea CO2 flux in a tank experiment. *Tellus Series B*, 58(5), 418-426.

-Notz D., 2005. Thermodynamic and fluid-dynamical processes in sea ice. *Univ. Cambridge*.

-Notz D. and M. G. Worster, 2008. In situ measurements of the evolution of young sea ice. *Journal of Geophysical Research*, *113*(C3), doi:10.1029/2007JC004333.

-Notz D. and M. G. Worster, 2009. Desalination processes of sea ice revisited. *Journal of Geophysical Research: Oceans*, *114*(C5), doi:10.1029/2008JC004885.

-Nozaki Y., J. Zhang and H. Amakawa, 1997. The fractionation between Y and Ho in the marine environment. *Earth Sci. Planet. Lett.*, 148, 329-340.

-Olenina I., et al., 2006. Biovolumes and size-classes of phytoplankton in the Baltic Sea. *Baltic Sea Environment Proceedings*, *106*, 1-144.

-Olson R.J., 1981. ^{15}N tracer studies of the primary nitrite maximum. *Journal of Marine Research*, 39(2), 203-238.

-Owens S.A., K.O. Buesseler and K.W.W. Sims, 2011. Re-evaluating the 238U-salinity relationship in seawater: Implications for the 238U–234Th disequilibrium method. *Marine Chemistry*, 127, 31-39.

-Paul D., G. Skrzypek and I. Fórizs, 2007. Normalization of measured stable isotopic compositions to isotope reference scales – a review. *Rapid Commun. Mass Sp.*, 21, 3006–3014.

-Park Y.-H., I. Durand, E. Kestenare, G. Rougier, M. Zhou, F. d'Ovidio, C. Cottéa and J.-H. Lee, 2014a. Polar Front around the Kerguelen Islands: an up-to-date determination and associated circulation of surface/subsurface waters. *J. Geophys. Res.–Oceans*, 119, 6575–6592, doi:10.1002/2014JC010061.

-Park Y.-H., F. Roquet, I. Durand and J.-L. Fuda, 2008. Large-scale circulation over and around the Northern Kerguelen Plateau. *Deep-Sea Res. Pt. II*, 55, 566–581.

-Park Y.H., J.H. Lee, I. Durand and C.S. Hong, 2014b. Validation of Thorpe-scale-derived vertical diffusivities against microstructure measurements in the Kerguelen region. *Biogeosciences*, 11, 6927-6937.

-Pennock J. R., D.J. Velinsky, J.M. Ludlam and J.H. Sharp, 1996. Isotopic fractionation of ammonium and nitrate during uptake by Skeletonema costatum: implications for δ^{15}N dynamics under bloom conditions. *Limnol. Oceanogr.*, 41, 451–459.

-Philippe M., et al., 2016. Ice core evidence for a 20th century increase in surface mass balance in coastal Dronning Maud Land, East Antarctica. *The Cryosphere*, *10*(5), 2501-2516, doi:10.5194/tc-10-2501-2016.

-Pike S.M., K.O. Buesseler, J. Andrews and N. Savoye, 2005. Quantification of 234Th recovery in small volume sea water samples by inductively coupled plasma-mass spectrometry. *Journal of Radioanalytical and Nuclear Chemistry*, 263, 355-360.

-Planchon F., A.J. Cavagna, D. Cardinal, L. André and F. Dehairs, 2013. Late summer particulate organic carbon export and twilight zone remineralisation in the Atlantic sector of the Southern Ocean. *Biogeosciences*, 10, 803-820.

-Planchon F., D. Ballas, A.-J. Cavagna, A.R. Bowie, D. Davies, T.W. Trull, E. Laurenceau, P. van der Merwe and F. Dehairs, 2015. Carbon export in the naturally iron-fertilized Kerguelen area of the Southern Ocean based on the ^{234}Th approach. *Biogeosciences,* 12, 3831-3848.

-Platt T., C.L. Gallegos and W.G. Harrison, 1980. Photoinhibition of photosynthesis in natural assemblages of marine phytoplankton. *J. Mar. Res.*, 38:687–701.

-Pongratz R. and K.G. Heumann,1999. Production of methylated mercury, lead, and cadmium by marine bacteria as a significant natural source for atmospheric heavy metals in polar regions. *Chemosphere*, 39, 89–102.

-Sholkovitz E.R., W.M. Landing and B.L. Lewis, 1994. Ocean particle chemistry: The fractionation of rare earth elements between suspended particles and seawater. *Geochim. Cosmochim. Acta*, 58, 1567-1579.

-Pringle D. and M. Ingham, 2009. Measuring sea ice thermal, electrical and hydraulic properties and processes. In: *Field Techniques for Sea Ice Research*, edited by H. Eicken, R. Gradinger, M. Salganek, K. Shirasawa, D. Perovich and M. Lepparanta, p. 592, University of Alaska Press, Fairbanks, Alaska.

-Priscu J.C., M.T. Downes, L.R. Priscu, A.C. Palmisano and C.W. Sullivan, 1990. Dynamics of ammonium oxidizer activity and nitrous-oxide (N2O) within and beneath Antarctic Sea Ice. Mar. Ecol. Prog. Ser 62, 37–46.

-Rafter P. A., P.J. DiFiore and D.M. Sigman, 2013. Coupled nitrate nitrogen and oxygen isotopes and organic matter remineralization in the Southern and Pacific Oceans. *J. Geophys. Res.–Oceans*, 118, 4781–4794, doi:10.1002/jgrc.20316.

-Randall K., M. Scarratt, M. Levasseur, S. Michaud, H. Xie and M. Gosselin, 2012. First measurements of nitrous oxide in Arctic sea ice. *J. Geophys. Res.*, *117*: C00G15.

-Rintala J. M., J. Piiparinen, J. Blomster, M. Majaneva, S. Müller, J. Uusikivi and R. Autio, 2014. Fast direct melting of brackish sea-ice samples results in biologically more accurate results than slow buffered melting. *Polar Biology*, *37*, 1811-1822.

-Rousset C., et al., 2015. The Louvain-La -Neuve sea ice model LIM 3.6: global and regional capabilities. *Geosci. Model Dev.*, *8*, 2991-3005.

-Rysgaard S., R.N. Glud, M.K. Sejr, M.E. Blicher and H.J. Stahl, 2008. Denitrification activity and oxygen dynamics in Arctic sea ice. *Polar Biology*, 5: 527-537.

-Rysgaard S., B. Delille, G.S. Dieckmann, R.N. Glud, H. Kennedy, J. Mortensen, S. Papadimitriou, D.N. Thomas and J.-L. Tison, 2011. Sea ice contribution to the air-sea CO_2 exchange in the Arctic and Southern Oceans. *Tellus 63B*: 823-830.

-Saenz B.T. and K.R. Arrigo, 2014. Annual primary production in Antarctic sea ice during 2005–2006 from a sea ice state estimate. *J. Geophys. Res.*, 119, 3645–3678.

-Sambrotto R.N. and B.J. Mace, 2000. Coupling of biological and physical regimes across the Antarctic Polar Front as reflected by nitrogen production and recycling. *Deep-Sea Research Part II*, 47, 3339-3367.

-Savoye N., F. Dehairs, M. Elskens, D. Cardinal, E.E. Kopczynska, T.W. Trull, S. Wright, W. Baeyens and B.F. Griffiths, 2004. Regional variation of spring N-uptake and new production in the Southern Ocean. *Geophysical Research Letters*, 31, L03301, doi:10.1029/2003GL018946.

-Savoye N., C. Benitez-Nelson, A.B. Burd, J.K. Cochran, M. Charette, K.O. Buesseler, G.A. Jackson, M. Roy-Barman, S. Schmidt and M. Elskens, 2006. ^{234}Th sorption and export models in the water column: A review. *Marine Chemistry*, 100, 234-249.

-Savoye N., T.W. Trull, S.H.M. Jacquet, J. Navez and F. Dehairs, 2008. ^{234}Th-based export fluxes during a natural iron fertilization experiment in the Southern Ocean (KEOPS). *Deep-Sea Research II*, 55, 841-855.

-Schloss P. D., et al., 2009. Introducing mothur: Open-Source, Platform-Independent, Community-Supported Software for Describing and Comparing Microbial Communities. *Appl. Environ. Microbiol.*, *75*(23), 7537-7541.

-Sigman D. M., M.A. Altabet, D.C. McCorkle, R. Francois and G. Fischer, 1999. The $\delta^{15}N$ of nitrate in the Southern Ocean: Consumption of nitrate in surface waters. *Global Biogeochem. Cy.*, 13, 1149-1166.

-Sigman D. M., M.A. Altabet, D.C. McCorkle, R. Francois and G. Fischer, 2000. The $\delta^{15}N$ of nitrate in the Southern Ocean: Nitrogen cycling and circulation in the ocean interior. *J. Geophys. Res.-Oceans*, 105, 19,599-19,614.

-Sigman D.M., K.L. Casciotti, M. Andreani, C. Barford, M. Galanter and J.K. Böhlke, 2001. A bacterial method for the nitrogen isotopic analysis of nitrate in seawater and freshwater. *Analytical Chemistry*, 73, 4145-4153.

-Sigman D. M., P.J. DiFiore, M.P. Hain, C. Deutsch, Y. Wang, D.M. Karl, A.N. Knapp, M.F. Lehmann and S. Pantoja, 2009. The dual isotopes of deep nitrate as a constraint on the cycle and budget of oceanic fixed nitrogen. *Deep-Sea Res. Pt. I*, 56, 1419–1439.

-Sigman D., J. Granger, P. DiFiore, M.M. Lehmann, R. Ho, G. Cane and A. van Geen, 2005. Coupled nitrogen and oxygen isotope measurements of nitrate along the eastern North Pacific margin. *Global Biogeochem. Cy.*, 19, GB4022, doi:10.1029/2005GB002458.

-Smetacek V., R. Scharek, L. I. Gordon, H. Eicken, E. Fahrbach, G. Rohardt and S. Moore, 1992. Early spring phytoplankton blooms in ice platelet layers of the southern Weddell Sea, Antarctica. *Deep Sea Research Part A. Oceanographic Research Papers*, *39*(2), 153-168.

-Smith R. E. H. and A. W. Herman, 1991. Productivity of sea ice algae: In situ vs. incubator methods. *Journal of marine Systems*, *2*(1-2), 97-110.

-Sohrin Y., S. Nakatsuka, T. Kono, E. Higo, T. Minami, K. Norisuye and S. Umetani, 2008. Multielemental determination of GEOTRACES key trace metals in seawater by ICP-MS after preconcentration using an ethylenediaminetriacetic acid chelating resin. *Anal. Chem.*, 80: 6267-6273.

-Song H. J., J. H. Lee, G. W. Kim, S. H. Ahn, H.-M. Joo, J. Y. Jeong, E. J. Yang, S.-H. Kang and S. H. Lee, 2016. In-situ measured primary productivity of ice algae in Arctic sea ice floes using a new incubation method. *Ocean Science Journal*, *51*(3), 387-396.

-Souchez R. and J. Jouzel, 1984. On the isotopic composition in δD and $\delta^{18}O$ of water and ice during freezing. *J. Glaciol.*, *30*(106), 369-372.

-Souchez R., J.-L. Tison and J. Jouzel, 1987. Freezing rate determination by the isotopic composition of the ice. *Geophys. Res. Lett.*, *14*(6), 599-602.

-Souchez R., J.-L. Tison and J. Jouzel, 1988. Deuterium concentration and growth rate of Antarctic first-year sea ice. *Geophys. Res. Lett.*, *15*(12), 1385-1388.

-Spindler M. and G.S. Dieckmann, 1986. Distribution and abundance of the planktonic foraminifer *Neogloboquadrina pachyderma* in sea ice of the Weddell Sea, (Antarctica). *Polar Biol.*, 5, p. 185-191.

-Stahl D. A. and J. de la Torre, 2012. Physiology and diversity of ammonia-oxidizing archaea. *Annu. Rev. Microbiol.*, 66, 88–101.

-Stefels J., M. Steinke, S. Turner, G. Malin and S. Belviso, 2007. Environmental constraints on the production and removal of the climatically active gas dimethylsulphide (DMS) and implications for ecosystem modeling. *Biogeochemistry*, 83, 245-275.

-Stefels J., G. Carnat, J.W. Dacey, T. Goossens, J.T.M. Elzenga and J.-L. Tison, 2012. The analysis of dimethylsulfide and dimethylsulfoniopropionate in sea ice: dry-crushing and melting using stable isotope additions. *Marine Chemistry*, 128-129: 34-43.

-Taylor S.R. and S.M. McLennan, 1985. The continental crust: its composition and evolution. Blackwell Scientific Publications, 312pp.

-Trull T. W., D. Davies and K. Casciotti, 2008. Insights into nutrient assimilation and export in naturally iron-fertilized waters of the Southern Ocean from nitrogen, carbon and oxygen isotopes. *Deep-Sea Res. Pt. II*, 55, 820–84.

-Thomas C., 1997. Identifying Marine Phytoplankton. Academic Press, Elsevier, California 858p.

-Thomas D. N., S. Papadimitriou and C. Michel, 2010. Biogeochemistry of sea ice. In: *Sea Ice*, edited by D. N. Thomas and G. S. Dieckmann, p. 621, Blackwell Publishing Ltd, Oxford, UK.

-Tison J.-L., A. Worby, B. Delille, F. Brabant, S. Papadimitriou, D. N. Thomas, J. de Jong, D. Lannuzel and C. Haas, 2008. Temporal evolution of decaying summer first-year sea ice in the Western Weddell Sea, Antarctica. *Deep Sea Research II*, *55*, 975-987.

-Tison J.-L., F. Brabant, I. Dumont and J. Stefels, 2010. High-resolution dimethyl sulfide and dimethylsulfoniopropionate time series profiles in decaying summer first-year sea ice at Ice Station Polarstern, western Weddell Sea, Antarctica. *Journal of Geophysical Research*, 115.

-Trenberth K. E., J. G. Olson and W. G. Large, 1989. A global ocean wind stress climatology based on ECMWF analyses. *Rep.*, 93 pp, National Center for Atmospheric Research, Boulder, Colorado.

-Trevena A. J. and G. B. Jones, 2006. Dimethylsulphide and dimethylsulphoniopropionate in Antarctic sea ice and their release during sea ice melting. *Marine Chemistry*, *98*, 210 – 222.

-Ütermöhl H., 1958. Zur Vervollkommung der quantitativen Phytoplankton-Methodik. *Mitteilungen Internationale Vereinigung für Theoretische und Angewandte Limnologie* 269–285.

-Vancoppenolle M., T. Fichefet, H. Goosse, S. Bouillon, G. Madec and M. A. M. Maqueda, 2009. Simulating the mass balance and salinity of Arctic and Antarctic sea ice. 1. Model description and validation. *Ocean Modelling*, *27*(1–2), 33-53.

-Vancoppenolle M., D. Notz, F. Vivier, J.-L. Tison, B. Delille, G. Carnat, J. Zhou, F. Jardon, P. Griewank, A. Lourenço and T. Haskell, 2013. Technical Note: On the use of the mushy-layer Rayleigh number for the interpretation of sea-ice-core data. *The Cryosphere Discuss.*, *7*(4), 3209-3230.

-Waser N. A. D., P.J. Harrison, B. Nielsen, S.E. Calvert and D.H. Turpin, 1998. Nitrogen isotope fractionation during the uptake and assimilation of nitrate, nitrite, ammonium and urea by a marine diatom. *Limnol. Oceanogr.*, 43, 215–224.

-Williams G., T. Maksym, J. Wilkinson, C. Kunz, C. Murphy, P. Kimball and H. Singh, 2014. Thick and deformed Antarctic sea ice mapped with autonomous under-water vehicles. *Nat. Geosci.*, 8, 1–7.

-Worby A.P., K.M. Meiners and S.F. Ackley, 2011. Antarctic sea-ice zone research during the International Polar Year, 2007–2009. *Deep Sea Res. II Top. Stud. Oceanogr*., 58, 993–998.

-Yoshida O., H. Y. Inoue, S. Watanabe, K. Suzuki and S. Noriki, 2011. Dissolved methane distribution in the South Pacific and the Southern Ocean in austral summer. *Journal of Geophysical Research: Oceans*, *116*(C7), C07008.

-Zhou J., B. Delille, H. Eicken, M. Vancoppenolle, F. Brabant, G. Carnat, N. X. Geilfus, T. Papakyriakou, B. Heinesch and J. L. Tison, 2013. Physical and biogeochemical properties in landfast sea ice (Barrow, Alaska): Insights on brine and gas dynamics across seasons. *Journal of Geophysical Research: Oceans*, *118*(6), 3172-3189.

-Zhou J., et al., 2014. Physical and bacterial controls on inorganic nutrients and dissolved organic carbon during a sea ice growth and decay experiment. *Marine Chemistry*, *166*, 59-69.

-Zhou J., J.-L. Tison, F. Brabant and B. Delille, 2011. Gas concentrations in Barrow landfast sea ice: the winter/spring contrasts. *Solas News*, *13*, 22–23.

10. ANNEX 1 – Copy of the publications

11. ANNEX 2 – Minutes of the follow-up committee meetings

Members of the Committee:

Tom Trull

Gerhard Dieckmann

Daniel Sigman

Damien Cardinal

Laurent Bopp

Minutes of the follow-up committee meeting held at BELSPO, Brussels, Sept. 3, 2012

Attended:

T. Trull; G. Dieckmann; L. André; J.-L. Tison; F. Fripiat (video conference with Princeton University); V. Schoemann, H. Goosse, S. Moreau; M. Vancoppenolle; J. Le Sommer; F. Dehairs; A.-J. Cavagna; A. Roukaerts.

Schedule:

10.00: Welcome

10.10: Gas transport in sea ice: How convection and diffusion processes might affect biological imprints… A challenge for modellers

J.-L. Tison, J. Zhou, D.N. Thomas, S. Rysgaard, H. Eicken, O. Crabeck, F. Deleu, M. Vancoppenolle, S. Moreau, H. Goosse and B. Delille

10.40: Modeling gas dynamics in first year sea-ice

S. Moreau, M. Vancoppenolle, Jiayun Zhou, J.-L. Tison, B. Delille and H. Goosse

11.10: The YROSIAE field Project: ongoing research

B. Delille, T. Haskell, V. Schoemann, J. Zhou, F. Fripiat, G. Carnat, W. Champenois, T. Goossens, M. Vancoppenolle, S. Moreau, J. de Jong, G. Dieckmann, H. Goosse and J.-L. Tison

11.40: First results on primary production and carbon export in the naturally Fe fertilised Kerguelen area (KEOPS 2)

A.-J. Cavagna, F. Planchon, D. Ballas, L. André and F. Dehairs

12.20: Planned sea-ice work during the upcoming SIPEX 2 expedition

A.-J. Cavagna, A. Roukaerts, F. Fripiat, J.-L. Tison, L ; André and F. Dehairs

12.30: Discussion round

13.00: Lunch break

14.00: Nitrogen isotopic composition in Antarctic Sea Ice (SIMBA+ISPOL) (PON, NO3, TDN).

F. Fripiat et al. Skype connection with Princeton

14.30: Vertical distribution of the isotopic composition of nitrate and silicic acid in the Antarctic Zone.

F. Fripiat et al. Skype connection with Princeton

14.40: Isotopic composition of nitrate in the naturally Fe fertilised Kerguelen area (KEOPS 2)

F. Dehairs, A.-J. Cavagna

15.00: BIOPERIANT05: a DRAKKAR model configuration for studying Southern Ocean biogeochemical cycles.

J. Le Sommer

15.30: Discussion round

17.00: End of workshop

Minutes of the BIGSOUTH meeting organised on 21/01/2014 Université Libre de Bruxelles

Attendants and talks:

Bruno Delille: The YROSIAE field Campaign an overview of available results

Jean-Louis Tison: The AWECS Weddell Sea winter cruise: preliminary results

Jiayun Zhou: The INTERICE V project: linking CO_2 fluxes to sea ice biogeochemistry and physics

Gauthier Carnat: Year-round evolution of Sulfur compounds in Antarctic landfast sea ice (McMurdo Sound - YROSIAE)

François Fripiat: N, Si cycling in sea ice (SIMBA - ISPOL - d'Umont d'Urville)

Véronique Schoemann: Biogeochemistry of trace metals in the sea ice

Arnout Roukaerts: Primary production and N cycling during SIPEX 2

Sebastien Moreau: 3D simulations of DIC and ALK incorporation in sea ice

Frank Dehairs: The biopump functioning in the Kerguelen area during KEOPS 2

François Fripiat: The significance of surface ocean nitrification during KEOPS 2

Further exchanges with the Follow-Up committee in the course of 2013 -2015

- Tom Trull :

Collaboration on POC/^{234}Th of size fractionated particles and nitrate isotopy during the KEOPS 2 (Oct.-Nov. 2011) expedition. Provided samples from sediment traps and continuous filtration system. Discussions on future collaboration (HEARD Island, Totten Ice shelf, MIZ) and assistance with analyses (nitrate isotopic analyses).

Frequent e-mail contacts and discussions in Hobart (March 10-14, 2014) during the 'International Sea Ice symposium in a changing environment'; also discussion via video-conference with F. Dehairs at LEGOS, OMP, Toulouse, 25/11/2014.

Contributed as co-author to papers by Frank Dehairs et al., in Biogeosciences and François Fripiat et al. in Biogeochemical Global Biogeochemical Cycles which appeared in 2015.

- Gerhard Dieckmann:

Set-up, training and drafting of a users guide (Jiayun Zhou and François Fripiat, ULB) of the AWI sediment traps and current meter that were deployed at Scott Base in August 2012. Discussions on sampling protocols.

Discussions during the International Sea Ice symposium in a changing environment, 2014, Hobart, Australia.

Contributed to several papers (Zhou et al., Janssens et al.) as a co-author.

- Daniel Sigman:

Collaboration for the analyses and discussion of sea ice nitrate $\delta^{15}N$ and $\delta^{18}O$ results. Providing the analytical facilities (2011-2013) to François Fripiat for the sea ice isotopic analyses of: nitrates, ammonium, total dissolved nitrogen, particulate nitrogen, and diatom N-bound. Contributed as co-author to paper by François Fripiat et al. in Global Biogeochemical Cycles and which was published in 2015.

- Damien Cardinal:

Collaboration in the coupling of the KEOPS 2 $^{13}C/^{15}N$ and ^{30}Si-incubations. Strongly implicated in the discussion about the $\delta^{30}Si$ results. Collaborations with Ivia Closset, PhD student Université Paris VI, under D. Cardinal's supervision.

Discussions at LOCEAN, Univ. Paris VI, December 2014.

Contributed as co-author to papers by Stephanie Jacquet et al. in Biogeosciences and which was published in 2015.

- Laurent Bopp:

Discussions during the PAGES SSC meeting, Paris, January 28, 2014, concerning the use of the NEMO-LIM-PISCES model.